Effective properties of randomly heterogeneous beams

by Jack Pierce-Brown

Thesis submitted to the University of Nottingham
for the degree of Doctor of Philosophy

June 2019



University of
Nottingham
UK | CHINA | MALAYSIA

Abstract

This research is concerned with the application of random fields to model material heterogeneity with implications on the usage of the stochastic finite element method to evaluate structural reliability. In particular, there is extensive consideration of the relationship between the effective modulus of elasticity of randomly heterogeneous timber beams and the underlying lognormal random field of elastic modulus. Under Euler-Bernoulli beam theory, the effective elastic modulus is shown to be a weighted harmonic mean and weighting functions are provided for a number of important loading conditions. Additionally, analytical expressions are derived for the moments of both the displacement and effective elastic modulus of the beam. In the case of multi-dimensional heterogeneity, a generalised weighted mean meta-model is introduced for the effective property of heterogeneous materials and a novel function optimisation algorithm is utilised to optimise the weighting function of this meta-model to the results of both one and two-dimensional finite element models with insights into the sensitivity of the effective property to both spatial weighting and minima of the random field of elastic modulus. Finally, the inference of the parameters of a random field model from effective local and global moduli of elasticity is considered and it is shown that the use of the midpoint approximation results in large epistemic biases which likely leads to underestimation of the variability of heterogeneous materials.

Acknowledgements

The author would like to express his sincere gratitude to his supervisors, Dr Luis C. Neves and Dr Donald L. Brown for their kindness encouragement and careful guidance that has culminated in the creation of this thesis. The author gratefully acknowledges the support provided by the Faculty of Engineering at the University of Nottingham that has facilitated the completion of this research project. The author also records his appreciation for the insightful comments of the internal examiner Dr Savvas P. Triantafyllou and the external examiner António Abel Henriques. Finally, the author thanks his family for their love during these years of study.

Contents

1 Introduction **1**

1.1 Meta-problem framework 5

1.2 Thesis overview and scope 8

2 Random fields: Theory, estimation and simulation **12**

2.1 Introduction 12

2.2 Stationarity 15

2.3 Mean square properties 17

2.4 Common covariance and correlation functions 18

2.4.1 Higher-dimensional correlation functions 25

2.5 Spectral representation 29

2.5.1 Common spectral density functions 32

2.5.2 Higher-dimensional spectral density functions 34

2.6 Non-Gaussian processes 35

2.7 Overview of estimation 37

2.8 Method of moments estimation 40

2.8.1 Efficient computation of the sample correlation function 42

2.9 Maximum likelihood estimation 44

2.10 Kriging 50

2.10.1 Kriging variance 54

2.10.2 Conditional random fields 55

2.11 Overview of simulation 56

2.12 Covariance matrix decomposition method 59

2.13 Fast Fourier transform method 60

2.13.1 Two-dimensional implementation 64

2.14 Evaluation of simulation methods 68

2.15 Conclusion 70

3 Theory of heterogeneous beams **72**

3.1 Introduction 72

3.2 Deterministic effective properties 76

3.2.1 Three-point loading 79

3.2.2 Uniformly distributed loading 83

3.2.3 Comparison of loading conditions 84

3.2.4 Analytical benchmark 87

3.2.5 Finite element model 90

3.3 Random effective properties 93

3.3.1 Analytical moments of displacement . . . 96
3.3.2 Stochastic finite element model . . . 99
3.3.3 Quasi-analytical moments of the effective elastic modulus . . . 101
3.4 Sensitivity analyses . . . 103
3.4.1 Variation of moments along the beam . . . 103
3.4.2 Variation of moments with the correlation length . . . 108
3.4.3 Variation of moments with the coefficient of variation . . . 110
3.4.4 Limitations . . . 114
3.5 Conclusion . . . 115

4 Meta-modelling of effective properties 117

4.1 Introduction . . . 117
4.2 Mean meta-models . . . 121
4.3 Functional optimisation . . . 125
4.3.1 Algorithm overview . . . 125
4.3.2 Optimisation investigation . . . 127
4.4 Three-point flexural test . . . 135
4.5 One-dimensional meta-modelling . . . 137
4.6 Two-dimensional meta-modelling . . . 144
4.7 Conclusion . . . 154

5 Inference from effective properties 157

5.1 Introduction . . . 157

5.2 Probabilistic modelling of timber . . . 161

5.3 Determination of the effective elastic modulus of timber . . . 168

5.4 Analysis of experimental data . . . 172

5.4.1 Marginal distribution . . . 174

5.4.2 Correlation structure . . . 178

5.5 Uncertainty quantification . . . 182

5.5.1 Distribution of the location parameter . . . 186

5.5.2 Distribution of the scale parameter . . . 188

5.5.3 Distribution of the correlation parameter . . . 190

5.5.4 Discussion of results . . . 192

5.6 Conclusion . . . 193

6 Conclusion **195**

6.1 General conclusions . . . 196

6.2 Recommendations for further research . . . 198

Bibliography **200**

Appendices **214**

A Calculations for Chapter 2 **215**

A.1 Constant of the power correlation function . . . 215

A.2 Spectral representations for FFT 216

A.3 Statistical properties of CMD 217

B Calculations for Chapter 3 **219**

B.1 Interchange of the order of integration 219

B.2 Equation of deflection for three-point loading 220

B.3 Weighting function for uniformly distributed loading 222

B.4 Weighting function for four-point loading 223

B.5 Moments of the reciprocal of a lognormal random variable 225

C Calculations for Chapter 5 **227**

C.1 Weighting function for the global modulus of elasticity 227

C.2 Weighting function for the local modulus of elasticity 230

Chapter 1

Introduction

The research presented by this thesis can be broadly placed within the discipline of reliability engineering which is a research area concerned with quantifying the probability of failure of engineering systems. Reliability engineering is motivated by a desire to inform decision making and manage risk with the intention of maximising the safety, sustainability and economic viability of the engineering system under consideration. It should be noted that a large range of different engineering systems fall within the scope of reliability engineering including transportation, energy and water networks; however, this thesis is primarily concerned with the subdiscipline of structural reliability which considers the probability of mechanical failure of constructed assets such as buildings, embankment dams and bridges resulting from uncertainties regarding loading, geometry and material properties. It is important to recognise that probabilistic approaches are becoming increasingly important for the analysis of structural systems in the face of the uncertainty arising from both changing environmental conditions and an increasingly interconnected world. Furthermore, the continuing development of modern computation is resulting in increasingly large datasets, in addition to the processing power necessary to analyse this data, and this implies that sophisticated methods for reliability engineering that were previously infeasible are becoming available.

The selection of an appropriate probabilistic model is essential to achieve an accurate quantification of the risk associated with engineering systems. In general, there are two approaches to obtain, and subsequently infer the parameters of, these probabilistic models which are respectively known as the *data driven* and *first principles* approaches. The

data driven approach selects a statistical model, or pool of candidate statistical models, a priori and then optimises the model parameters to a historical dataset. For instance, the frequency of an event such as an earthquake can be modelled using a Poisson point process whose rate parameter is estimated on the basis of the historical frequency of earthquakes within the region and the associated extent of structural collapse can be estimated based on records of building damage. The data driven approach is useful under the condition that a sufficiently large dataset is available and that the recorded past occurrences of the phenomena are predictive of its future frequency and intensity. However, in the case of rare events with low frequency, such as large magnitude earthquakes, or phenomena whose past is not predictive of their future, such as floods due to changing environmental conditions, then caution should be exercised in the use of purely data driven approaches.

The alternative approach to structural reliability is to adopt the first principles approach which utilises probabilistic models that are derived from fundamental physical laws that govern the structural system. The advantage of this approach is that the probabilistic model is not selected a priori, a source of considerable subjectivity, and that the predictive power of the first principles model is dependent on the accuracy of the physical laws rather than the availability of historical data. Furthermore, the first principles approach is useful to evaluate system reliability against rare events that, whilst having adequately large consequences as to pose a significant risk, have sufficiently low frequency that there is no record of their occurrence in the historical dataset. It is suggested that a balanced approach to structural reliability that takes advantage of the strengths of both methods is obtained through the combination of the first principles and data driven approaches with the objective of either optimising the parameters of a derived physical model to a suitable dataset or, alternatively, validating a data driven model through verification against physical first principles.

The research direction pursued within this thesis is to adopt a physics-based probabilistic model to quantify the structural reliability associated with randomly heterogeneous materials. This is motivated by the fact that all materials are to some extent heterogeneous with uncertainty associated with their physical properties and, consequently, there is always a risk that a material will not perform in the way that is expected. In order to mitigate against this, engineers seek an approach to structural design that minimises this risk to an acceptable level. The traditional approach is to perform a determinis-

tic analysis that models the material as homogeneous with mechanical properties given by a representative value and to address uncertainty through the use of safety factors. Unfortunately, this deterministic approach is subject to a number of disadvantages: the first disadvantage is that there is no consideration of probability of failure since homogeneous materials do not fail under stresses below their representative strength; the second disadvantage is that this theory does not account for heterogeneous behaviour such as the differential settlement of soil or the non-symmetrical bending of beams; the third disadvantage is that the use of safety factors may result in over-design since this approach to account for the spatial variation of material properties is overly simplistic. This motivates the development of structural design methods that account for material heterogeneity in a more sophisticated manner in order to produce increasingly reliable, sustainable and economical structures.

One of the most important physical models for structures composed of randomly heterogeneous materials is the stochastic finite element method which utilises random field theory to model the stochastic spatial variation of material properties. This can be considered a first principles approach to structural reliability since the distribution of macroscale structural behaviour is not assumed but rather arises as a physical consequence of the random field that models the microscale distribution of material properties. It is important to note that the accuracy of the stochastic finite element method is dependent on the degree to which the random field model suitably represents the innate spatial variation of material properties. One criticism of considerable weight is that random fields model heterogeneity as a continuous function which it may be argued is an inappropriate representation of many heterogeneous materials, such as soil and timber, since their microstructure is binary with any point in the material being associated with either a solid or a void. This issue is resolved by Ostoja-Starzewski (2008) through the rationale that the random field constitutes a *mesoscale continuum approximation* to the heterogeneous material that is obtained by passing a moving average window over its binary microstructure as illustrated in Figure 1.1. The advantage of the continuous mesoscale model of heterogeneity is that this representation is compatible with continuum mechanical models thereby facilitating structural analysis and, provided that the size of the moving average window is sufficiently small, the use of the mesoscale continuum approximation renders a suitably accurate representation of material heterogeneity.

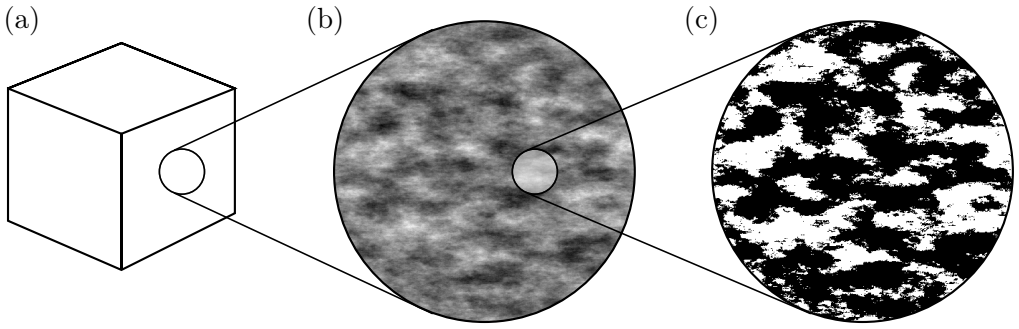


Figure 1.1: Representations of the material at different scales: (a) macrostructure, (b) mesoscale continuum approximation and (c) binary microstructure.

An additional factor affecting the accuracy of the stochastic finite element method, in addition to the mesoscale continuum approximation, is the uncertainty associated with the inferences of the parameters of the random field model. A significant source of inferential uncertainty is that material properties are experimentally determined over a non-zero sample volume of the material and, consequently, these experimentally determined material properties are effective properties of the material given by some type of average over the sample volume. The relationship between the effective properties, which describe material behaviour at the macroscale, and the random field model, which describes mesoscale material behaviour, is not well understood and as a result of this traditional inferential methodologies have resorted to treating the average-type effective properties as point samples of the random field. The typical approach is to approximate effective properties as point samples located at the centroid of the sample volume through an approach known as the *midpoint approximation* (Kiureghian and Ke, 1988). In particular, the usage of this approximation is investigated within this thesis since it is considered to be a source of substantial epistemic uncertainty that potentially causes the stochastic finite element method to be an unconservative approach to quantify structural reliability.

It is the contribution of this thesis to specifically consider the relationship between the effective elastic modulus in bending of randomly heterogeneous timber beams and the underlying random field of elastic modulus known as the *stiffness profile*. The consideration of timber is important since this material offers a sustainable alternative to other commonly used construction materials; however, the adoption of this material within the construction industry is limited by the variability of its material properties. Conse-

quently, the development of structural reliability methods that account for this variability are critical to the production of sustainable timber structures. Furthermore, the consideration of timber beams is also motivated by the availability of a 4-point bending dataset from Sousa et al. (2014) which enables the investigation of the uncertainty associated with fitting the random field model to experimental data. The first consideration in examining the relationship between the effective elastic modulus and the stiffness profile is the determination of the nature of the average that the effective elastic modulus constitutes over the sample volume and this is known as the *predictive forward problem*. The second consideration is the investigation of appropriate inferential methodologies to estimate the parameters of the stiffness profile from experimentally determined effective properties and this is known as the *inferential inverse problem* which is discussed in further detail in the following section.

1.1 Meta-problem framework

This section presents the meta-problem framework which provides a structure to understand the general contributions of this thesis relating to the problems of prediction and inference associated with the experimentally determined effective properties of random field models. However, prior to the presentation of this framework, it is useful to first introduce the mathematical notation adopted within this thesis to describe randomly heterogeneous materials. An arbitrary spatially distributed random material property is notated $Z(x)$ where x is a spatial index parameter; however, for specific material properties such as either elastic modulus or strength then the random field is notated as $E(x)$ or $f(x)$ respectively. A real one-dimensional random field $Z(x)$ can be formally defined as a function that maps the following two measurable spaces (Sudret and Kiureghian, 2000):

$$Z(x) : (Q, \mathcal{F}, P) \mapsto \mathbb{R} \tag{1.1}$$

where Q is the sample space i.e. the set of all possible outcomes, $\mathcal{F}$ is a σ-algebra on Q containing the events to be considered, P is a probability measure returning the probability of each event and $\mathbb{R}$ is the set of real numbers which is the range of $Z(x)$. However, within this thesis it is often the case that the range of $Z(x)$ is restricted to the

positive real numbers $\mathbb{R}^+$ since non-positive values are not physically realisable for many properties of interest such as either elastic modulus or strength. The effective property Z^* of the random field $Z(x)$ over a sample volume Ω is given by:

$$Z^* = H(Z(x)) \tag{1.2}$$

where $H(.)$ is the homogenisation function that takes the material property Z that varies with the spatial parameter x and returns a spatially constant material property Z^* that is equivalent to the random field $Z(x)$ over the sample volume Ω.

The meta-problem framework that is presented in this section is divided into two overarching themes which respectively relate to the problems of prediction and inference. The problem of prediction is concerned with determination of the effective property Z^* of the random field $Z(x)$ which requires consideration of the homogenisation function H. In contrast, the problem of inference is concerned with estimation of the statistical properties of the random field $Z(x)$ from its effective properties Z^* which involves consideration of the inverse homogenisation function H^{-1}. The problems of prediction and inference can be considered in both the stochastic case of a random material property $Z(x)$ and in the deterministic case of a single realisation $Z(x, q)$ of the random field $Z(x)$ for a single point q in the sample space $q \in Q$. It should be noted that in the case that the variation in material properties is deterministic $Z(x, q)$ then the associated effective property will also be deterministic $Z^*(q)$. In total, the meta-problem framework consists of four meta-problems: the first two meta-problems consider the problem of prediction whilst the last two meta-problems consider the problem of inference.

Meta-problem 1 – deterministic prediction

This meta-problem is concerned with prediction of the effective property Z^* of a realisation $Z(x, q)$ of the random field. *Meta-problem 1 – deterministic prediction* is notated:

$$Z(x, q) \longrightarrow Z^*(q) \tag{1.3}$$

where the direction of the arrow $\longrightarrow$ denotes that predictions of the deterministic effective property $Z^*(q)$ are to be made given the realisation $Z(x, q)$. The meta-problem

of deterministic prediction is important since it considers prediction of the macroscale behaviour of a structure composed of a heterogeneous material given its deterministic mesoscale variation $Z(x, q)$. This meta-problem is considered extensively in the one-dimensional case in the first half of *Chapter 3 – Theory of heterogeneous beams* and the two-dimensional case is considered in *Chapter 4 – Meta-modelling of effective properties*. This meta-problem is presented first since it is the simplest of the four meta-problems and, furthermore, it is through an understanding of this meta-problem that approaches can be developed to the later meta-problems associated with prediction in the stochastic case.

Meta-problem 2 – stochastic prediction

This meta-problem is concerned with prediction of the distribution of the effective property Z^* of the random field $Z(x)$. *Meta-problem 2 – stochastic prediction* is notated:

$$Z(x) \longrightarrow Z^* \tag{1.4}$$

In contrast to *meta-problem 1 – deterministic prediction*, this meta-problem considers prediction of the effective property Z^* in the stochastic case. This meta-problem is considered extensively in the one-dimensional case in the second half of *Chapter 3 – Theory of heterogeneous beams* where it is observed that the relationship between the effective elastic modulus E^* and the stochastic stiffness profile $E(x)$ is non-analytical and, therefore, the homogenisation function H can not be determined exactly. As a result of this, the exact distribution of the effective elastic modulus E^* is intractable and, consequently, the adopted approach is to approximate the moments of the effective elastic modulus E^* through a quasi-analytical theory of heterogeneous beams.

Meta-problem 3 – stochastic inference

The meta-problem is concerned with inferring the distribution of a random field $Z(x)$ from its effective property Z^*. *Meta-problem 3 – stochastic inference* is notated:

$$Z^* \longrightarrow Z(x) \tag{1.5}$$

where $\longrightarrow$ denotes that inferences about the parameters of the random field $Z(x)$ are

to be made given the distribution of the effective property Z^*. It is noted that the process of inference is associated with significantly greater uncertainty than the process of prediction. This is because the determination of the distribution of the random field $Z(x)$ from the distribution of the effective property Z^* is an ill-posed problem with no unique solution for the inverse homogenisation function H^{-1}. This meta-problem is considered most extensively in *Chapter 5 – Inference from effective properties* which details the quantification of uncertainty associated with random field parameters estimated from the experimental dataset of Sousa et al. (2014) under the midpoint approximation.

Meta-problem 4 – deterministic inference

This meta-problem is concerned with the inference of a realisation $Z(x, q)$ of a random field from its effective property $Z^*(x, q)$. *Meta-problem 4 – deterministic inference* is notated:

$$Z^*(q) \longrightarrow Z(x, q) \tag{1.6}$$

The importance of this meta-problem is that, in contrast to *meta-problem 3 – stochastic inference*, this meta-problem is concerned with the inference of a deterministic material profile $Z(x, q)$ that has actually occurred rather than the ensemble of possibilities of the stiffness profile that the random field $Z(x)$ represents. This meta-problem is primarily considered at the end of *Chapter 2 – Random fields: Theory, estimation and simulation* as well as *Chapter 5 – Inference from effective properties*. This meta-problem is considered after *meta-problem 3 – stochastic inference* since the accurate inference of a realisation of the material property profile depends on the parameters of the random field describing central tendency, scale and smoothness.

1.2 Thesis overview and scope

This section presents an overview of each chapter of the thesis and provides commentary on the scope of the analysis contained within that chapter with reference to the meta-problem framework developed in the previous section.

Chapter 1 – Introduction

This chapter contains an introduction to reliability analysis with particular consideration of the structural risk associated with assets constructed from heterogeneous materials. The data driven and first principles approaches to probabilistic modelling are considered with an evaluation of the relative benefits and disadvantages of each approach. The use of the stochastic finite element method is scrutinised with respect to its evaluation of the structural risk associated with heterogeneous materials including examination of both the mesoscale continuum approximation, as well as, inferential difficulties that arise from the estimation of the parameters of the random field model under the midpoint approximation. Finally, the meta-problem framework is presented and commentary is provided as to the manner by which this thesis addresses each meta-problem with reference to the relevant chapters.

Chapter 2 – Random fields: Theory, estimation and simulation

This chapter outlines the theory of random fields including an explanation of concepts relating to marginal distributions, stationarity and mean square properties. The second moment structure of random fields is also considered with extensive discussion of both covariance and spectral density functions. Furthermore, inferential methodologies for the estimation of random field parameters are presented including method of moments and maximum likelihood estimation with consideration of the numerical formulation of these estimators for the case of multiple realisations. Additionally, the simulation techniques of covariance matrix decomposition (CMD) and the fast Fourier transform method (FFT) are investigated and it is verified that CMD is the most efficient method for the simulation of a high number of realisations of a small to medium sized random field whilst FFT is the most efficient method for the simulation of a large random field. Finally, it is noted that the numerical techniques discussed in this chapter for the estimation and simulation of random fields have been implemented in the Matlab toolbox `RFbox`[1].

Chapter 3 – Theory of heterogeneous beams

This chapter presents the theory of heterogeneous beams under Euler-Bernoulli beam theory for the case of both a deterministic and stochastic stiffness profile. The work of Bechtel (1985) is extended to show that effective elastic modulus can be formulated

[1]Matlab toolbox: `RFbox` `https://github.com/jackpiercebrown/RFbox`

as a weighted harmonic mean for any point along the beam including the derivation of weighting functions for a number of important loading conditions. In the case of a deterministic stiffness profile, an equation is presented for both the deflection and effective property of a beam under 3-point loading with linear variation in elastic modulus. In the stochastic case, analytical expressions are derived for the first two moments of deflection and quasi-analytical expressions are derived for first two moments of the effective elastic modulus under the approximation that displacement is lognormally distributed. Finally, it is verified that the quasi-analytical expressions for the mean and variance of effective elastic modulus show good agreement with the results of a stochastic finite element model.

Chapter 4 – Meta-modelling of effective properties

This chapter presents an extension to the one-dimensional theory of heterogeneous beams, as presented in Chapter 3, to the case of multidimensional heterogeneity. This is achieved through the development of a generalised weighted mean meta-model with applicability to both average-type effective properties, such as elastic modulus, as well as extreme-type effective properties such as strength. Furthermore, the acceptance-rejection functional optimisation algorithm of Bocchini and Deodatis (2008) is extended and utilised to optimise the weighting function of the meta-model. In the one-dimensional case, convergence of the weighting functions to the analytical solution derived by Bechtel (1985) is verified and the error associated with the arithmetic, geometric and harmonic meta-models is quantified. In the two dimensional-case, the meta-models are trained to a plane-stress stochastic finite element model and it is shown that the effective elastic modulus of a beam with two-dimensional heterogeneity is bound by the harmonic and geometric means with additional insights into the spatial weighting of this effective property.

Chapter 5 – Inference from effective properties

This chapter considers the inference of the parameters of a random field model from experimentally determined effective properties. A detailed analysis is conducted into local and global test procedures according to BS EN 408:2010 including derivation of weighting functions for the local and global elastic moduli. A lognormal random field model is fitted to the experimental dataset of Sousa et al. (2014) using method of moment estimators under the midpoint approximation with commentary on the assessment of stationarity

as well as the selection of the marginal distribution. The values of the estimated parameters of the random field, namely the location, scale and correlation parameters, are reported and an uncertainty quantification is performed, based on Pierce-Brown et al. (2018), in order to quantify the epistemic and aleatoric uncertainty associated with these parameter estimates. Finally, it is shown that random fields inferred under the midpoint approximation likely underestimate material heterogeneity.

Chapter 6 – Conclusion

This chapter provides an overview of the general conclusions of each chapter of the thesis with reference to the meta-problem framework. The analytical, numerical and inferential insights of the thesis into the relationship between the effective modulus of elasticity and the random field of elastic modulus are summarised. In particular, conclusions are provided on the applicability of random fields to model material heterogeneity with implications on the usage of the stochastic finite element method to evaluate structural reliability. Finally, recommendations are made, based on the limitations identified within this thesis, for further research with a view to increasing the adoption, accessibility and accuracy of the stochastic finite element method as a means to quantify the risk and reliability of structures composed of randomly heterogeneous materials.

Bibliography and Appendices

References are provided throughout this thesis to relevant literature in order to support a particular point under consideration or, alternatively, to provide a source of additional information relating to a particular subject. The citations for each chapter are compiled into a single bibliography at the end of this thesis which has been sorted alphabetically by the surname of the first author. In order to improve the readability of this thesis, the derivation of a pertinent result is often omitted from the argument at hand through the provision of a reference to one of three appendices and the calculations within these appendices have been ordered chronologically according the order in which they are referenced.

Chapter 2

Random fields: Theory, estimation and simulation

2.1 Introduction

Random processes and their multidimensional counterparts, known as random fields, are widely used to mathematically model the stochastic variation of a number spatio-temporal phenomena including the spatial variation of material properties (Hajek, 2015, p. 103). The convention adopted within this chapter is to notate a random process as $Z(x)$ where the index variable x belongs to a subset of one-dimensional space $x \in D \subset \mathbb{R}^1$ where D is the domain of the random process $Z(x)$. The variability of the material at any point x_i in the domain $x_i \in D$ is modelled with a single random variable $Z(x_i)$ and the collection of these random variables is known as a random process $Z(x) = \{Z(x_i) : x_i \in D\}$. The higher dimensional counterpart to a random process, a two-dimensional random field, is notated $Z(x, y)$ where the index variables (x, y) belongs to a subset of two-dimensional space $(x, y) \in D \subset \mathbb{R}^2$. Furthermore, it is noted that a random field of arbitrary dimension n can be obtained by taking the domain to be a subset of n-dimensional space $D \subset \mathbb{R}^n$. However, only one $Z(x)$ or two-dimensional $Z(x, y)$ random fields are explicitly considered within this thesis. Furthermore, it is noted that it is seldom useful to distinguish between random processes and fields therefore these terms tend to be interchanged freely.

The majority of the theory of random fields introduced within this chapter is presented for the case of a one-dimensional random process $Z(x)$; however, in general it is possible to extend this theory to the higher dimensional cases without difficulty unless explicitly stated otherwise. An additional comment on notation is that if the state space of $Z(x)$ is discrete then $Z(x)$ is referred to as a discrete-valued random process and if the state space is continuous then $Z(x)$ is referred to as a continuous-valued random process. Furthermore, if the index set x is discrete then $Z(x)$ is referred to as a discrete-space random process and if x is continuous then $Z(x)$ is referred to as a continuous-space random process. It is noted that, in the case that the random field $Z(x)$ is discrete-space, then $Z(x)$ can be equivalently represented by a random column vector $\boldsymbol{Z} = [Z(x_1), Z(x_2), \ldots, Z(x_J)]^\intercal$ where the number of random variables J is finite. This thesis primarily considers continuous-space models for material properties, however, it is observed later in this chapter that it is often necessary to approximate a continuous-space model with a discrete-space approximation for the purposes of simulation.

It is conventional that every random variable $Z(x_i)$ in the domain D is distributed according to the same probability density function $f(Z(x,q))$ which is known as the *marginal distribution* of the random process $Z(x)$. The process $Z(x)$ is then customarily referred to by its marginal distribution; for example, if every point x_i in the domain D is associated with a normally distributed random variable then $Z(x)$ is known as a Gaussian process. It is noted that Gaussian processes are popular in many disciplines due to a number of convenient properties inherited from the normal distribution (Fenton and Griffiths, 2008, p. 93): firstly, every linear combination of samples from a Gaussian process has a joint normal distribution; secondly, any linear transformation of a Gaussian process is also a Gaussian process; thirdly, a Gaussian process is completely defined by its first two statistical moments. The first moment of a random process $Z(x)$ is described by the mean $\mu(x)$ which is given by:

$$\mu(x) = \mathbb{E}[Z(x)] \tag{2.1}$$

where $\mathbb{E}[.]$ is the expected value operator. In the case that the random process $Z(x)$ is discrete-space then the first moment can be represented by a mean vector $\boldsymbol{\mu} = [\mu(x_1), \mu(x_2), \ldots, \mu(x_J)]^\intercal$.

The second moment of a random process $Z(x)$ can be completely represented by the covariance function $C(x_i, x_j)$ that describes the joint variability of the random variables $Z(x_i)$ and $Z(x_j)$ where x_i and x_j are two points in the domain D. The covariance function $C(x_i, x_j)$ is given by:

$$C(x_i, x_j) = \text{Cov}\left[Z(x_i), Z(x_j)\right] \tag{2.2}$$

$$= \mathbb{E}[(Z(x_i) - \mu(x_i))(Z(x_j) - \mu(x_j))] \tag{2.3}$$

The magnitude of the covariance function $C(x_i, x_j)$ can be difficult to interpret and consequently it is convenient to instead work with its normalisation, the correlation function $\rho(x_i, x_j)$ with range $-1 \leq \rho \leq 1$, that describes the degree of linear dependence between $Z(x_i)$ and $Z(x_j)$. The correlation function $\rho(x_i, x_j)$ is given by:

$$\rho(x_i, x_j) = \frac{C(x_i, x_j)}{\sigma(x_i)\sigma(x_j)} \tag{2.4}$$

where $\sigma(x)$ is the standard deviation of the random variable $Z(x)$ given by:

$$\sigma(x) = \sqrt{\text{Var}[Z(x)]} = \sqrt{\mathbb{E}[(Z(x) - \mu(x))^2]} \tag{2.5}$$

Additionally, if the random process $Z(x)$ is discrete-space then its second moment structure can be represented with a covariance matrix $\boldsymbol{C}$ given by:

$$\boldsymbol{C} = \begin{bmatrix} C(x_1, x_1) & C(x_2, x_1) & \dots & C(x_J, x_1) \\ C(x_1, x_2) & C(x_2, x_2) & \dots & C(x_J, x_2) \\ \vdots & \vdots & \dots & \vdots \\ C(x_1, x_J) & C(x_2, x_J) & \dots & C(x_J, x_J) \end{bmatrix} \tag{2.6}$$

It is noted that a covariance matrix $\boldsymbol{C}$ is valid if it is both symmetric and positive semidefinite whilst a covariance function $C(x_i, x_j)$ is only valid if it is positive definite. The positive semidefiniteness of a symmetric matrix, such as the covariance matrix $\boldsymbol{C}$, can be verified by ensuring its eigenvalues Λ_i are non-negative $\Lambda_i \geq 0$ (Rasmussen and Williams, 2006, p. 80).

The fourth convenient property of Gaussian processes is that the joint probability density function $f(.)$ of a discrete-space process $\boldsymbol{Z}$ with mean vector $\boldsymbol{\mu}$ and covariance matrix $\boldsymbol{C}$ is analytically given by:

$$f(\boldsymbol{Z}(q)) = (2\pi \det(\boldsymbol{C}))^{-\frac{1}{2}} \exp\left((\boldsymbol{Z}(q) - \boldsymbol{\mu})^{\intercal} \boldsymbol{C}^{-1} (\boldsymbol{Z}(q) - \boldsymbol{\mu})\right) \tag{2.7}$$

where: $\boldsymbol{Z}(q)$ is a realisation of the discrete-space process $\boldsymbol{Z}$,
$\det(\boldsymbol{C})$ is the determinant of the covariance matrix $\boldsymbol{C}$,
$\exp(.)$ is the exponential function.

2.2 Stationarity

The stationarity of a random process is an important consideration since it describes the regularity of the distribution of the random process over space. A random process $Z(x)$ is said to be stationary if it is invariant to translations in the spatial input space x. Furthermore, a random process $Z(x)$ is said to be *strongly stationary*, also known as *strictly stationary*, if its probability density function $f(\boldsymbol{Z})$ is invariant under an arbitrary translation h (Chilès and Delfiner, 2012, p. 16):

$$f(Z(x_1 + h), Z(x_2 + h), \ldots, Z(x_J + h)) = f(Z(x_1), Z(x_2), \ldots, Z(x_J)) \tag{2.8}$$

The property of *strong stationarity* implies that all of the statistical moments of $Z(x)$ are invariant to translations in the input space and, consequently, the statistical moments are constant with x.

A process $Z(x)$ is said to be *weakly stationary*, also known as *wide-sense stationary*, if only its first and second moments are invariant to translations in the input space x (Rasmussen and Williams, 2006). This implies that the mean is spatially constant $\mu(x) = \mu$ and that the covariance function $C(x_i, x_j)$ is only dependent on the relative separation of points $s = x_i - x_j$:

$$C(|s|) = C(|x_i - x_j|) = C(x_i, x_j) \tag{2.9}$$

The stationarity of the covariance function also implies that the variance of the process is constant $\sigma^2(x) = \sigma^2$. Therefore, the correlation function of a second-moment stationary process is given by:

$$\rho(|s|) = \frac{C(|s|)}{\sigma^2} = \frac{C(|s|)}{C(0)} \tag{2.10}$$

In the case of a Gaussian process, it is useful to note that the property of weak stationarity also implies strong stationarity. The property of weak stationarity is also referred to as *homogeneity* (Yaglom, 1962); however, this terminology is not pursued here since a stationary process has the potential to be confused with a process whose realisations are constant-valued. The property of weak stationarity is an important characteristic for many simulation and estimation techniques; consequently, it is of interest to obtain a weakly stationary process from its nonstationary counterpart. A process $Z(x)$ with nonstationary mean $\mu(x)$ and variance $\sigma^2(x)$ can be transformed into a process $Z'(x)$ with stationary mean and variance through (Vanmarcke, 1988, p. 182):

$$Z'(x) = \frac{Z(x) - \mu(x)}{\sigma(x)} \tag{2.11}$$

The operations of subtracting the mean $\mu(x)$ and dividing by the standard deviation $\sigma(x)$ are referred to as *detrending* and *normalising* respectively. It is important to note that the operations of detrending and normalising are not sufficient to yield a weakly stationary process in the case that the correlation function $\rho(x_i, x_j)$ is nonstationary. Figure 2.1 shows a realisation of a stationary random process $Z(x)$ with a Gaussian marginal distribution $f(Z)$ along with an illustration of the location parameter μ, scale parameter σ and a correlation parameter θ known as the correlation length which is introduced in Section 2.4.

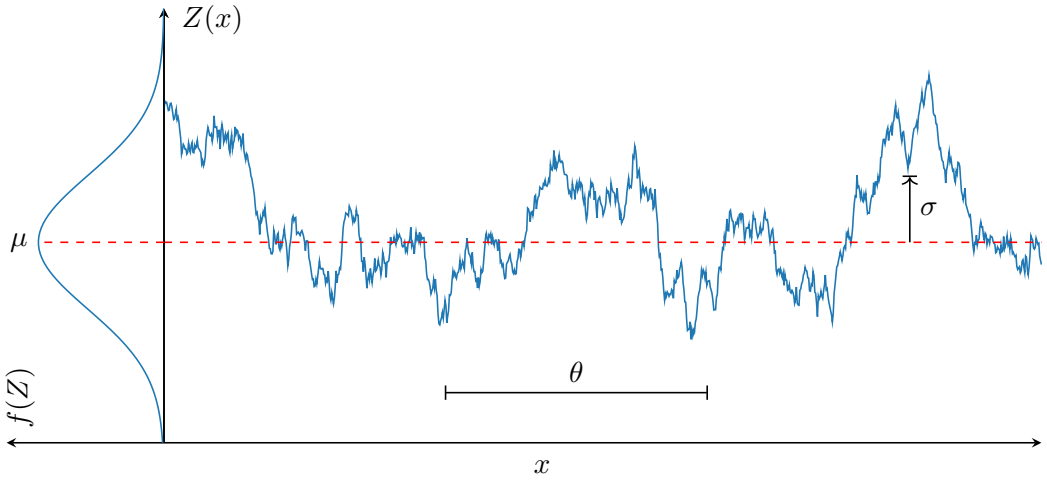


Figure 2.1: Single realisation of the random field $Z(x)$ whose marginal distribution $f(Z)$ is shown on the left-hand side with location parameter μ, scale parameter σ and correlation parameter θ shown for illustrative purposes.

2.3 Mean square properties

The continuity and differentiability of random fields is an important consideration for a number of simulation and estimation techniques. It is noted that the properties of the random field and its realisations are determined by the behaviour of the covariance function at the origin (Paciorek, 2003, p. 33). The mean square properties of the random field are considered since it is difficult to determine the properties of realisations of the random field directly. However, it should be noted that whilst mean square properties are easy to determine, there is no simple relationship between the covariance function and the realisations of an arbitrary random process (Stein, 1999, p. 20). Fortunately, in the case of a Gaussian process that is separable as defined by Doob (1997, p. 51), mean square properties do imply sample path properties.

A random process $Z(x)$ is *mean square continuous* if (Yaglom, 1962, p. 22):

$$\lim_{h \to 0} \mathbb{E}\left[|Z(x+h) - Z(x)|^2\right] = 0 \tag{2.12}$$

A necessary and sufficient condition for mean square continuity is that the covariance function $C(s)$ is continuous at the origin $s = 0$. It is important to note that whilst

mean square continuity is a necessary condition for continuity of the realisations of the random process $Z(x)$ it is not a sufficient condition. However, mean square continuity does imply continuity of realisations in the case of a separable Gaussian process.

A random process $Z(x)$ is *mean square differentiable* if (Chilès and Delfiner, 2012, p. 60):

$$\lim_{h \to 0} \mathbb{E}\left[\frac{Z(x+h) - Z(x)}{h} - \dot{Z}(x)\right] = 0 \tag{2.13}$$

were $\dot{Z}(x)$ is the mean square derivative of the random process $Z(x)$. A necessary and sufficient condition for mean square differentiability is that the second derivative $\ddot{C}$ of the covariance function exists at the origin. This implies that the the derivative of the covariance function is zero at the origin $\dot{C}(0) = 0$ since the covariance function $C(s)$ is an even function. It is worth emphasising again that mean square properties do not generally imply sample path properties and, consequently, mean square differentiability does not imply differentiability of realisations for an arbitrary random process. However, mean square continuity does imply continuity of realisations in the case that the random process is both Gaussian and separable.

2.4 Common covariance and correlation functions

In the consideration of the second moment structure of a random process, the case of statistical independence may superficially appear to be the simplest concrete construction of a stochastic process. However, it is observed in this section that the use of an uncorrelated process is unpragmatic for many applications of interest. Consider the white noise process which is a stationary random process $Z_N(x)$ given by an uncountably infinite set of independent mean-zero random variables $\{Z_N(x_1), Z_N(x_2), \ldots, Z_N(x_J)\}$ on the domain D with variance σ^2. The correlation function $\rho_N(x_i, x_j)$ of white noise can be taken to be the Kronecker delta function (Arfken et al., 2013):

$$\rho_N(s) = \begin{cases} 1 & \text{if } s = 0 \\ 0 & \text{if } s \neq 0 \end{cases} \tag{2.14}$$

where $s = x_i - x_j$. White noise is usually defined as being wide-sense stationary with

constant variance σ^2 and, consequently, its covariance function $C_N(s)$ is given by:

$$C_N(s) = \begin{cases} \sigma^2 & \text{if } s = 0 \\ 0 & \text{if } s \neq 0 \end{cases} \tag{2.15}$$

The singular behaviour of this covariance function at the origin means that realisations of the white noise process $Z_N(x)$ are neither continuous nor differentiable. The Kronecker delta definition of white noise has been adopted by many authors (Box et al., 2016, p. 48), however, it should be noted that processes with this covariance function have been shown to be unmeasurable (Kallianpur, 1980, p. 10). The property of non-measurability implies that the integral of Kronecker delta white noise is undefined which is problematic since the integral of white noise is sought for many applications such as the modelling of Brownian motion. This issue of non-measurability can be avoided by instead defining the covariance function of white noise as the Dirac delta function. However, the variance σ^2 of a process with the Dirac delta covariance function cannot be considered to be finite and this can be heuristically understood by considering the following loose definition of the Dirac delta function $\delta(s)$ (Desoer and Kuh, 1969, p. 31):

$$C_N(s) = \delta(s) = \begin{cases} +\infty, & s = 0 \\ 0, & s \neq 0 \end{cases} \tag{2.16}$$

subject to the requirement that $\delta(s)$ satisfies:

$$\int_{-\infty}^{\infty} \delta(s) \, = 1 \tag{2.17}$$

In order that the correlation function is one at the origin $\rho_N(0) = 1$ then the variance σ_N^2 of Dirac delta white noise cannot be finite. It is important to note that the Dirac delta function is not formally defined as a function but rather as a distribution or a measure (Fenton and Griffiths, 2008, p. 104); however, the heuristic definition given above does provide insights into the difficulty of defining the seemingly trivial case of an uncorrelated random process in the spatial domain D. It is noted that a more rigorous definition of Dirac delta white noise is obtained through its frequency domain representation as detailed in Section 2.5. In conclusion, whilst the case of Kronecker delta white noise does

not form a profitable basis for a theory of random fields due its lack of measurability, the case of Dirac delta white noise is more fruitful since many finite variance processes can be defined as the integral of this infinite variance process.

The process $Z_W(t)$ is known as the Wiener process and models Brownian motion which is the phenomena associated with the random movement of a particle suspended in a fluid (Wiener, 1923). Within the context of Brownian motion, the index set t describes the evolution of the system $Z_W(t)$ with time. It is useful to note that the Wiener process $Z_W(t)$ is often used to model the integral of Gaussian white noise (defined with the Dirac delta function):

$$Z_W(t) = \int_0^t Z_N(x)\,\mathrm{d}x \tag{2.18}$$

The properties of the Wiener process are that: it is a second-moment non-stationary Gaussian process with zero-mean $\mu_W = 0$, non-stationary variance $\sigma_W^2 = t$ and a non-stationary correlation function $\rho_W(t_i, t_j)$; its increments are independent and Gaussian; its expected future value is given by the current value of the process and processes with this property are known as *martingales* (Le Gall, 2013, p. 49); it is mean-square continuous with continuous realisations (Wiener, 1923).

The covariance function $C_W(t_i, t_j)$ of the Wiener process $Z_W(t)$ is given by:

$$C_W(t_i, t_j) = \min(t_i, t_j) \tag{2.19}$$

The correlation function $\rho_W(t_i, t_j)$ of the Wiener process $Z_W(t)$ is given by:

$$\rho_W(t_i, t_j) = \frac{\min(t_i, t_j)}{\sqrt{t_i t_j}} \tag{2.20}$$

The non-stationarity of the Wiener process suggests that it is a good model for systems whose uncertainty increases with the index parameter, however, it is noted that stationary models are preferred as a starting point for modelling the spatial variation in material properties unless there is significant evidence of non-stationarity.

There are a number of popular correlation functions for the spatial modelling of material

properties. The first is known as the *Gaussian* or *squared-exponential* correlation function (Rasmussen and Williams, 2006) and is given by:

$$\rho_G(s) = \exp\left(-\pi\left(\frac{s}{\theta}\right)^2\right) \tag{2.21}$$

where θ is a correlation parameter known as the *correlation length* (Fenton and Griffiths, 2008, p. 103) or *scale of fluctuation* and is defined by Vanmarcke (1988, p. 14) as satisfying the following integral of the correlation function:

$$\theta = \int_{-\infty}^{\infty} \rho(s)\,\mathrm{d}s = 2\int_{0}^{\infty} \rho(s)\,\mathrm{d}s \tag{2.22}$$

Fenton and Griffiths (2008, p. 103) note that this definition is only for strictly non-negative correlation functions $0 \leq \rho(s) \leq 1$ and, consequently, the correlation length is not well-defined for periodic correlation functions such as the sinusoidal correlation function which is a popular correlation function for modelling the autocorrelation structure of wind generated ocean waves since it has range $-1 \leq \rho(s) \leq 1$ (Latta and Bailie, 1968). Furthermore, it should be noted that the correlation length can not truly be defined independently of the correlation function that is parametrises since fitting different correlation functions to the same data results in different estimations of the correlation length θ.

An intuitive interpretation of the correlation length θ is that it is the distance within which the process exhibits significant self-correlation and beyond which the self-correlation becomes insignificant (Fenton and Griffiths, 2008, p. 103). Heuristically, the correlation length describes the smoothness of a process where a large correlation length renders a smooth process whilst a small correlation length renders a rough process. In the limiting case, as $\theta \to \infty$, the process becomes homogeneous and, as $\theta \to 0$, the process becomes the infinitely rough Kronecker delta white noise process. Figure 2.2 illustrates the effect of varying the correlation length on the realisations of a random process $Z_G(x)$ with the Gaussian correlation function $\rho_G(s)$. It can be seen that the process with the small correlation length ($\theta = 0.01L$) exhibits substantial high frequency oscillation whilst, in comparison, the process with the large correlation length ($\theta = 0.2L$) exhibits substantial low frequency oscillations. Additionally, it is noted that all of the realisations of the random process are smooth since $\dot{\rho}_G(0) = 0$ and this has led to the criticism that this

correlation function produces realisations which are not sufficiently rough to be realistic of the true variation in material properties (Stein, 1999, p. 30).

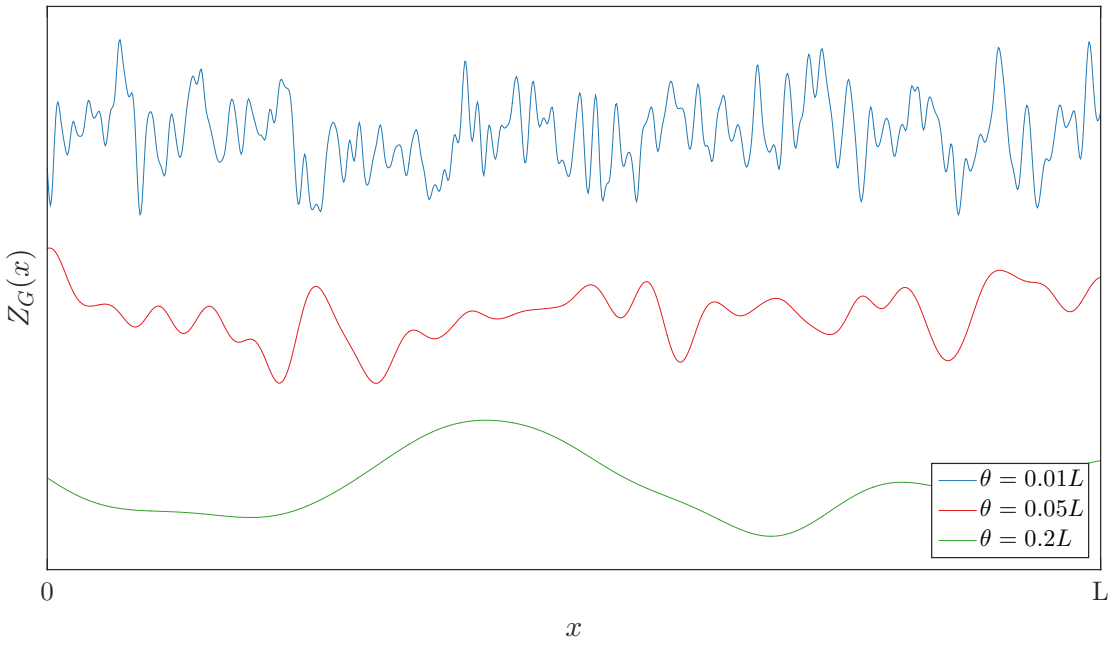


Figure 2.2: Three realisations of a random process $Z_G(x)$ with the Gaussian correlation function $\rho_G(s)$ parametrised with correlation lengths $\theta = 0.01L$, $0.05L$ and $0.2L$.

A popular correlation function that produces non-smooth realisations is the *Markov* or *exponential* correlation function (Rasmussen and Williams, 2006, p. 85):

$$\rho_M(s) = \exp\left(-\frac{2|s|}{\theta}\right) \tag{2.23}$$

This correlation function is also referred to in the literature as the Ornstein-Uhlenbeck correlation function since it was originally derived by Uhlenbeck and Ornstein (1930) to describe the velocity of a massive Brownian particle under the influence of friction. A process with this correlation function is said to be Markovian since the future of the process depends only on the current state and is independent of any previous states (Fenton and Griffiths, 2008, p. 110). A stationary process with this correlation function is not a martingale since the future expected value of the process is closer to the mean than the current state and, consequently, this process is said to exhibit *mean-reversion*. An important consideration is that the derivative of the Markov correlation function is discontinuous at $s = 0$ and, as a result of this, a process with this correlation function is not mean square differentiable since $\dot{\rho}_M(0) \neq 0$.

It is observed that the exponential and squared-exponential correlation function can be generalised into a correlation function $\rho_P(s)$ of arbitrary power λ which is given by (Rasmussen and Williams, 2006, p. 86):

$$\rho_P(s) = \exp\left(-C\left(\frac{|s|}{\theta}\right)^{\lambda}\right) \quad \text{if } 0 \leq \lambda < 2 \tag{2.24}$$

It is noted that if the correlation length θ is required to satisfy the integration requirement of Vanmarcke (1988), as given by Equation 2.22, then the constant C is given by (see Appendix A.1):

$$C = \left(\frac{1}{2\Gamma\left(1+\lambda^{-1}\right)}\right)^{-\lambda} \tag{2.25}$$

where $\Gamma(.)$ is the Gamma function.

A common approach to construct a correlated random process is to take an unweighed moving arithmetic average over the Dirac delta white noise process:

$$Z_T(x) = \frac{1}{\theta}\int_{x-\theta/2}^{x+\theta/2} Z_N(t)\,\mathrm{d}t \tag{2.26}$$

The correlation function $\rho_T(s)$ of the process $Z_T(s)$ is known as the *triangular* correlation function and is given by:

$$\rho_T(s) = \begin{cases} 1 - \dfrac{|s|}{\theta} & \text{if } |s| \leq \theta \\ 0 & \text{if } |s| \geq \theta \end{cases} \tag{2.27}$$

The derivative of the triangular correlation function $\dot{\rho}_T(s)$ is discontinuous at both the origin $s = 0$ and at separations equalling the correlation length $s = \theta$. Additionally, in contrast to both the Markov $\rho_M(s)$ and Gaussian $\rho_G(s)$ correlation functions, points separated by a distance greater than the correlation length $s > \theta$ are statistically independent. Figure 2.3 shows a comparison of the Markov $\rho_M(s)$, Gaussian $\rho_G(s)$ and triangular $\rho_T(s)$ correlation functions. It is observed that initially the Markov correlation function

falls off the quickest, followed by the triangular correlation function with the Gaussian correlation function exhibiting the highest initial correlation. For medium separations, the triangular correlation function exhibits the highest correlation whilst the Markov and Gaussian correlation functions are approximately equal. For large separations, the Markov correlation function has the highest correlation, the Gaussian correlation function has lower correlation and, finally, the triangular function has zero correlation.

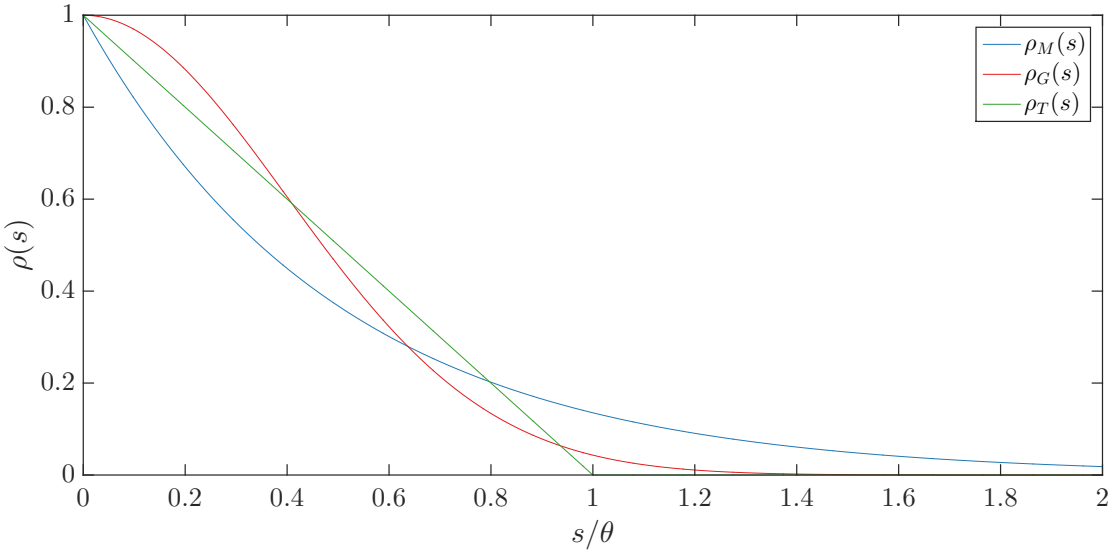


Figure 2.3: Variation of the Markov $\rho_M(s)$, Gaussian $\rho_G(s)$ and triangular $\rho_T(s)$ correlation functions with spatial separation s normalised by the correlation length θ.

Figure 2.4 shows three realisations associated with the Markov $\rho_M(s)$, Gaussian $\rho_G(s)$ and triangular $\rho_T(s)$ correlation functions that have all been parametrised with the same correlation length $\theta = 0.1L$ for the purposes of visual comparison. The Markov-correlated process $Z_M(x)$ has the greatest short-scale variability and the smallest long-scale variability, in comparison, the Gaussian-correlated process $Z_G(x)$ has the greatest long-scale variability and the smallest short-scale variability and, finally, the triangular-correlated process $Z_T(x)$ has the greatest medium-range correlations. It should be noted that the consideration of correlation functions within this section has not been exhaustive; for alternative correlation functions consider the polynomial decaying (Fenton and Griffiths, 2008), rational quadratic (Rasmussen and Williams, 2006), spherical (Cressie, 1993) and fractional Gaussian noise correlation functions (Mandelbrot and Van Ness, 1968). However, this thesis will restrict its consideration to solely the Markov, Gaussian and Triangular correlation functions and their higher dimensional extensions.

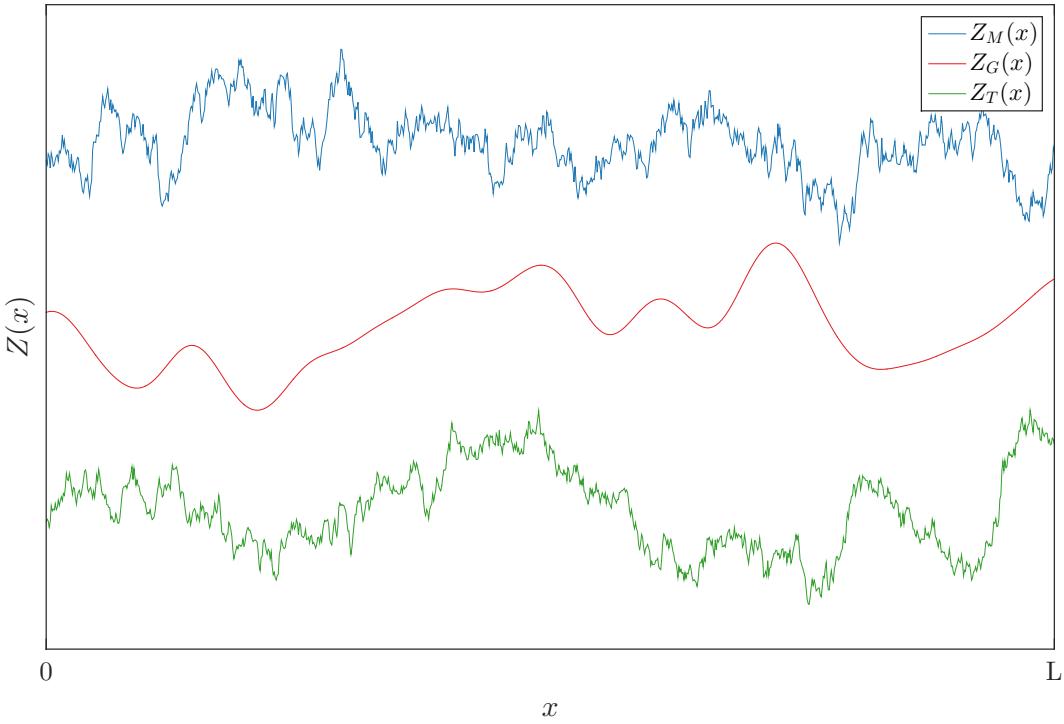


Figure 2.4: Realisation of the Markov-correlated $Z_M(x)$, Gaussian-correlated $Z_G(x)$ and triangular-correlation $Z_T(x)$ Gaussian processes with constant standard deviation and correlation length.

2.4.1 Higher-dimensional correlation functions

The definition of a two-dimensional random field $Z(x, y)$ requires that the correlation functions defined in the previous section be extended to the multidimensional case. This is not a trivial task since a correlation function that is positive definite in $\mathbb{R}^1$ may not be positive definite in $\mathbb{R}^2$. One example of this is the triangular correlation function $\rho_T(s)$ which is not valid in any dimension higher than one (Cressie, 1993, p. 22) and this has unfortunately resulted in researchers occasionally fitting invalid covariance functions that run the risk of yielding negative variances. The simplest approach to obtain a two-dimensional correlation function is to take the product of the two orthogonal one-dimensional correlation functions as follows (Fenton and Griffiths, 2008, p. 118):

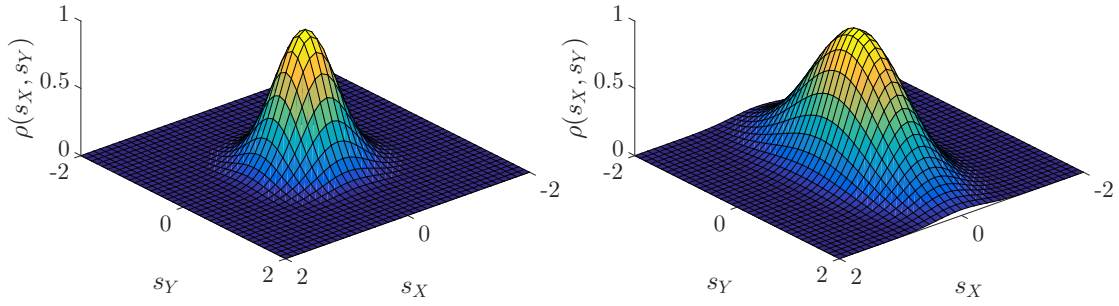
$$\rho_{X,Y}(s_X, s_Y) = \rho_X(s_X) \cdot \rho_Y(s_Y) \tag{2.28}$$

where s_X and s_Y are the spatial separations in the x and y-directions respectively. In

order to avoid an unnecessarily cluttered notation, the subscript of these correlation functions is dropped since the input arguments provide sufficient clarity with regards to the spatial direction of the correlation function. Correlation functions that can be decomposed according to Equation 2.28 are known as *separable*. The two-dimensional separable extension of the Gaussian correlation function is given by:

$$\rho_G(s_X, s_Y) = \exp\left(-\pi\left[\left(\frac{s_X}{\theta_X}\right)^2 + \left(\frac{s_Y}{\theta_Y}\right)^2\right]\right) \tag{2.29}$$

where θ_X and θ_Y are the correlation lengths in the x and y-direction respectively. It is noted that this correlation function corresponds to the ℓ^2-norm over the correlation length adjusted domain. Figure 2.5 illustrates the ℓ^2-norm Gaussian correlation function in the cases of (a) equal correlation lengths and (b) unequal correlation lengths. In the case of equal correlation lengths $\theta_X = \theta_Y$, this correlation function is said to be *isotropic* since it is invariant to rotations in the input space (Fenton and Griffiths, 2008, p. 118). In the case of unequal correlation lengths $\theta_X \neq \theta_Y$, this correlation function is said to be *ellipsoidal* since contours of constant correlation form ellipses in $\mathbb{R}^2$. Additionally, it is observed that the continuity of the derivative of the one-dimensional Gaussian correlation function is also preserved in its two-dimensional ℓ^2-norm extension.



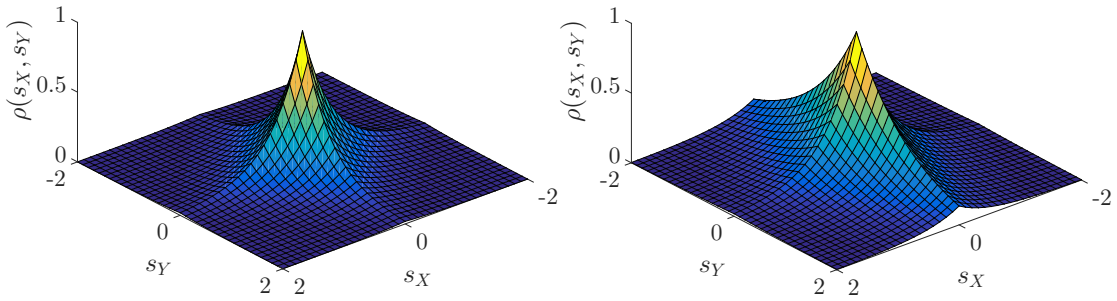
(a) $\theta_X = \theta_Y = 1$ (b) $\theta_X = 1$, $\theta_Y = 2$

Figure 2.5: ℓ^2-norm Gaussian correlation function in $\mathbb{R}^2$.

The separable two-dimensional Markov correlation function is given by:

$$\rho_M(s_X, s_Y) = \exp\left(-2\left(\frac{|s_X|}{\theta_X} + \frac{|s_Y|}{\theta_Y}\right)\right) \tag{2.30}$$

This correlation function corresponds to an ℓ^1-norm over the correlation length adjusted domain and hence is referred to as the ℓ^1-norm Markov correlation function. Figure 2.6 illustrates the ℓ^1-norm Markov correlation function in the case of (a) equal correlation lengths and (b) unequal correlation lengths. It is observed that this correlation function is non-differentiable both at the origin and along lines corresponding to $s_X = 0$ and $s_Y = 0$. Furthermore, it can be seen that, even in the case of equal correlation lengths, correlations are strongest along the orthogonal coordinate directions due to the ℓ^1-norm. The lack of isotropy in the case of equal correlation lengths $\theta_X = \theta_Y$ is difficult to justify since it implies dependency of the correlation structure on the arbitrarily chosen orthogonal coordinate directions x and y. As a result of this, the use of correlation functions that correspond to the ℓ^1-norm in $\mathbb{R}^2$ is not pursued further.



(a) $\theta_X = \theta_Y = 1$ (b) $\theta_X = 1$, $\theta_Y = 2$

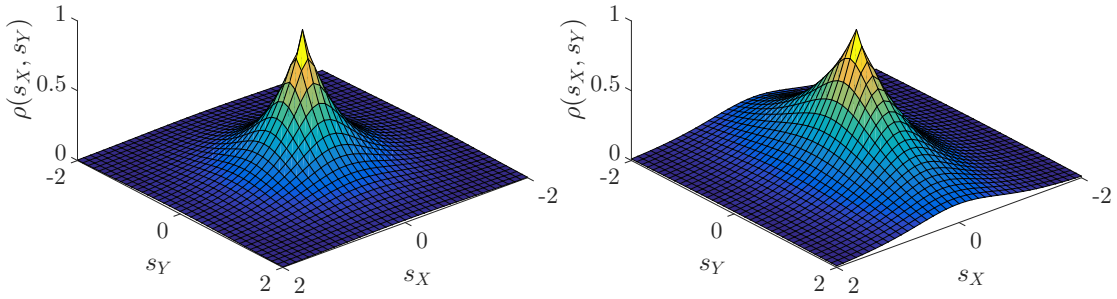
Figure 2.6: ℓ^1-norm Markov correlation function in $\mathbb{R}^2$.

An ellipsoidal non-separable two-dimensional Markov correlation function can be produced by taking the ℓ^2-norm over the correlation length adjusted domain:

$$\rho_M(s_X, s_Y) = \exp\left(-2\sqrt{\left(\frac{s_X}{\theta_X}\right)^2 + \left(\frac{s_Y}{\theta_Y}\right)^2}\right) \tag{2.31}$$

Figure 2.7 illustrates the ℓ^2-norm Markov correlation function in the case of (a) equal correlation lengths and (b) unequal correlation lengths. It is observed in the case of equal correlation lengths that this correlation function is isotropic and, consequently, it is preferred to the ℓ^1-norm Markov correlation function for the modelling of heterogeneous materials. Additionally, it can be seen that similar to its one-dimensional counterpart, this correlation function is only non-differentiable at the origin; however, it is important

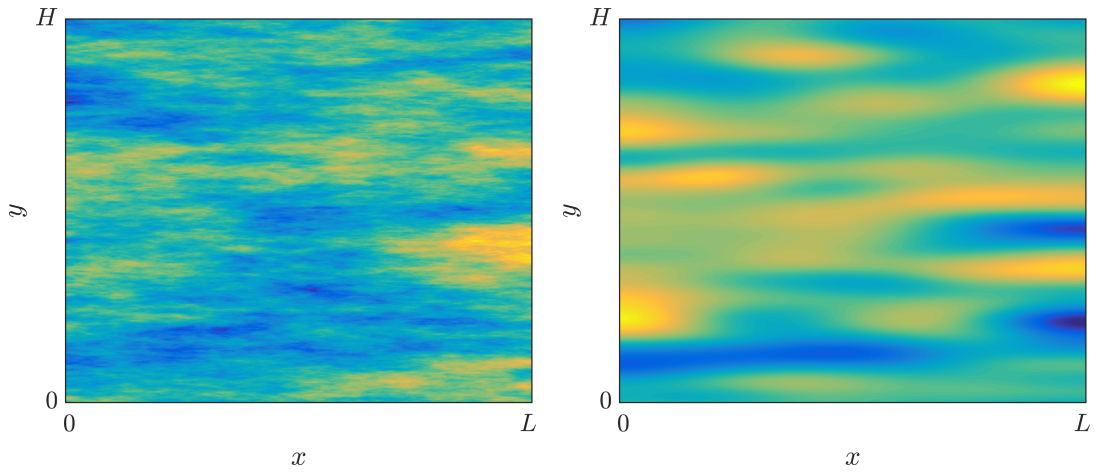
to note that the Markovian property exhibited in one-dimensional space does not hold for higher dimensions (Fenton and Griffiths, 2008, p. 123).



(a) $\theta_X = \theta_Y = 1$ (b) $\theta_X = 1$, $\theta_Y = 2$

Figure 2.7: ℓ^2-norm Markov correlation function in $\mathbb{R}^2$.

Figure 2.8 shows two realisations of a two-dimensional random field $Z(x, y)$ with the (a) ℓ^2-norm Markov correlation function and the (b) ℓ^2-norm Gaussian correlation function. It is observed that the higher dimensional Markov correlation function is associated with rough non-differentiable realisations due to the non-existence of the second derivative $\ddot{C}_M$ of the Markov correlation function at the origin whilst, in comparison, the Gaussian correlation function generates smooth realisations due the existence of $\ddot{C}_G(0)$. Additionally, it should be noted that all of the higher dimensional correlation functions considered in this section are *quadrant symmetric* since $\rho(s_X, s_Y) = \rho(-s_X, s_Y) = \rho(s_X, -s_Y) = \rho(-s_X, -s_Y)$. Finally, the only higher dimensional case considered in this section is the two-dimensional case; however, it is noted that an ellipsoidal correlation function in $\mathbb{R}^n$ can be formed by taking the ℓ^2-norm over the correlation length adjusted domain in the n-spatial dimensions.



(a) ℓ^2-norm Markov correlation function (b) ℓ^2-norm Gaussian correlation function

Figure 2.8: Realisations of a two-dimensional random field $Z(x, y)$ with $\theta_X = 0.1L$ and $\theta_Y = 0.5H$.

2.5 Spectral representation

In the context of random field theory, spectral representation refers specifically to the decomposition of a random field $Z(x)$ into a basis consisting of independent orthogonal sinusoidal functions (Stefanou, 2009). In contrast, decomposition with respect to other orthogonal basis functions are referred to differently, for instance, decomposition into eigenfunctions is known as the Karhunen-Loève expansion (Loève, 1978). In the spectral representation, the second moment structure of the random process $Z(x)$ is expressed in terms of the *two-sided spectral density function* $S(f)$ where f is a frequency index parameter. It is noted that the spectral density function $S(f)$ is the frequency domain equivalent to the covariance function $C(s)$.

The decomposition of a weakly-stationary mean-square-continuous mean-zero Gaussian process $Z(x)$ into sinusoids of random amplitude and phase angle was first given by Rice (1944):

$$Z(x) = \sum_{m=0}^{\infty} C_m \cos(f_m x + \phi_m) \tag{2.32}$$

where ϕ_m is a uniformly distributed phase angle on the interval $[0, 2\pi]$ and C_m is an

amplitude coefficient that is often defined deterministically as being equal to (Shinozuka and Jan, 1972):

$$C_m = \sqrt{2S(f_m)\Delta f} \tag{2.33}$$

where Δf is the size of the frequency interval that approaches zero in the limit $\Delta f \to 0$ as the number of sinusoids becomes large $m \to \infty$. The formulation of the spectral representation as an infinite summation is considered here since it is more intuitively understood, however, a rigorous definition of the spectral representation in terms of a Fourier-Stieltjes integral can be found in Yaglom (1962, p. 37).

The spectral representation given by Equation 2.32 can be written equivalently as (Rice, 1944, p. 287):

$$Z(x) = \sum_{m=0}^{\infty} \left[A_m \sin\left(f_m x\right) + B_m \cos\left(f_m x\right)\right] \tag{2.34}$$

where the amplitudes A_m and B_m are mean-zero normally distributed random variables whose variance is given by:

$$\mathbb{E}\left[A_m^2\right] = \mathbb{E}\left[B_m^2\right] = S(f_m)\Delta f \tag{2.35}$$

The two-sided spectral density function $S(f)$ and the covariance-function $C(s)$ are related through the Wiener-Khinchin theorem and are expressed as the following Fourier transform pairs:

$$C(s) = \int_0^{\infty} S(f)\cos(fs)\,\mathrm{d}f \tag{2.36}$$

$$S(f) = \frac{1}{2\pi}\int_0^{\infty} C(s)\cos(fs)\,\mathrm{d}s \tag{2.37}$$

Fenton and Griffiths (2008, p. 97) note that since the spectral density function $S(f)$ is an even function $S(f) = S(-f)$ then it is convenient to instead work with the one-sided spectral density function $G(f)$:

$$G(f) = 2S(f) \quad \text{if } f \geq 0 \tag{2.38}$$

In the case that the process $Z(x)$ is weakly stationary, the Wiener-Khinchin transforms can be expressed as:

$$G(f) = \frac{2\sigma^2}{\pi} \int_0^\infty \rho(s) \cos(fs)\, \mathrm{d}s \tag{2.39}$$

$$\rho(s) = \frac{1}{\sigma^2} \int_0^\infty G(f) \cos(fs)\, \mathrm{d}f \tag{2.40}$$

From a heuristic perspective, the spectral density function $G(f)$ describes how the variance σ^2 of the random process $Z(x)$ is distributed with respect to each frequency f. A smooth process, where θ is large compared to the domain D, has its power concentrated in the low frequencies whilst a rough process, where θ is small compared to the domain D, has its power concentrated in the high frequencies. The total variance of the process is then given by the summation over the whole frequency spectrum:

$$\sigma^2 = \int_{-\infty}^\infty S(f)\, \mathrm{d}f = 2 \int_0^\infty G(f)\, \mathrm{d}f \tag{2.41}$$

The spectral representation of a two-dimensional random field $Z(x, y)$ is given by (Shinozuka and Deodatis, 1996):

$$Z(x,y) = \sum_{n=0}^{\infty} \sum_{m=0}^{\infty} C_{m,n} \cos(f_m x + f_n y + \phi_{m,n}) \tag{2.42}$$

$$= \sum_{n=0}^{\infty} \sum_{m=0}^{\infty} \left[A_{m,n} \sin\left(f_m x + f_n y\right) + B_{m,n} \cos\left(f_m x + f_n y\right) \right] \tag{2.43}$$

where the deterministic amplitude C_m is given by (Shinozuka and Deodatis, 1996):

$$C_{m,n} = \sqrt{G(f_m, f_n) \Delta f_m \Delta f_n} \tag{2.44}$$

and the random amplitudes $A_{m,n}$ and $B_{m,n}$ are normally distributed with mean-zero and variance given by:

$$\mathbb{E}\left[A_{m,n}^2\right] = \mathbb{E}\left[B_{m,n}^2\right] = \frac{G(f_m, f_n)\Delta f_m \Delta f_n}{2} \tag{2.45}$$

Finally, it is noted that the two-dimensional one-sided spectral density function $G(f_X, f_X)$ is given by the Fourier transform of the respective two-dimensional correlation function $\rho(s_X, s_Y)$:

$$G(f_X, f_Y) = \left(\frac{2}{\pi\sigma}\right)^2 \int_0^\infty \int_0^\infty \rho(s_X, s_Y) \cos(f_X s_X) \cos(f_Y s_Y)\, \mathrm{d}s_X\, \mathrm{d}s_Y \tag{2.46}$$

2.5.1 Common spectral density functions

This section presents the spectral density functions associated with a number of the correlation functions presented in Section 2.4. The spectral representation is an especially useful representation for random processes that do not posses a finite second moment such as Dirac delta white noise $Z_N(x)$ whose spectral density function G_N is given by the Fourier transform of the Dirac delta function:

$$G_N(f) = G_0 \quad \text{if } f \geq 0 \tag{2.47}$$

where G_0 is the value of the spectral density function at the origin known as the *white noise intensity*. The spectral density function is uniform across all frequencies and it is in this sense that the variance of Dirac delta correlated white noise can be understood to be infinite:

$$\sigma_N^2 = 2\int_0^\infty G_N(f)\, \mathrm{d}f = \infty \tag{2.48}$$

For finite variance processes, it is useful to define the intercept of the spectral density function at the origin as (Fenton and Griffiths, 2008, p. 103):

$$G_0 = G(0) = \frac{\sigma^2\theta}{\pi} \tag{2.49}$$

The spectral density function $G_M(f)$ associated with the Markov covariance function $C_M(s)$ is given by:

$$G_M(f) = \frac{G_0}{1 + (\theta f/2)^2} \quad \text{if } f \geq 0 \tag{2.50}$$

It is noted that the Markov spectral density function $G_M(f)$, unlike the Markov covariance function $C_M(s)$, is continuous at the origin and of rational quadratic form (Rasmussen and Williams, 2006, p. 86).

The spectral density function $G_G(f)$ associated with the Gaussian covariance function $C_G(s)$ is given by:

$$G_G(f) = G_0 \exp\left(-\frac{\theta^2 f^2}{4\pi}\right) \quad \text{if } f \geq 0 \tag{2.51}$$

It is observed that the Gaussian spectral density function $G_G(f)$ is of the same squared exponential form as its associated covariance function $C_G(s)$.

The spectral density function $G_T(f)$ associated with the triangular covariance function $C_T(s)$ is given by:

$$G_T(f) = G_0 \left[\text{sinc}\left(\frac{f\theta}{2}\right)\right]^2 \quad \text{if } f \geq 0 \tag{2.52}$$

where sinc(.) is given by:

$$\text{sinc}\left(\frac{f\theta}{2}\right) = \frac{2\sin(f\theta/2)}{f\theta} \tag{2.53}$$

It is noted that the triangular covariance function $\rho_T(s)$ is linear and non-differentiable at both $s = 0$ and $s = \theta$; however, in contrast the triangular spectral density function $G_T(f)$ is of trigonometric form and everywhere differentiable. One numerical consideration

associated with the triangular spectral density function is that it needs to be ensured that $G_T(0) = G_0$ since the following limit is difficult to obtain numerically:

$$\lim_{f \to 0} \operatorname{sinc}\left(\frac{f\theta}{2}\right) = 1 \tag{2.54}$$

Figure 2.9 shows that initially the Markov spectral density function $G_M(f)$ decreases the quickest and hence has greater high frequency content which characterise the roughness of its realisations. In comparison, the Gaussian spectral density function $G_G(f)$ initially decreases the slowest and hence has greater low frequency content which characterises the smoothness of its realisations. Additionally, the triangular spectral density function $G_T(f)$ initially decreases faster than $G_G(f)$ but not as quickly as $G_M(f)$, however, unlike either $G_G(f)$ or $G_M(f)$ this function is not strictly monotonically decreasing and exhibits oscillatory behaviour that is attributed to the discontinuity of $\rho_T(s)$ at a separation equalling the correlation length $s = \theta$.

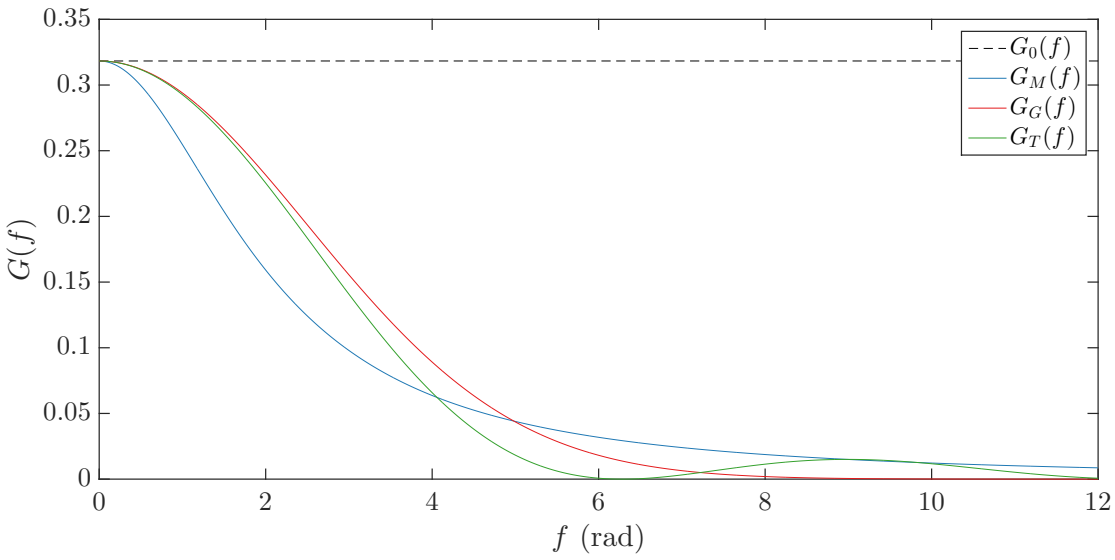


Figure 2.9: A comparison of the white noise $G_0(f)$, Markov $G_M(f)$, Gaussian $G_G(f)$ and triangular $G_T(f)$ spectral density functions against frequency f in radians ($\sigma = 1$, $\theta = 1$).

2.5.2 Higher-dimensional spectral density functions

Higher-dimensional spectral functions can be obtained from the higher-dimensional covariance function in Section 2.4 through the relationship given by Equation 2.46. In the

case of the ℓ^2-norm two-dimensional Markov correlation function, the equivalent spectral density function is given by:

$$G_M(f_X, f_Y) = \frac{\sigma^2 \theta_X \theta_Y}{2\pi \left[1 + \left(\frac{\theta_X f_X}{2}\right)^2 + \left(\frac{\theta_Y f_Y}{2}\right)^2\right]^{\frac{3}{2}}} \tag{2.55}$$

In the case of the ℓ^2-norm two-dimensional Gaussian correlation function, the equivalent spectral density function is given by:

$$G_G(f_X, f_Y) = \frac{\sigma^2 \theta_X \theta_Y}{\pi^2} \exp\left(-\frac{\theta_X^2 f_X^2 + \theta_Y^2 f_Y^2}{4\pi}\right) \tag{2.56}$$

The two-dimensional realisations shown in Figure 2.8 (a) and (b) were generated through the spectral representation of a random field with the two-dimensional ℓ^2-norm Markov and ℓ^2-norm Gaussian spectral density functions respectively through a simulation method known as the Fast Fourier transform method which is detailed in Section 2.13.

2.6 Non-Gaussian processes

So far this chapter has only considered Gaussian processes, however, for many phenomena non-positive values are not physically admissible and, consequently, the use of a marginal normal distribution may be inappropriate. Therefore, it is of interest to obtain a random process $Z(x)$ with an arbitrary non-Gaussian marginal distribution. This can be achieved through *translation theory* (Grigoriu, 1995) whereby a random process $Z(x)$ with marginal cumulative density function $F(.)$ is obtained through the following transformation of an underlying Gaussian process $\underline{Z}(x)$:

$$Z(x) = F^{-1}\left(\underline{F}\left(\underline{Z}(x)\right)\right) \tag{2.57}$$

where $\underline{F}(.)$ is the cumulative distribution function of the normal distribution. However, it is important to note that this transformation alters the statistical moments of $\underline{Z}(x)$ and, consequently, it is necessary to back-configure the parameters $\underline{\mu}$, $\underline{\sigma}$, $\underline{\rho}(s)$ such that

the non-Gaussian process $Z(x)$ has the desired statistical moments. Finding a general relationship between Gaussian and non-Gaussian statistical moments is challenging and has led to the development of algorithms to match the Gaussian and non-Gaussian spectral density functions (Shields et al., 2011, Bocchini and Deodatis, 2008). However, it is useful to note that if the random process $Z(x)$ has a lognormal marginal distribution then these relationships are analytically tractable. This is due to the simplicity of the following relationship between a lognormal random process $Z(x)$ with mean μ, variance σ^2 and correlation function $\rho(s)$ and the underlying normal $\underline{Z}(x)$:

$$Z(x) = \exp\left(\underline{Z}(x)\right) \tag{2.58}$$

The statistics of the non-Gaussian process $Z(x)$ are given by (Vanmarcke, 1988, p. 54):

$$\mu = \exp\left(\underline{\mu} + \frac{1}{2}\underline{\sigma}^2\right) \tag{2.59}$$

$$\sigma^2 = \left(\exp(\underline{\sigma}^2\underline{\rho}(s) - 1)\right)\exp\left(2\underline{\mu} + \underline{\sigma}^2\right) \tag{2.60}$$

$$\rho(s) = \frac{\exp\left(\underline{\sigma}^2\underline{\rho}(s)\right) - 1}{\exp(\underline{\sigma}^2) - 1} \tag{2.61}$$

Consequently, in order to obtain a lognormal process with statistics μ, σ, $\rho(s)$ the statistics of Gaussian process $\underline{Z}(x)$ are back-configured according to:

$$\underline{\mu} = \ln\left(\mu\left(1 + \frac{\sigma^2}{\mu^2}\right)^{-\frac{1}{2}}\right) \tag{2.62}$$

$$\underline{\sigma}^2 = \ln\left(1 + \frac{\sigma^2}{\mu^2}\right) \tag{2.63}$$

$$\underline{\rho}(s) = \frac{\ln\left[\left(\exp\left(\sigma^2\right) - 1\right)\rho(s) + 1\right]}{\sigma^2} \tag{2.64}$$

Figure 2.10 shows the effect of exponentiation on a Markov correlation function $\underline{\rho}(s)$ of a Gaussian process $\underline{Z}(x)$ for varying desired coefficients of variation c_v of the obtained lognormal process $Z(x)$. It is observed that, for small coefficients of variation c_v of the

lognormal process $Z(x)$, the error induced in the correlation structure caused by not back-configuring the correlation function $\underline{\rho}(s)$ of the Gaussian process $\underline{Z}(x)$ is small.

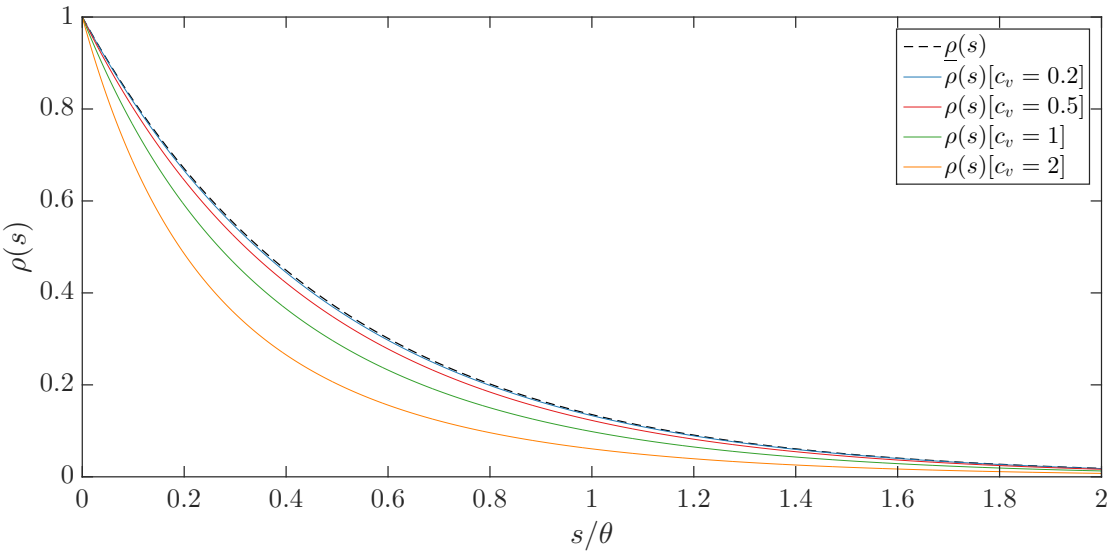


Figure 2.10: Effect of exponentiation on the Markov correlation function $\underline{\rho}(s)$ of an underlying Gaussian process $\underline{Z}(x)$ for four different coefficients of variation c_v of the obtained lognormal process $Z(x)$.

2.7 Overview of estimation

The use of random field models to quantify the risk associated with heterogeneous materials requires that the random field parameters $\mathbf{\Phi} = \{\mu, \sigma, \theta\}$ are accurately inferred from experimental data. The quality of these inferences depends on the choice of estimation methodology which in turn affects the accuracy of the quantification of risk achieved through the usage of the random field model. This section considers the application of two frequentist techniques namely the method of moments (MM) and maximum likelihood estimation (MLE) in order to infer the parameters $\mathbf{\Phi}$ of a random field. The literature on the estimation of random field parameters has primarily focussed on inference from a single realisation of the random field as elucidated by the following quote:

> "In geotechnical engineering, we generally only have one 'experiment' — our planet as we see it. Rather than showing variability over an ensemble, our one realization shows variability over space." (Fenton and Griffiths, 2008, p. 180)

In contrast to the previous focus of the literature on the case of a single realisation, this thesis considers the theory of estimation for the more general case of multiple realisations of the random field. This is motivated by the fact that this thesis considers the application of random fields to timber wherein each tree of the same species can be considered a distinct realisation of the same underlying random process. In the case of a single realisation, a concept of great importance is ergodicity which describes the ability to make inferences from a single realisation of infinite extent (Fenton and Griffiths, 2008, p. 180). However, ergodicity is also an important consideration for the case of multiple realisations since it affects the number of realisations required to achieve an ensemble that is representative of the variability of the random field.

In the formal mathematical definition, a random process $Z(x)$ is ergodic if a particular probabilistic descriptor can be deduced from a realisation of infinite extent. A realisation is said to be of infinite extent if the volume $|D|$ of the domain is taken in the following limit $D \to \infty$ where this limit is to be understood in the mean square sense (Chilès and Delfiner, 2012, p. 20). The particular probabilistic descriptor is usually taken to be the mean, however, ergodicity can also be considered with respect to other probabilistic descriptors such as covariance. A random process $Z(x)$ is *mean-ergodic* if (Chilès and Delfiner, 2012, p. 19):

$$\lim_{D\to\infty} \frac{1}{|D|} \int_D Z(x,q)\,\mathrm{d}x = \mu \tag{2.65}$$

A sufficient condition for a process to be ergodic in mean is that as the separation between points in the domain becomes large $s \to \infty$ then these points become statistically independent i.e. their covariance becomes zero $C(s) \to 0$ (Adler and Taylor, 2007, p. 145). An example of a process that is not mean-ergodic is the Wiener process and this can be explained by recalling that this process is a martingale. In contrast, a process such as white noise is not only ergodic but *micro-ergodic* since its statistical properties can be deduced from infinite sampling density over a finite domain (Chilès and Delfiner, 2012, p. 22). It is useful to note that if a process is ergodic then it is also strongly stationary, however, the converse is not necessarily true and an example of this is the process with constant-valued realisations (Cressie, 1993, p. 57).

At this point it important to note that the consideration of realisations of infinite extent

is not pragmatic since, in practice, samples of realisations can only be obtained over a finite domain. Consequently, it is useful to introduce a heuristic concept known as *reasonable ergodicity* which describes whether the correlation of the realisation over the sampling domain is sufficiently negligible in order that samples can be considered to be reasonably statistically independent. If the correlations over the sampling domain are significant then estimations of the random field parameters, especially the scale and correlation parameters, may be subject to substantial uncertainty. The assessment of whether a process is reasonably ergodic over the domain requires the determination of whether a trend exists within the data. This requires significant engineering judgement and can not be determined with absolute confidence; however, if a trend is observed then it needs to be determined whether this trend is due to a trend in the mean $\mu(x)$ or should instead be attributed to the covariance structure $C(s)$ of the random field (Cressie, 1993, p. 25). If the observed trend is attributed to a non-stationary mean $\mu(x)$ then the process can be considered to be reasonably ergodic and the data should be detrended prior to estimates of the covariance structure. However, if the observed trend is attributed to the covariance structure of the process then the process can not be considered to be reasonably ergodic and, consequently, parameter estimates may be subject to substantial uncertainty.

Finally, it should be recognised that conventional inferential methodologies consider the data points to constitute samples of the random field at a single point in space. However, as discussed in Chapter 1, experimentally determined material properties are in fact effective material properties determined over a non-zero sample volume. Thus, experimentally determined material properties are averages over the sample volume and can, at best, only be approximated as samples of the random field at a single point in space. This discrepancy between the point scale characteristics of the random field model and the macroscale nature of experimentally determined material properties is not addressed within this chapter, however, this discrepancy is considered extensively in *Chapter 5 – Inference from effective properties*. This chapter is instead focussed on the extension of conventional methodologies for estimation, such as method of moments and maximum likelihood estimation, to the case of multiple realisations.

2.8 Method of moments estimation

The estimation technique known as method of moments involves estimating population moments from the samples then solving equations for the parameters of interest (Devore, 2012, p. 256). The benefit of this approach is that it is simple and fast, however, it should be noted that the derived estimators can often be biased. Consequently, method of moments is often a suitable approach to obtain an initial approximation to a parameter value in the case that other methods are intractable (Casella and Berger, 2002, p. 312). For the case of a Gaussian random process, the parameters μ and σ are simply given by the sample mean and variance, however, determination of the correlation parameter θ is more complex since it requires the derivation of a relationship between the sample correlation function $\hat{\rho}(s)$ and the analytical correlation function $\rho(s)$ to be fitted.

Consider a stationary Gaussian process $Z(x)$ with R realisations where each realisation Z_r has been sampled at J equispaced spatial locations. One approach to estimate the mean μ and variance σ^2 from these samples is to use the following classical estimators:

$$\hat{\mu} = \frac{1}{JR} \sum_{r=1}^{R} \sum_{j=1}^{J} Z_r(x_j) \tag{2.66}$$

$$\hat{\sigma}^2 = \frac{1}{JR} \sum_{r=1}^{R} \sum_{j=1}^{J} \left(Z_r(x_j) - \hat{\mu}\right)^2 \tag{2.67}$$

The estimator for the variance σ^2 is biased since the denominator is not $R(J-1)$, however, this biased estimator is preferred over the unbiased estimator since it ensures positive semidefinite covariance matrices (Fenton, 1999). These classical estimators yield acceptable results if the samples are reasonably ergodic or if samples from many realisations are available, however, in the case of a limited number of realisations that are not reasonably ergodic then these classical estimators may perform poorly. It is possible to derive improved estimators that depend on the correlation structure, as shown in Section 2.9, however it is noted that many authors continue to use the classical estimators due to their simplicity (Lloret-Cabot et al., 2014),.

The second-moment structure of the random process $Z(x)$ can be estimated using the sample covariance function also known as the *covariogram* (Cressie, 1993, p. 67). This

approach requires that the spatial locations at which the process $Z(x)$ has been sampled to be equispaced so that the correlation at the k^{th} spatial separation s_k can be estimated. The usual estimate of the covariance function, adapted for the case of multiple realisations, is given by (Box et al., 2016, p. 31):

$$\hat{C}(s_k) = \frac{1}{JR} \sum_{r=1}^{R} \sum_{j=1}^{J-k} \left(Z_r(x_j) - \hat{\mu}\right) \left(Z_r(x_{j+k}) - \hat{\mu}\right) \quad \text{for } k = 0, 1, \ldots, K \tag{2.68}$$

It is noted that the use of a variable denominator, given by $R(J-k)$, is not pursued here due to issues with non-positive definiteness (Jenkins and Watts, 1968, p. 182). The sample correlation function, also known as the *correlogram*, is given by (Montegomery et al., 2008, p. 30):

$$\hat{\rho}(s_k) = \frac{\hat{C}(s_k)}{\hat{C}(s_0)} \tag{2.69}$$

where $\hat{C}(s_0) = \hat{\sigma}^2$. The correlation parameter θ is estimated through regression by considering the error between the sample correlation function $\hat{\rho}(s, \theta)$ and the theoretical correlation function $\rho(s, \theta)$ to be fitted:

$$\epsilon(\theta) = \frac{1}{k} \sum_{j=1}^{k} \left(\hat{\rho}(s_j|\theta) - \rho(s_j|\theta)\right)^2 \tag{2.70}$$

The method of moments estimate of the correlation length θ is obtained by finding the value of θ that minimises the error function $\epsilon(\theta)$:

$$\hat{\theta} = \operatorname{argmin} \epsilon(\theta) \tag{2.71}$$

The minimisation of the error function $\epsilon(\theta)$ is often approached numerically due to the non-linear form of many theoretical correlation functions. In the case that there are many theoretical correlation models to be selected between, the regression procedure is repeated for each correlation function and the correlation function with the lowest error ϵ is selected.

2.8.1 Efficient computation of the sample correlation function

For a large number of realisations R or spatial sampling locations J, the computation of the sample correlation function given by Equation 2.68 can become computationally expensive. Consequently, it is useful to consider an efficient method to compute the sample correlation function $\hat{\rho}(s)$ through the use of Fourier transforms. The correlation function of a weakly stationary mean-zero random process $Z(x)$ can be defined as the cross-correlation of $Z(x)$ with itself at lag s (Papoulis, 1962, p. 242):

$$\rho(s) = Z(s) * \overline{Z}(-s) = \int_{-\infty}^{\infty} Z(x)\overline{Z}(x-s)\,\mathrm{d}x \tag{2.72}$$

where $\overline{Z}(s)$ is the complex conjugate of $Z(s)$ and $*$ is the convolution operator. This definition of the theoretical correlation function $\rho(s)$ can be utilised to develop a computationally efficient method to compute the sample correlation function $\hat{\rho}(s)$ through the use of the convolution theorem which states that the Fourier transform of convolution is equal the pointwise product of Fourier transforms: $\mathcal{F}\{f * g\} = \mathcal{F}\{f\} \cdot \mathcal{F}\{g\}$. Consequently, the correlation function $\rho(s)$ can be expressed as:

$$\rho(s) = \mathcal{F}^{-1}\big\{\mathcal{F}\{Z(s)\} \cdot \overline{\mathcal{F}}\{Z(s)\}\big\} \tag{2.73}$$

If the J samples of a single realisation $Z_r(x_j)$ are formulated as the following column vector:

$$\boldsymbol{Z}_r = \begin{bmatrix} Z_r(x_1) \\ Z_r(x_2) \\ \vdots \\ Z_r(x_J) \end{bmatrix} \tag{2.74}$$

then the vectorised sample correlation function $\hat{\boldsymbol{\rho}}$ of the single realisation $Z_r(x_j)$ can be computed efficiently through (Press et al., 1997, p. 538):

$$\hat{\boldsymbol{\rho}} = \mathcal{F}^{-1}\big\{\mathcal{F}\{\boldsymbol{Z}_r - \hat{\mu}\} \circ \overline{\mathcal{F}}\{\boldsymbol{Z}_r - \hat{\mu}\}\big\} \tag{2.75}$$

where $\circ$ is the entrywise product also known as the Hadamard product (Horn and Johnson, 2013, p. 371). Note that the sample mean is subtracted from the sample vector $\boldsymbol{Z}_r$ in the above expression since Equation 2.73 is only valid for mean-zero random processes. It is of interest to consider the efficient computation of the sample correlation function $\hat{\boldsymbol{\rho}}$ for the case of multiple realisations; in the case that there is an equal sized column vector of samples $\boldsymbol{Z}_r$ for each realisation then the matrix of samples is given by:

$$\boldsymbol{Z'} = \begin{bmatrix} \boldsymbol{Z}_1 & \boldsymbol{Z}_2 & \dots & \boldsymbol{Z}_R \end{bmatrix} \tag{2.76}$$

Additionally, the Fourier operator is defined for matrix inputs such that:

$$\mathcal{F}(\boldsymbol{Z'}) = \begin{bmatrix} \mathcal{F}(\boldsymbol{Z}_1) & \mathcal{F}(\boldsymbol{Z}_2) & \dots & \mathcal{F}(\boldsymbol{Z}_R) \end{bmatrix} \tag{2.77}$$

It is observed that since the discrete Fourier transform is a linear operator, the averaging associated with the outer summation in Equation 2.68 can be applied within the frequency domain. Consequently, the vectorised sample correlation function $\hat{\boldsymbol{\rho}}$ for the case of multiple realisations is given by:

$$\hat{\boldsymbol{\rho}} = \mathcal{F}^{-1}\left\{ \left(\mathcal{F}\{\boldsymbol{Z'} - \hat{\mu}\} \circ \overline{\mathcal{F}}\{\boldsymbol{Z'} - \hat{\mu}\} \right) \frac{\mathbf{1}}{R} \right\} \tag{2.78}$$

where $\mathbf{1}$ is a column vector with R entries all equal to one.

The limitation of the method of moments approach to compute the second moment structure of the random process $Z(x)$ is that the observations of each realisation are required to be equispaced. However, it is often the case that observations are either irregularly spaced or that there are an inconsistent number of observations for each realisation; consequently, it is of interest to pursue a more flexible approach for the inference of model parameters which is known as maximum likelihood estimation.

2.9 Maximum likelihood estimation

This section considers a frequentist estimation technique known as maximum likelihood estimation (MLE) which is an alternative to the method of moment approach considered in the previous section. MLE makes use of the likelihood function $\mathcal{L}(\boldsymbol{Z}|\boldsymbol{\Phi})$ that describes the probability of samples $\boldsymbol{Z}$ given a vector of parameter values $\boldsymbol{\Phi} = \{\mu, \sigma, \theta\}$. The maximum likelihood estimate of the vector of parameters $\boldsymbol{\Phi}$ is given by (Hogg et al., 2013, p. 323):

$$\hat{\boldsymbol{\Phi}} = \operatorname{argmax} \mathcal{L}(\boldsymbol{Z}|\boldsymbol{\Phi}) \tag{2.79}$$

Consequently, MLE finds the vector of parameters $\hat{\boldsymbol{\Phi}} = \{\hat{\mu}, \hat{\sigma}, \hat{\theta}\}$ that gives the samples $\boldsymbol{Z}$ the maximum probability of occurring (Casella and Berger, 2002, p. 316). One of the key advantages of maximum likelihood estimators are their asymptotic properties which are the properties of the estimator as the number of samples grows large $n \to \infty$ (Devore, 2012, p. 262). Under certain regularity conditions (Hogg et al., 2013, p. 322), these asymptotic properties are: the MLE are consistent; the MLE are efficient and constitute the minimum variance unbiased estimator since the variance of the estimator approaches the Cramér-Rao lower bound (Hogg et al., 2013, p. 327); finally, the MLE are approximately unbiased and normally distributed about the true parameter values. However, it should be noted that for small sample sizes the MLE are neither unbiased nor minimum variance and, in certain circumstances, method of moment estimators may be superior (Hosking and Wallis, 1987). A disadvantage of the maximum likelihood approach is that the likelihood may be computationally expensive to evaluate or intractable requiring that the likelihood be approximated numerically. Furthermore, for certain distributions the partial derivatives of the likelihood function can not be obtained in closed analytical form requiring the use of numerical optimisation algorithms to find the arguments that maximise the likelihood function (Devore, 2012, p. 261). One example of a distribution for which all of the partial derivatives can not be obtained analytically are Gaussian processes since it is not possible, in the general case, to calculate a partial derivative with respect to the correlation parameter θ.

In the case that the n samples are from a single realisation $\boldsymbol{Z}_r$ of a Gaussian random process $Z(x)$, the likelihood function $\mathcal{L}(\boldsymbol{Z}_r)$ is simply equal to the multivariate normal

probability density function given by Equation 2.7:

$$\mathcal{L}(\boldsymbol{Z}_r) = f(\boldsymbol{Z}_r) = (2\pi)^{-\frac{n}{2}} \det(\boldsymbol{C}_r)^{-\frac{1}{2}} \exp\left((\boldsymbol{Z}_r - \boldsymbol{\mu}_r)^\intercal \boldsymbol{C}_r^{-1} (\boldsymbol{Z}_r - \boldsymbol{\mu}_r)\right) \tag{2.80}$$

where $\boldsymbol{C}_r$ and $\boldsymbol{\mu}_r$ are the covariance matrix and mean vector of $\boldsymbol{Z}_r$ respectively. If the process $Z(x)$ is weakly stationary then the likelihood function is given by:

$$\mathcal{L}(\boldsymbol{Z}_r) = \left(2\pi\sigma^2\right)^{-\frac{n}{2}} \det(\boldsymbol{\rho}_r)^{-\frac{1}{2}} \exp\left(\frac{(\boldsymbol{Z}_r - \mu\mathbf{1}_r)^\intercal \boldsymbol{\rho}_r^{-1} (\boldsymbol{Z}_r - \mu\mathbf{1}_r)}{2\sigma^2}\right) \tag{2.81}$$

It is noted that the likelihood tends to be vanishing and consequently it is preferable to instead consider the log-likelihood function (Fenton, 1999):

$$\log \mathcal{L}(\boldsymbol{Z}_r) = -\frac{n}{2}\log(2\pi) - \frac{n}{2}\log(\sigma^2) - \frac{1}{2}\log(\det(\boldsymbol{\rho}_r)) - \frac{(\boldsymbol{Z}_r - \mu\mathbf{1}_r)^\intercal \boldsymbol{\rho}_r^{-1} (\boldsymbol{Z}_r - \mu\mathbf{1}_r)}{2\sigma^2} \tag{2.82}$$

where the constant $-\frac{n}{2}\log(2\pi)$ may be neglected since it does not affect the location of the maximum of $\log \mathcal{L}(\boldsymbol{Z}_r)$. Assuming that the likelihood function is unimodal with derivative zero only at the maximum, an estimator for the location parameter μ can be derived by taking the partial derivative of the log-likelihood function with respect to μ, setting it equal to zero and rearranging to give (Fenton, 1999):

$$\hat{\mu} = \frac{\mathbf{1}_r^\intercal \boldsymbol{\rho}_r^{-1} \boldsymbol{Z}_r}{\mathbf{1}_r^T \boldsymbol{\rho}_r^{-1} \mathbf{1}_r} \tag{2.83}$$

This estimator is equal to the classical mean estimator when there is no correlation between samples i.e. when $\boldsymbol{\rho}_r = \boldsymbol{I}$ where $\boldsymbol{I}$ is the identity matrix. However, as the correlation between samples increases this estimator has reduced variance compared to the classical estimator of the mean. An estimator for the variance σ^2 is obtained by taking a partial derivative of the log-likelihood function with respect to σ^2, setting it equal to zero and rearranging to give (Fenton, 1999):

$$\hat{\sigma}^2 = \frac{1}{n}(\boldsymbol{Z}_r - \hat{\mu}_r\mathbf{1}_r)^T \boldsymbol{\rho}_r^{-1} \boldsymbol{Z}_r \tag{2.84}$$

This estimator for variance is a substantial improvement over the classical estimator of variance in the case that samples are correlated. Closed formed estimators for both the location μ and scale parameter σ have been presented, however, the partial derivative with respect to the correlation parameter θ can not always be obtained since closed form solutions for the derivative of the determinant of the correlation matrix do not always exist (Fenton and Griffiths, 2008, p. 197). Instead, numerical optimisation is used to find the value of the correlation parameter θ that maximises the log-likelihood function. It is important to note that the expressions for $\hat{\mu}$ and $\hat{\sigma}$, given by Equations 2.83 and 2.84, give the maximum likelihood estimates of μ and σ for each θ_i and, consequently, optimisation of the likelihood function reduces to numerical optimisation of a single parameter namely the correlation parameter θ.

The theory of maximum likelihood estimation for Gaussian processes presented above is only for the case of samples belonging to a single realisation, however, it is of interest to consider the case of samples belonging to an ensemble of realisations $\boldsymbol{Z}$. Two methods are considered for extending the MLE theory presented above to the case of multiple realisations. The first approach is to note that the likelihood of the ensemble $\boldsymbol{Z}$ is simply given by the product of their individual likelihoods:

$$\mathcal{L}(\boldsymbol{Z}|\boldsymbol{\Phi}) = \prod_{r=1}^{R} f(\boldsymbol{Z}_r) \tag{2.85}$$

or in the case of log-likelihood by the summation of their individual log-likelihoods:

$$\log \mathcal{L}(\boldsymbol{Z}|\boldsymbol{\Phi}) = \sum_{r=1}^{R} \log f(\boldsymbol{Z}_r) \tag{2.86}$$

where $\boldsymbol{Z}_r$ is the r^{th} realisation of the random field belonging to the ensemble $\boldsymbol{Z}$. The approach would then be to take partial derivatives of this expression for log-likelihood and attempt to derive expressions for $\hat{\mu}$ and $\hat{\sigma}$. The second approach, and the approach pursued here, is to vectorise the R realisations into a single column vector given by:

$$\boldsymbol{Z} = \begin{bmatrix} \boldsymbol{Z}_1 \\ \boldsymbol{Z}_2 \\ \vdots \\ \boldsymbol{Z}_R \end{bmatrix} \tag{2.87}$$

with global correlation matrix $\boldsymbol{\rho}$ given by:

$$\boldsymbol{\rho} = \begin{bmatrix} \boldsymbol{\rho}_1 & 0 & \dots & 0 \\ 0 & \boldsymbol{\rho}_2 & \dots & 0 \\ \vdots & \vdots & \ddots & \vdots \\ 0 & 0 & \dots & \boldsymbol{\rho}_R \end{bmatrix} \tag{2.88}$$

where $\boldsymbol{\rho}_r$ is the correlation matrix of the r^{th} realisation $\boldsymbol{Z}_r$.

Let $\boldsymbol{a}$ and $\boldsymbol{b}$ denote the solutions to the following system of linear equations:

$$\boldsymbol{\rho a} = \boldsymbol{Z} \tag{2.89}$$

$$\boldsymbol{\rho b} = \mathbf{1} \tag{2.90}$$

where $\mathbf{1}$ is a column vector of ones with size equal to $\boldsymbol{Z}$. The maximum likelihood estimates of the mean and standard deviation inferred from the global sample vector $\boldsymbol{Z}$ of the random field are given by:

$$\hat{\mu} = \frac{\mathbf{1}^T \boldsymbol{a}}{\mathbf{1}^T \boldsymbol{b}} \tag{2.91}$$

$$\hat{\sigma} = \frac{1}{n}(\boldsymbol{Z} - \hat{\mu}\mathbf{1})^T \boldsymbol{a} \tag{2.92}$$

where n is the total number of samples in $\boldsymbol{Z}$. The maximum likelihood estimate $\hat{\theta} = \operatorname{argmax} \log \mathcal{L}(\boldsymbol{Z}|\theta)$ is then obtained through numerical optimisation of the log-likelihood function given by:

$$\log \mathcal{L}(\boldsymbol{Z}|\theta) = -\frac{n}{2}\log(\hat{\sigma}^2) - \frac{1}{2}\log(\det(\boldsymbol{\rho}(\theta))) - \frac{(\boldsymbol{Z} - \hat{\mu}\mathbf{1})^T \boldsymbol{\rho}(\theta)^{-1}(\boldsymbol{Z} - \hat{\mu}\mathbf{1})}{2\hat{\sigma}^2} \tag{2.93}$$

In the case of a large number of realisations, the direct computation of the solutions $\boldsymbol{a}$ and $\boldsymbol{b}$ is computationally expensive and should be avoided by taking advantage of the sparse and symmetric nature of the global correlation matrix $\boldsymbol{\rho}$. Note that the following manipulations are based on elementary linear algebra and the properties of determinants (Axler, 1997). It is observed that since the global correlation matrix $\boldsymbol{\rho}$ is a block diagonal matrix then its inverse is equal to the inverse of each of its elements:

$$\boldsymbol{\rho}^{-1} = \begin{bmatrix} \boldsymbol{\rho}_1 & 0 & \cdots & 0 \\ 0 & \boldsymbol{\rho}_2 & \cdots & 0 \\ \vdots & \vdots & \ddots & \vdots \\ 0 & 0 & \cdots & \boldsymbol{\rho}_R \end{bmatrix}^{-1} = \begin{bmatrix} \boldsymbol{\rho}_1^{-1} & 0 & \cdots & 0 \\ 0 & \boldsymbol{\rho}_2^{-1} & \cdots & 0 \\ \vdots & \vdots & \ddots & \vdots \\ 0 & 0 & \cdots & \boldsymbol{\rho}_R^{-1} \end{bmatrix}. \tag{2.94}$$

Furthermore, since the system of equations corresponding to each local correlation matrix $\boldsymbol{\rho}_r$ are independent then the solutions, $\boldsymbol{a}$ and $\boldsymbol{b}$, to the linear system of equations are given by:

$$\boldsymbol{a} = \boldsymbol{\rho}^{-1}\boldsymbol{Z} = \begin{bmatrix} \boldsymbol{\rho}_1^{-1}\boldsymbol{Z}_1 \\ \boldsymbol{\rho}_2^{-1}\boldsymbol{Z}_2 \\ \vdots \\ \boldsymbol{\rho}_R^{-1}\boldsymbol{Z}_R \end{bmatrix} \tag{2.95}$$

$$\boldsymbol{b} = \boldsymbol{\rho}^{-1}\mathbf{1} = \begin{bmatrix} \boldsymbol{\rho}_1^{-1}\mathbf{1}_1 \\ \boldsymbol{\rho}_2^{-1}\mathbf{1}_2 \\ \vdots \\ \boldsymbol{\rho}_R^{-1}\mathbf{1}_R \end{bmatrix} \tag{2.96}$$

where $\mathbf{1}_r$ is the r^{th} column vector of ones with size equal to r^{th} realisation $\boldsymbol{Z}_r$. Note that for computational reasons, the solution to this linear system of equations should be found through Gaussian elimination rather than through direct computation of the inverse of the correlation matrix $\boldsymbol{\rho}_r$. A further numerical consideration is that the determinant of a large correlation matrix $\boldsymbol{\rho}$ can be so large that it can not be represented accurately using single or double precision and, therefore, the direct computation of the determinant of $\boldsymbol{\rho}$ should be avoided. It is noted that the global correlation matrix $\boldsymbol{\rho}$ is a block diagonal matrix and, consequently, its determinant is given by:

$$\det(\boldsymbol{\rho}) = \prod_{r=1}^{R} \det(\boldsymbol{\rho}_r) \tag{2.97}$$

Similarly, the log determinant of the global correlation matrix $\boldsymbol{\rho}$ is given by:

$$\log(\det(\boldsymbol{\rho})) = \sum_{r=1}^{R} \log(\det(\boldsymbol{\rho}_r)) \tag{2.98}$$

Additionally, in the case that the correlation matrices are equal $\boldsymbol{\rho}_1 = \boldsymbol{\rho}_2 = \cdots = \boldsymbol{\rho}_R$ (i.e. the realisations have all been sampled at the same spatial locations) then the log-determinant is given by $\log(\det(\boldsymbol{\rho})) = R\log(|\boldsymbol{\rho}_1|)$. Furthermore, it can be shown that the log-determinant of a matrix does not need to be computed directly provided that the matrix permits the following Cholesky decomposition (Wicklin, 2012):

$$\boldsymbol{\rho}_r = \boldsymbol{\psi}\boldsymbol{\psi}^{\intercal} \tag{2.99}$$

where $\boldsymbol{\psi}$ is a lower triangular square matrix. It should be recognised that Cholesky decomposition requires a positive definite matrix which is a stronger condition than that satisfied by correlation matrices which are only required to be positive semidefinite. The log-determinant of the correlation matrix $\boldsymbol{\rho}_r$ is given by:

$$\begin{aligned}
\log(\det(\boldsymbol{\rho}_r)) &= \log(\det(\boldsymbol{\psi}\boldsymbol{\psi}^{\intercal})) && (2.100)\\
&= \log(\det(\boldsymbol{\psi})\det(\boldsymbol{\psi}^{\intercal})) && (2.101)\\
&= \log(\det(\boldsymbol{\psi})^2) && (2.102)\\
&= 2\log(\det(\boldsymbol{\psi})) && (2.103)
\end{aligned}$$

Observing that the determinant of a lower triangular matrix $\boldsymbol{\psi}$ is simply given by the product of its diagonal elements $\boldsymbol{\psi}_{i,i}$ and, consequently, the log-determinant of the correlation matrix $\boldsymbol{\rho}_r$ is given by:

$$\log(\det(\boldsymbol{\rho}_r)) = 2\log\left(\prod_{i=1}^{I}\boldsymbol{\psi}_{i,i}\right) \tag{2.104}$$

$$= 2\sum_{i=1}^{I}\log\boldsymbol{\psi}_{i,i} \tag{2.105}$$

Therefore, it has been shown that the log-determinant of the correlation matrix $\boldsymbol{\rho}_r$, and similarly the global correlation matrix $\boldsymbol{\rho}$ given by Equation 2.98, can be obtained without direct computation of the determinant through the use of Cholesky decomposition. It is important to recognise that the advantage of this approach is that it offers both greater computational efficiency and numerical stability over direct computation of the log-determinant.

2.10 Kriging

Kriging is an interpolation method that aims to estimate the value of a realisation of a random process at a location different from those that it has been sampled at. In the case that the random process is Gaussian, it is observed that the kriging estimator is both unbiased and the minimum variance estimator (Journel and Huijbregts, 1978, p. 304). This method of interpolation was used by its namesake, Krige (1951), to predict the spatial distribution of gold-ore and, within the context of geostatistics, its mathematical basis was formalised by Matheron (1973). However, it should be recognised that this interpolation technique has a long history: it was first developed by Kolmogrov (1941) and Wiener (1964) and has been referred to by many names including Gaussian process regression (Rasmussen and Williams, 2006, p. 30) and time series forecasting (Box et al., 2016, p. 129).

The advantage of kriging over other interpolation techniques such as cubic splines (Press et al., 1997, p. 107) is that the kriging estimator takes into account the expected value and correlation structure of the samples through the use of random field models. This section only considers the case of *simple kriging*, which assumes that the parameters of the random field are both constant and known, however, for more sophisticated implementations such as kriging with an unknown constant mean, known as *ordinary kriging*, or kriging with an unknown non-stationary polynomial mean, known as *universal krig-*

ing, refer to Fenton and Griffiths (2008, p. 130). The kriging estimate $\hat{Z}$ of a realisation at location x_i is given by:

$$\hat{Z}(x_i) = \mu\mathbf{1} + \boldsymbol{\beta}_i^{\mathsf{T}} (\boldsymbol{Z} - \mu\mathbf{1}) \tag{2.106}$$

where $\mathbf{1}$ is a column vector of ones with size equal to $\boldsymbol{Z}$, $\boldsymbol{\beta}_i$ is a column vector that weights the detrended value of the samples $\boldsymbol{Z}$ and $\boldsymbol{Z}$ is a column vector of the observations of the realisation sampled at spatial locations $\boldsymbol{x}_{\boldsymbol{\alpha}}$:

$$\boldsymbol{Z} = Z(\boldsymbol{x}_{\boldsymbol{\alpha}}) = \begin{bmatrix} Z(x_1) \\ Z(x_2) \\ \vdots \\ Z(x_J) \end{bmatrix} \tag{2.107}$$

The values of the vector $\boldsymbol{\beta}_i$, containing the coefficients $\beta_{i,j}$, that minimises the variance of the error of the estimator at location x_i is given by:

$$\boldsymbol{\beta}_i = \boldsymbol{C}^{-1}\boldsymbol{b}_i \tag{2.108}$$

where $\boldsymbol{C}$ is the covariance matrix of $\boldsymbol{Z}$ and $\boldsymbol{b}_i$ is a vector of covariances between the samples $\boldsymbol{Z}$ and the value to be estimated $Z(x_i)$:

$$\boldsymbol{b}_i = \begin{bmatrix} \mathrm{Cov}(Z(x_i), Z(x_1)) \\ \mathrm{Cov}(Z(x_i), Z(x_2) \\ \vdots \\ \mathrm{Cov}(Z(x_i), Z(x_J) \end{bmatrix} \tag{2.109}$$

The above equations consider the kriging estimate of the realisation at a single point x_i, however, it is often the case in practice that a kriging estimate $\hat{Z}$ is desired at many spatial locations $\{x_1, \ldots, x_I\}$. This can be achieved by concatenating the vectors of covariances $\boldsymbol{b}_i$ for every i^{th} point to be predicted into a single matrix given by:

$$\boldsymbol{b} = \begin{bmatrix} \boldsymbol{b}_1 & \boldsymbol{b}_2 & \dots & \boldsymbol{b}_I \end{bmatrix} \tag{2.110}$$

where $\boldsymbol{b}$ is a J by I matrix where J is the number of samples and I is the number of locations that an estimate of the realisation is desired at. Similar to Equation 2.108, the spatial weights $\boldsymbol{\beta}$ are given by:

$$\boldsymbol{\beta} = \boldsymbol{C}^{-1}\boldsymbol{b} \tag{2.111}$$

where $\boldsymbol{\beta}$ is also a J by I matrix. Similar to Equation 2.106, the column vector of predictions $\hat{\boldsymbol{Z}} = \{\hat{Z}(x_1), \dots, \hat{Z}(x_I)\}$ is given by:

$$\hat{\boldsymbol{Z}} = \mu\mathbf{1} + \boldsymbol{\beta}^{\mathsf{T}}\left(\boldsymbol{Z} - \mu\mathbf{1}\right) \tag{2.112}$$

Figure 2.11 shows the effect that the choice of correlation length θ has on the kriging estimate $\hat{Z}(x)$ of samples $\boldsymbol{Z}$ for the Markov correlation function $\rho_M(s)$. It is noted that the kriging estimate depends on the mean parameter which has arbitrarily been taken to be $\mu = 7$. It is also noted that the kriging estimate is independent of the scale parameter σ. The scale parameter σ only affects the confidence intervals associated with the kriging estimate since the kriging estimate is, in effect, an expected value calculation. It is observed that as the correlation length is taken in the limit $\theta \to \infty$ then the kriging interpolation using the Markov correlation function approaches linear interpolation and, as $\theta \to 0$, the kriging interpolation increasingly regresses towards the mean $\mu = 7$. In the case of extrapolation, the kriging estimate tends asymptotically towards the mean and the rate at which this occurs decreases as the value of the correlation length θ increases.

Figure 2.12 shows the effect of the choice of correlation length θ on the kriging estimate $\hat{Z}(x)$ of samples $\boldsymbol{Z}$ for the Gaussian correlation function $\rho_G(s)$. The kriging estimate shown in Figure 2.12 is significantly different than the kriging estimate shown in Figure 2.11 despite identical random field parameters and, consequently, it is concluded that the choice of correlation function has a large influence on the kriging estimate. In particular, the derivative of the Gaussian kriging estimate is continuous at sampling locations $\boldsymbol{x_\alpha}$ whilst the derivative of the Markov kriging estimate is discontinuous at $\boldsymbol{x_\alpha}$ and this is attributed to the fact that the derivative of the Gaussian correlation function $\rho_G(s)$ is

continuous at the origin whilst the derivative of the Markov correlation function $\rho_M(s)$ is not. It should be noted that in general the kriging estimate $\hat{Z}(x)$ is less variable than a typical realisation of $Z(x)$ since the kriging estimate is effectively an average over the set of all possible realisations of $Z(x)$.

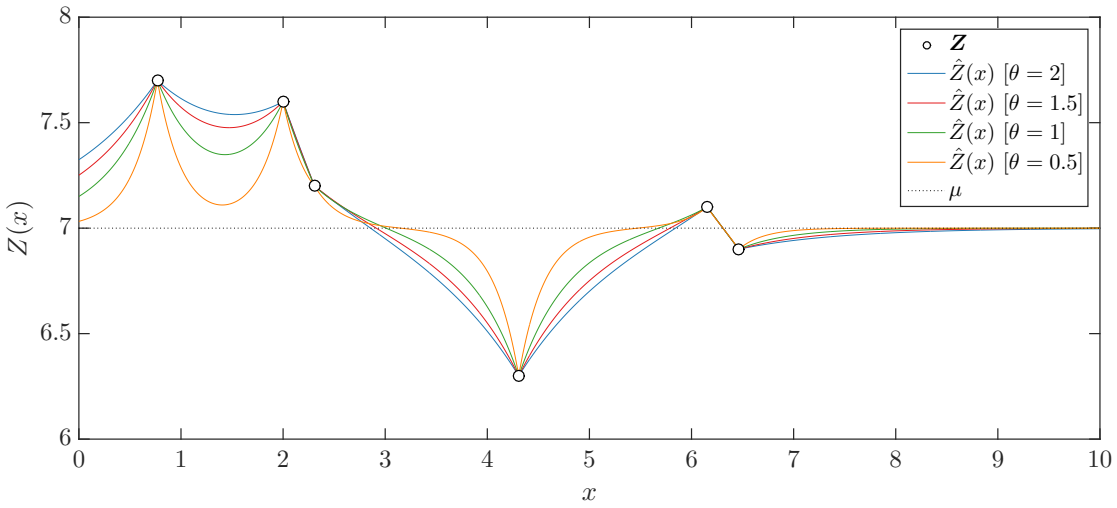


Figure 2.11: Variation of the kriging estimate $\hat{Z}(x)$ with the Markov correlation function $\rho_M(s)$ for four different values of the correlation length θ.

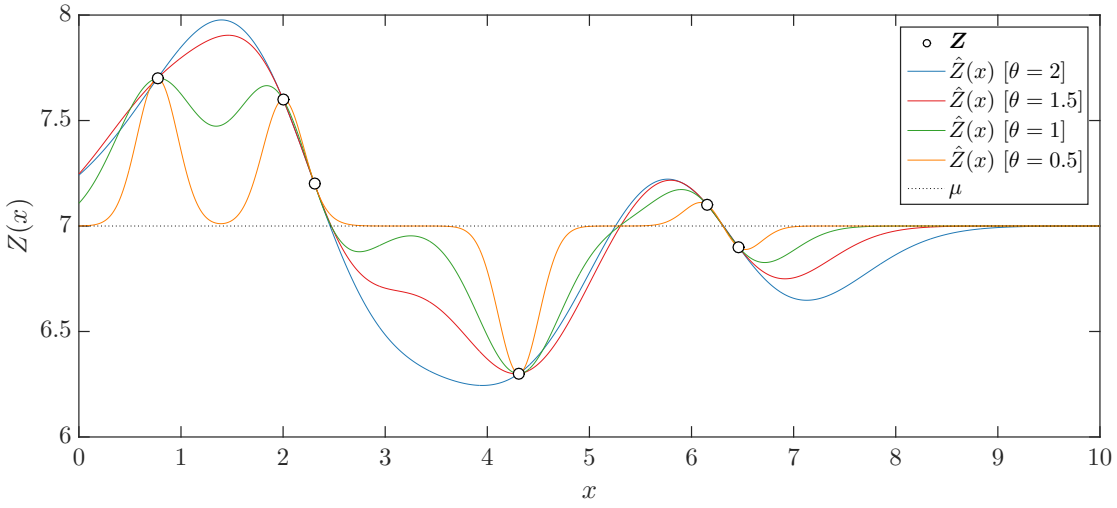


Figure 2.12: Variation of the kriging estimate $\hat{Z}(x)$ with the Gaussian correlation function $\rho_G(s)$ for four different values of the correlation length θ.

2.10.1 Kriging variance

It is desirable to quantify the uncertainty associated with the kriging interpolation $\hat{Z}(x)$ and this can be achieved through consideration of kriging error $\epsilon = \hat{Z}(x) - Z(x)$. For Gaussian processes, the error ϵ is normally distributed with mean zero and variance given by (Fenton and Griffiths, 2008, p. 129):

$$\sigma_{\epsilon}^2(x_i) = \text{Var}\left[Z(x_i) - \hat{Z}(x_i)\right] \tag{2.113}$$

$$= \sigma^2 - \boldsymbol{\beta}_i^{\intercal}\boldsymbol{C}\boldsymbol{\beta}_i \tag{2.114}$$

$$= \sigma^2 - \boldsymbol{\beta}_i^{\intercal}\boldsymbol{b}_i \tag{2.115}$$

The kriging error ϵ is homoscedastic since its variance σ_{ϵ}^2 only depends on the covariance structure, and not on the values, of the conditioning data (Chilès and Delfiner, 2012, p. 161). Consequently, in the case that the process is Gaussian, the confidence intervals based on the kriging standard deviation σ_{ϵ} constitute conditional confidence intervals. Furthermore, since the error ϵ is normally distributed then the approximate 95% confidence intervals are given by:

$$\left[\hat{Z}(x) - 2\sigma_{\epsilon}(x), \hat{Z}(x) + 2\sigma_{\epsilon}(x)\right] \tag{2.116}$$

If the kriging variance is required not only at a single location x_i, but rather at a number of locations $\{x_1, \ldots, x_I\}$, then it is an observation of this thesis that the column vector $\boldsymbol{\sigma}_{\boldsymbol{\epsilon}}^{\mathbf{2}} = \{\sigma_{\epsilon}^2(x_1), \ldots, \sigma_{\epsilon}^2(x_I)\}$ is given by:

$$\boldsymbol{\sigma}_{\boldsymbol{\epsilon}}^{\mathbf{2}} = \sigma^2\mathbf{1} - \mathbf{1}\boldsymbol{\beta}^{\intercal}\boldsymbol{b} \tag{2.117}$$

Figure 2.13 shows the 95% confidence intervals associated with the kriging estimate $\hat{Z}(x)$ of the samples $\boldsymbol{Z}$ with the Gaussian correlation function $\rho_G(s)$ and random field parameters $\mu = 7$, $\sigma = 0.5$, $\theta = 2$. It is observed that extrapolation is associated with the largest uncertainty and, as the distance from the kriging estimate $Z(x_i)$ to the nearest sample $\boldsymbol{Z}_j$ becomes large, the kriging variance approaches the variance of the random field $\sigma_{\epsilon}^2 \to \sigma^2$. Furthermore, it is observed that the interpolation between

samples is associated with moderate uncertainty that decreases to zero as the location of the kriging estimate approaches the location of a sample. It is useful to note that in the kriging methodology considered here, namely simple kriging, the uncertainty in the data is assumed to be zero; however, for kriging methodologies that takes into account experimental error consider *noisy kriging* (Picheny and Ginsbourger, 2014).

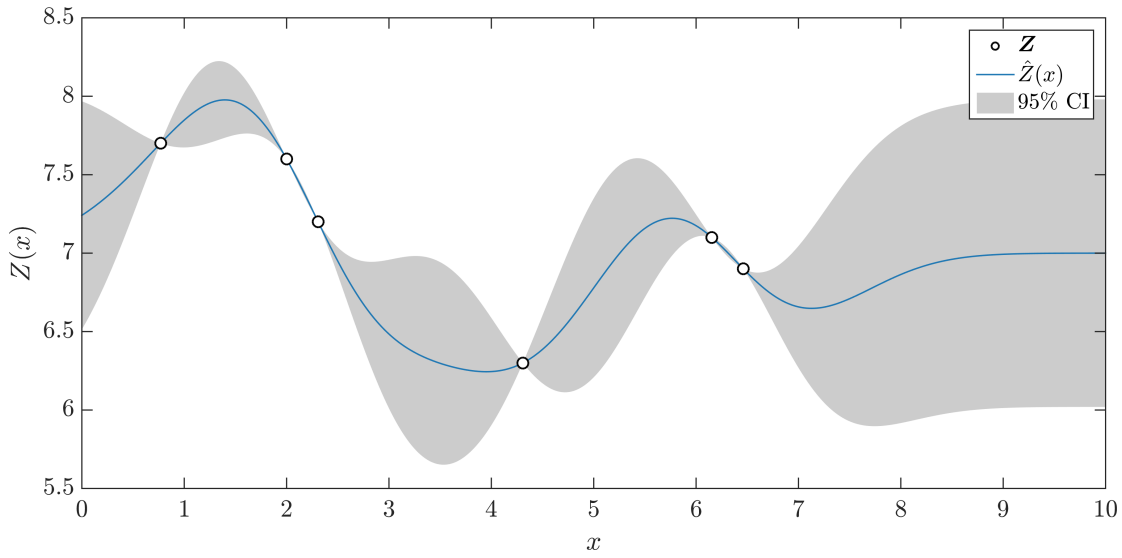


Figure 2.13: Kriging estimate $\hat{Z}(x)$ of samples $\boldsymbol{Z}$ with 95% confidence intervals shown in grey (Gaussian correlation function $\rho_G(s)$, $\mu = 7$, $\sigma = 0.5$, $\theta = 2$).

2.10.2 Conditional random fields

The theory of kriging is not only useful for estimation but can also be utilised for the efficient simulation of conditional random fields. The simulation of conditional random fields is useful to quantify the uncertainty associated with samples of a random process $\boldsymbol{Z} = Z(\boldsymbol{x_\alpha})$ located at spatial locations $\boldsymbol{x_\alpha}$. A conditional random field $Z_C(x)$ is a random field whose realisations always take the same values at the spatial locations $x = \boldsymbol{x_\alpha}$. Realisations of a conditional random field $Z_C(x)$ are given by (Journel and Huijbregts, 1978, p. 495):

$$Z_C(x) = Z_U(x) + Z_K(x) - Z_{KU}(x) \tag{2.118}$$

where: $Z_U(x)$ is an unconditional realisation of the random field,

$Z_K(x)$ is the simple kriging estimate of the samples $\boldsymbol{Z}$,

$Z_{KU}(x)$ is the simple kriging estimate of the values of $Z_U(\boldsymbol{x_a})$.

Figure 2.14 shows three realisations of a conditional random field $Z_C(x)$ whose realisations have fixed values at spatial locations $\boldsymbol{x_\alpha}$. It is observed that the realisations remain roughly within the 95% confidence intervals illustrated in Figure 2.13. Furthermore, it is worth recognising that the kriging interpolation and variance can be intuitively thought of as equivalent to simulating an infinite number of conditional realisations through the sample points and then computing the mean and variance of this ensemble respectively. The remainder of this chapter presents and evaluates methods to simulate the unconditional realisations of a random field.

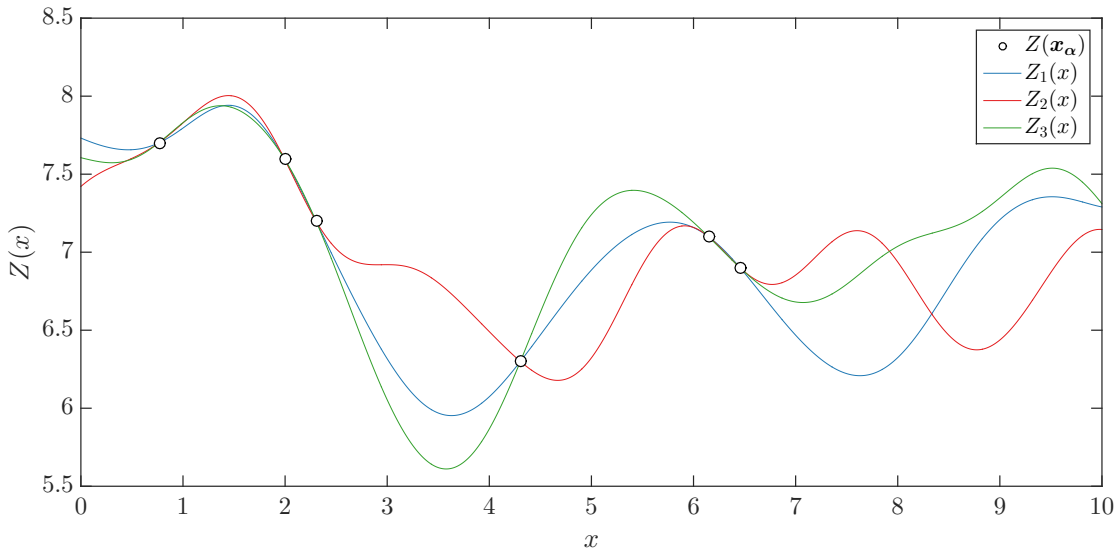


Figure 2.14: Three realisations of a conditional random field $Z_C(x)$ whose realisations take the same values $\boldsymbol{Z}$ at spatial locations $\boldsymbol{x_\alpha}$.

2.11 Overview of simulation

The simulation of random fields requires the discretisation of a continuous random field $Z(x)$ into a discrete-space approximation given by a random vector $\boldsymbol{Z}$ and it should be noted that the accuracy of this approximation is dependent on the choice of discretisation method. Sudret and Kiureghian (2000, p. 9) identify three types of discretisation methods for random fields namely *point discretisation*, *average discretisation* and *series expansion*. In both point and average discretisation methods, the domain D is subdivided into a finite number of elements $\boldsymbol{\Omega} = \{\Omega_1, \Omega_2, \ldots, \Omega_N\}$ and the field $Z(x)$ is then

approximated in each element Ω_i as:

$$Z_i = \int_{\Omega_i} \omega(x) Z(x) \, \mathrm{d}\Omega_i \tag{2.119}$$

where $\omega(x)$ is the spatial weighting function. The random vector $\boldsymbol{Z}$ that approximates $Z(x)$ is then given by:

$$\boldsymbol{Z} = \begin{bmatrix} Z_1 & Z_2 & \dots & Z_N \end{bmatrix}^{\mathsf{T}} \tag{2.120}$$

The point discretisation method considered in this thesis is the *midpoint method* which approximates the field in each element using as random variable Z_i equal to the value of the field at the centroid x_c of the element as follows (Sudret and Kiureghian, 2000, p. 10):

$$Z_i = Z(x_c), \quad x_c \in \Omega_i \tag{2.121}$$

The midpoint method is equivalent to taking the weighting function $\omega(x)$ in Equation 2.119 to be the Dirac delta function $\delta(x - x_c)$ so that a point sample at the centroid x_c is obtained. The advantage of the midpoint method is its simplicity, however, it should be noted that the midpoint method has been shown to over-represent the variability of the random field in each element Ω_i (Kiureghian and Ke, 1988). This motivates the use of spatial average methods, such as the method proposed by Vanmarcke and Grigoriu (1983), where the weighting function $\omega(x)$ that is taken to be uniform over the element Ω_i. The advantage of spatial average methods is that they better represent the variability of the random field; however, the disadvantage is that the determination of the correct type of average can be complex especially for the non-linear averages associated with many types of effective properties.

The final discretisation technique, known as the series expansion method, decomposes the random field with respect to orthogonal basis functions and this expansion is then truncated in order to render a discretised approximation to the continuous random field. This thesis adopts a unified approach to discretisation under the midpoint approximation and, consequently, the orthogonal basis functions are only evaluated at the centroids of

the element Ω_i. This approach promotes consistency between the discretisation methods, however, it should be noted that this approach does not take full advantage of series expansion methods which are detailed further in Sudret and Kiureghian (2000). The truncated series expansion of the random field $Z(x)$ in each element is given by:

$$Z_i = \sum_{m=0}^{M-1} \omega_m(x) Z_m(x) \tag{2.122}$$

The effect of truncating the expansion at $m = M - 1$ is that the variance of the random field is artificially decreased and it should be recognised that the extent of reduction of variance depends on the magnitude of M. It is noted that this reduction in variance is to some extent compensated by the over-representation of variability associated with the midpoint approximation. Figure 2.15 shows a comparison of local average and midpoint discretisation methods for a single realisation of a random field. The use of local average discretisation is not considered further within this thesis, instead this thesis focusses on two methods to simulate random fields under the midpoint approximation namely covariance matrix decomposition and the fast Fourier transform method.

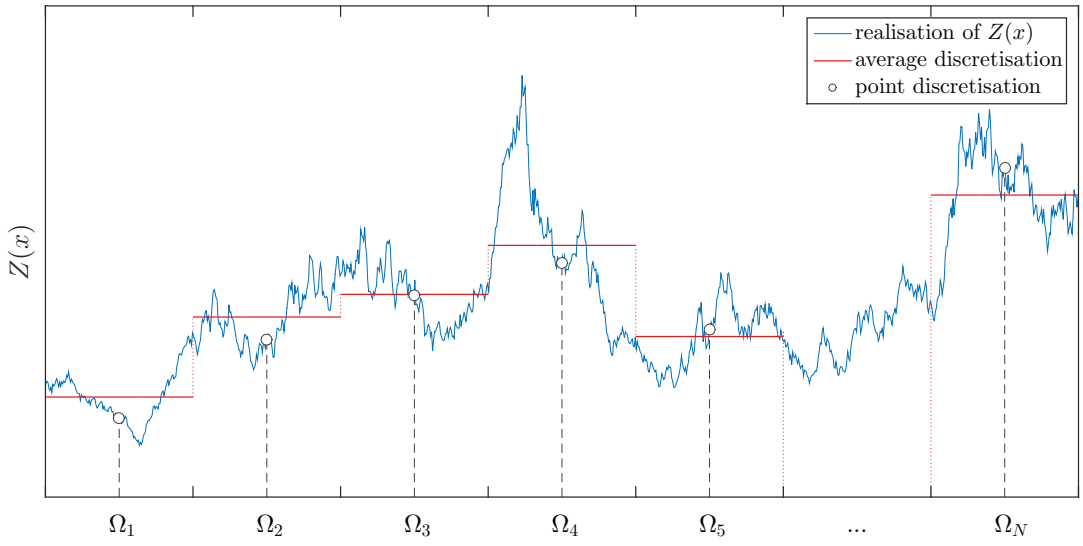


Figure 2.15: Illustrative comparison of local average and midpoint discretisation of a single realisation of the random field $Z(x)$ discretised into N elements Ω_i.

2.12 Covariance matrix decomposition method

A method to simulate a random column vector $\boldsymbol{Z}$ consisting of N normally distributed random variables with mean μ, standard deviation σ and correlation matrix $\boldsymbol{\rho}$ was first presented by Scheuer and Stoller (1962). This method later came to be known as the covariance matrix decomposition (CMD) method and is based on the following decomposition of the random vector $\boldsymbol{Z}$ (Fenton, 1994):

$$\boldsymbol{Z} = \mu + \sigma\boldsymbol{\psi}\boldsymbol{\xi} \tag{2.123}$$

where $\boldsymbol{\xi}$ is a column vector of N uncorrelated mean-zero, unit variance normal random variables and $\boldsymbol{\psi}$ is an N by N matrix that satisfies the following decomposition of the correlation matrix $\boldsymbol{\rho}$:

$$\boldsymbol{\rho} = \boldsymbol{\psi}\boldsymbol{\psi}^{\intercal} \tag{2.124}$$

The effect of multiplying the column vector of independent normal random variables $\boldsymbol{\xi}$ by the square matrix $\boldsymbol{\psi}$ is to introduce statistical dependency according to the desired correlation structure. A verification that the random vector $\boldsymbol{Z}$ has the desired statistical properties can be found in Appendix A.3. Two methods are considered to obtain the matrix $\boldsymbol{\psi}$: the first method utilises Cholesky decomposition whilst the second method utilises eigendecomposition. In the Cholesky implementation of CMD, the square matrix $\boldsymbol{\psi}$ is obtained as a real lower triangular matrix through a modified from of Gaussian elimination. In comparison, the eigendecomposition implementation is based on the following decomposition of of $\boldsymbol{\rho}$ (Zhang and Ellingwood, 1994):

$$\boldsymbol{\rho} = \boldsymbol{V}\boldsymbol{\Lambda}\boldsymbol{V}^{-1} \tag{2.125}$$

where $\boldsymbol{V}$ is a square $N \times N$ matrix whose i^{th} column is the eigenvector V_i of $\boldsymbol{\rho}$ and $\boldsymbol{\Lambda}$ is a diagonal matrix whose elements are the corresponding eigenvalues. Since $\boldsymbol{\Lambda}$ is a diagonal matrix then it can be factorised such that the correlation matrix $\boldsymbol{\rho}$ is given by:

$$\boldsymbol{\rho} = \boldsymbol{V}\sqrt{\boldsymbol{\Lambda}}\sqrt{\boldsymbol{\Lambda}}\boldsymbol{V}^{-1} \tag{2.126}$$

where $\sqrt{\boldsymbol{\Lambda}}$ is simply given by the pointwise square root of each of the diagonal entries of $\boldsymbol{\Lambda}$. The desired square matrix $\boldsymbol{\psi}$ is then given by:

$$\boldsymbol{\psi} = \boldsymbol{V}\sqrt{\boldsymbol{\Lambda}} \tag{2.127}$$

It has been observed that the eigendecomposition implementation of CMD is closely related to the Karhunen-Loève expansion of a random field under the midpoint approximation (Zhang and Ellingwood, 1994). Additionally, the simulation of realisations of a two-dimensional random field can be achieved through CMD by vectorising the discretised two-dimensional field into a single column vector $\boldsymbol{Z}$ as discussed in Section 2.7. A numerical issue that often occurs with certain covariance functions, such as the Gaussian correlation function $\rho_G(s)$, is that the correlation between neighbouring points in the covariance matrix becomes one due to numerical round-off errors and this renders the computed covariance matrix invalid since it is not positive semi-definite (Fenton and Griffiths, 2008, p. 111). This problem is resolved through the method proposed by Higham (2002) that finds the so-called *nearest correlation matrix* through the minimisation of the Frobenius norm.

2.13 Fast Fourier transform method

The spectral representation of a random field is of great utility since it implies that realisations of the random field can be simulated through the summation of random sinusoids provided that the sinusoidal expansion is suitability truncated and that the frequency spectrum is suitably discretised. If this method is implemented in conjunction with fast Fourier transform (FFT) algorithms (Cooley and Tukey, 1965) then random field realisations can be simulated with great computational efficiency. However, the disadvantage of the FFT method is that both the spatial and frequency domains must be discretised into an equal number of elements and that the number of elements must be equal to a power of 2. Section 2.5 presents two equivalent spectral representations of a stochastic process $Z(x)$ namely the random phase angle and random amplitude formulations. In

the limiting case, as the number of sinusoids becomes large $M \to \infty$, then these representations are equal; however, in the case that the spectral representation is truncated then these formulations can no longer be said to be equal. Consequently, the discrete spectra approximation $\bar{Z}(x) \approx Z(x)$ is associated with different errors and computational costs depending on whether the random phase angle or random amplitude formulation is adopted. The random phase angle formulation is the most popular representation (Stefanou, 2009), however, it is an observation of this section that this representation is associated with several fundamental limitations. The discretised random phase angle formulation is given by a truncation of Equation 2.32:

$$\bar{Z}(x_j) = \sqrt{2} \sum_{m=0}^{M-1} \sqrt{G(f_m)\Delta f} \cos(f_m x_j + \phi_m) \tag{2.128}$$

where: M is the number of sinusoidal terms,

$G(f_m)$ is the one-sided spectral density function at frequency f_m,

Δf is the non-zero interval of frequency discretisation,

ϕ_m is a uniform random variable on $[0, 2\pi]$.

In order to take advantage of FFT algorithms, the random phase angle formulation can be rewritten using Euler's formula as (see Appendix A.2):

$$\bar{Z}(x_j) = \mathrm{Re}\left\{ \sqrt{2} \sum_{m=0}^{M-1} \sqrt{G(f_m)\Delta f}\, \mathrm{e}^{\mathrm{i}\phi_m} \mathrm{e}^{\mathrm{i} f_m x_j} \right\} \tag{2.129}$$

where Re{.} is the real part operator. The discretised random amplitude formulation is given by a truncation of Equation 2.34:

$$\bar{Z}(x_j) = \sum_{m=0}^{M-1} \left[A_m \cos(f_m x_j) + B_m \sin(f_m x_j) \right] \tag{2.130}$$

where the random amplitudes, A_m and B_m, are mean-zero random variables. It is useful to note that the random amplitude formulation can similarly be written into a form suitable to take advantage of FFT algorithms (see Appendix A.2):

$$\bar{Z}(x_j) = \mathrm{Re}\left\{\sum_{m=0}^{M}(A_m - iB_m)\mathrm{e}^{\mathrm{i}f_m x_j}\right\} \tag{2.131}$$

In both the random phase angle and random amplitude formulations the spectral density function is discretised into M components. As a result of this, the truncated spectral density function $G(f_m)$ is only defined for $0 \leq m < M$ and, consequently, $G(f_M)$ is undefined. It is observed that it is useful to define the truncated spectral density function periodically so that $G(f_m) = G(f_{m+M})$ and, consequently, this implies that $G(f_M) = G(f_0)$. This simplifies the definition of the variances of the random amplitudes, A_m and B_m, which are given by:

$$\mathbb{E}\left[A_m^2\right] = \begin{cases} \frac{1}{2}G(f_m)\Delta f & \text{if } m = 0 \\ \frac{1}{4}\left[G(f_m) + G(f_{M-m})\right]\Delta f & \text{if } m = 1, \ldots, \frac{M}{2} - 1 \\ G(f_m) & \text{if } m = \frac{M}{2} \end{cases} \tag{2.132}$$

$$\mathbb{E}\left[B_m^2\right] = \begin{cases} 0 & \text{if } m = 0, \frac{M}{2} \\ \frac{1}{4}\left[G(f_m) + G(f_{M-m})\right]\Delta f & \text{if } m = 1, \ldots, \frac{M}{2} - 1 \end{cases} \tag{2.133}$$

The variances of A_m and B_m are identical except at the edge point $m = 0$ and midpoint $m = M/2$. At the midpoint, the variance of A_m is doubled whilst at the edge point and midpoint the variance of B_m is zero. The random amplitudes, A_m and B_m, do not need to be generated over the whole domain due to the following symmetry conditions (noting the antisymmetry relationship for B_m):

$$\left.\begin{aligned} A_m &= A_{M-m} \\ B_m &= -B_{M-m} \end{aligned}\right\} \quad \text{if } \frac{M}{2} < m < M \tag{2.134}$$

Figure 2.16 shows the symmetry conditions of the random amplitudes, A_m and B_m, in one-dimensional space $\mathbb{R}^1$ where the filled circles indicate points at which the random amplitudes need to be generated and the hollow circles where they are given by symmetry. It has been observed that the covariance structure of random fields generated using the fast Fourier transform technique are always symmetric about the mid-lines of the field

(Fenton, 1994). This problem is resolved by generating a field twice as larger as desired and only keeping the first half.

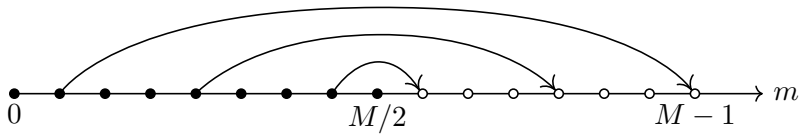


Figure 2.16: Illustration of the symmetries of the random amplitudes, A_m and B_m, in $\mathbb{R}^1$ where filled circles indicates the random amplitudes to be generated and hollow circles indicate random amplitudes given by symmetry.

The random phase angle formulation, given by Equation 2.128, and the random amplitude formulation, given by Equation 2.130, both have comparative advantages and disadvantages. The advantage of the random amplitude formulation is that the realisations are *strongly ergodic* (Grigoriu, 1993) which implies that all realisations are ergodic. However, in comparison, realisations of the random amplitude formulation are only *weakly ergodic* which implies that only some realisations are ergodic. In practical terms, the effect of this is that the deterministic coefficient formulation converges more rapidly to the desired statistics (Fenton, 1990, p. 15). A further advantage of the random phase angle formulation is that it is less computationally expensive since only half the number of random variables are required to be simulated for each realisation in comparison to the random amplitude formulation. However, the disadvantage of the random phase angle formulation is that the simulated realisations have an artificial lower and upper bound since the absolute value of the realisations is subject to the following inequality:

$$|\overline{Z}(x_j)| \leq \sqrt{2} \sum_{m=0}^{M-1} \sqrt{G(f_m)\Delta f} \tag{2.135}$$

Furthermore, an additional disadvantage of the random phase angle formulation is that the marginal distribution of the realisations is only approximately Gaussian for a large number M of sinusoidal terms (Grigoriu, 1993). In conclusion, if computational efficiency is prioritised then the random phase angle formulation is recommended; however, if accuracy is prioritised, as is the case within this thesis, then the random amplitude formulation should be pursued. Finally, it is worth briefly considering the effects of discretisation on the accuracy of the simulated realisations. If the spatial domain $[0, L]$

is discretised into J points then the spatial interval of discretisation Δx is given by:

$$\Delta x = \frac{L}{J-1} \tag{2.136}$$

Since space and frequency are discretised equally $M = J$ then the frequency interval Δf is given by (Fenton, 1994):

$$\Delta f = \frac{2\pi}{J\Delta x} = \frac{2\pi(J-1)}{JL} \approx \frac{2\pi}{L} \tag{2.137}$$

It is observed that the frequency interval Δf is approximately independent of the degree of discretisation J. This implies that the size of the domain L needs to be sufficiently large in order that a sufficiently fine discretisation of the spectral density function is achieved. If the domain is not sufficiently large then the spectral density function will be coarsely discretised resulting in distortion of the correlation structure. Consequently, it may be necessary to generate a field with domain L larger than required and discard the excess. A further consideration is the frequency beyond which the spectral density is neglected, known as the cut-off frequency f_U, which is given by:

$$f_U = \Delta f(J-1) \approx \frac{2\pi(J-1)}{L} \tag{2.138}$$

The effect of increasing the size of the domain L, without an approximately equal increase in the degree of discretisation J, is to decrease the cut-off frequency f_U. This may lead to an excessive truncation of the spectral density function which, in turn, results in decreased variance of the simulated realisations. Consequently, in order to achieve accurate simulation with the fast Fourier transform method, it needs to be ensured that the field is both sufficiently large with an adequately high degree of discretisation.

2.13.1 Two-dimensional implementation

The same approach to use fast Fourier transform algorithms to efficiently generate realisations of a random process $Z(x)$ through its spectral representation can be utilised to efficiently generate realisations of a random field $Z(x, y)$. The truncation of the two-

dimensional random phase angle formulation is not considered here, however, details of its implementation can be found in Shinozuka and Deodatis (1996). The discretised random amplitude spectral representation of a random field $Z(x, y)$ is given by the truncation of Equation 2.43:

$$\bar{Z}(x_j, y_k) = \sum_{n=0}^{N-1} \sum_{m=0}^{M-1} \left[A_{m,n} \cos(f_m x_j + f_n y_k) + B_{m,n} \cos(f_m x_j + f_n y_k) \right] \tag{2.139}$$

This can be rewritten in a form suitable for the use of fast Fourier transform algorithms using Euler's formula (see Appendix A.2):

$$\bar{Z}(x_j, y_k) = \mathrm{Re} \left\{ \sum_{n=0}^{N-1} \mathrm{e}^{i f_n y_k} \sum_{m=0}^{M-1} (A_{m,n} - \mathrm{i} B_{m,n}) \mathrm{e}^{\mathrm{i} f_m x_j} \right\} \tag{2.140}$$

Similar to the one-dimensional case, it is noted that simplified expressions for the variances of the random amplitudes, $A_{m,n}$ and $B_{m,n}$, are obtained by defining the truncated spectral density function periodically such that $G(f_m, f_n) = G(f_{m+M}, f_n) = G(f_m, f_{n+N})$. The variances of the mean-zero normally distributed random amplitudes, $A_{m,n}$ and $B_{m,n}$, are given by:

$$\mathbb{E}\left[A_{m,n}^2\right] = \begin{cases} \Delta f_m \Delta f_n G(f_m, f_n) & \text{if } m = 0, \frac{M}{2} \text{ and } n = 0, \frac{N}{2} \\ \dfrac{\Delta f_m \Delta f_n}{8} \left[G(f_m, f_n) + G(f_{M-m}, f_n) + G(f_m, f_{N-n}) + G(f_{M-m}, f_{N-n}) \right] & \text{otherwise} \end{cases} \tag{2.141}$$

$$\mathbb{E}\left[B_{m,n}^2\right] = \begin{cases} 0 & \text{if } m = 0, \frac{M}{2} \text{ and } n = 0, \frac{N}{2} \\ \dfrac{\Delta f_m \Delta f_n}{8} \left[G(f_m, f_n) + G(f_{M-m}, f_n) + G(f_m, f_{N-n}) + G(f_{M-m}, f_{N-n}) \right] & \text{otherwise} \end{cases} \tag{2.142}$$

The variance of $A_{m,n}$ and $B_{m,n}$ are identical except at the corner points ($m = 0, \frac{M}{2}$ and $n = 0, \frac{N}{2}$) where the variance of $A_{m,n}$ is doubled and the variance of $B_{m,n}$ is zero. If the spectral density function is quadrant symmetric, the random amplitudes have two symmetry lines at $m = M/2$ and $n = N/2$. Consequently, the random amplitudes exhibit the following horizontal symmetries:

$$\left.\begin{aligned} A_{m,n} &= A_{M-m,n} \\ B_{m,n} &= B_{M-m,n} \end{aligned}\right\} \text{ if } \frac{M}{2} < m < M, \frac{N}{2} < n < N \tag{2.143}$$

and the following vertical symmetries (noting the antisymmetry relationship for $B_{m,n}$):

$$\left.\begin{aligned} A_{m,n} &= A_{m,N-n} \\ B_{m,n} &= -B_{m,N-n} \end{aligned}\right\} \text{ if } \frac{M}{2} < m < M, \frac{N}{2} < n < N \tag{2.144}$$

Only the case of quadrant symmetric spectral density functions, as presented in Subsection 2.4.1, have been considered here, however, for the case of a non-quadrant symmetric spectral density function consider Fenton (1994). The symmetries of the random amplitudes are illustrated in Figure 2.17 where the lines of symmetry are shown as dashed lines, the filled circles indicate the points at which the random amplitudes are to be generated and the hollow circles indicate the random amplitudes that are given by symmetry. Similar to the one-dimensional case, the covariance structure of the field is symmetric about the midlines and, consequently, a field four times as large as is required is to be generated and the excess discarded.

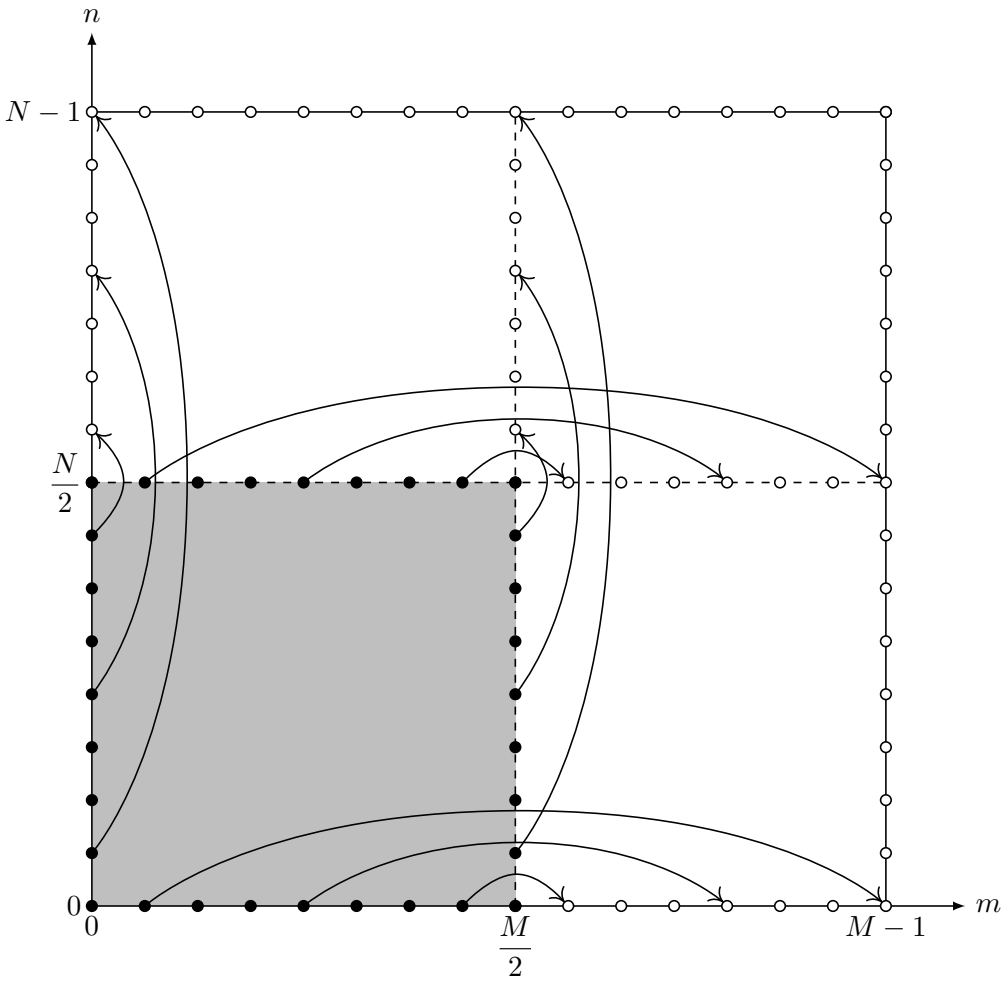


Figure 2.17: Symmetries of random amplitudes, $A_{m,n}$ and $B_{m,n}$, of a quadrant symmetric random field where lines of symmetry are shown as dashed lines, filled circles indicate random amplitudes to be generated and hollow circles indicate random amplitudes given by symmetry.

2.14 Evaluation of simulation methods

This section presents the results of a computer experiment designed to evaluate the computational performance of the simulation methods presented within this chapter. The methods that are compared are the Cholesky and eigendecomposition implementations of covariance matrix decomposition (CMD) as well as the random amplitude implementation of the fast Fourier transform (FFT) method. The analysis has been performed on a PC with an i3-4150 CPU and 16 GB of ram and the results are only valid for the specific implementation of the CMD and FFT algorithms in the Matlab toolbox `RFbox`. Figure 2.18 shows the computational time t in seconds to generate realisations of a random field consisting of $N_\Omega = 1000$ elements against the number of realisations N_R for all three simulation methods. The FFT method has a negligible initial cost whilst the CMD methods have significant initial costs associated with the decomposition of the covariance matrix. It is observed that the initial cost, for the case of $N_\Omega = 1000$ elements, is substantially larger for the eigendecomposition implementation of CMD in comparison to the Cholesky implementation. As the number of simulated realisations N_R increases, the computational cost associated with all simulation methods increases linearly where the gradients of the Cholesky and eigendecomposition implementations of CMD are approximately equal whilst the gradient of FFT is higher. It is concluded that as the required number of realisations of the random field increases, the relative computational efficiency of CMD compared to FFT increases. Consequently, if a large number of realisations are to be generated then CMD is the most computationally efficient simulation method.

Figure 2.19 shows a logarithmic plot of the computational time t in seconds to generate $N_R = 1000$ realisations of a random field against number of elements N_Ω for all three simulation methods. It is observed that if the field consists of a small number of elements N_Ω then the Cholesky and eigendecomposition implementations of CMD are significantly more efficient than FFT. However, as the size of the field increases the computational cost of FFT scales linearly with the number of elements N_Ω whilst the computational cost associated with both implements of the CMD method increases non-linearly. It is concluded that the rapid increase in computational cost associated with CMD, especially the eigendecomposition implementation, implies that this method is unsuitable for the simulation of large random fields.

In the evaluation of simulation methods, it is important to consider the computational

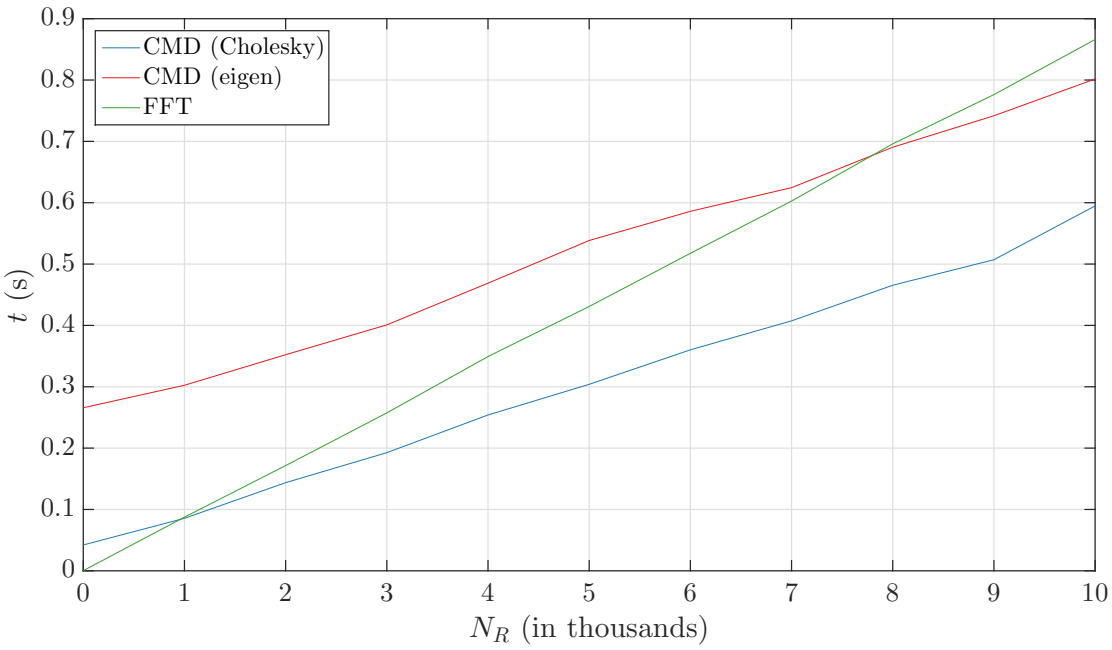


Figure 2.18: Computational time t in seconds to generate N_R realisations of a random field consisting of $N_\Omega = 1000$ elements for the three simulation methods.

efficiency and accuracy of each method. The most efficient method for the simulation of small to medium sized random fields is CMD, however, both implementations of CMD suffer from faster than linear scaling of computational cost t with the number of elements N_Ω. It is observed that the eigendecomposition implementation of CMD is computationally inferior to the Cholesky implementation; however, eigendecomposition may be advantageous in the case of near singular covariance matrices for which the Cholesky algorithm would be unstable and produce inaccurate results (Straka et al., 2013). For the simulation of large random fields, FFT is more computationally efficient due to the linear scaling of the computational cost t with the number of elements N_Ω. However, the disadvantages of FFT are that the representation of the covariance structure of the random field is less accurate due to the discretisation of the spectral density function and that the accurate simulation of lognormal random processes requires matching of the spectral density functions (Shields et al., 2011). Finally, it should be noted that in the two-dimensional case, the computational cost associated with FFT is doubled due to the requirement that a field approximately four times larger than desired is generated whereas in the one-dimensional case only a field twice as large is required.

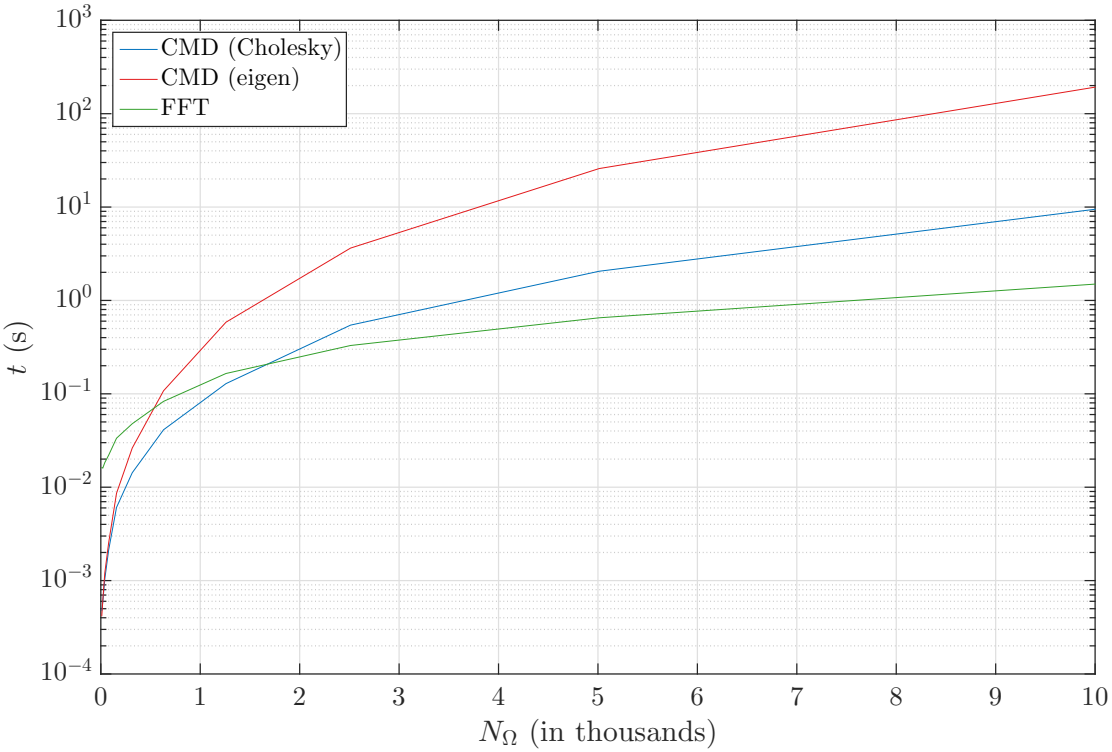


Figure 2.19: Logarithmic computational time t in seconds to generate $N_R = 1000$ realisations of a random field consisting of N_Ω elements for the three simulation methods.

2.15 Conclusion

This chapter has presented and developed upon the theory of random fields relating to their analytical properties, methodologies to estimate their parameters and techniques to simulate their realisations. In particular, the contribution of this chapter has been to present the theory of random fields with a focus on the situation where samples of multiple realisations are available. The case of multiple realisations has not received in much attention within the literature since random fields have primarily been applied within the geotechnical domain for which there is only a single realisation namely the Earth. However, the application of random fields to timber requires a more general approach since each tree of a species is considered to be a different realisation of the same stochastic process. The key achievements of this chapter are summarised as:

- A wide range of correlation functions have been considered with respect to the properties of their sample paths, higher-dimensional extensions and equivalent spectral representations in the frequency domain. It has been recommended that the use of white noise processes within a structural context is not to be pursued due to

issues with measurability as recognised by Kallianpur (1980). Additionally, an analytical closed form expression for the constant of the generalised power function parametrised with the correlation length as defined by Vanmarcke (2015) has been presented.

- The theory for the estimation of random fields has been presented including techniques to infer the parameters of a random field, such as method of moments and maximum likelihood estimation, as well as the technique of kriging which estimates the value of a realisation at an unobserved location. Furthermore, analysis has been presented with regards to the efficient computation of the sample correlation function using Fourier transforms and the efficient computation of the likelihood function for the case of multiple realisations.

- The theory for the simulation of random fields has been presented including discussion of discretisation methods with particular reference to the simulation techniques of covariance matrix decomposition and the fast Fourier transform method. A periodic definition of the discretised spectral density function has been introduced and an evaluation of the three simulation methods has been presented including recommendations on when each method should be utilised with respect to both computational cost and accuracy.

The techniques presented in this chapter relating to estimation and simulation have been implemented in the Matlab toolbox `RFbox`. The theory of random fields presented within this chapter, in conjunction with this toolbox, is used in the following chapters of this thesis to analyse the behaviour of randomly heterogeneous beams.

Chapter 3

Theory of heterogeneous beams

3.1 Introduction

A beam is a slender structural element that offers resistance to applied load through flexure which induces shear forces and bending moments within the beam resulting in internal stresses and strains that are in equilibrium with the external forces. The *flexural rigidity* of a beam is a material property that is related to the magnitude of resistance offered by the beam whilst undergoing flexural deformation during bending. A beam is considered heterogeneous if its flexural rigidity is not spatially constant but rather a function of position v along the length of the beam. There are many causes of variation in flexural rigidity, however, this variation can fundamentally be attributed to either irregularity of the cross-section, leading to non-constant area moment of inertia I or to spatially varying material properties leading to non-constant modulus of elasticity. In the case of steel beams, a common cause of variation in flexural rigidity is the inclusion of web-openings which provide access for services such as pipelines and air conditioning and cause a fluctuating second moment of area I (Redwood and Cho, 1993). An additional cause of variable second moment of area I are tapered beam profiles which are utilised since less steel can be used in regions with low internal bending moment leading to both financial and weight savings.

A less visually apparent, yet equally significant, source of variation in flexural rigidity is the use of heterogeneous materials with non-constant material properties in the construction of beams. Many commonly used materials for the construction of beams are highly

heterogeneous such as concrete, a composite of fine and coarse aggregates combined with cement (Mosley et al., 2007), and timber which a severely anisotropic naturally produced composite grown for the purposes of the tree rather than a material optimised for beam performance (Porteous and Kermani, 2007). The uncertain material properties associated with these heterogeneous materials can pose a significant risk and, consequently, approaches have been developed to mitigate the risk associated with the heterogeneity of these materials. In the case of concrete, the proportion of aggregates is carefully controlled and vibratory techniques are used to ensure correct aggregate distribution in order to mitigate against the occurrence of a dangerous degree of inhomogeneity. In the case of timber, beams are graded into structural classes based on the effective modulus of elasticity and this ensures that the beam has sufficient flexural characteristics prior to structural usage.

In the consideration of the causes of beam heterogeneity, it is important to not only consider innate factors relating to cross-section design or choice of material but also the influence of environmental factors over time. For instance, the resistance of timber to flexural deflection is known to be significantly affected by atmospheric moisture content as well as the load-duration effect (Köhler and Svensson, 2011). Furthermore, the exposure of a beam to non-uniform environmental conditions can be a significant cause of heterogeneity; for example, a steel beam exposed to high temperatures caused by fire can lead to non-uniform reduction in the modulus of elasticity (Kodur and Dwaikat, 2009). Additionally, the flexural rigidity of reinforced concrete beams can be non-uniformly degraded over time through corrosion resulting from either carbonation or chlorine attack which leads to oxidation of the steel reinforcement and the formation of rust. It is observed that the effect that corrosion of steel rebar has on flexural rigidity is often modelled through the local reduction of beam cross-section (Coronelli and Gambarova, 2004, Stewart, 2009). However, it should be recognised that rust has a greater volume than steel and, consequently, corrosion is not associated with a change in cross-section but rather a change in material properties. This demonstrates that variation in flexural rigidity can to a large extent be modelled through the variation of either elastic modulus E and/or second moment of area I and that these properties are largely interchangeable for the purposes of analysis. For reasons of simplicity, this chapter only considers variation in elastic modulus E since this is the material property that has principally been considered within random field modelling of beams (Kline et al., 1986, Taylor and Bender, 1991, Wang and Foschi, 1992). However, it should be noted that the results

presented within this chapter equally apply to the effect that variation of the second moment of area I has on flexural rigidity.

There has been extensive research to quantify the risk associated with heterogeneous beams, however, this research has mostly relied on the stochastic finite element method (Stefanou, 2009) to analyse the behaviour of: cantilevers (Vanmarcke and Grigoriu, 1983, Spanos and Ghanem, 1989, Ishida, 2001); simply supported beams under 3-point (García and Rosales, 2017, Sasikumar et al., 2014), 4-point (Kandler and Füssl, 2017, Casciati and Domaneschi, 2007) and uniformly distributed loading (Wang and Foschi, 1992, Chang and Chang, 1994); as well as the heterogeneous tensile behaviour of cantilevers (Füssl et al., 2016). Additionally, there has been some limited consideration of the analytical behaviour of stochastic beams namely the second order characteristics of the displacement profile (Arwade and Deodatis, 2011, Shen et al., 2014, Elishakoff et al., 1995), moments of vibration (Kukla and Owczarek, 2005, Grigoriu, 2015) as well as analysis under the assumption of periodic heterogeneity (Buannic and Cartraud, 2001).

The research direction adopted within this chapter is to develop an analytical approach to heterogeneous beam behaviour based on the formulation of the effective elastic modulus of Euler-Bernoulli beams as a weighted harmonic mean. This result was first presented by Bechtel (1985), however, this contribution has received relatively little attention in the intermediary years. It is shown in this chapter that the manipulation of this formulation yields an elegant approach to the formidable challenge associated with the analysis of randomly heterogeneous beams. This research is motivated by the following quote:

> "Even for the simplest structural configurations such as beams whose elastic properties may be viewed as realizations of a one-dimensional stationary random process, the challenge to the analyst is formidable." (Vanmarcke and Grigoriu, 1983)

The specific case considered by Bechtel (1985) was the midspan deflection of an Euler-Bernoulli beam under 3-point loading. The contribution of this chapter is to extend this theory by formulating the effective elastic modulus at any point along the beam as a weighted harmonic mean for the case of 3-point, 4-point and uniformly distributed loading conditions. The weighting functions corresponding to each of these loading conditions are derived and it is then shown how the variance of displacement of a randomly

heterogeneous beam is given by an expression which integrates over these weighting functions.

It is of interest to consider how the contributions of this chapter fit into the wider literature on mean field homogenisation theory which is concerned with the prediction of the macroscale behaviour of systems with microscale variation. It is noted that mean field theory originated within statistical physics, however, it has since found wide application in a range of disciplines including computer science, statistics and communication theory (Opper and Saad, 2007). The theory is concerned with the development of multi-scale methods that substitute an average, known as an effective property, in order to simplify systems that exhibit scale dependent behaviour such as partial differential equations with rapidly oscillating coefficients which are often used to model the mechanical behaviour of heterogeneous materials (Pavliotis and Stuart, 2007). In particular, mean field theory is interested in the determination of *representative volume elements* which are deterministic continuum equivalents to the microscale variability of materials. It is noted that the determination of representative volume elements is achieved through asymptotic homogenisation which assumes that if the volume of the element is sufficiently large then, in the limiting case as $L/\theta \to \infty$, the material properties become deterministic (Bakhvalov and Panasenko, 1989). However, Ostoja-Starzewski (2006) states that in practice this assumption may be hard to justify since it assumes that the microscale heterogeneity is periodic thereby facilitating what is known as *separation of scales* so that the scale of microscale heterogeneity may be considered small in comparison to the size of the volume element. In the case that separation of scales can not be justified, the alternative is to instead consider *statistical volume elements* which are randomly distributed effective material properties corresponding to the homogenisation of non-periodic microstructure (Ostoja-Starzewski and Wang, 1999). Within this context, it is important to note that the effective material properties considered within this thesis are statistical volume elements that are variable for any particular realisation of the stiffness profile rather than representative volume elements.

To provide an overview, this chapter is primarily concerned with the meta-problems of prediction, in particular, the prediction of the displacement U and effective modulus of elasticity E^* of an Euler-Bernoulli beam with a stochastic stiffness profile $E(v)$. In Section 3.2, a single realisation of elastic modulus $E(v, q)$ is considered and the determination of the corresponding deterministic displacement profile $U(x, q)$ and effective

elastic modulus $E^*(x,q)$ is detailed including the derivation of the spatial weighting function $\omega(v)$. In Section 3.3, an ensemble of stiffness profiles $E(v)$ is considered including the derivation of analytical expressions for the moments of the stochastic displacement profile $U(x)$ and quasi-analytical moments of the random effective elastic modulus $E^*(x)$. In Section 3.4, a sensitivity analysis is performed investigating the variation of the moments of displacement U, and the effective elastic modulus E^*, with the distance x along a simply supported beam as well as the variation of these moments with the coefficient of variation c_v and correlation length θ of the stiffness profile $E(v)$. Finally, the key contributions of this chapter are summarised in Section 3.5 and recommendations are made for the direction of future research.

3.2 Deterministic effective properties

Within the context of the meta-problem framework outlined in Chapter 1, this section considers *meta-problem 1 – deterministic prediction*:

$$E(v,q) \longrightarrow U(x,q) \longrightarrow E^*(x,q) \tag{3.1}$$

where $E(v,q)$ is a realisation of the one-dimensional random field $E(v)$ for a single point q in the sample space $q \in Q$ and $U(x,q)$ is the observed deterministic vertical displacement of the beam from which the deterministic effective elastic modulus $E^*(x,q)$ is calculated. It is shown in this section how the effective elastic modulus $E^*(x,q)$ can be formulated as a weighted harmonic mean which facilitates the analytical computation of the displacement $U(x,q)$ of a heterogeneous beam. In order to simplify the notation, the parameter q is dropped when it is sufficiently from context that only a single realisation of the random field is under consideration.

The fundamental result of this section is to show that, for a range of different loading conditions, the effective elastic modulus E^* of an Euler-Bernoulli beam can be formulated as a weighed harmonic mean:

$$E^*(x) = \left(\int_0^L \omega(v|x) \cdot E(v)^{-1} \, \mathrm{d}v \right)^{-1} \tag{3.2}$$

where $(.)^{-1}$ denotes the pointwise reciprocal such that $E(v)^{-1} = \left\{ v_i \in D | \frac{1}{E(v_i)} \right\}$ where D is the domain of the integration $D = [0, L]$ with L being the length of the beam. The weighting function $\omega(v|x)$ expresses the dependency of displacement U, at position x, on the elastic modulus E, at position v, and satisfies the following property:

$$\int_0^L \omega(v|x)\,\mathrm{d}v = 1 \tag{3.3}$$

where the units of the weighting function $\omega(v|x)$ are given by the reciprocal of the units of the domain D so that the right-hand side of this equation is dimensionless. It is important to note that Euler-Bernoulli beam theory neglects the effects of shear and, consequently, the weighting functions derived in this chapter, as well as the resulting analysis, only strictly apply to slender beams for which the negligence of shear effects is reasonable.

The Euler-Bernoulli equation relates the second derivative of vertical displacement U to the internal bending moment M as follows:

$$\frac{\mathrm{d}^2 U(x)}{\mathrm{d}x^2} = \frac{M(x)}{E(x)I} \tag{3.4}$$

where E is the modulus of elasticity and I is the second moment of area which is assumed to be constant within this thesis. It is noted that the traditional method to obtain the vertical deflection U of the beam is the method of double integration. Before continuing further, it is useful to make a remark on the notation adopted within this chapter for the description of variation along the length of the beam. Vertical deflection U and effective elastic modulus E^* are parametrised with the variable x and the bending moment M, elastic modulus E and the derived weighting functions ω are parametrised with the variable v. The utility of this notation is that the dependency of the vertical deflection U, or the effective elastic modulus E^*, at a point x can be expressed in terms of the modulus of elasticity E at any point v along the span. To further complicate the issue, it is good practice to avoid writing multiple integrals as integrals of the same variable and, consequently, the first integral associated with Equation 3.4 is with respect to the parameter u whilst the second integral is with respect to the parameter v.

The first derivative of displacement is obtained through the standard integration of

Equation 3.4:

$$\frac{\mathrm{d}U(x)}{\mathrm{d}x} = \frac{1}{I}\int_0^x \frac{M(u)}{E(u)}\,\mathrm{d}u + C \tag{3.5}$$

where C is the first constant of integration and the limits of this indefinite integral are associated with the variable change discussed above. The first derivative of displacement has a useful physical interpretation as the slope of the beam at any position x. The standard method of integration is then repeated to obtain the vertical deflection $U(x)$ of the beam as follows:

$$U(x) = \frac{1}{I}\int_0^x \int_0^u \frac{M(v)}{E(v)}\,\mathrm{d}v\,\mathrm{d}u + Cx + D \tag{3.6}$$

where D is the second constant of integration. For the case of a simply supported beam, the constants of integration are determined by the following boundary conditions:

$$U|_{x=0} = 0 \implies D = 0 \tag{3.7}$$

$$U|_{x=L} = 0 \implies C = -\frac{1}{LI}\int_0^L \int_0^u \frac{M(v)}{E(v)}\,\mathrm{d}v\,\mathrm{d}u \tag{3.8}$$

Substituting these expressions for the constants of integration, C and D, into Equation 3.6 gives:

$$U(x) = \frac{1}{I}\int_0^x \int_0^u \frac{M(v)}{E(v)}\,\mathrm{d}v\,\mathrm{d}u - \frac{x}{LI}\int_0^L \int_0^u \frac{M(v)}{E(v)}\,\mathrm{d}v\,\mathrm{d}u \tag{3.9}$$

Through an interchange of the order of integration, the double integral is reduced to a single integral (see appendix B.1):

$$U(x) = \frac{1}{I}\int_0^x \frac{M(v)(x-v)}{E(v)}\,\mathrm{d}v - \frac{x}{LI}\int_0^L \frac{M(v)(L-v)}{E(v)}\,\mathrm{d}v \tag{3.10}$$

The analysis of the displacement of a simply supported beam continues with the consideration of three expressions for bending moment $M(v)$ corresponding to 3-point $M_3(v)$,

4-point $M_4(v)$ and uniformly distributed $M_0(v)$ loading. It is shown in this section how the weighting functions associated with each of these loading conditions can be derived through the formulation of the effective elastic modulus E^* as a weighted harmonic mean. Furthermore, the steps of algebraic manipulation are shown explicitly for the case of 3-point loading so that the method by which the weighting function is derived can be understood thereby facilitating the repetition of this calculation for other loading and boundary conditions of interest.

3.2.1 Three-point loading

The 3-point bending test, as shown in Figure 3.1, is used extensively to evaluate the flexural properties of materials such as rigid plastics (BS EN 178:2010), biomaterials (Temenoff and Mikos, 2008) and timber (Johansson, 2003). In particular, the machine grading of timber utilises a continuous rolling flatwise implementation of the 3-point bending test (Porteous and Kermani, 2007, p. 12) and, consequently, the effective elastic modulus E^* is not constant but instead varies with the spatial parameter x. The advantage of the 3-point bending test is that it is simple to implement since it only requires the application of a single point load, however, this test has been criticised for the highly non-uniform stress distribution induced by the single point load which leads to an effective elastic modulus E_3^* that is not particularly representative of the whole span stiffness profile $E(v)$.

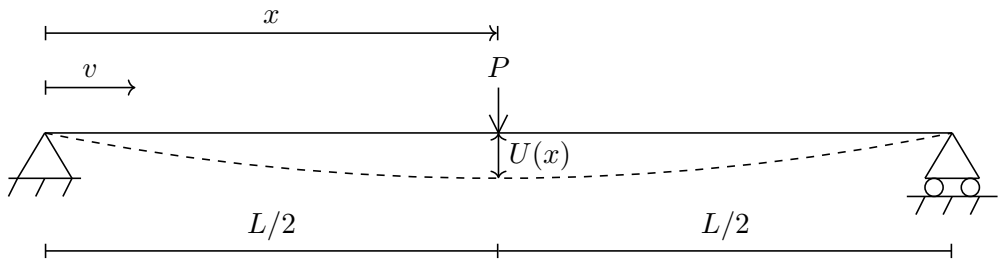


Figure 3.1: One-dimensional model of a simply supported beam of length L under 3-point loading of magnitude P resulting in vertical displacement $U(x)$.

The bending moment $M_3(v)$ induced by the 3-point load of magnitude P is given by:

$$M_3(v) = \begin{cases} -\dfrac{Pv}{2} & \text{if } 0 \leq v \leq \dfrac{L}{2} \\ -\dfrac{P(L-v)}{2} & \text{if } \dfrac{L}{2} \leq v \leq L \end{cases} \tag{3.11}$$

The equation for bending moment $M_3(v)$ is a piecewise function whose domain is split into subdomains at the midspan $v = L/2$ due to the point load. Substituting the expression for bending moment under 3-point loading $M_3(v)$ into the expression for the deflection $U(x)$ of a simply supported beam, given by Equation 3.10, and considering the case of $0 \leq x \leq L/2$ gives:

$$U(x) = \frac{1}{I}\int_0^x -\frac{Pv(x-v)}{2E(v)}\,\mathrm{d}v - \frac{x}{LI}\left(\int_0^{L/2} -\frac{Pv(L-v)}{2E(v)}\,\mathrm{d}v + \int_{L/2}^{L} -\frac{P(L-v)^2}{2E(v)}\,\mathrm{d}v\right) \tag{3.12}$$

$$= \frac{P}{2I}\left(\int_0^x -\frac{v(x-v)}{E(v)}\,\mathrm{d}v + \int_0^{L/2} \frac{xv(L-v)}{LE(v)}\,\mathrm{d}v + \int_{L/2}^{L} \frac{x(L-v)^2}{LE(v)}\,\mathrm{d}v\right) \tag{3.13}$$

Splitting the interval of integration of the middle term so that the domains of integration of each term do not overlap gives:

$$\begin{aligned} U(x) = \frac{P}{I}\Bigg(&\int_0^x -\frac{vL(x-v)}{LE(v)}\,\mathrm{d}v + \int_0^x \frac{xv(L-v)}{LE(v)}\,\mathrm{d}v \\ &+ \int_x^{L/2} \frac{xv(L-v)}{LE(v)}\,\mathrm{d}v + \int_{L/2}^{L} \frac{x(L-v)^2}{LE(v)}\,\mathrm{d}v\Bigg) \end{aligned} \tag{3.14}$$

Noting that $xv(L-v) - vL(x-v) = v^2(L-x)$, the first and second terms combine to give:

$$U(x) = \frac{P}{2LI}\left(\int_0^x \frac{v^2(L-x)}{E(v)}\,\mathrm{d}v + \int_x^{L/2} \frac{xv(L-v)}{E(v)}\,\mathrm{d}v + \int_{L/2}^{L} \frac{x(L-v)^2}{E(v)}\,\mathrm{d}v\right) \tag{3.15}$$

It is important to note that this expression for vertical displacement $U(x)$ is only valid for $0 \leq x \leq L/2$ with the other case $L/2 \leq x \leq L$ being given by (see Appendix B.2):

$$U(x) = \frac{P}{2LI}\left(\int_0^{L/2} \frac{v^2(L-x)}{E(v)}\,\mathrm{d}v + \int_{L/2}^{x} \frac{v(L-v)(L-x)}{E(v)}\,\mathrm{d}v + \int_x^L \frac{x(L-v)^2}{E(v)}\,\mathrm{d}v\right) \tag{3.16}$$

Thus, an expression for the vertical deflection of a heterogeneous beam at any point x in the domain $D = [0, L]$ is given through the consideration of Equations 3.15 – 3.16. In order to obtain an expression for the 3-point effective elastic modulus $E_3^*(x)$, this result must be combined with an equivalent expression for deflection under homogeneous beam theory. The deflection U of a beam, for $0 \leq x \leq L/2$, under 3-point loading with constant modulus of elasticity $E_3^*(x)$ is given by:

$$U(x) = \frac{Px\left(3L^2 - 4x^2\right)}{48E_3^*(x)I} \tag{3.17}$$

An expression for the effective modulus of elasticity $E_3^*(x)$ is obtained through a change in the subject of the equation:

$$E_3^*(x) = \frac{Px\left(3L^2 - 4x^2\right)}{48\,U(x)\,I} \tag{3.18}$$

Substituting the expression for displacement $U(x)$ for $0 \leq x \leq L/2$, given by Equation 3.15, into this expression for the effective elastic modulus $E_3^*(x)$ and simplifying gives:

$$E_3^*(x) = \frac{xL\left(3L^2 - 4x^2\right)}{24\left(\int_0^x \frac{v^2(L-x)}{E(v)}\,\mathrm{d}v + \int_x^{L/2} \frac{xv(L-v)}{E(v)}\,\mathrm{d}v + \int_{L/2}^{L} \frac{x(L-v)^2}{E(v)}\,\mathrm{d}v\right)} \tag{3.19}$$

The variables P and I cancel due to the independence of the effective modulus of elasticity from either the load P or the second moment of area I. It can now be seen that the 3-point effective elastic modulus $E_3^*(x)$ is of the form of a weighted harmonic mean given by:

$$E_3^*(x) = \left(\int_0^L \omega_3(v|x) \cdot E(v)^{-1}\,\mathrm{d}v\right)^{-1} \tag{3.20}$$

where $\omega_3(v|x)$ is the 3-point weighting function which, for $0 \leq x \leq L/2$, is given by:

$$\omega_3(v|x) = \begin{cases} \dfrac{24v^2(L-x)}{xL(3L^2-4x^2)} & \text{if } 0 \le v \le x \\ \dfrac{24v(L-v)}{L(3L^2-4x^2)} & \text{if } x \le v \le \dfrac{L}{2} \\ \dfrac{24(L-v)^2}{L(3L^2-4x^2)} & \text{if } \dfrac{L}{2} \le v \le L \end{cases} \tag{3.21}$$

It is noted that the case of $L/2 \le x \le L$ can be obtained via symmetry through the substitution of $L - x$ in place of x in Equation 3.21. Figure 3.2 illustrates the 3-point weighting function $\omega_3(v|x)$ for six different locations x of displacement U. It is observed that the 3-point weighting function $\omega_3(v|x)$ is unimodal and always attains a maximum at midspan independent of the point x at which deflection is observed. Consequently, it is concluded that the 3-point effective elastic modulus $E_3^*(x)$ is always most representative of the midspan stiffness of the beam. Furthermore, it can be seen, for any x, that as $v \to 0$ then $\omega_3 \to 0$ and, consequently, it is concluded that the stiffness of the beam near the supports always has a negligible contribution to both the displacement U and the effective elastic modulus $E_3^*(x)$. Finally, it is noted that the derivative of the weighting function $\omega_3(v|x)$ is discontinuous at the midspan $v = L/2$ and the point $v = x$ at which deflection U is observed.

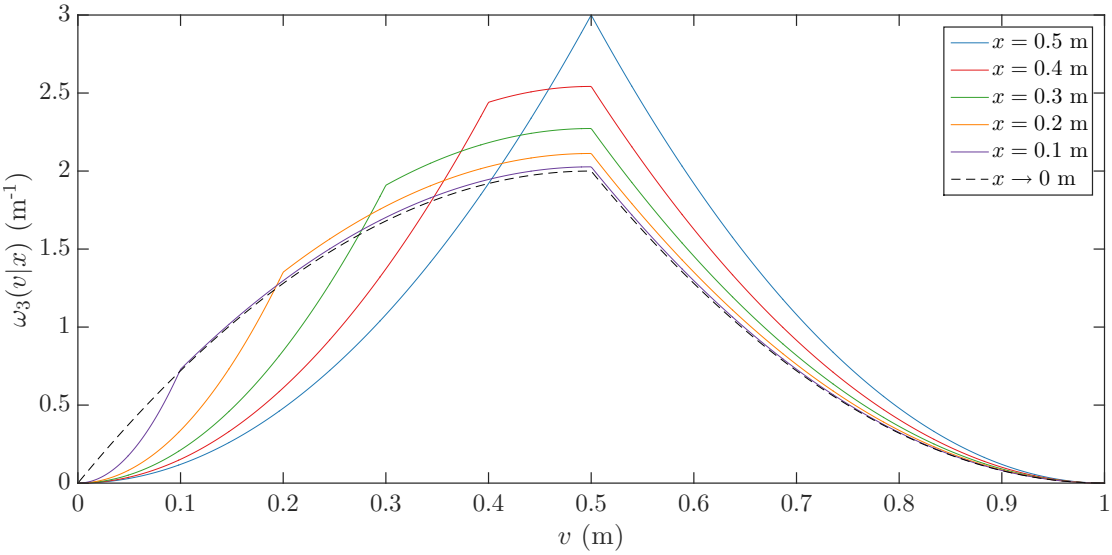


Figure 3.2: 3-point weighting function $\omega_3(v|x)$ against position v along the beam for six different points x of observed deflection ($L = 1$ m).

3.2.2 Uniformly distributed loading

It is useful to recognise that all loads are to some extent distributed loads, however, when the size of the distribution is small in comparison to the length of the beam then the distributed load can reasonably be approximated as a point load. For example, it is often appropriate to model the load imparted by a secondary beam onto a primary beam as a point load corresponding to the 3-point loading condition. Whilst this is a reasonable approximation in the majority of cases, it should be noted that this may not always result in a sufficiently accurate stress distribution which motivates the direct consideration of distributed loads. In particular, this chapter only considers the case of uniformly distributed loading (UDL) over the whole length of the beam, as shown in Figure 3.3, which results from sources of loading such as self-weight or slab loading.

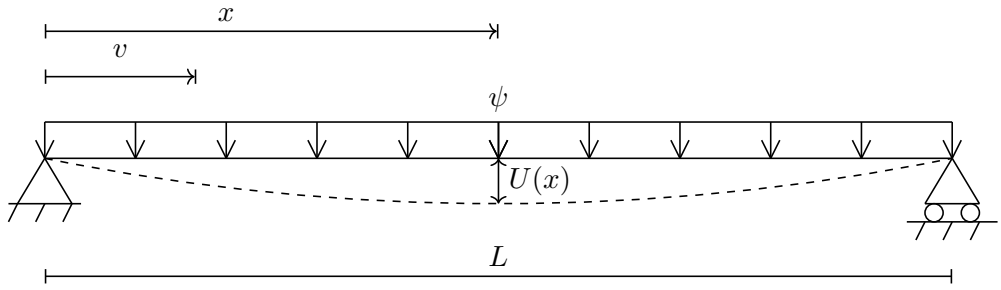


Figure 3.3: One-dimensional model of a simply supported beam of length L under uniformly distributed loading of magnitude ψ resulting in vertical displacement $U(x)$.

The bending moment $M_0(v)$ resulting from the UDL of magnitude ψ is given by:

$$M_0(v) = \frac{\psi v(L-v)}{2} \tag{3.22}$$

and the associated UDL weighting function $\omega_0(v|x)$ for the case of $0 \leq x \leq L$ is given by (see Appendix B.3):

$$\omega_0(v|x) = \begin{cases} \dfrac{12(L-v)v^2}{xL(L^2+xL-x^2)} & \text{if } 0 \leq v \leq x \\ \dfrac{12(L-v)^2 v}{L(L-x)(L^2+xL-x^2)} & \text{if } x \leq v \leq L \end{cases} \tag{3.23}$$

Figure 3.4 illustrates the UDL weighting function $\omega_0(v|x)$ for six different points x of

observed displacement U. In the case that $L/3 \leq x \leq 2L/3$, the UDL weighting function $\omega_0(v|x)$ attains a maximum at the point at which deflection U is observed $v = x$. However, in the case that stiffness is observed near to the supports, as either $x < L/3$ or $x > 2L/3$, then the maximum is attained at either $v = L/3$ or $v = 2L/3$ respectively. The varying location of maximum weighting associated with the UDL weighting function $\omega_0(v|x)$ is in contrast with the constant location of the maximum of the 3-point weighting function $\omega_3(v|x)$ which is always located midspan $v = L/2$. A further contrast between the UDL $\omega_0(v|x)$ and 3-point $\omega_3(v|x)$ weighting functions is that the gradient of $\omega_0(v|x)$ has at most a single discontinuity whilst the gradient of $\omega_3(v|x)$ has two discontinuities. However, the similarities between the UDL $\omega_0(v|x)$ and 3-point $\omega_3(v|x)$ weighting functions include the fact that they are both unimodal and that as $v \to 0$ then $\omega \to 0$. Finally, it is useful to note that the shape of the weighting function is invariant to changes in the length L of the beam; however, the weighting function must scale so that its integral over the length of the beam remains equal to one.

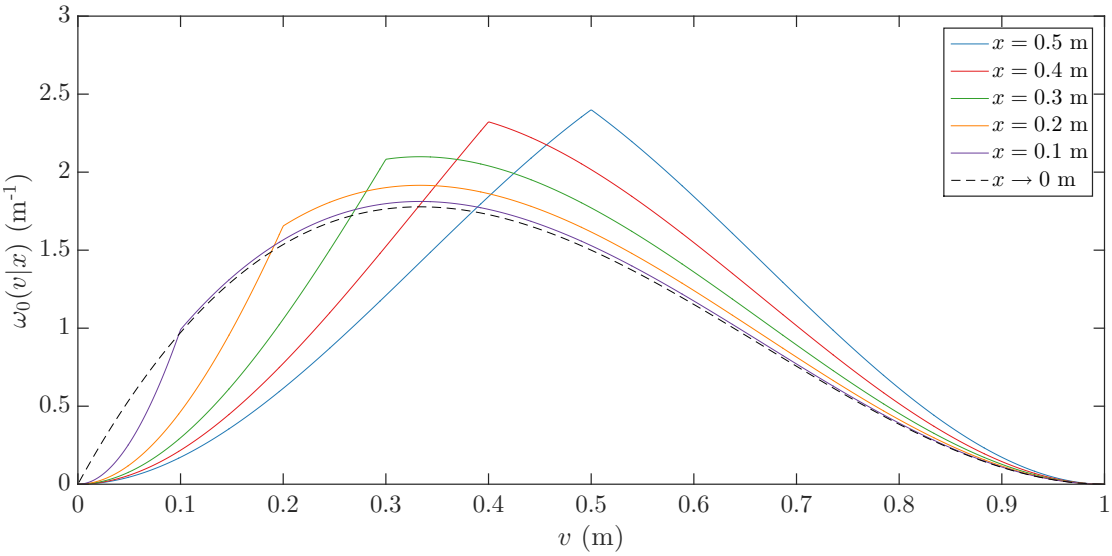


Figure 3.4: Variation of the UDL weighting function $\omega_0(v|x)$ against position v along the beam for six points x of observed deflection U ($L = 1$ m).

3.2.3 Comparison of loading conditions

This subsection contains a comparison of the 3-point, 4-point and UDL bending tests in terms of the dependency of the effective elastic modulus on the underlying stiffness profile $E(v)$ as quantified by the weighting functions $\omega(v|x)$. It is noted that the methods to experimentally determine the effective elastic modulus E^*, through either 3-point

(Johansson, 2003) or 4-point loading (BS EN 408:2010), exclusively consider the midspan effective elastic modulus $E_c^* = E^*(x_c)$. The importance of the midspan displacement of a simply supported beam under symmetrical loading is that, under homogeneous theory, this is the location of maximum deflection and, under heterogeneous theory, this is the point for which the weighting functions are symmetric.

The 3-point weighting function $\omega_3(v|x_c)$ for midspan deflection $U_3(x_c)$ is given by:

$$\omega_3(v|x_c) = \begin{cases} \dfrac{12v^2}{L^3} & \text{if } 0 \leq v \leq \dfrac{L}{2} \\ \dfrac{12(L-v)^2}{L^3} & \text{if } \dfrac{L}{2} \leq v \leq L \end{cases} \tag{3.24}$$

The UDL weighting function $\omega_0(v|x_c)$ for midspan deflection $U_0(x_c)$ is given by:

$$\omega_0(v|x_c) = \begin{cases} \dfrac{96(L-v)v^2}{5L^4} & \text{if } 0 \leq v \leq \dfrac{L}{2} \\ \dfrac{96(L-v)^2v}{5L^4} & \text{if } \dfrac{L}{2} \leq v \leq L \end{cases} \tag{3.25}$$

Another loading condition of great importance is 4-point bending which is the standard test for the static grading of timber according to BS EN 408:2010. Figure 3.5 shows an illustration of the four-point loading set-up with two point loads of magnitude $P/2$ at the ternary points $v = L/3$ and $v = 2L/3$. The advantage of the 4-point being test is that the central region of the beam is placed under a constant bending moment resulting in an effective elastic modulus E_4^* which is more representative of the whole span stiffness profile in comparison to the 3-point bending test.

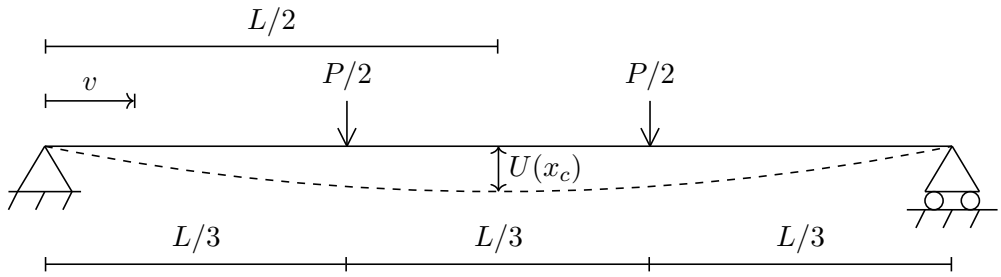


Figure 3.5: One-dimensional model of a simply supported beam of length L undergoing 4-point bending with two loads of magnitude $P/2$ which results in vertical midspan displacement $U(x_c)$.

The bending moment $M_4(v)$ associated with 4-point loading is given by:

$$M_4(v) = \begin{cases} -\dfrac{Pv}{2} & \text{if } 0 \le v \le \dfrac{L}{3} \\ -\dfrac{PL}{6} & \text{if } \dfrac{L}{3} \le v \le \dfrac{2L}{3} \\ -\dfrac{P(L-v)}{2} & \text{if } \dfrac{2L}{3} \le v \le L \end{cases} \tag{3.26}$$

The 4-point weighting function $\omega_4(v|x_c)$ for midspan deflection $U_4(x_c)$ is given by (see Appendix B.4):

$$\omega_4(v|x_c) = \begin{cases} \dfrac{324v^2}{23L^3} & \text{if } 0 \le v \le \dfrac{L}{3} \\ \dfrac{108vL}{23L^3} & \text{if } \dfrac{L}{3} \le v \le \dfrac{L}{2} \\ \dfrac{108(L-v)L}{23L^3} & \text{if } \dfrac{L}{2} \le v \le \dfrac{2L}{3} \\ \dfrac{324(L-v)^2}{23L^3} & \text{if } \dfrac{2L}{3} \le v \le L \end{cases} \tag{3.27}$$

Figure 3.6 shows a comparison between the 3-point $\omega_3(v|x_c)$, 4-point $\omega_4(v|x_c)$ and UDL $\omega_0(v|x_c)$ weighting functions. In terms of the midspan $v = L/2$, the 3-point weighting function ω_3 assigns the highest weighting of 3.00 m^{-1} and the 4-point weighting function ω_4 assigns the lowest weighting of 2.35 m^{-1} with the UDL weighting function ω_0 assigning an intermediate weight of 2.40 m^{-1}. This order is reversed at the ternary points, $v = L/3$ and $v = 2L/3$, with the 4-point weighting function ω_4 assigning the highest weighting of 1.57 m^{-1}, followed by the UDL weighting function ω_0 assigning an intermediate weighting of 1.42 m^{-1} with the 3-point ω_3 assigning the lowest weighting of 1.33 m^{-1}. In conclusion, if it is desired that the effective elastic modulus E^* be most representative of midspan stiffness then the 3-point bending test is recommended; however, if an effective elastic modulus that is most representative of the whole stiffness profile of $E(v)$ is desired then the 4-point bending test is recommended. Finally it is noted that the UDL bending test offers a comparable alternative to the 4-point bending test with respect to the spatial weighting over the stiffness profile $E(v)$.

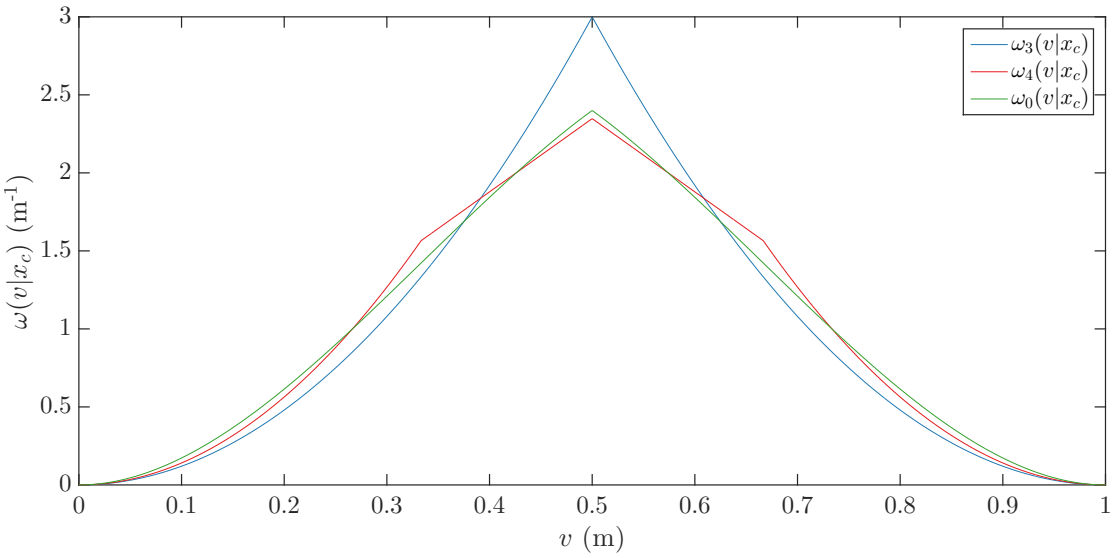


Figure 3.6: Comparison between the 3-point $\omega_3(v|x_c)$, 4-point $\omega_4(v|x_c)$ and UDL $\omega_0(v|x_c)$ weighting functions for midspan deflection $U(x_c)$ ($L = 1$ m).

3.2.4 Analytical benchmark

Benchmarks have been used extensively to verify the performance of finite element models and ensure numerical convergence to the analytical solution (Huebner et al., 2001, Bursi and Jaspart, 1997, Sze et al., 2004). An analytical benchmark is introduced here for the case of a simply supported beam under 3-point loading with linear variation of elastic modulus along the length of the beam. The reason for the consideration of linear variation in elastic modulus is that it is the simplest example of a heterogeneous beam. In particular, the contribution of this subsection is to present a novel analytical expression for the displacement profile and midspan effective elastic modulus of a simply supported beam with linear variation in stiffness under 3-point loading.

The linear stiffness profile of the benchmark heterogeneous is given by:

$$E(v) = E_0 + \frac{(E_L - E_0)\, v}{L} \quad \text{if } 0 \leq v \leq L \tag{3.28}$$

where E_0 is the value of elastic modulus at the left-hand pin support and E_L is the value of elastic modulus at the right-hand roller support. The integrals in the expression for the displacement of an Euler-Bernoulli beam under 3-point loading, given by Equation 3.15 – 3.16, have been evaluated analytically using the software Wolfram Mathematica 10.4

developed by Wolfram Research. This integration is performed under the assumption that the following variables are subsets of the positive real numbers $x, v, L, E_0, E_L \in \mathbb{R}^+$ as well as the assumption that the stiffness profile is strictly increasing $E_L > E_0$. However, the assumption that the stiffness profile is strictly increasing is only a trivial limitation since the case of $E_0 = E_L$ is given by homogeneous theory and the case of $E_0 > E_L$ is given by symmetry. It is observed that since the equation for the 3-point bending moment $M_3(v)$, given by Equation 3.11, is split into two cases at the midspan $v = v_c = L/2$ then the equation of deflection $U(x)$ is similarly subdivided. For an Euler-Bernoulli beam under 3-point loading with linear variation in elastic modulus, the displacement profile $U(x)$ for the case of $0 \leq x \leq L/2$ is given by:

$$\begin{aligned} U(x) = \frac{LP}{8E_L^3 I}\Bigg[& 4E_0^2L^2 \ln\left(\frac{E_L x}{E_0 L} + 1\right) - 4E_0^2 Lx \ln\left(\frac{L(2E_0 + E_L)}{2(E_0 L + E_L x)}\right) \\ & - 4E_0^2 Lx \ln\left(\frac{E_L x}{E_0 L} + 1\right) - 4E_0 E_L Lx \\ & - 4E_0 E_L Lx \ln\left(\frac{L(2E_0 + E_L)}{E_0 L + E_L x}\right) + E_0 E_L Lx \ln(16) \\ & + 8Lx(E_0 + E_L)^2 \tanh^{-1}\left(\frac{E_L}{4E_0 + 3E_L}\right) - E_L^2 Lx - 2E_L^2 x^2\Bigg] \end{aligned} \tag{3.29}$$

where $\ln(.)$ is the natural logarithm and $\tanh^{-1}(.)$ is the inverse hyperbolic tangent function. The displacement profile $U(x)$ for the case of $L/2 \leq x \leq L$ is given by:

$$\begin{aligned} U(x) = -\frac{LP}{8E_L^3 I^2}\Bigg[& 4E_0^2 Lx \ln\left(\frac{E_0 L + E_L x}{E_0 L + E_L L}\right) + 8E_0^2 L(x - L) \tanh^{-1}\left(\frac{E_L}{4E_0 + E_L}\right) \\ & + 4E_L^2 Lx \ln\left(\frac{E_0 L + E_L x}{E_0 L + E_L L}\right) + 4E_0 E_L L^2 - 4E_0 E_L Lx \\ & - 4E_0 L(E_0 + E_L)(L - x) \ln\left(\frac{L(2E_0 + E_L)}{2(E_0 L + E_L x)}\right) \\ & + 8E_0 E_L Lx \ln\left(\frac{E_0 L + E_L x}{E_0 L + E_L L}\right) + E_L^2 L^2 + E_L^2 Lx - 2E_L^2 x^2\Bigg] \end{aligned} \tag{3.30}$$

In addition to obtaining the analytical deflection profile from the weighted harmonic mean formulation, it is also possible to obtain an analytical expression for the effective elastic modulus E^*. The midspan effective property $E_c^* = E^*(x_c)$ of an Euler-Bernoulli beam under 3-point loading, obtained by evaluating Equation 3.19, is given by:

$$E_c^* = \frac{(E_0 - E_L)^3}{3\left[E_0^2\left(\ln(16) - 4\ln\left(\frac{E_0 + E_L}{E_0}\right) - 2\right) + E_L^2\left(8\tanh^{-1}\left(\frac{E_0 - E_L}{E_0 + 3E_L}\right) + 2\right)\right]} \tag{3.31}$$

According to homogeneous theory, the equation of displacement is a cubic equation and, consequently, it is of interest to investigate the extent to which the displacement profile $U(x)$ of a heterogeneous beam deviates from this cubic equation. Figure 3.7 shows the displacement profiles associated with four different heterogeneity ratios E_L/E_0 that, in order to facilitate comparison, have been normalised by dividing the displacement profile $U(x)$ by its maximum value $\max[U(x)]$. As the stiffness towards the right-hand support E_L increases, the location of maximum deflection deviates from midspan towards the left-hand support. However, even for large heterogeneity ratios E_L/E_0 the deviation of the location of maximum deflection from the midspan is small and, consequently, the location of maximum displacement is considered to be in a stable equilibrium (Synge and Griffith, 1949, p. 216). It is worth noting that current grading procedures only consider midspan displacement and do not take into account the location of maximum displacement. It is suggested that through consideration of the whole displacement profile using techniques such as computer vision (Olsson et al., 2013), that more accurate inferences on the stiffness profile of heterogeneous beams can be made.

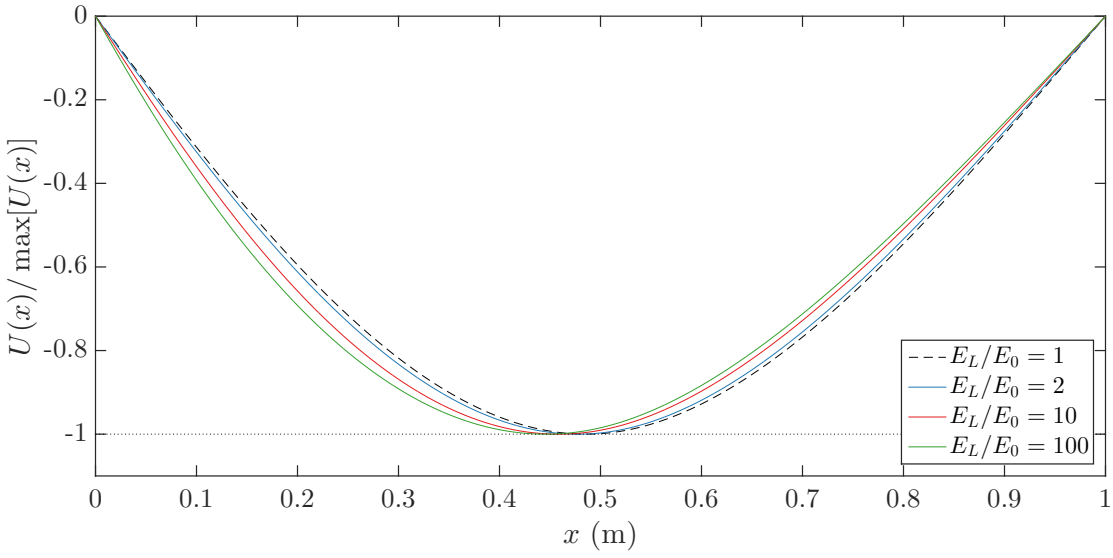


Figure 3.7: Deviation of the displacement profile $U(x)$ from a cubic equation as the heterogeneity ratio E_L/E_0 increases from the homogeneous case $E_L/E_0 = 1$ to the highly heterogeneous case $E_L/E_0 = 100$.

3.2.5 Finite element model

This subsection details the development of a finite element model (FEM) of a heterogeneous beam and the verification of this model against the benchmark presented in the previous section. Finite element modelling is a numerical technique, frequently utilised within engineering disciplines, to obtain approximate solutions to boundary value problems for partial differential equations through the discretisation of the domain D into a finite number of elements $\boldsymbol{\Omega} = \{\Omega_1, \ldots, \Omega_N\}$. The approach adopted within this chapter is to model the heterogeneous beams as a set of interconnected homogeneous beams thereby reducing the continuous variation in elastic modulus to a discrete idealisation that is accessible to numerical solution. Through the consideration of an approximation to the linear elastic constitutive equation based on the weak-form of Euler-Bernoulli theory, the local stiffness matrix $\boldsymbol{K}_i$ of the i^{th} homogeneous beam element is given by the following symmetric square matrix (Zienkiewicz and Taylor, 2005, p. 294):

$$\boldsymbol{K}_i = E_i I \begin{bmatrix} \frac{12}{L_i^3} & \frac{6}{L_i^2} & -\frac{12}{L_i^3} & \frac{6}{L_i^2} \\ \frac{6}{L_i^2} & \frac{4}{L_i} & -\frac{6}{L_i^2} & \frac{2}{L_i} \\ -\frac{12}{L_i^3} & -\frac{6}{L_i^2} & \frac{12}{L_i^3} & -\frac{6}{L_i^2} \\ \frac{6}{L_i^2} & \frac{2}{L_i} & -\frac{6}{L_i^2} & \frac{4}{L_i} \end{bmatrix} \tag{3.32}$$

where E_i and L_i are the elastic modulus and length of the i^{th} homogeneous beam element Ω_i respectively and I is the second moment of area which is treated as constant within this thesis. The stiffness matrix of the entire assemblage is obtained through the direct stiffness method which constructs the global stiffness matrix $\boldsymbol{K}$ through the summation of the local stiffness matrices $\boldsymbol{K}_i$ to a square matrix of zeroes with size equal to the number of degrees of freedom of the entire structure (Bathe, 1996, p. 151). Due to the sequential connection of the elements, the global stiffness matrix $\boldsymbol{K}$ is given by the following diagonal matrix:

$$\boldsymbol{K} = \begin{bmatrix} \boldsymbol{K}_1 & 0 & \dots & 0 \\ 0 & \boldsymbol{K}_2 & \dots & 0 \\ \vdots & \vdots & \ddots & \vdots \\ 0 & 0 & \dots & \boldsymbol{K}_N \end{bmatrix} \tag{3.33}$$

It should be noted that structural beam elements with cubic interpolation functions are exact within the context of Euler-Bernoulli beam theory (Bathe, 1996, p. 153) and, consequently, the local stiffness matrix $\boldsymbol{K}_i$ given by Equation 3.32 is exact if the beam is homogeneous. However for the case of a heterogeneous beam, the finite element model is associated with an error resulting from the approximation of the stiffness profile $E(v)$ with a piecewise constant function $\overline{E}(v)$ that has discontinuities at the element boundaries as shown in Figure 3.8.

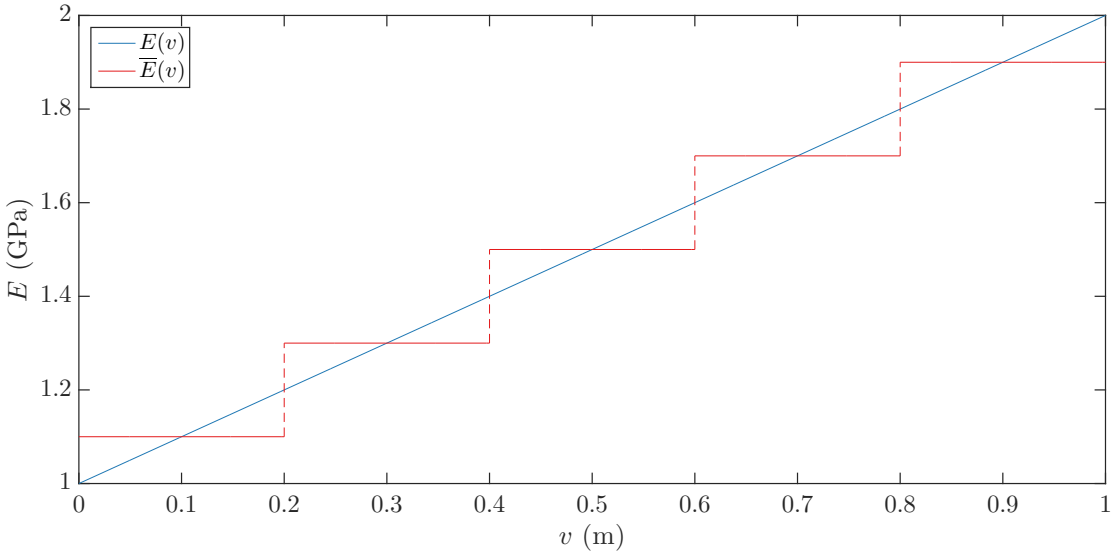


Figure 3.8: Piecewise constant approximation $\overline{E}(v)$ to the stiffness profile $E(v)$ for $N = 5$ elements ($L = 1$ m).

Prior to the application of boundary conditions, the global stiffness matrix $\boldsymbol{K}$ is singular and can not be inverted. The approach to apply the boundary conditions, given by Equations 3.7 – 3.8, is the method of reduction which involves deleting the appropriate rows and columns of the global stiffness matrix associated with zero displacement (Zienkiewicz and Taylor, 2005). The response quantity of vertical displacement $\boldsymbol{U}$ is then given under linear elastic theory by:

$$\boldsymbol{U} = \boldsymbol{K}^{-1}\boldsymbol{F} \tag{3.34}$$

For computational reasons, it is recommended that the inverse of the stiffness matrix $\boldsymbol{K}$ is not obtained directly but rather that the linear system $\boldsymbol{F} = \boldsymbol{K}\boldsymbol{U}$ is solved through the use of an iterative solver, such as the SPIKE algorithm (Polizzi and Sameh, 2006), which is less computationally expensive and more accurate. Furthermore, direct construction of the global stiffness matrix $\boldsymbol{K}$ should be avoided since handling sparse matrices is both computationally expensive and an inefficient usage of computer memory. Instead, the global stiffness matrix $\boldsymbol{K}$ should be stored as a skyline matrix (Felippa, 1975) which takes advantage of both the symmetry and sparsity of the global stiffness matrix $\boldsymbol{K}$.

A numerical investigation has been performed to investigate the effect that the number of elements N has on the accuracy of the numerical displacement profile $\overline{U}(x)$ obtained by the finite element model in comparison to the exact displacement profile $U(x)$ given by Equations 3.29 – 3.30. Figure 3.9 shows the maximum absolute percentage error MAPE[.] of the numerical displacement profile $\overline{U}(x)$ against the number N of finite elements. It is observed that for a discretisation greater than $N = 100$, the error in the numerical displacement profile $\overline{U}(x)$ obtained through the finite element model is negligible and, consequently, it is concluded that a discretisation of the order $N > 100$ suitably discretises the linear stiffness profile $E(v)$.

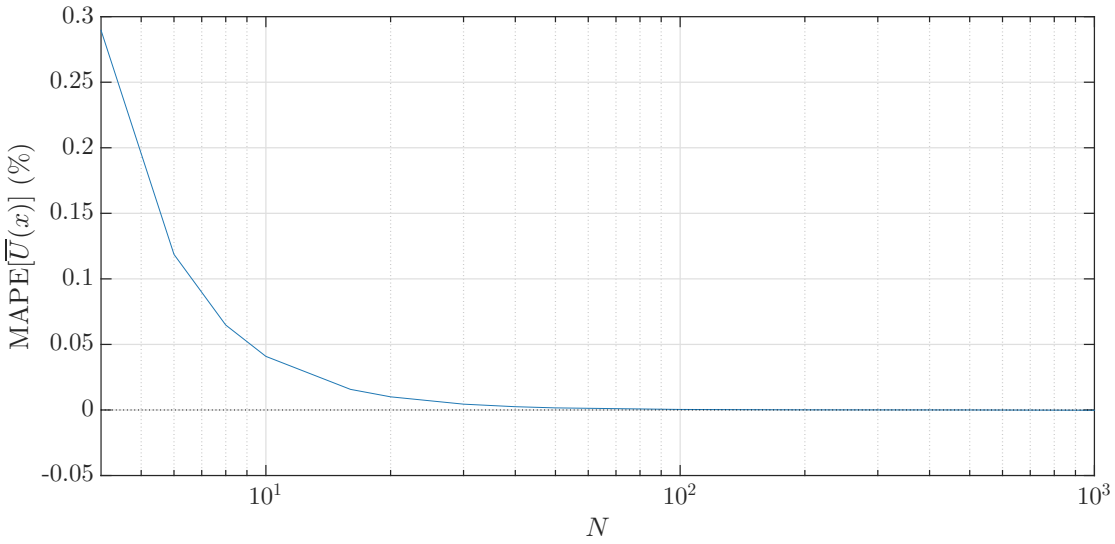


Figure 3.9: Maximum absolute percentage error of the FEM displacement profile $\overline{U}(x)$ against the number of finite elements N.

3.3 Random effective properties

Within the context of the meta-problem framework, as outlined in Chapter 1, this section considers *meta-problem 2 – stochastic prediction*:

$$E(v) \longrightarrow U(x) \longrightarrow E^*(x) \tag{3.35}$$

where $E(v)$ is a one-dimensional random field, $U(x)$ is the random displacement profile and $E^*(x)$ is the random effective elastic modulus. It has been shown in subsection 3.2.4 that, for a deterministic stiffness profile $E(v, q)$, it is possible to analytically compute the corresponding deterministic displacement profile $U(x, q)$ and effective elastic modulus $E^*(x, q)$. In the case that the stiffness profile $E(v)$ is randomly distributed, it is not possible to find the full distribution of either the displacement profile $U(x)$ or the effective modulus of elasticity $E^*(x)$. However, it is the observation of this thesis that if the distribution of the stiffness profile $E(v)$ is closed under the reciprocal operation then the moments of displacement $U(x)$ can be obtained analytically. In theory, it is possible to obtain an expression for the n^{th} moment of displacement $U(x)$; however, expressions are only derived for the first two moments of $U(x)$ and then, under the approximation that $U(x)$ is lognormally distributed, quasi-analytical expressions are derived for the first two moments of $E^*(x)$.

The choice of marginal distribution of the stiffness profile $E(v)$ has a significant effect on the extent to which the moments of displacement $U(x)$ are tractable. A popular model for stiffness profiles $E(v)$ has been Gaussian processes due to the useful analytical properties associated with the normal distribution. However, the choice of the normal distribution to model properties such as elastic modulus is problematic since displacement is proportional to the reciprocal of elastic modulus:

$$U \propto \frac{1}{E} \tag{3.36}$$

It is noted that if the marginal distribution of $E(v)$ has non-zero probability that the elastic modulus is zero $E = 0$ then the reciprocal process $E(v)^{-1}$ will not have finite moments (Robert, 1991). If $E(v)^{-1}$ does not have finite moments then neither will

the displacement profile $U(x)$ nor the effective property $E^*(x)$. Consequently, it is the recommendation of this thesis that the marginal distribution of properties such as elastic modulus be defined so that there is zero probability of non-positive values. Furthermore, if the analytical moments of displacement $U(x)$ are desired then it is recommended that the marginal distribution of $E(v)$ is chosen such that it is closed under the reciprocal operation. A random variable X is considered closed under the reciprocal operation if X and $1/X$ have the same distribution. It is useful to note that a random variable that is closed under the reciprocal operation can be obtained through the exponentiation of any symmetrically distributed variable Y where symmetrically distributed implies that Y and $-Y$ have the same distribution. A convenient choice for a process that is closed under the reciprocal operation is the lognormal process $E(v)$ which is given by:

$$E(v) = \exp\left(\underline{E}(v)\right) \tag{3.37}$$

where $\underline{E}(v)$ is the underlying Gaussian process with mean $\underline{\mu}$, variance $\underline{\sigma}^2$ and correlation function $\underline{\rho}(v_i, v_j)$. The stiffness profile $E(v)$ with mean μ, variance σ^2 and correlation function $\rho(v_i, v_j)$ is lognormally distributed according to:

$$E(v) \sim \mathcal{LN}(\underline{\mu}, \underline{\sigma}^2 \underline{\rho}(v_i, v_j)) \tag{3.38}$$

Therefore, the reciprocal process $E(v)^{-1}$ is given by:

$$E(v)^{-1} = \exp\left(-\underline{E}(v)\right) \tag{3.39}$$

It is important to note that taking the negative of a random variable only the changes the sign of its expected value and does not change its second moment structure. Consequently, the Gaussian process $-\underline{E}(v)$ that underlies the reciprocal process $E(v)^{-1}$ is distributed according to:

$$-\underline{E}(v) \sim \mathcal{N}\left(-\underline{\mu}, \underline{\sigma}^2 \underline{\rho}(v_i, v_j)\right) \tag{3.40}$$

Thus, the reciprocal lognormal process $E(v)^{-1}$ is distributed according to:

$$E(v)^{-1} \sim \mathcal{LN}\left(-\underline{\mu}, \underline{\sigma}^2 \underline{\rho}(v_i, v_j)\right) \tag{3.41}$$

It is observed that the reciprocal operation alters the first two moments of the lognormal process $E(v)$. The mean and variance of the reciprocal process $E(v)^{-1}$ are respectively given by (see Appendix B.5):

$$\mathbb{E}[E(v)^{-1}] = \frac{\mu^2 + \sigma^2}{\mu^3} \tag{3.42}$$

$$\mathrm{Var}[E(v)^{-1}] = \frac{\sigma^2 \left(\mu^2 + \sigma^2\right)^2}{\mu^8} \tag{3.43}$$

However, it is important to note that the correlation structure of the stiffness profile $E(v)$ and its reciprocal $E(v)^{-1}$ are identical and that this preservation of correlation structure is a useful property that is exploited to compute the analytical moments of displacement $U(x)$. Figure 3.10 shows a single realisation of the lognormal process $E(v)$ (with units of GPa) and its reciprocal $E(v)^{-1}$ (with units of GPa^{-1}) with identical correlation structures.

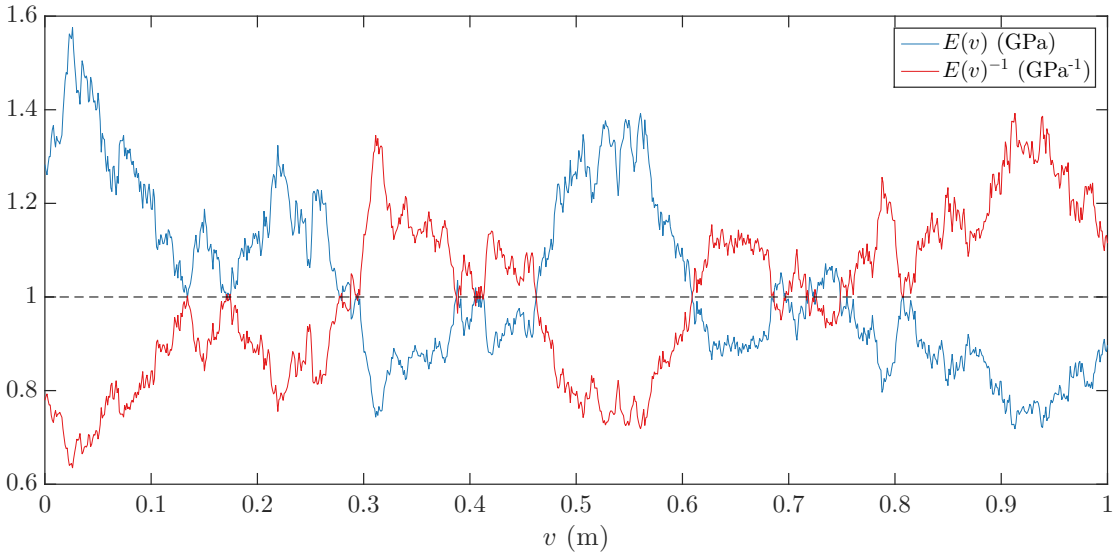


Figure 3.10: A single realisation of the lognormal process $E(v)$ (with units of GPa) and the associated realisation of the reciprocal process $E(v)^{-1}$ (with units of GPa^{-1}).

3.3.1 Analytical moments of displacement

The deflection $U(x)$ of a heterogeneous beam is simply given through the substitution of the effective elastic modulus $E^*(x)$ into the homogeneous equation for deflection. For the case of a simply supported beam under 3-point loading, the deflection $U_3(x)$ is given by:

$$U_3(x) = \begin{cases} \dfrac{Px\left(3L^2 - 4x^2\right)}{48E_3^*(x)I} & \text{if } 0 \leq x \leq \dfrac{L}{2} \\ \dfrac{P(L-x)(4x^2 - 8xL + L^2)}{48E_3^*(x)I} & \text{if } \dfrac{L}{2} \leq x \leq L \end{cases} \tag{3.44}$$

Let $U^*(x)$ denote the zero-variance displacement profile that is obtained as the variance of $E(v)$ is taken to zero $\sigma^2 \to 0$ i.e. as the realisations of the random process $E(v)$ become spatially constant. In this limiting case, the realisations $E(v, q)$ of the stiffness profile are deterministic whose value is simply given by the mean value of the random field $E(v, q) = \mathbb{E}[E(v)] = \mu$. Similarly in the case of homogeneous realisations, the effective elastic modulus E^* is simply equal to the constant value of the realisations $E^* = \mu$.

Let $\eta(x)$ denote a *scale factor* which is given by:

$$\eta(x) = U^*(x) \cdot \mu \tag{3.45}$$

The utility of defining this scale factor $\eta(x)$ is that the expressions for the moments of $U(x)$ derived in this section are generalised for any loading or boundary conditions. In the case of 3-point loading, the scale factor $\eta_3(x)$ is given by:

$$\eta_3(x) = \begin{cases} \dfrac{Px\left(3L^2 - 4x^2\right)}{48I} & \text{if } 0 \leq x \leq \dfrac{L}{2} \\ \dfrac{P(L-x)(4x^2 - 8xL + L^2)}{48I} & \text{if } \dfrac{L}{2} \leq x \leq L \end{cases} \tag{3.46}$$

Noting that the deflection $U(x)$ of any heterogeneous beam is given by:

$$U(x) = \eta(x) \cdot E^*(x)^{-1} \tag{3.47}$$

Substituting the expression for the effective elastic modulus E^* formulated as a weighted harmonic mean, given by Equation 3.2, into the above expression for displacement $U(x)$ gives:

$$U(x) = \eta(x) \int_0^L \omega(v|x) \cdot E(v)^{-1} \, \mathrm{d}v \tag{3.48}$$

It is desirable to obtain the full distribution of displacement $U(x)$; however, it is well known that the sum of lognormal random variables is neither lognormally distributed nor has a closed form distribution (Beaulieu and Xie, 2004). In spite of this, the moments of $U(x)$ can be calculated analytically and, as previously noted, this subsection presents results for the mean and variance of $U(x)$. It should be observed that in the case that the scale factor $\eta(x)$ and the weighting function $\omega(v|x)$ are symmetric about the midspan then the moments of displacement are also similarly symmetric. Although, it is important to note that this does not imply that any realisation of the displacement profile $U(x, q)$ is symmetric.

Taking the expected value of Equation 3.48, the first moment of displacement $U(x)$ is given by:

$$\mathbb{E}\left[U\right] = \mathbb{E}\left[\eta(x) \int_0^L \omega(v) \cdot E(v)^{-1} \, \mathrm{d}v\right] \tag{3.49}$$

$$= \eta(x) \int_0^L \omega(v) \cdot \mathbb{E}\left[E(v)^{-1}\right] \, \mathrm{d}v \tag{3.50}$$

The expected value of the reciprocal process $E(v)^{-1}$, given in Equation 3.42, is independent of the spatial parameter v so can be removed from the integral as follows:

$$\mathbb{E}\left[U(x)\right] = \eta(x) \left(\frac{\mu^2 + \sigma^2}{\mu^3}\right) \int_0^L \omega(v) \, \mathrm{d}v \tag{3.51}$$

As stated in section 3.2, the weighting function $\omega(v)$ satisfies the property that $\int_0^L \omega(v) \, \mathrm{d}v = 1$ and, therefore, the expected value of displacement $\mathbb{E}\left[U(x)\right]$ is simply given by a multiple of the scale factor $\eta(x)$:

$$\mathbb{E}\left[U(x)\right] = \eta(x)\left(\frac{\mu^2+\sigma^2}{\mu^3}\right) \tag{3.52}$$

Consequently, it is observed that the expected value of displacement $U(x)$ is independent of the correlation structure of $E(v)$. Parametrising the above expression with the coefficient of variation $c_v = \sigma/\mu$ yields:

$$\mathbb{E}\left[U(x)\right] = \frac{\eta(x)}{\mu}\left(1+c_v^2\right) \tag{3.53}$$

$$= \left(1+c_v^2\right)U^*(x) \tag{3.54}$$

It is shown that for non-zero variance of the stiffness profile $\sigma^2 > 0$ that the expected value of displacement $U(x)$ is greater than the zero-variance displacement profile $U^*(x)$ and that the magnitude of this increase depends on the coefficient of variation c_v of the stiffness profile $E(v)$. The reason that the expected value of displacement $\mathbb{E}\left[U(x)\right]$ of a heterogeneous beam is not equal to the zero-variance displacement profile $U^*(x)$ is because the effective elastic modulus E^* is a harmonic mean which is disproportionately sensitive to low values of elastic modulus. If the effective property E^* were given by an arithmetic mean then the expected value of displacement would be equal to the zero-variance displacement profile $U^*(x)$.

The variance of displacement $U(x)$ is expressed as:

$$\mathrm{Var}\left[U(x)\right] = \mathbb{E}\left[U(x)^2\right] - \mathbb{E}\left[U(x)\right]^2 \tag{3.55}$$

where $\mathbb{E}\left[U(x)^2\right]$ is given by:

$$\mathbb{E}\left[U(x)^2\right] = \left(\eta(x)\int_0^L \omega(v)\,\mathbb{E}\left[E(v)^{-1}\right]\mathrm{d}v\right)\left(\eta(x)\int_0^L \omega(u)\,\mathbb{E}\left[E(u)^{-1}\right]\mathrm{d}u\right) \tag{3.56}$$

$$= \eta(x)^2\int_0^L\int_0^L \omega(v)\,\omega(u)\,\mathbb{E}\left[E(v)^{-1}\right]\,\mathbb{E}\left[E(u)^{-1}\right]\,\mathrm{d}v\,\mathrm{d}u \tag{3.57}$$

and $\mathbb{E}\left[U(x)\right]^2$ is given by:

$$\mathbb{E}\left[U(x)\right]^2 = \eta(x)^2 \int_0^L \int_0^L \mathbb{E}\left[\omega(v)\,\omega(u)\,E(v)^{-1}\,E(u)^{-1}\right]\,\mathrm{d}v\,\mathrm{d}u \tag{3.58}$$

$$= \eta(x)^2 \int_0^L \int_0^L \omega(v)\,\omega(u)\,\mathbb{E}\left[E(v)^{-1}\,E(u)^{-1}\right]\,\mathrm{d}v\,\mathrm{d}u \tag{3.59}$$

Substituting Equation 3.57 and 3.59 into Equation 3.55 gives:

$$\mathrm{Var}\left[U(x)\right] = \eta(x)^2 \int_0^L \int_0^L \omega(v)\,\omega(u)\,\left(\mathbb{E}\left[E(v)^{-1}\right]\,\mathbb{E}\left[E(u)^{-1}\right] - \mathbb{E}\left[E(v)^{-1}\,E(u)^{-1}\right]\right)\,\mathrm{d}v\,\mathrm{d}u \tag{3.60}$$

$$= \eta(x)^2 \int_0^L \int_0^L \omega(v)\,\omega(u)\,\mathrm{Cov}\left[E(v)^{-1}, E(u)^{-1}\right]\,\mathrm{d}v\,\mathrm{d}u \tag{3.61}$$

If the stiffness profile $E(v)$ is strictly stationary then the reciprocal process $E(v)^{-1}$ is also strictly stationary with covariance function given by $C(|v-u|) = \mathrm{Cov}\left[E(v)^{-1}, E(u)^{-1}\right] = \mathrm{Var}\left[E(v)^{-1}\right]\rho(|v-u|)$ and, consequently, the variance of displacement $\mathrm{Var}[U(x)]$ is given by:

$$\mathrm{Var}\left[U(x)\right] = \eta(x)^2\,\mathrm{Var}\left[E(v)^{-1}\right] \int_0^L \int_0^L \omega(v)\,\omega(u)\,\rho(|v-u|)\,\mathrm{d}v\,\mathrm{d}u \tag{3.62}$$

$$= \eta(x)^2 \left(\frac{\sigma^2\left(\mu^2+\sigma^2\right)^2}{\mu^8}\right) \int_0^L \int_0^L \omega(v)\,\omega(u)\,\rho(|v-u|)\,\mathrm{d}v\,\mathrm{d}u \tag{3.63}$$

This expression for $\mathrm{Var}\left[U(x)\right]$ consists of the multiplication of three elements namely the square of the scale factor $\eta(x)$, the variance of the reciprocal process $\mathrm{Var}[E(x)^{-1}]$ given by Equation 3.43 and, finally, a double integral of two instances of the weighting function $\omega(.)$ that are multiplied by the correlation function $\rho(|v-u|)$.

3.3.2 Stochastic finite element model

It is important to note that only the moments of the displacement profile $U(x)$ can be obtained analytically and, consequently, numerical methods are required in order to obtain full distribution of $U(x)$. This is achieved through the development of a stochastic finite element model (SFEM) that combines the deterministic finite element model in

Subsection 3.2.5 with the Monte Carlo method (Robert and Casella, 2004). A numerical approximation $\overline{U}(x)$ to the distribution of displacement $U(x)$ is obtained through repeated experimental involving: the simulation of a realisation of the stiffness profile $E(v, q)$; the determination of deterministic displacement profiles $U(x, q)$ that correspond to the realisations of the stiffness profile $E(v, q)$; the determination of the effective elastic modulus $E^*(x, q)$ corresponding to the deterministic displacement profile $U(x, q)$; finally, through repeated experimental runs an ensemble of realisations $E(v, q)$ that sufficiently approximates the random field $E(v)$ is obtained thereby suitably approximating the full distribution of $U(x)$ with an ensembles of realisations $U(x, q)$ of the displacement profile. Only the traditional implementation of the Monte Carlo method is pursued here rather than importance sampling techniques such as Markov Chain Monte Carlo (Hastings, 1970) since these techniques utilise correlated sequential samples which leads to difficulties in parallelisation.

The deterministic convergence study in Chapter 3.2.5 can not be used to directly verify the stochastic case and, consequently, a second convergence study is performed to assess the influence of the number of finite elements N on the accuracy of the numerical approximation $\overline{U}(x)$ to the displacement profile $U(x)$. It is observed that the mean of $U(x)$, given by Equation 3.52, is independent of the discretion of heterogeneity and, hence, convergence is only considered with respect to the variance of $U(x)$. It is noted that the double integral in the expression for the variance of displacement, given by Equation 3.63, is evaluated numerically using the tiled quadrature method (Shampine, 2008). Figure 3.11 shows the maximum absolute percentage error in the finite element solution against the number of elements N. It can be seen that, similar to the deterministic convergence study in subsection 3.2.4, that a discretisation of $N > 100$ elements provides suitable discretisation of the stochastic stiffness profile $E(v)$. It is also important to note that the variance of the finite element displacement profile $\overline{U}(x)$ converges from above which implies that under-discretisation of the stiffness profile $E(v)$ is associated with an overprediction of the variance of displacement $U(x)$.

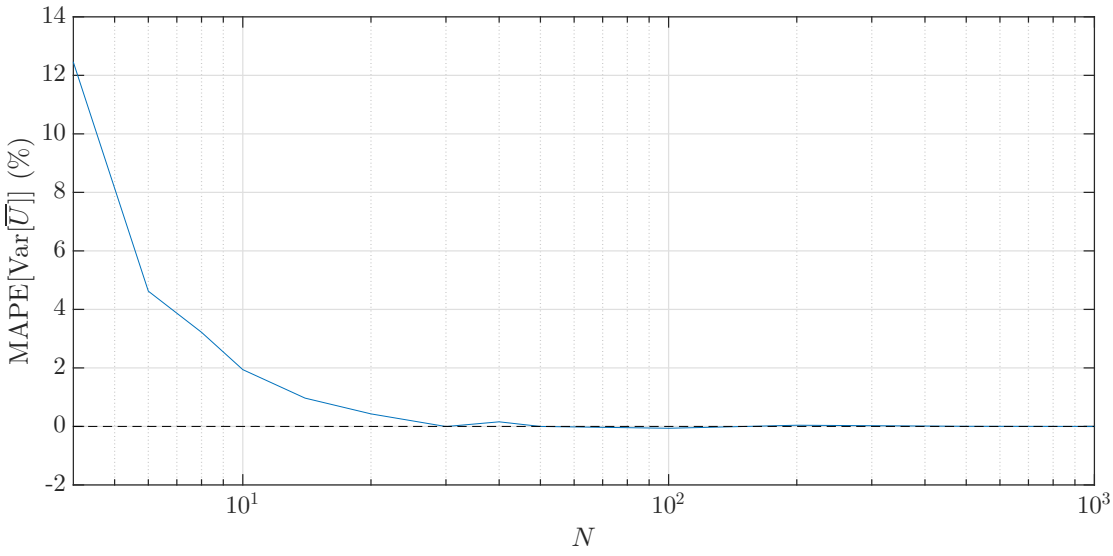


Figure 3.11: Maximum absolute percentage error in the variance of displacement $\mathrm{Var}[\overline{U}]$ against the number of finite elements N.

3.3.3 Quasi-analytical moments of the effective elastic modulus

The method to obtain expressions for the first two moments of the effective elastic modulus E^* begins with the observation that E^* is proportional to the reciprocal of displacement U:

$$E^*(x) = \eta(x) \cdot U(x)^{-1} \tag{3.64}$$

Unfortunately, the full distribution of $U(x)$ is not available analytically and, consequently, the moments of the effective elastic modulus E^* can not be determined exactly. The approach adopted is to derive quasi-analytical expressions for the moments of E^* by approximating displacement U as lognormally distributed and to once again take advantage of the fact that the lognormal distribution is closed under the reciprocal operation. The error associated with the quasi-analytical expressions for the moments of the effective elastic modulus E^*, due to the approximation of displacement U as lognormal, is investigated in the following section.

Displacement $U(x)$ is approximately lognormally distributed according to:

$$U(x) \overset{\text{approx}}{\sim} \mathcal{LN}(\underline{\mu}_U(x), \underline{\sigma}_U^2(x)) \tag{3.65}$$

where the underlying normal parameters $\underline{\mu}_U(x)$ and $\underline{\sigma}_U^2(x)$ are given through method of moments as (Devore, 2012, p. 239):

$$\underline{\mu}_U(x) = \ln\left(\frac{\mathbb{E}\left[U(x)\right]}{\sqrt{1 + \text{Var}\left[U(x)\right] \cdot \mathbb{E}\left[U(x)\right]^{-2}}}\right) \tag{3.66}$$

$$\underline{\sigma}_U^2(x) = \ln\left(1 + \frac{\text{Var}\left[U(x)\right]}{\mathbb{E}\left[U(x)\right]^2}\right) \tag{3.67}$$

where $\mathbb{E}\left[U(x)\right]$ and $\text{Var}\left[U(x)\right]$ are given by Equations 3.52 and 3.63 respectively.

The reciprocal of displacement $U(x)^{-1}$ is approximately lognormally distributed according to:

$$U(x)^{-1} \overset{\text{approx}}{\sim} \mathcal{LN}(-\underline{\mu}_U(x), \underline{\sigma}_U^2(x)) \tag{3.68}$$

Consequently, through the consideration of Equation 3.64 it is apparent that the effective elastic modulus E^* is approximately lognormally distributed according to:

$$E^*(x) \overset{approx}{\sim} \mathcal{LN}(-\underline{\mu}_U(x) + \ln[\eta(x)],\ \underline{\sigma}_U^2(x)) \tag{3.69}$$

The quasi-analytical mean of the effective elastic modulus E^* is given by:

$$\mathbb{E}\left[E^*(x)\right] \approx \exp\left(-\underline{\mu}_U(x) + \ln[\eta(x)] + \frac{1}{2}\underline{\sigma}_U^2(x)\right) \tag{3.70}$$

The quasi-analytical variance of the effective elastic modulus E^* is given by:

$$\text{Var}\left[E^*(x)\right] \approx \eta(x)^2 \left(\exp[\underline{\sigma}_U^2(x)] - 1\right) \exp\left(-2\underline{\mu}_U(x) + \underline{\sigma}_U^2(x)\right) \tag{3.71}$$

3.4 Sensitivity analyses

This section contains three sensitivity analyses which investigate the variation of the moments of displacement U and the effective elastic modulus E^* with respect to a number of parameters. The first sensitivity analysis investigates the variation of these moments with respect to the position x along the beam, the second with the correlation length θ and the third with the coefficient of variation c_v of the stiffness profile $E(v)$. In particular, the variation of these moments are considered for a simply supported beam under 3-point loading for three different correlation functions of the stiffness profile $E(v)$ namely the Markov $\rho_M(s)$, Gaussian $\rho_G(s)$ and triangular $\rho_T(s)$ correlation functions. The (quasi)-analytical moments associated with the Markov, Gaussian and triangular-correlated stiffness profiles are respectively denoted $E_M(v)$, $E_G(v)$, $E_T(v)$ whilst the moments computed through the SFEM are respectively denoted $\overline{E}_M(v)$, $\overline{E}_G(v)$, $\overline{E}_T(v)$ where the bar indicates that the stiffness profile has been discretised in accordance with the finite elements. The benefit of comparing the quasi-analytical and SFEM approaches is two fold: firstly, for the moments of U, this comparison serves to validate the performance of the stochastic finite element model and secondly, for the moments of E^*, this comparison provides a means to assess the accuracy of the approximate quasi-analytical expressions derived in Subsection 3.3.3. The value of the parameters of the heterogeneous beam utilised in the following sensitivity analyses are detailed in Table 3.1 and it is noted that the discretisation parameters only apply to the stochastic finite element model.

3.4.1 Variation of moments along the beam

Figure 3.12 shows that the variance of displacement $\text{Var}[U]$ increases from zero at the supports and is maximised at midspan for all three correlation functions. In particular, it is observed that the variance is greatest for the Gaussian correlation function $\rho_G(s)$, followed by the triangular correlation function $\rho_T(s)$ and, finally, the variance is lowest for the Markov correlation function $\rho_M(s)$. Good agreement is observed between the stochastic finite element method and the analytical solution, given by Equation 3.63, which verifies that the degree of discretisation $N = 2 \times 10^2$ and the number of Monte Carlo simulations $R = 1 \times 10^6$ is sufficient to obtain accurate predictions of the variance of displacement. It is useful to note that the variance of displacement $\text{Var}[U]$ shares the

properties of the zero-variance profile $U^*(x)$ of being both symmetric about the midspan $x = L/2$ as well as being first-derivative continuous.

It is informative to not only consider the variance of displacement $\text{Var}[U]$ but also the coefficient of variation $\text{CV}[U]$. The utility of the coefficient of variation is that it controls for the increase in mean displacement $\mathbb{E}[U(x)]$ thus providing insights into the relative variability of displacement U. The coefficient of variation of displacement is given by:

$$\text{CV}\left[U(x)\right] = \frac{\sqrt{\text{Var}[U(x)]}}{|\mathbb{E}[U(x)]|} \tag{3.72}$$

where $|.|$ is the absolute value operator. Figure 3.13 shows the variation in the coefficient of variation of displacement $\text{CV}\left[U\right]$ against the position x along the beam. It is observed that $\text{CV}\left[U\right]$ is maximised at the midspan for all three correlation functions, however, the relative increase in $\text{CV}\left[U\right]$ towards the midspan is small compared to the increase observed for $\text{Var}\left[U\right]$ as shown in Figure 3.12. Based on the analysis contained within this section, it is concluded that the increase in the variability of displacement is attributable to both the increase in the expected value of displacement $\mathbb{E}[U]$ and, to a lesser extent,

Table 3.1: Parameter values for the sensitivity analyses.

Parameter name	Symbol	Value	Units
Random field parameters			
Location parameter	μ	12.0	GPa
Scale parameter	σ	3.6	GPa
Coefficient of variation	c_v	0.3	–
Correlation length	θ	1.0	m
Structural parameters			
Beam length	L	1.0	m
Second moment of area	I	3.7×10^{-7}	m^4
Load	P	10^4	N
Discretisation parameters			
Beam discretisation	N	200	–
Number of runs	R	10^6	–

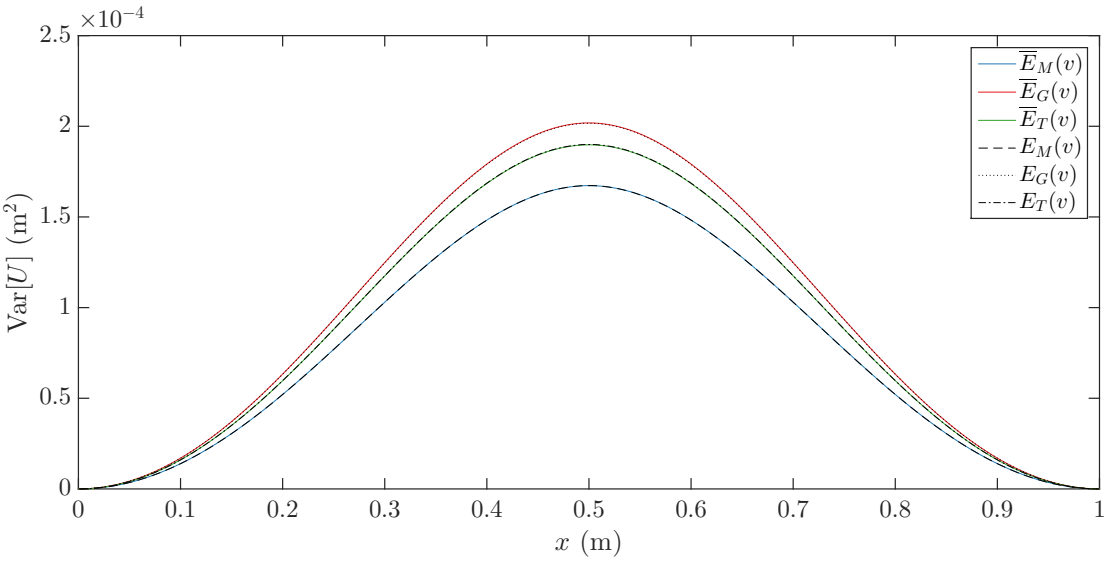


Figure 3.12: Variance of displacement Var$[U]$ against the distance x along the beam.

the increase in relative variability as quantified by the coefficient of variation CV$[U]$. Additionally, it shown that the coefficient of variation of displacement CV $[U]$ is, for all three correlation functions, smaller than the coefficient of variation c_v of the stiffness profile $E(v)$ due to the fact that the effective elastic modulus E^* is a harmonic mean which averages, and hence reduces the variability, of the stiffness profile $E(v)$. Finally, it can be seen that the limiting value of CV $[U]$ is non-zero at the supports (i.e. as $x \to 0$ and $x \to L$) and it noted that this behaviour is similar to the behaviour of the well-known sinc(x) function as $x \to 0$ (see Subsection 2.5.1).

Figure 3.14 shows how the expected value of the effective modulus of elasticity Mean$[E^*]$ varies with the distance x along the beam. The expected value of the effective elastic modulus $\mathbb{E}[E^*]$ is always lower than the expected value of the stiffness profile $\mathbb{E}[E(v)] =$ 12 GPa and this is due to the effective elastic modulus E^* being given by a harmonic mean which tends towards minima. It is observed that calculating the effective property E^* based on the midspan displacement $x = L/2$ maximises its expected value whilst calculating E^* from displacement near the supports minimises its expected value and it is important that this is taken into account when comparing different procedures to calculate the effective elastic modulus E^*. For instance, it has been suggested that in the case of 4-point bending that the effective property E^* be calculated based on the average of displacement under both loads (Bechtel, 2007). It is concluded that this method of calculating the effective elastic modulus E^* will reduce its expected in comparison to the traditional calculation based solely on midspan displacement.

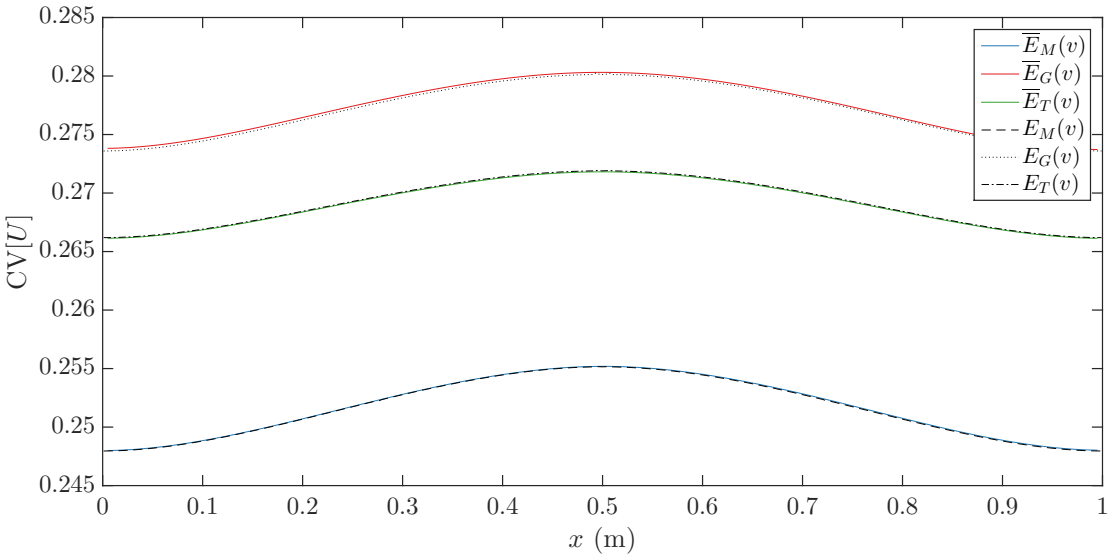


Figure 3.13: Coefficient of variation of displacement CV$[U]$ against the distance x along the beam.

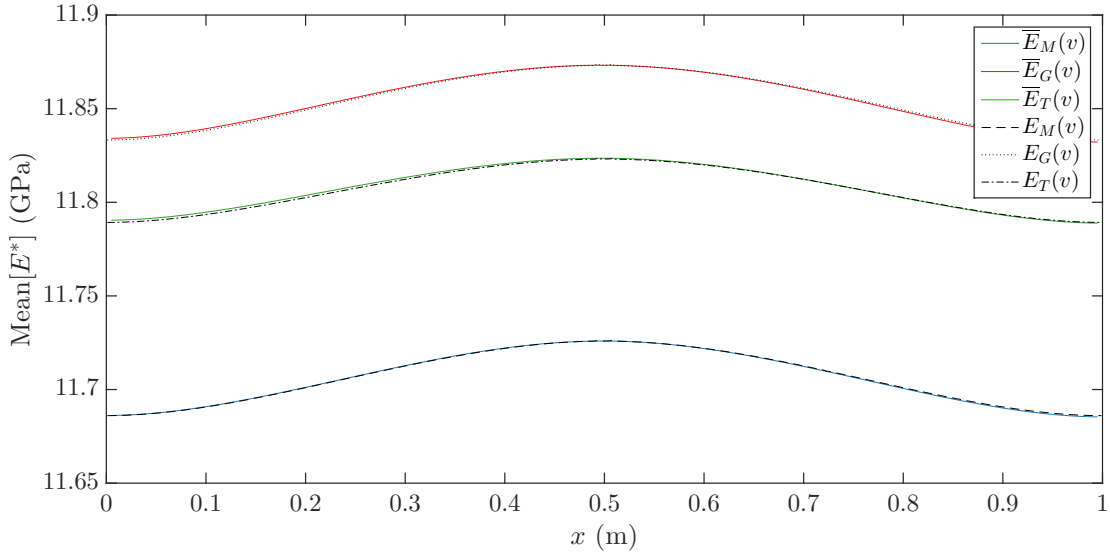


Figure 3.14: Mean of the effective elastic modulus Mean$[E^*]$ against the distance x along the beam.

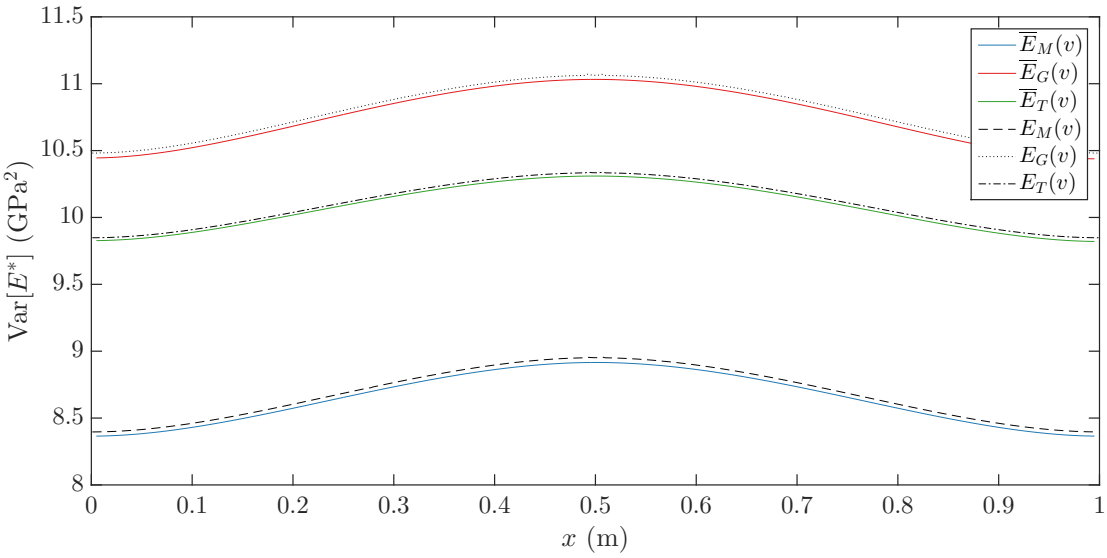


Figure 3.15: Variance of the effective elastic modulus Var$[E^*]$ against the distance x along the beam.

Figure 3.15 shows how the variance of the effective elastic modulus Var$[E^*]$ varies with distance x along the beam. It can be seen, similar to the expected value of the effective elastic modulus $\mathbb{E}[E^*]$, that the variance of the effective elastic modulus Var$[E^*]$ is also maximised midspan. It is observed by inspection that the estimate of Var$[E^*]$ associated with the quasi-analytical approach $\{E_M(v), E_G(v), E_T(v)\}$ exhibits a small positive bias compared to the more accurate estimates associated with the stochastic finite element model $\{\overline{E}_M(v), \overline{E}_G(v), \overline{E}_T(v)\}$. This small positive bias is primarily attributed to the error induced through the approximation of displacement U as being lognormally distributed. Finally, it is concluded that for heterogeneous beams with parameters similar to those detailed in Table 3.1, this error is small thus validating that the quasi-analytical theory developed in subsection 3.3.3 is a reasonable approximation of the moments of the effective elastic modulus E^*.

For all of the moments of displacement U and the effective elastic modulus E^* considered in this section, the value of the moment is always maximal for the Gaussian correlation function $\rho_G(s)$, lower for the triangular correlation function $\rho_T(s)$ and minimal for the Markov correlation function $\rho_M(s)$ in spite of all three correlation functions being parametrised by the same correlation length $\theta = 1$ m. An explanation for this phenomena is obtained by considering that, as shown in Figure 2.3, the Gaussian correlation function $\rho_G(s)$ has the greatest short-range correlation, the triangular correlation function $\rho_T(s)$ has the greatest mid-range correlation and the Markov correlation function

$\rho_M(s)$ has the greatest long-range correlation. It is concluded that since heterogeneous beam behaviour appears to be dominated by short-range correlation then the Gaussian-correlated stiffness profile $E_G(v)$ results in macroscale beam behaviour that would be associated with a triangular-correlated stiffness profile $E_T(v)$ with a greater correlation length or a Markov-correlated stiffness profile $E_M(v)$ with an even greater correlation length.

3.4.2 Variation of moments with the correlation length

This subsection presents the results of a sensitivity analysis investigating how the moments of midspan displacement $U_c = U(x_c)$ and the midspan effective elastic modulus $E_c^* = E^*(x_c)$ vary with the correlation length θ of the stiffness profile $E(v)$. The parameter values of this sensitivity analysis are once again given by Table 3.1; however, instead of a constant correlation length, the effect of varying the correlation length θ on the interval $(0, 1]$ is analysed. It is important to recognise that the expected value of midspan displacement $\mathbb{E}[U_c]$, given by Equation 3.52, is independent of the correlation length θ and, consequently, the expected value of midspan displacement $\mathbb{E}[U_c]$ is not considered within this sensitivity analysis. Figure 3.16 shows the variation in the variance of midspan displacement $\text{Var}[U_c]$ with the correlation length θ. It is observed that as the beam becomes increasingly homogeneous, $\theta \to \infty$, the variance of midspan displacement $\text{Var}[U_c]$ increases for all of the correlation functions and, as $\theta \to 0$, the variance of midspan displacement $\text{Var}[U_c]$ approaches zero due to the statistical homogeneity of Kronecker delta correlated white noise. Finally, the variance of midspan displacement of the heterogeneous beam is lowest for the Markov correlation function $\rho_M(s)$ and highest for the Gaussian correlation function $\rho_G(s)$ with the triangular correlation function $\rho_T(s)$ resulting in similar beam behaviour up to a correlation length of $\theta = 0.3$ m.

Figure 3.17 shows that the mean of the midspan effective elastic modulus $\text{Mean}[E_c^*]$ increases with the correlation length θ for all three correlation functions. This function is concave since its second derivative is negative and, consequently, as the beam becomes increasingly heterogeneous, $\theta \to \infty$, the magnitude of the relative increase in the expected value of the effective elastic modulus $\text{Mean}[E^*]$ reduces. Furthermore, as the beam becomes increasingly heterogeneous, $\theta \to 0$, the expected value of the effective elastic modulus $\text{Mean}[E^*]$ approaches a lower-bound $\mathbb{E}_{LB}[E_c^*]$ that appears to be well

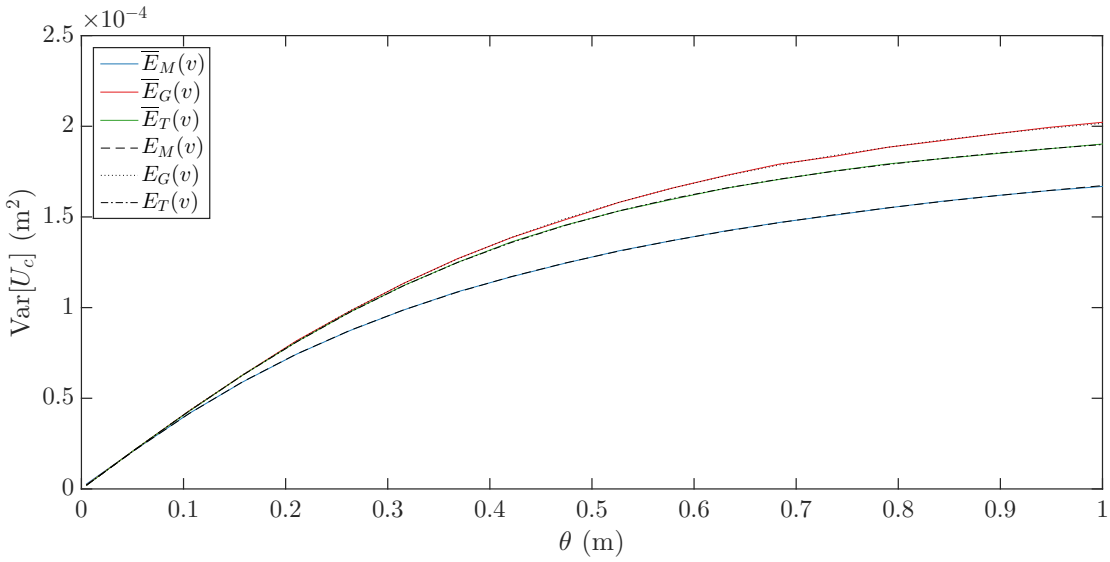


Figure 3.16: Variance of midspan displacement $\mathrm{Var}[U_c]$ against the correlation length θ.

approximated by:

$$\mathbb{E}_{LB}[E_c^*] \approx \frac{\mu}{1+c_v^2} \tag{3.73}$$

where c_v is the coefficient of variation of the lognormal stiffness profile $E(v)$. Additionally, it is important to recognise that the behaviour of the stiffness profile $E(v)$ at zero-correlation length $\theta = 0$ is not well-defined. This is due to the stiffness profile $E(v)$ becoming the white noise process with the Kronecker Delta correlation function whose integral is undefined (see Section 2.4) and, consequently, the mean of the effective elastic modulus $\mathbb{E}[E_c^*]$ at zero correlation length $\theta \to 0$ has not been evaluated nor plotted.

Figure 3.18 shows the variance of the midspan effective elastic modulus $\mathrm{Var}[E_c^*]$ against the correlation length θ of the stiffness profile $E(v)$. It is observed that the variance of the midspan effective elastic modulus $\mathrm{Var}[E_c^*]$ increases with the correlation length θ and in the limiting case, as $\theta \to \infty$, the variance of the effective elastic modulus approaches the variance of the random field $\mathrm{Var}[E_c^*] \to \sigma^2$. It can be seen that the estimate of the variance of the midspan effective elastic modulus $\mathrm{Var}[E_c^*]$ associated with the quasi-analytical moments $\{E_M(v), E_G(v), E_T(v)\}$ systematically underpredicts the true variance of the midspan effective elastic modulus compared to the estimates obtained through the SFEM $\{\overline{E}_M(v),\ \overline{E}_G(v),\ \overline{E}_T(v)\}$. In addition to the systematic uncertainty associated with the quasi-analytical moments, it is also worth considering

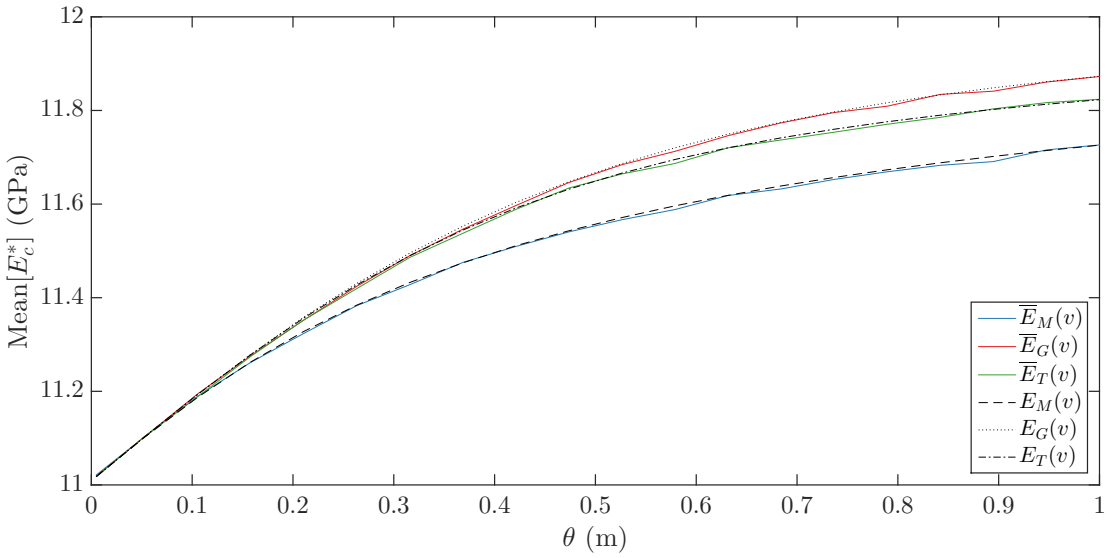


Figure 3.17: Mean of the midspan effective elastic modulus Mean$[E_c^*]$ against the correlation length θ.

the statistical uncertainty associated with the limited sample size associated with the Monte Carlo method. It is observed, for a fixed sample size $R = 1 \times 10^6$, that as the correlation length θ increases then the accuracy of the estimate of the variance of the effective elastic modulus reduces since the realisations associated with a large correlation length θ are less ergodic.

3.4.3 Variation of moments with the coefficient of variation

This subsection contains a sensitivity analysis investigating how the moments of midspan displacement U_c and the midspan effective elastic modulus E_c^* vary with the coefficient of variation c_v of the stiffness profile $E(v)$. The parameters are identical to those given by Table 3.1, however, instead of a constant coefficient of variation c_v, the effect of varying c_v on the interval $(0, 1]$ is analysed. Figure 3.19 shows that the mean of midspan displacement Mean$[U_c]$ increases with the coefficient of variation c_v and that this increase is independent of the type of correlation function. This increase in the expected value of midspan displacement Mean$[U_c]$ is due to the effective elastic modulus E^* being given by a harmonic mean which is disproportionately sensitive to weak zones of the stiffness profile $E(v)$. In the limiting case as the coefficient of variation approaches zero, $c_v \to 0$, then the expected value of midspan displacement approaches the midspan displacement of the zero-variance profile $\mathbb{E}[U_c] \to U^*(x_c)$.

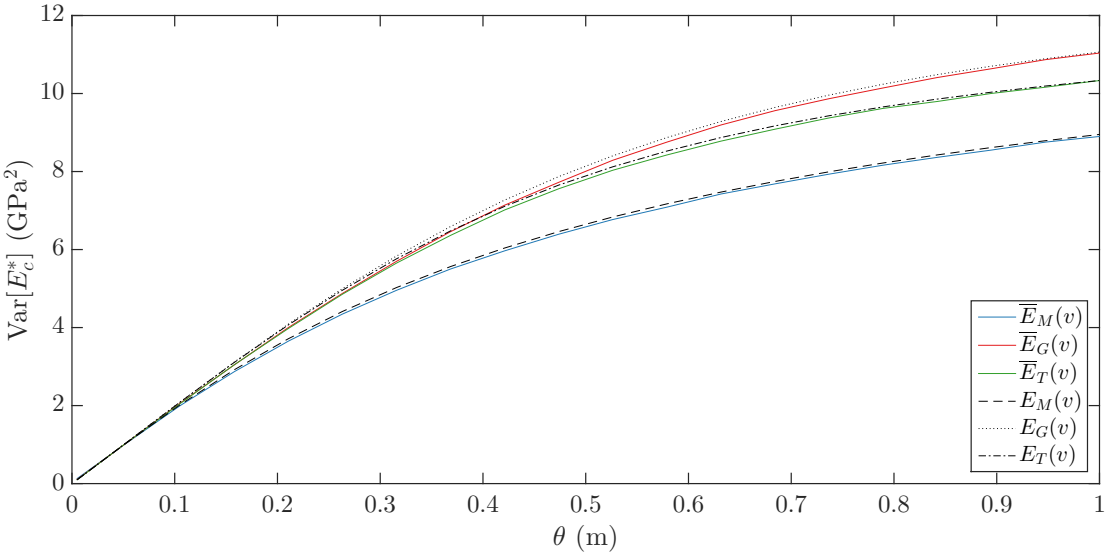


Figure 3.18: Variance of the midspan effective elastic modulus Var$[E_c^*]$ against the correlation length θ.

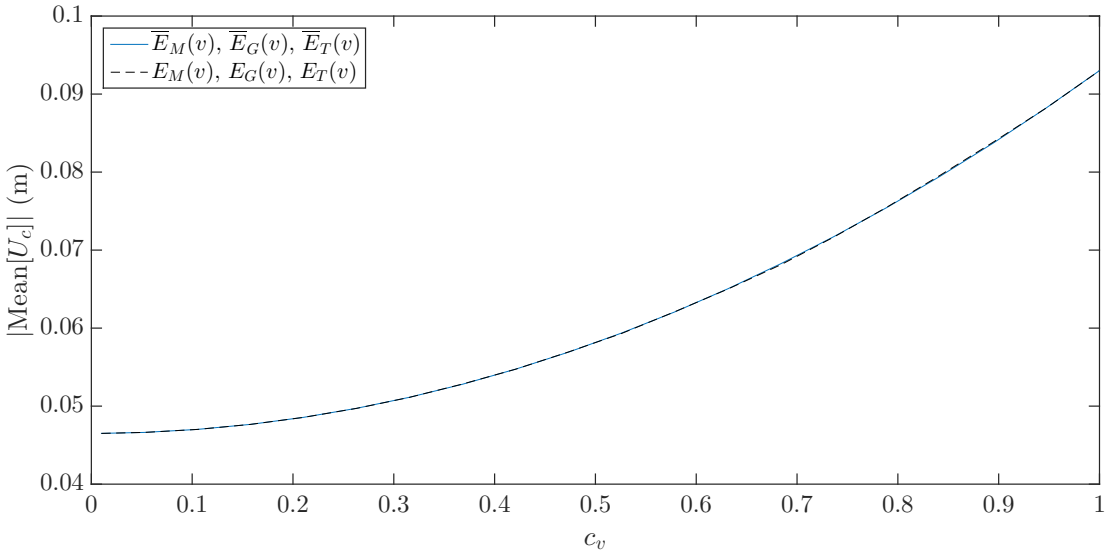


Figure 3.19: Absolute value of the mean of the midspan displacement |Mean$[U_c]$| against the coefficient of variation c_v of the stiffness profile $E(v)$.

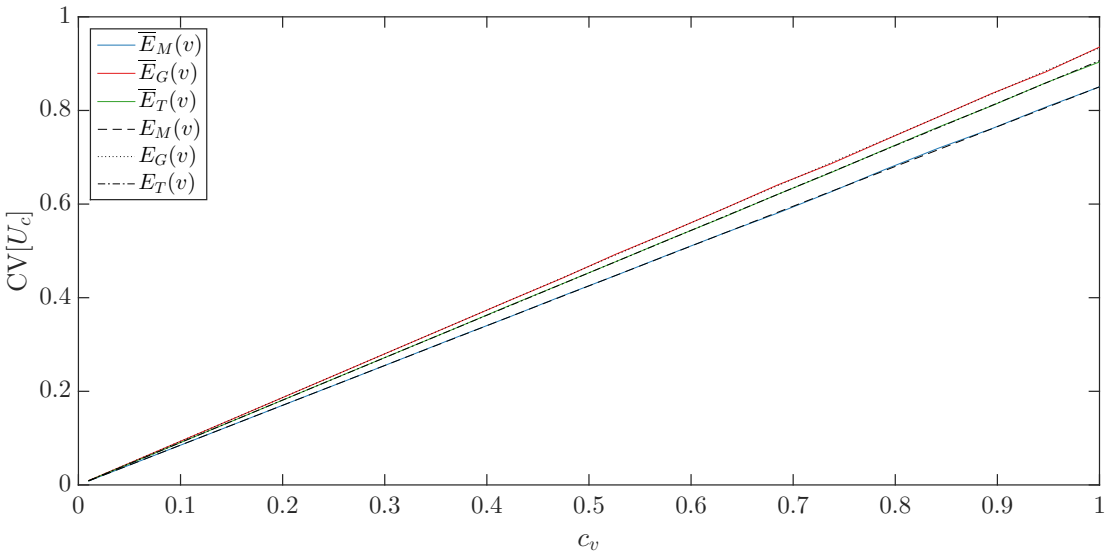


Figure 3.20: Coefficient of variation of midspan displacement CV$[U_c]$ against the coefficient of variation c_v of the stiffness profile $E(v)$.

Figure 3.20 shows the coefficient of variation of midspan displacement CV$[U_c]$ against the coefficient of variation c_v of the stiffness profile $E(v)$. It is observed that, for all correlation functions, the coefficient of variation of midspan displacement CV$[U_c]$ increases linearly with the coefficient of variation c_v of the stiffness profile $E(v)$ with a gradient of slightly less than one. The fact that the coefficient of variation of midspan displacement CV$[U_c]$ is always less than the coefficient of variation c_v of the stiffness profile $E(v)$ is due to the fact that the effective elastic modulus E^* is a harmonic mean which acts to average over, and hence reduce the variability of, the stiffness profile $E(v)$. This reduction in variability is dependent on the correlation structure of the stiffness profile with the reduction being the greatest in the case of the Markov-correlated process $E_M(v)$ and smallest in the case of the Gaussian-correlated process $E_G(v)$.

Figure 3.21 shows how the mean of the midspan effective elastic modulus Mean$[E_c^*]$ varies with the coefficient of variation c_v of the stiffness profile $E(v)$. It can be seen that as the heterogeneity of the beam increases, $c_v \to \infty$, the expected value of the effective elastic modulus decreases to zero and as the beam becomes increasingly homogeneous, $c_v \to 0$, the expected value of the effective elastic modulus approaches the expected value of the random field Mean$[E_c^*] \to \mathbb{E}[E(v)] = 12$ GPa. Furthermore, it is observed that an increase in the coefficient of variation c_v also leads to an increase in the epistemic error associated with the quasi-analytical moments $\{E_M(v), E_G(v), E_T(v)\}$ which results in the quasi-analytical moments over-predicting Mean$[E_c^*]$ for all three correlation functions.

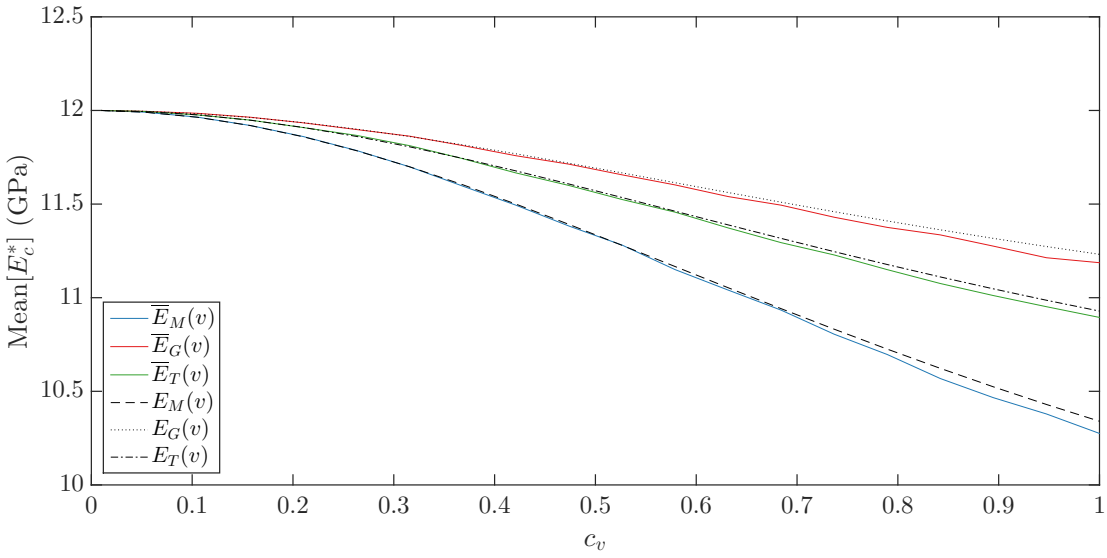


Figure 3.21: Mean of the midspan effective elastic modulus Mean$[E_c^*]$ against the coefficient of variation c_v of the stiffness profile $E(v)$.

This is explained by considering that as the coefficient of variation of the lognormally distributed variables increases their summation increasingly deviates from the lognormal distribution and, consequently, the accuracy of the quasi-analytical moments decreases.

Figure 3.22 shows the coefficient of variation of the midspan effective elastic modulus CV$[E_c^*]$ against the coefficient of variation c_v of the stiffness profile $E(v)$. It is observed that the coefficient of variation of the midspan effective elastic modulus E_c^* increases approximately linearly with the coefficient of variation c_v. Similar to the relationship observed in Figure 3.20, the gradient is less than one due to the reduction in variability resulting from the averaging associated with the effective elastic modulus E^*. However unlike the relationship observed in Figure 3.20, the quasi-analytical moments $\{E_M(v), E_G(v), E_T(v)\}$ are not exact and, as the coefficient of variation c_v becomes large, the quasi-analytical moments increasingly over-predict the coefficient of variation of the effective elastic modulus CV$[E_c^*]$ in comparison to the moments obtained through the stochastic finite element model $\{\overline{E}_M(v), \overline{E}_G(v), \overline{E}_T(v)\}$. However, the magnitude of this over-prediction is small thus validating the accuracy of the quasi-analytical theory developed in Section 3.3 for most coefficients of variation of timber observed in practice which typically tend to be within the range 0.2 – 0.4 (Thelandersson, 2003).

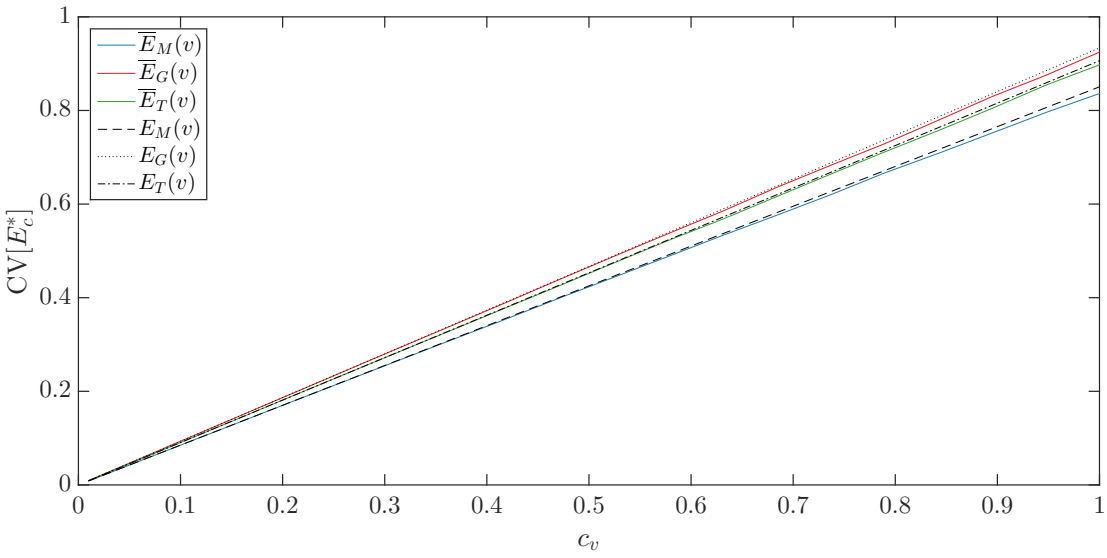


Figure 3.22: Coefficient of variation of the midspan effective elastic modulus CV$[E_c^*]$ against the coefficient of variation c_v of the stiffness profile $E(v)$.

3.4.4 Limitations

The theory of heterogeneous beams as presented in this chapter is subject to a number of limitations which include: restriction of the analysis to the case of Euler-Bernoulli beams thus neglecting the contributions of shear effects to displacement and the consideration of only the first and second moments of displacement $U(x)$ rather than its full distribution. This limitation is due to the fact that the full distribution of $U(x)$ can not be obtained through analytical methods and, consequently, if consideration of the full distribution of $U(x)$ is required then the use of numerical methods such as the stochastic finite element method is necessary. Figure 3.23 shows the mean and 95% confidence intervals of the displacement profile $U(x)$ as well as the zero-variance profile $U^*(x)$ obtained through the stochastic finite element model of a heterogeneous beam whose parameters are given by Table 3.1. It can be seen that the mean displacement profile Mean$[U(x)]$ is 9% greater than the zero-variance profile $U^*(x)$ as a result of the factor $(1 + c_v^2)$ in Equation 3.54. One limitation of the quasi-analytical theory developed in this chapter is that it may not be suitable for the simulation of confidence intervals which depend heavily on the tails of the distribution. If confidence intervals are to be determined then it is recommended that this be achieved through numerical methods such as the stochastic finite element method. Finally, in spite of the limitations identified here, it is concluded that the quasi-analytical theory developed within this chapter has great utility for engineering calculations that depend on the moments of either displacement U or the effective elastic modulus E^*.

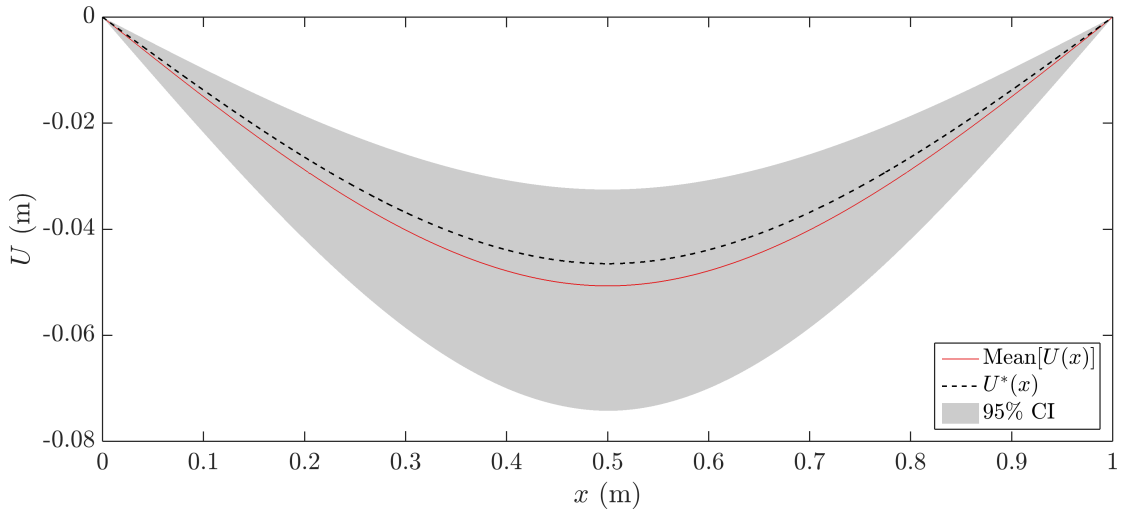


Figure 3.23: Mean displacement profile Mean$[U(x)]$, zero-variance displacement profile $U^*(x)$ and 95% confidence intervals against distance x along the beam.

3.5 Conclusion

This chapter has developed a novel theory of heterogeneous beams based on the formulation of the effective elastic modulus as a weighted harmonic mean. The key achievements of this chapter are summarised as:

- The formulation of the effective elastic modulus at any point along a heterogeneous Euler-Bernoulli beam as a weighted harmonic mean with weighting functions derived for the 3-point, 4-point and uniformly distributed loading conditions. The properties of these weighting functions have been analysed with insights into the relationship between the effective elastic modulus E^* and the stiffness profile $E(v)$. Finally, analytical expressions have been obtained for both the displacement and effective elastic modulus of a beam under 3-point loading with linear variation in elastic modulus and these analytical expressions have been used as a benchmark to evaluate a finite element model.

- Analytical expressions have been derived for the first two moments of displacement and quasi-analytical expressions for the effective elastic modulus of a randomly heterogeneous beam with a lognormally distributed stiffness profile $E(v)$. These quasi-analytical moments have been validated against a stochastic finite element model in a series of sensitivity analyses investigating the behaviour of randomly heterogeneous beams with respect to the location x of displacement U along the

beam, as well as, the correlation length θ and coefficient of variation c_v of the stiffness profile $E(v)$.

The following suggestions are made for future research based on the quasi-analytical theory of heterogeneous beam developed in this chapter:

- This chapter has only considered the case of a simply supported beam and, consequently, it is of interest to investigate the dependency of the effective elastic modulus on the support conditions of the beam. It is noted that an understanding of the influence of the flexibility of the joints would be relevant to the risk analysis of large structures consisting of numerous jointed heterogeneous elements. In particular, it is suggested that the quasi-analytical theory developed within this chapter could be used to mitigate against the large computational cost associated with the analysis of such large structures.

- Expressions have only be obtained for the first two moments of displacement and, consequently, it is of interest to extend the theory of heterogeneous beams through the derivation of a general expression for the n^{th} moment of displacement. Moreover, the theory can be further generalised by deriving a general expression for the weighting function $\omega(v)$ in terms of the internal bending moment $M(v)$. These developments would facilitate the analytical theory of heterogeneous beams as a computationally efficient and exact alternative to stochastic finite element modelling for the purposes of reliability analysis.

The theory of heterogeneous beams, developed using the theory of random fields presented in Chapter 2, forms the basis for the higher-dimensional analysis of the effective properties of heterogeneous beams detailed in the remainder of this thesis. In Chapter 4, the problem of approximating the relationship between the higher-dimensional effective modulus of elasticity E^* and the underlying stiffness field $E(x, y)$ is considered including the optimisation of two-dimensional weighting functions. Finally, Chapter 5 considers the problem of inferring the parameters of a two-dimensional random field $E(x, y)$ from experimentally determined effective moduli in order to model the spatial variation of elastic modulus.

Chapter 4

Meta-modelling of effective properties

4.1 Introduction

The development of methodologies to determine effective material properties is important to disciplines of engineering concerned with the analysis of materials that exhibit a significant degree of heterogeneity. The utility of effective properties is that they describe the property of a homogeneous region that is equivalent to a heterogeneous region of a material. The process of substituting an equivalent homogeneous region is known as homogenisation or upscaling and has been investigated extensively within the discipline of reservoir engineering which is a field of research primarily concerned with predicting the effective permeability of randomly porous media with the aim of accurately forecasting the production of a petroleum reservoir (Brown and Vasilyeva, 2016). It should be noted that this chapter draws upon many of the concepts developed within reservoir engineering and demonstrates how the methodologies to analyse porous media can be adapted to determine the effective modulus of elasticity of randomly heterogeneous beams. In particular, the research contained within this chapter is motivated by the following quote:

> "One of the most pervasive problems in the description of an heterogeneous medium is the problem of averaging from one scale to another. A medium

> property is observed at one scale on a particular support (volume) of measurement, but the value of that property 'averaged' over a different volume size at a different location is needed" (Journel et al., 1986)

It is of interest to consider higher dimensional heterogeneity, as modelled by random fields, since many heterogeneous materials such as soil, concrete and timber have mechanical properties that are variable in all three spatial dimensions and, consequently, one-dimensional random processes may be an inadequate approximation of such phenomena. It has been shown in Chapter 3 that the effective elastic modulus of an Euler-Bernoulli beam is given exactly by a weighted harmonic mean; however, the extension of this theory beyond the one-dimensional case is inhibited by the fact that the relationship between a multidimensional field, describing the variation in a material property, and the effective property, describing the macroscale behaviour of that material, is not analytical. The approach adopted within this chapter to overcome the non-analytical nature of higher-dimensional effective properties is to utilise meta-models, also known as surrogate models (Sudret, 2012), which offer an approximate approach to the problem of upscaling. It is important that the meta-model is carefully selected since the meta-model needs to be simple enough in order to function as a meta-model, however, the meta-model should not be so simple as to fail to appropriately model the nature of the phenomena. A novel contribution of this chapter is to introduce a meta-model for the effective properties of heterogeneous materials of the form of a weighted generalised mean thereby extending the analysis contained within Chapter 3 as well as drawing on concepts from the research field of reservoir engineering.

Meta-models have also been extensively applied within the discipline of structural reliability in order to model the relationship between the input and output of probabilistic models (Sudret, 2012). It is noted that the primary motivation for the use of these meta-models has been to mitigate against the high computational cost associated with repeated calls to numerical methods such as the stochastic finite element method (Wang and Shan, 2007). In particular, commonly used parametric meta-models include polynomial models, polynomial chaos expansions (Choi et al., 2004) and kriging models (Sacks et al., 2004, Gaspar et al., 2014) and it has been observed that first order reliability methods (Hasofer and Lind, 1974) are in fact linear polynomial meta-models. In addition to parametric meta-models, there has also been extensive use of non-parametric meta-models in order to predict the reliability of constructed assets such as heteroge-

neous cohesive slopes (Chok et al., 2016) and concrete structures with uncertain material properties (Most and Bucher, 2007) through the training of artificial neural networks to the output of finite element models.

The research direction adopted within this chapter is to utilise analytical parametric meta-models to model the relationship between the realisations of a random field and the associated effective properties. It is suggested that there are significant advantages beyond a mere reduction in computational cost that motivate the use of meta-models to compute the effective property of realisations of a random field. In particular, analytical meta-models have the potential to offer conceptual insights into research questions concerning the sensitivity of the effective property to extrema of the material field, as well as, the relative spatial importance of different regions in the domain to the effective property. For instance, Le et al. (2015) utilised the stochastic finite element method to analyse the behaviour of heterogeneous slopes and observed by inspection that the permeability at the surface of the embankment has the greatest contribution to the effective permeability. However, the problem with non-analytical methods such as the finite element method is that these methods often function as a black-box which, in spite of being an invaluable tool for solving intractable mechanics problems, inhibits explicit investigation of the relationship between model inputs and outputs. This motivates the use of analytical meta-models in order to explicitly characterise the opaque behaviour of these numerical methods thereby offering a quantitative post hoc interpretation of the relationship between the effective property and the realisation of the random field (Montavon et al., 2018).

A secondary motivation for the use of analytical meta-models is that their useful properties facilitate analysis of both the input and output quantities. For instance, it has been shown in Chapter 3 that analytical expressions for the moments of displacement can be obtained through manipulation of the weighted harmonic mean formulation of the effective elastic modulus of an Euler-Bernoulli beam. Furthermore, this type of analytical formulation provides a framework to obtain the model input from its output through *inversion* which is the process of inferring a stiffness profile from its experimentally determined effective properties. Within the discipline of heterogeneous mechanics, the problem of inversion has previously been approached through finite element modelling (Maniatty et al., 1989) in a procedure that has come to be known as the inverse finite element method (Kefal et al., 2017). In particular, one advantage of the analytical

meta-models introduced in the following section is that they permit an approach to the problem of inversion through Fourier deconvolution (Bracewell, 2000). Finally, it should be noted that extensive discussion of the application of such inversion methodologies is beyond the scope of this chapter; however, for further information on the inversion of effective modulus of elasticity to recover the stiffness profile consider Foschi (1987), Lam et al. (1991) and Pope and Matthews (1995).

Within the context of the meta-problem framework outlined in Chapter 1, this chapter is primarily concerned with developing an approximate approach to *meta-problem 1 – deterministic prediction* in the multi-dimensional case:

$$Z(x, y, q) \xrightarrow{\text{approx}} Z^*(q) \tag{4.1}$$

where $Z(x, y, q)$ is a deterministic field describing the spatial variation of material properties, $Z^*(q)$ is the deterministic effective property and these two quantities are approximately related using a meta-model. However, it is important to note that the development of an approximate analytical meta-modelling approach to *meta-problem 1 – deterministic prediction* also lends itself to the development of analytical approaches to both *meta-problem 2 – stochastic prediction*, since the meta-model enables the analytical calculation of moments of displacement, and to *meta-problem 4 – deterministic inference* since the meta-model facilitates an analytical approach to the problem of inversion. It should be noted that in this chapter the effective property Z^* is spatially constant, located at midspan, and that both the random field $Z(.)$ and the weighting function $\omega(.)$ are parametrised with the spatial parameters $\{x, y, z\}$ rather than the spatial parameter v utilised in Chapter 3.

This chapter can be roughly divided into two halves: the first half presents a class of meta-models for the effective properties of heterogeneous structures as well as an algorithm to optimise these meta-models to the output of a finite element model and the second half presents an investigation into the application of these meta-models to analyse heterogeneous beam behaviour. In total, this chapter consists of seven sections: the first section is *introduction* which contains this chapter overview; the second section is *mean meta-models* which presents the generalised weighted mean meta-model with specific consideration of arithmetic, geometric and harmonic means; the third section

is *functional optimisation* which presents a novel gradient-free functional optimisation algorithm, investigates its convergence on a benchmark problem and makes parameter recommendations to optimise algorithm performance; the fourth section is *three-point flexural test* which provides an overview of a multidimensional quasi-analytical model for the effective property of a beam under 3-point loading; the fifth section is *one-dimensional meta-modelling* which investigates the application of the functional optimisation algorithm to optimise the meta-models to the results of a 1D finite element model; the sixth section is *two-dimensional meta-modelling* which investigates the application of the functional optimisation algorithm to optimise the meta-models to the results of a 2D finite element model; finally, the seventh section is *conclusion* which provides an overview of the contribution of this chapter and makes recommendations for future research into the meta-modelling of effective properties.

4.2 Mean meta-models

Analytical mean meta-models have been used extensively within the research field of reservoir engineering to model the effective permeability of rock formations. In particular, the most commonly used models have been the arithmetic, geometric and harmonic means which are collectively referred to as the Pythagorean means (King, 1987). Additionally, it is useful to note that these three means can be generalised into a single mean of arbitrary power and that this generalised mean meta-model offers greater predictive power due to its variable sensitivity to extrema of the underlying field (Journel et al., 1986). Furthermore, it is also desirable that these meta-models account for spatial weighting since it has been observed, in flow problems, that the value of the material property at some points in the domain has been found to have a greater contribution to the effective property. For instance, details of an investigation into the varying spatial dependency of the effective permeability of a well on the field of permeability for the case of a harmonic mean can be found in Oliver (1990) and Desbarats (1992). It is a novel contribution of this thesis to present an expression for a meta-model suitable for modelling the effective properties of multidimensional randomly heterogeneous beams. The generalised weighted mean meta-model for the effective property Z^* of a material whose properties vary in three-spatial dimensions $Z(x, y, z)$ is presented in integral form as:

$$Z^* = \left(\int_D \omega(x, y, z) \cdot Z(x, y, z)^m \, \mathrm{d}V \right)^m \tag{4.2}$$

where D is the domain of integration, $\omega(x, y, z)$ is the weighting function, m is the power of the mean and $\mathrm{d}V$ is a differential volume element. In order to satisfy the traditional definition of a mean, the weighting function $\omega(x, y, z)$ should satisfy the following integration requirement:

$$\int_D \omega(x, y, z) \, \mathrm{d}V = 1 \tag{4.3}$$

Observing that the right-hand side of this equation is dimensionless, it is noted that the units of the weighting function $\omega(x, y, z)$ are given by the reciprocal of the units of the domain D.

The power m controls the extent to which the meta-model for the effective property Z^* tends towards the extrema of the random field $Z(x, y, z)$. As m increases, the effective property Z^* tends towards the maxima of the random field $Z(x, y, z)$ and, as m decreases, Z^* tends towards the minima of $Z(x, y, z)$. In the limiting case, as $m \to -\infty$, the effective property Z^* is equal to the minima of $Z(x, y, z)$ which is useful for modelling minima-type effective properties such as the strength of a brittle material. When the power $m = 1$, the effective property Z^* is the arithmetic mean Z_A^* of the random field $Z(x, y, z)$, as $m \to 0$ then Z^* tends to the geometric mean Z_G^* of $Z(x, y, z)$ and when $m = -1$ then Z^* is the harmonic mean Z_H^* of $Z(x, y, z)$. It is the observation of Cardwell and Parsons (1945) that average-type effective properties, such as permeability, are bounded by the harmonic and arithmetic mean. Consequently, in the case that $-1 \leq m \leq 1$, the effective property models average-type effective properties such as permeability, elastic modulus and electrical conductivity. Finally, it is important to note that this chapter will only consider the case of average-type effective properties given by the three Pythagorean means rather than effective properties with an arbitrary power m. This is because the simultaneous optimisation of both the power m and the weighting function $\omega(x, y, z)$ is beyond the scope of this research and, therefore, only the optimisation of the weighting function $\omega(x, y, z)$ is pursued within this chapter.

The arithmetic mean ($m = 1$) can be considered the simplest of the three Pythagorean means since the relationship between the effective property Z^* and the random field

$Z(x, y, z)$ is linear. The weighted arithmetic mean Z_A^* is given by:

$$Z_A^* = \int_D \omega_A(x, y, z) \cdot Z(x, y, z) \, \mathrm{d}V \tag{4.4}$$

This meta-model is an exact model for material properties such as effective density, as well as the idealised case of effective permeability where heterogeneity is solely perpendicular to the direction of flow which is known as a series system (Fuchs et al., 2013). However due to the simplicity and attractive analytical properties of this linear system, the arithmetic mean Z_A^* has also been used to model non-arithmetic effective properties, such as effective elastic modulus, in a parallel system (Bulleit and Chapman, 2004). If the integration requirement of the weighting function is met $\int_D \omega(x, y, z) \, \mathrm{d}V = 1$ then, in the case that the random field $Z(x, y, z)$ has a finite stationary expected value, the arithmetic mean Z_A^* has the useful property of mean preservation since the expected value of the effective property Z_A^* is equal to the expected value of the random field $\mathbb{E}[Z_A^*] = \mathbb{E}[Z(x, y, z)]$. However, the property of mean preservation inhibits the use of this meta-model for properties that are dominated by low values, such as modulus of elasticity, since these properties do not exhibit mean preservation $\mathbb{E}[Z^*] < \mathbb{E}[Z(x, y, z)]$. It is the novel observation of this thesis that this limitation can be overcome by relaxing the integration requirement of the weighting function $\omega(x, y, z)$ such that $\int_D \omega_A(x, y, z) \, \mathrm{d}V < 1$. This facilitates the use of the arithmetic mean Z_A^* to model geometric or harmonic effective properties without the risk of systematically overpredicting the true value of the effective property.

The harmonic mean ($m = -1$) is a non-linear model for the relationship between the effective property Z^* and the material property $Z(x, y, z)$. The weighted harmonic mean Z_H^* is given by:

$$Z_H^* = \left(\int_D \omega_H(x, y, z) \cdot Z(x, y, z)^{-1} \, \mathrm{d}V \right)^{-1} \tag{4.5}$$

where $(.)^{-1}$ does not signify the inverse of the function, but rather the pointwise reciprocal such that $Z(x)^{-1} = \{x_i \in D | Z(x_i)^{-1}\}$. The harmonic mean Z_H^* exactly models effective permeability where heterogeneity is solely parallel to the direction of flow (Fuchs et al., 2013) and has been shown, in Chapter 3, to exactly model the effective elastic modulus of an Euler-Bernoulli beam. The harmonic mean Z_H^* is more strongly influenced

by minima than the arithmetic mean and, consequently, does not exhibit the property of mean preservation since the expected value of the harmonic meta-model Z_H^* is lower than the expected value of the random field $\mathbb{E}[Z_H^*] < \mathbb{E}[Z(x,y,z)]$.

The final Pythagorean mean is the geometric mean Z_G^* which is obtained by taking the limit $m \to 0$ in the generalised power mean meta-model. The weighted geometric mean Z_G^* is given by:

$$Z_G^* = \exp\left(\int_D \omega_G(x,y,z) \cdot \ln Z(x,y,z)\,\mathrm{d}V\right) \tag{4.6}$$

It is useful to note that if all the weighting functions are equal $\omega_A = \omega_G = \omega_H$ and $Z(x,y,z)$ denotes a set with at least two non-equal values then the following inequality holds for the Pythagorean means: $Z_H^* < Z_G^* < Z_A^*$ (Xia et al., 1999). Therefore, the geometric model Z_G^* can be considered an intermediary between the harmonic Z_H^* and arithmetic Z_A^* means since it is affected by minima to a greater degree than Z_A^* but not to the extent that Z_H^* is affected by minima. It has been suggested that the geometric mean is the best model for effective permeability in the case of multidimensional heterogeneity with spatial variation both parallel and perpendicular to flow since, similar to the one-dimensional case, the effective property Z^* tends towards minima values however, unlike the one-dimensional case, the flow can avoid regions of low permeability therefore the sensitivity to minima is reduced (Matheron, 1968).

An additional factor to consider in the choice between the Pythagorean means is that the geometric and harmonic models are only well-defined for the case that both the random field of the material property $Z(x,y,z)$ and the weighting function $\omega(x,y,z)$ are strictly positive. Thus, the geometric and harmonic means are appropriate models for many strictly positive mechanical properties such as permeability, electrical resistivity and elastic modulus. However for properties that take negative values, or for noisy measurements of strictly positive properties, the arithmetic model Z_A^* is recommended due to its robustness to both negative values as well as values close to zero. Finally, all of the mean models have been presented for the 3D case, however, the 1D and 2D cases can easily be obtained by taking the weighting function $\omega(x,y,z)$ and the random field $Z(x,y,z)$ as constant in the y or z-direction as required.

4.3 Functional optimisation

This section presents a novel functional optimisation algorithm suitable for the optimisation of the weighting function of the generalised mean meta-model. The objective of mathematical optimisation is to find the input argument that minimises or maximises the output of a function. This section considers the optimisation of a particular type of function known as a *functional* which, in simplest terms, can be described as a function whose input argument is also a function. Consequently, the objective of functional optimisation is to find an optimal input function that minimises the functional. The history of functional optimisation began with calculus of variations which is an analytical approach used to solve problems such as the Brachistochrone problem, as well as, the so-called 'heavy-chain' problems (Gelfand and Fomin, 1963). Following the advent of modern computation, numerical approaches to gradient-based functional optimisation have been developed (Dreyfus, 1962) in a field of research that is now known as optimal control theory (Bryson, 1996). In this chapter, an algorithm that treats the functional to be minimised as a black box is sought and, consequently, a derivative free approach is pursued. In particular, an algorithm is developed as an extension to the acceptance-rejection perturbation algorithm proposed by Bocchini and Deodatis (2008) wherein the perturbations are no longer of deterministic shape with random sign but rather realisations of a random field.

4.3.1 Algorithm overview

Let $\bar{f}(x)$ denote the optimal function that minimises the error functional $\epsilon(f(x))$. The objective of the algorithm is to obtain an approximation $\hat{f}(x)$ to the optimal function $\bar{f}(x)$ through an iterative acceptance-rejection approach. At each step of the algorithm, a new approximation $\hat{f}_p(x)$ is proposed to the current iteration of the approximation $\hat{f}_i(x)$ such that:

$$\hat{f}_p(x) = \hat{f}_i(x) + \xi(x) \tag{4.7}$$

where $\xi(x)$ is a random perturbation. If the proposed function $\hat{f}_p(x)$ decreases the error functional i.e. if $\epsilon(\hat{f}_p(x)) < \epsilon(\hat{f}_i(x))$ then the perturbation is accepted:

$$\hat{f}_{i+1}(x) = \hat{f}_p(x) \tag{4.8}$$

Otherwise, the perturbation is rejected:

$$\hat{f}_{i+1}(x) = \hat{f}_i(x) \tag{4.9}$$

At the initialisation of the algorithm, an initial approximation $\hat{f}_0(x)$ to the optimal function $\bar{f}(x)$ is required. If a priori information about the form of $\bar{f}(x)$ is available then this can be included in the specification of the initial approximation $\hat{f}_0(x)$, otherwise, if a priori information about $\bar{f}(x)$ is unavailable then the initial approximation $\hat{f}_0(x)$ can be taken to be uniform and located at the best estimate of the centroid of $\bar{f}(x)$. Additionally, it should be noted that the perturbations $\xi(x)$ are of arbitrary form, for instance Bocchini and Deodatis (2008) took the perturbations to be of Gaussian form:

$$\xi(x) = \alpha \exp\left[-\frac{(x - x_0)^2}{\beta^2}\right] \tag{4.10}$$

where α, β and x_0 are the amplitude, scale and location parameters respectively. Bocchini and Deodatis (2008) took α as a constant with random sign, $\beta^2 = 40$ and x_0 as uniformly distributed on the domain D over which the approximation $\hat{f}(x)$ is to be optimised. The disadvantage of taking the perturbations $\xi(x)$ to be of Gaussian form is that they are of constant symmetric shape and constitute a solely positive or negative modification to the current iteration of the approximation $\hat{f}_i(x)$. It is a contribution of this thesis to propose a novel acceptance-rejection algorithm that is more robust and overcomes these limitations by taking these perturbations $\xi(x)$ to be realisations of a Gaussian random field:

$$\xi(x) \sim \mathcal{N}(\mu_\xi, \sigma_\xi^2 \rho_\xi(s)) \tag{4.11}$$

where μ_ξ, σ_ξ and $\rho_\xi(s)$ are the mean, standard deviation and correlation function of the random field perturbations respectively. If it is desired that the approximation $\hat{f}(x)$ is smooth, then it is recommended that the correlation function of the perturbations $\rho_\xi(s)$ is given by the Gaussian correlation function:

$$\rho_\xi(s) = \exp\left(-\pi\left(\frac{s}{\theta_\xi}\right)^2\right) \tag{4.12}$$

where θ_ξ is the correlation length and s is the absolute separation between two points.

4.3.2 Optimisation investigation

This section evaluates the performance of the novel functional acceptance-rejection optimisation algorithm on a benchmark problem. In particular, the convergence characteristics of the algorithm are evaluated and recommendations are made on the selection of the parameters of the random field perturbations. In this optimisation investigation, the benchmark function and hence the optimal function $\bar{f}(x)$ to iteratively approximate is given by:

$$\bar{f}(x) = \frac{\sin(11x) + \cos(19x) + \cos(29x)}{3} \tag{4.13}$$

where optimisation is only considered over the domain $x \in D = [0, 1]$ which is discretised into N equispaced points. The error functional $\epsilon(f(x))$, and hence the function to minimise, is given by the mean square error (MSE) between the approximation $\hat{f}(x)$ and the optimal function $\bar{f}(x)$:

$$\epsilon(\hat{f}(x)) = \text{MSE}[\hat{f}(x)] = \frac{1}{N}\sum_{i=1}^{N}\left(\hat{f}(x_i) - \bar{f}(x_i)\right)^2 \tag{4.14}$$

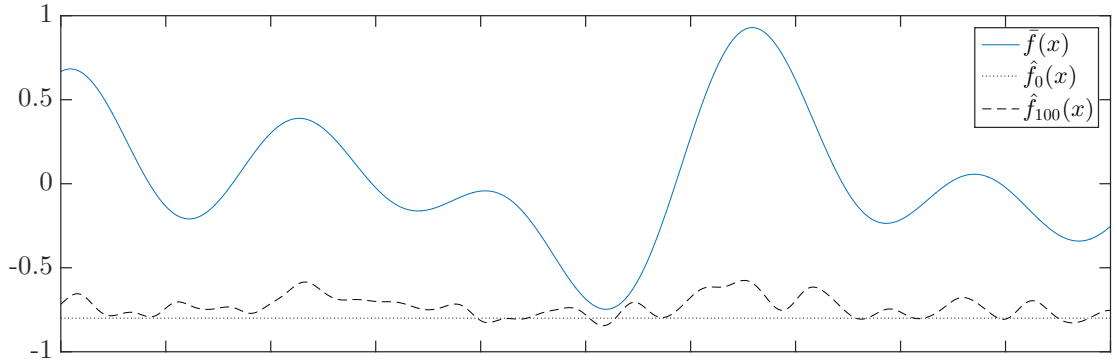
Table 4.1 shows the parameter values of the random field perturbations $\xi(x)$ and the value of the initial approximation $\hat{f}_0(x)$ utilised for the optimisation investigation. For fastest convergence, the uniform initial function $\hat{f}_0(x)$ should be located at the centroid of the optimal function $\bar{f}(x)$, however, $\hat{f}_0(x)$ has been deliberately offset to -0.8 to investigate optimisation under suboptimal conditions. The number of elements N that are used to discretise the approximation $\hat{f}(x)$ does not significantly affect algorithm convergence and has arbitrarily been taken equal to 10^3. Additionally, it is noted that the perturbation parameters, namely the number of perturbations R_ξ as well as the location μ_ξ, scale σ_ξ and correlation θ_ξ parameters, have been selected based on rules of thumb presented at the end of this section. Furthermore, the effect of varying the perturbation parameters

from those given in Table 4.1 on the convergence of the acceptance-rejection functional optimisation algorithm is investigated through sensitivity analyses contained within this section.

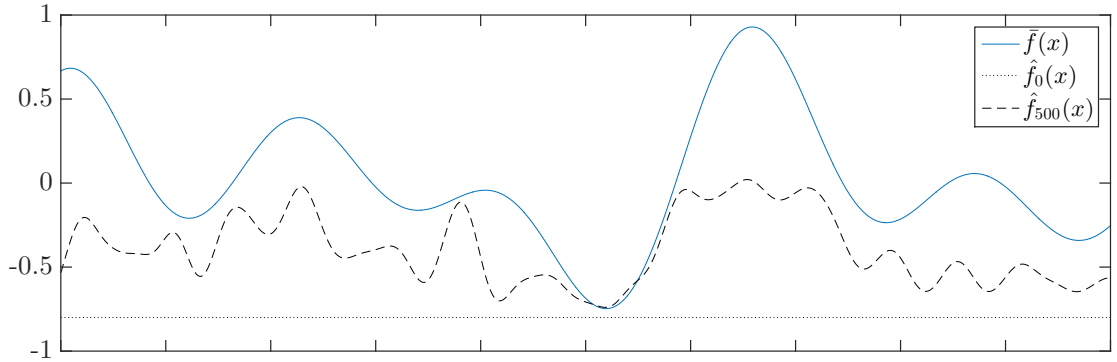
Table 4.1: Parameter values selected for the convergence study of the functional optimisation algorithm.

Parameter name	Symbol	Value
Uniform initial approximation	$\hat{f}_0(x)$	-0.8
Discretisation of the domain	N	10^3
Number of perturbations	R_ξ	10^5
Location parameter	μ_ξ	0
Scale parameter	σ_ξ	0.01
Correlation length	θ_ξ	0.1

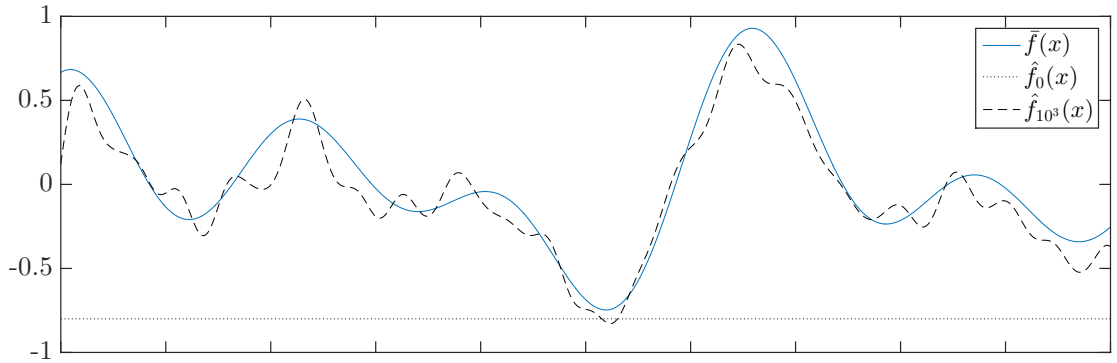
Figure 4.1 shows the convergence of the approximation $\hat{f}(x)$ to the optimal function $\bar{f}(x)$ as the number of perturbations increases from (a) $R_\xi = 100$ to (d) $R_\xi = 10^5$. The convergence of $\hat{f}(x)$ to $\bar{f}(x)$ can be roughly divided into two stages: the first is a coarse adjustment phase, observed in subfigures (a) to (c), and the second is the fine adjustment phase, observed is subfigures (c) to (d). The coarse adjustment phase is primarily concerned with vertically translating the initial approximation $\hat{f}_0(x)$ to the centroid of $\bar{f}(x)$ whilst the fine adjustment phase is concerned with adapting the approximation $\hat{f}(x)$ to closely match the shape of $\bar{f}(x)$. However, it should be noted that even during the early stages $R_\xi = 100$ of the coarse adjustment phase, the approximation $\hat{f}(x)$ already shows evidence of beginning to adopt the minima and maxima pattern of $\bar{f}(x)$ which is indicative of fine scale optimisation. Consequently, the coarse and fine adjustment phases should not be considered absolutely distinct stages, but rather a framework for understanding the convergence of the algorithm. It is evident by inspection that for $R_\xi = 10^5$ perturbations, good agreement has been achieved between the approximation $\hat{f}_{10^5}(x)$ and the optimal function $\bar{f}(x)$. However, two systematic inaccuracies in the approximation $\hat{f}_{10^5}(x)$ should be elucidated: firstly, at the local minima and maxima there is evidence of overshooting which is attributed to the influence of the correlation length θ_ξ in excessively smoothing $\hat{f}(x)$ and, secondly, the optimisation of $\hat{f}(x)$ at the boundaries of the domain is less accurate since the value of the function outside the domain cannot penalise, and thereby constrain, the derivative of $\hat{f}(x)$.



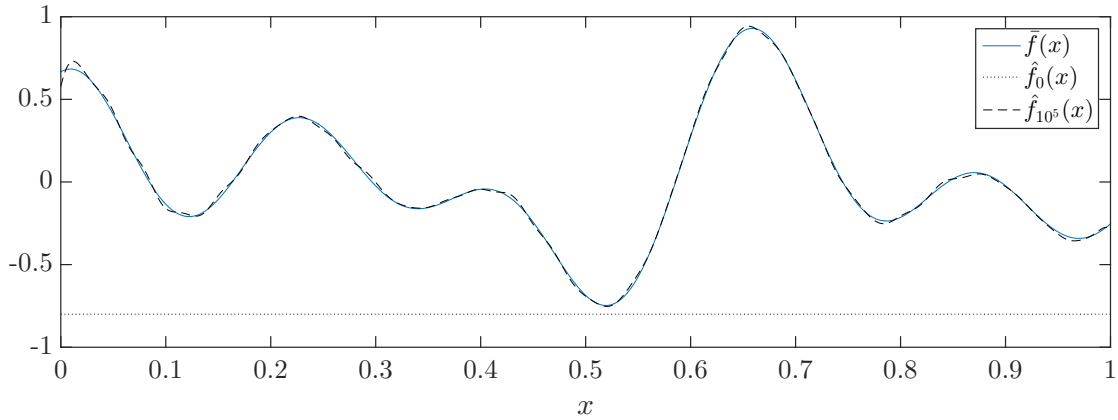
(a) $R_\xi = 100$



(b) $R_\xi = 500$



(c) $R_\xi = 10^3$



(d) $R_\xi = 10^5$

Figure 4.1: Convergence of the approximation $\hat{f}(x)$ to the benchmark optimal function $\bar{f}(x)$ for a varying number R_ξ of random field perturbations.

In addition to the acknowledgement of the positive performance of the optimisation algorithm on the benchmark problem, as illustrated in Figure 4.1, a word of caution is required with regards to two major limitations of the functional optimisation algorithm. The first limitation is that the algorithm is extremely sensitive to local minima of the error functional $\epsilon(f(x))$ and can only reasonably be expected to approximate a locally optimal function $\bar{f}(x)$. This is because the algorithm only accepts perturbations that strictly minimise the error functional $\epsilon(f(x))$ and, consequently, the algorithm has no ability to escape local minima in order to find a global minima. The second limitation is that the parameters of the random field perturbations have a significant affect on the accuracy of the approximation $\hat{f}(x)$ obtained within a finite number R_ξ of perturbations. In order to investigate this limitation, a number of sensitivity analyses have been performed to analyse the dependency of convergence of the functional optimisation algorithm on the parameters of the random field perturbations and the results of these sensitivity analyses are contained at the end of this section. In particular, the influence of taking the standard deviation σ_ξ and the correlation length θ_ξ to be one order of magnitude smaller and greater than the values specified in Table 4.1 is investigated.

Figure 4.2 shows the rate of convergence of the approximation $\hat{f}(x)$ to the optimal function $\bar{f}(x)$ for $R_\xi = 10^5$ perturbations with a small $\sigma_\xi = 0.001$, medium $\sigma_\xi = 0.01$ and large standard deviation $\sigma_\xi = 0.1$. It is evident that the large standard deviation $\sigma_\xi = 0.1$ results in fast convergence during the coarse adjustment phase, however, the large standard deviation appears to then inhibit fine-scale adjustment since the perturbations are too large to be accepted at a suitable rate. In contrast, the small standard deviation $\sigma_\xi = 0.001$ results in slower convergence during the coarse adjustment phase, however, the rate of convergence is consistent and, for a large number of perturbations $R_\xi = 10^5$, the best convergence is achieved. Additionally, in comparison to the small $\sigma_\xi = 0.001$ and large $\sigma_\xi = 0.1$ standard deviation, the intermediary standard deviation $\sigma_\xi = 0.01$ offers acceptable convergence during both the coarse-scale and fine-scale adjustment phases. Finally, it is concluded that the optimal choice of the scale parameter σ_ξ depends on the number of perturbations R_ξ that are proposed since if $R_\xi = 10^2$ then $\sigma_\xi = 0.1$ offers the best convergence, whilst if $R_\xi = 10^4$ then $\sigma_\xi = 0.01$ offers the best convergence and, lastly, if $R_\xi = 10^5$ then $\sigma_\xi = 0.001$ offers the best convergence.

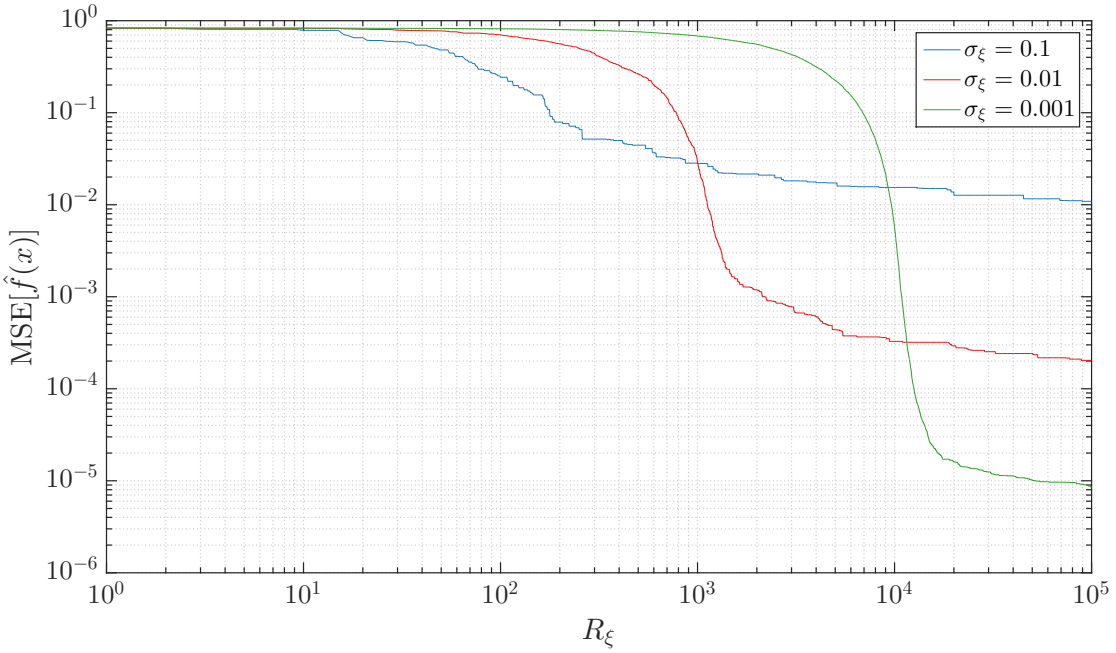


Figure 4.2: Mean square error MSE between the approximation $\hat{f}(x)$ and the optimal function $\bar{f}(x)$ against number of perturbations R_ξ for three different values of the standard deviation σ_ξ.

On the basis of the sensitivity analysis conducted to investigate the dependency of convergence of the functional optimisation algorithm on the scale parameter σ_ξ, it is recommended that if an estimate of the range of the optimal function $\hat{\chi} \approx \max[\hat{f}(x)] - \min[\hat{f}(x)]$ is available then the following rule of thumb can be utilised to select the scale parameter σ_ξ of the perturbations:

$$\sigma_\xi = \frac{\hat{\chi}}{\sqrt[B]{R_\xi}} \tag{4.15}$$

where the root B can typically be taken to be equal to 2. However, it is useful to note that faster convergence can be achieved by taking $B > 2$ at the expense of fine-scale adjustment or, alternatively, more accurate fine-scale adjustment can be achieved by taking $B < 2$ at the expense of the rate of coarse-scale adjustment.

In addition to consideration of the scale parameter σ_ξ, the rate of convergence of the algorithm with respect to the correlation parameter θ_ξ is also investigated. Figure 4.3 shows the optimised approximation $\hat{f}(x)$ for $R_\xi = 10^5$ perturbations with the small correlation length $\theta_\xi = 0.005$. It is observed that the choice of the correlation length

θ_ξ not only affects the rate of convergence, but also has a significant impact of the final optimised shape of $\hat{f}(x)$. Additionally, it is noted that this correlation length θ_ξ is unsuitably small and results in an overfitted approximation $\hat{f}(x)$ that, whilst following the general trend of the optimal function $\bar{f}(x)$, exhibits highly oscillatory behaviour. In the case that an overly rough final approximation is obtained, two solutions are suggested to rectify this issue: firstly, the optimisation could be repeated with a larger correlation length in order to impose sufficient regularity on the optimised approximation $\hat{f}(x)$ or, secondly, a moving average of the optimised approximation $\hat{f}(x)$ could be taken since $\hat{f}(x)$ oscillates around the optimal function $\bar{f}(x)$.

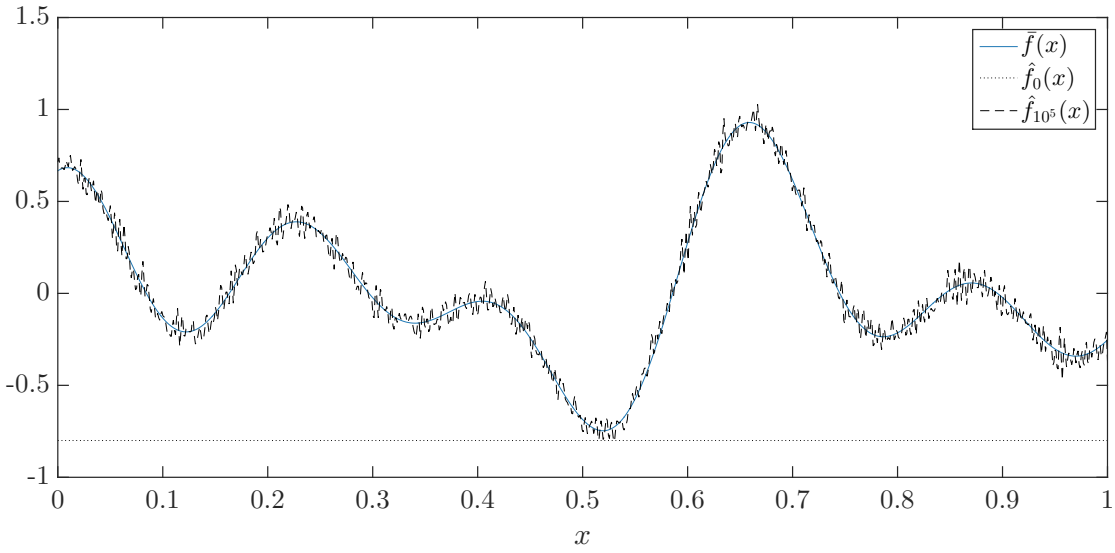


Figure 4.3: Convergence of the approximation $\hat{f}(x)$ to the optimal function $\bar{f}(x)$ for $R_\xi = 10^5$ perturbations with an unsuitably small correlation length $\theta_\xi = 0.005$.

Figure 4.4 shows the optimised approximation $\hat{f}(x)$ for $R_\xi = 10^5$ perturbations with a large correlation length $\theta_\xi = 0.5$. It is observed that this correlation length is unsuitably large since it results in an underfitted optimised approximation $\hat{f}(x)$ that is too smooth to capture the detailed variation of $\bar{f}(x)$. It is evident that choosing a correlation length that is either too small or too large has a negative effect on the approximation $\hat{f}(x)$. However, it should be recognised that the overfitting phenomena associated with an unsuitably small correlation length is more easily detected than the underfitting phenomena associated with an unsuitably large correlation length. For instance, it would be easy to believe that the optimised function $\hat{f}(x)$ in Figure 4.4 had converged to the optimal function if the true optimal function $\bar{f}(x)$ were not known. Consequently, it is recommended in the choice of the correlation length θ_ξ that, in the face of uncertainty,

a small correlation length should be favoured since problems in convergence are more easily detected.

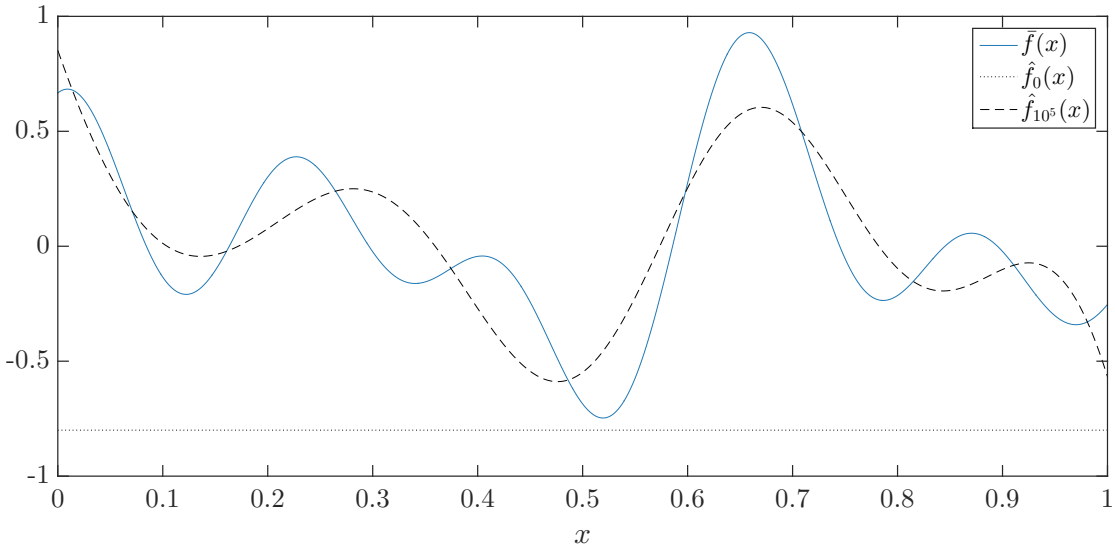


Figure 4.4: Convergence of the approximation $\hat{f}(x)$ to the optimal function $f(x)$ for $R_\xi = 10^5$ perturbations with an unsuitably large correlation length $\theta_\xi = 0.5$.

Figure 4.5 shows the rate of convergence of the approximation $\hat{f}(x)$ to the optimal function $\bar{f}(x)$ for $R_\xi = 10^5$ perturbations with a small $\theta_\xi = 0.005$, medium $\theta_\xi = 0.05$ and large $\theta_\xi = 0.5$ correlation length. It is evident that a large correlation length $\theta_\xi = 0.5$ results in initially faster convergence (i.e. for less than $R_\xi = 10^3$ perturbations), however for a large number of perturbations $R_\xi = 10^5$, the error remaining after optimisation is significant and this is due to the approximation $\hat{f}(x)$ underfitting the optimal function $\bar{f}(x)$ as shown in Figure 4.4. In contrast, the small correlation length $\theta_\xi = 0.005$ results in slower convergence initially, although, a better fit is ultimately achieved for $R_\xi > 3 \times 10^3$ perturbations despite the issue of over-fitting as shown in Figure 4.3. However, the convergence achieved for $R_\xi > 10^3$ perturbations with a medium correlation length $\theta_\xi = 0.05$ is superior to the convergence achieved for either the small $\theta_\xi = 0.005$ or large $\theta_\xi = 0.5$ correlation lengths. Finally, it is observed that whilst the choice of the standard deviation σ_ξ is based on the desired rate of convergence during both the coarse and fine-scale adjustment phases, in comparison, the choice of the correlation length θ_ξ is constrained by the fundamental smoothness of the optimal function $\bar{f}(x)$. This is because the value of θ_ξ does not just affect the convergence rate of the algorithm but also the optimised shape of $\hat{f}(x)$. Consequently, it is concluded that the convergence of the functional optimisation algorithm is highly sensitive to the choice of correlation

length θ_ξ.

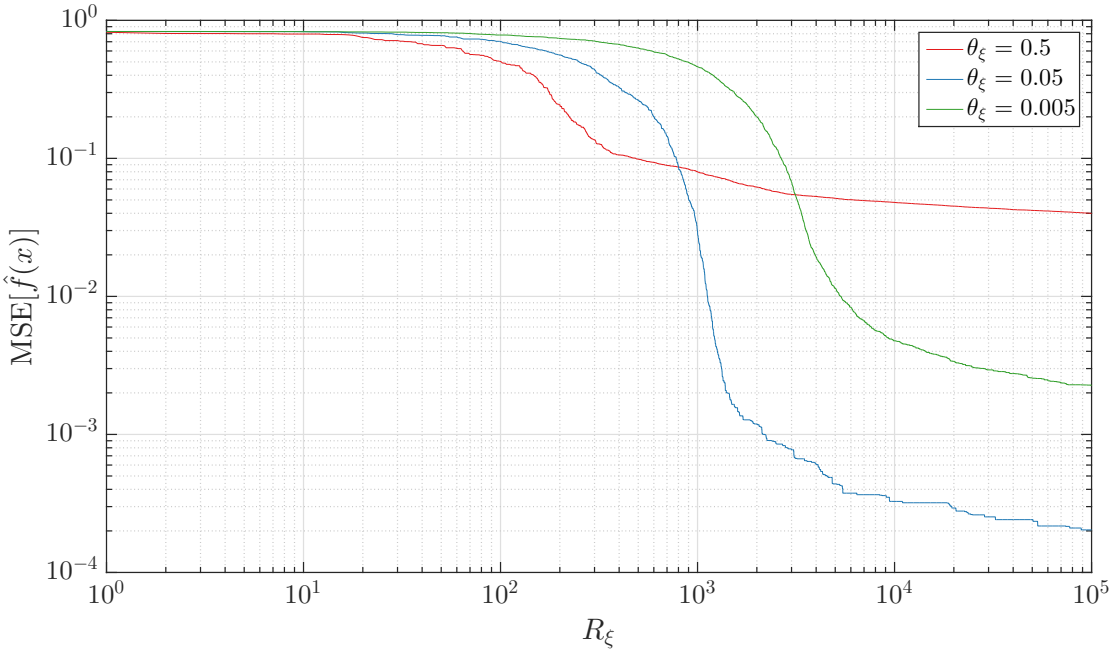


Figure 4.5: Mean square error MSE between the approximation $\hat{f}(x)$ and the optimal function $\bar{f}(x)$ against the number of perturbations R_ξ for three different values of the correlation length θ_ξ.

On the basis of the sensitivity analysis conducted to investigate the dependency of convergence on the correlation length θ_ξ, it is recommended that if an estimate of the number of maxima $\hat{N}_{\max}$ and minima $\hat{N}_{\min}$ of the optimal function $f(x)$ is available then the following rule of thumb can be used to select the correlation length θ_ξ of the perturbations:

$$\theta_\xi = \frac{L}{C\left(\hat{N}_{\max} + \hat{N}_{\min}\right)} \tag{4.16}$$

where L is the size of the domain D over which the approximation $\hat{f}(x)$ is to be optimised and C is a constant whose value is selected to mitigate against underfitting. In order to provide sufficient protection against overfitting, it is recommended to take the constant such that $C \geq 2$, however, if underfitting is not a significant concern then the constant can be taken such that $C = 1$.

The investigation contained within this section into the performance of the functional

optimisation algorithm for different values of the standard deviation σ_ξ and correlation length θ_ξ demonstrates the sensitivity of the algorithm to the parameters of the random field perturbations. During the coarse adjustment phase, it is clear that perturbations with a large standard deviation σ_ξ are optimal, however, as the algorithm progresses into the fine adjustment phase, perturbations with a small standard deviation σ_ξ are required. It is suggested that the performance of the functional optimisation algorithm could be improved by making the algorithm adaptive with respect to the scale parameter σ_ξ by setting a target acceptance rate and, if too few perturbations are being accepted, then σ_ξ is to be decreased, otherwise, if too many perturbations are being accepted then σ_ξ is to be increased. An investigation would be required to identify a rule of thumb for the optimal acceptance rate of perturbations, however, for other algorithms such as Metropolis-Hastings Markov Chain Monte Carlo an acceptance rate of 0.234 has been suggested (Roberts and Rosenthal, 2001). Finally, it is noted that adaptation with respect to the correlation length θ_ξ is challenging since the optimal choice of this parameter depends on the intrinsic smoothness of the optimal function $\bar{f}(x)$ and does not solely depend on the desired rate of convergence. It is suggested that an adaptive algorithm for the correlation length θ_ξ would need to make inferences about the smoothness of $\bar{f}(x)$ based on the iterations of the approximation $\hat{f}_i(x)$. This can be achieved by estimating the number of local minima and maxima of $\hat{f}_i(x)$ and using Equation 4.16 to adaptively select the correlation length θ_ξ of the random field perturbations.

4.4 Three-point flexural test

It has been found in Chapter 3 that the effective elastic modulus of a one-dimensional heterogeneous beam is given exactly by a harmonic mean with a quadratic weighting function. The contribution of the remainder of this chapter is to consider the case of a two-dimensional beam with heterogeneity in both the x and y-directions for which analytical expressions for the effective elastic modulus E^* are not readily available thus motivating the use of meta-models. Consequently, the weighted mean meta-models for effective properties, developed in Section 4.2, as well as the functional optimisation algorithm to optimise the weighting functions of these meta-models, developed in Section 4.3, are applied to the case of a simply supported beam under 3-point loading as shown in Figure 4.6. It is noted that three-point beam bending is an excellent problem for the

application of the weighted mean meta-models since the effective elastic modulus of a beam exhibits a strong spatial dependency which is to be quantified through optimisation of the weighting function to the results of the finite element model. Furthermore, in the one-dimensional case, it is possible to evaluate convergence of the harmonic meta-model to the analytical solution and, additionally, in the case of arithmetic and geometric means it is possible to investigate the effect of modelling a harmonic system using non-harmonic means. In the two-dimensional case, the effective property can only be accurately found by a finite element model and, consequently, the advantage of meta-models is that they provide conceptual insights into the relationship between the effective elastic modulus and the random field of elastic modulus.

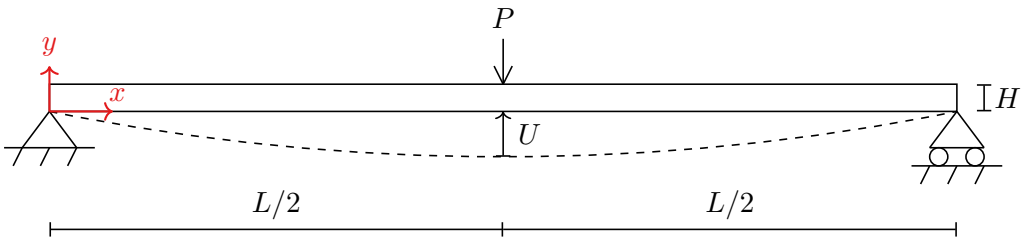


Figure 4.6: Idealised model of a simply supported beam of length L and cross-section height H under 3-point loading of magnitude P resulting in midspan vertical displacement U.

Under Euler-Bernoulli theory, the midspan displacement U of simply supported beam under 3-point loading is given by:

$$U = \frac{PL^3}{48E^*I} \tag{4.17}$$

where P is the midspan point load, L is the length of the beam, I is the second moment of area of the cross-section and E^* is the effective modulus of elasticity. In the case that the elastic modulus E only varies longitudinally in the x-direction then the effective elastic modulus E^* is given by (Bechtel, 1985):

$$E^* = \left(\int_0^L \omega_X(x) \cdot E(x)^{-1} \, \mathrm{d}x \right)^{-1} \tag{4.18}$$

where $\omega_X(x)$ is the weighting function in the x-direction that is given by:

$$\omega_X(x) = \begin{cases} \dfrac{12x^2}{L^3} & \text{if } 0 \leq x \leq \dfrac{L}{2} \\ \dfrac{12(L-x)^2}{L^3} & \text{if } \dfrac{L}{2} \leq x \leq L \end{cases} \tag{4.19}$$

This result was further extended by Bechtel (1985) to the case where elastic modulus E also varies transversely in the y-direction. However, it is important to note that this higher-dimensional extension is still under the assumption of one-dimensional behaviour since it is assumed that the neutral axis is at the centroid of the beam and that plane sections remain plane. Consequently, the expression for the 2D effective elastic modulus is not analytical but rather quasi-analytical and is given by:

$$E^*_{AH} = \left(\int_0^L \omega_X \left(\int_0^H \omega_Y(y) \cdot E(x,y) \, \mathrm{d}y \right)^{-1} \mathrm{d}x \right)^{-1} \tag{4.20}$$

where $\omega_Y(y)$ is the weighting function in the y-direction that is given by:

$$\omega_Y(y) = \frac{12\left(y - \frac{H}{2}\right)^2}{H^3} \quad \text{if } 0 \leq y \leq H \tag{4.21}$$

The weighting function $\omega_Y(y)$ assigns zero weight to the vertical centroid of the beam and quadratically increases towards the top and bottom of the beam section. It should be recognised that the neutral axis of a heterogeneous beam is distinct from its vertical centroid. Finally, the reason that this quasi-analytical effective property is notated E^*_{AH} is that it is a hybrid model consisting of an arithmetic mean E^*_A in the y-direction and a harmonic mean E^*_H in the x-direction.

4.5 One-dimensional meta-modelling

The stochastic finite element model detailed in Chapter 3 has been utilised within this section to investigate the application of the mean meta-models to a one-dimensional heterogeneous beam under 3-point loading. It is noted that only two beam elements are required in the homogeneous case to obtain the exact midspan deflection of a beam under 3-point loading (Zienkiewicz and Taylor, 2005). However, a larger number of elements $N = 1000$ are utilised in the heterogeneous case in order to appropriately discretise the

stiffness profile $E(x)$ which is modelled as a lognormal random process with mean $\mu =$ 12 GPa, standard deviation $\sigma = 3.6$ GPa and the exponential correlation function:

$$\rho(s_X) = \exp\left(-\frac{2|s_X|}{\theta_X}\right) \tag{4.22}$$

where $\theta_X = 0.6$ m. It is noted that these parameter values have been chosen as plausible values for the along-grain elastic modulus of timber in agreement with values reported in the literature (Bulleit and Chapman, 2004, Füssl et al., 2016). The exponential correlation function has been selected since it produces non-smooth realisations which, in comparison to differentiable realisations, is a more realistic model for the variation of physical properties (Stein, 1999). In total $R = 1000$ realisations of the random process $E(x)$ have been generated using the covariance matrix decomposition method detailed in Chapter 2 and, for each realisation, an effective property E^* has been obtained using the finite element model. For illustrative purposes, a single realisation of the stiffness profile is shown in Figure 4.7 along with its computed effective property $E^* = 11.1$ GPa as calculated by the finite element model.

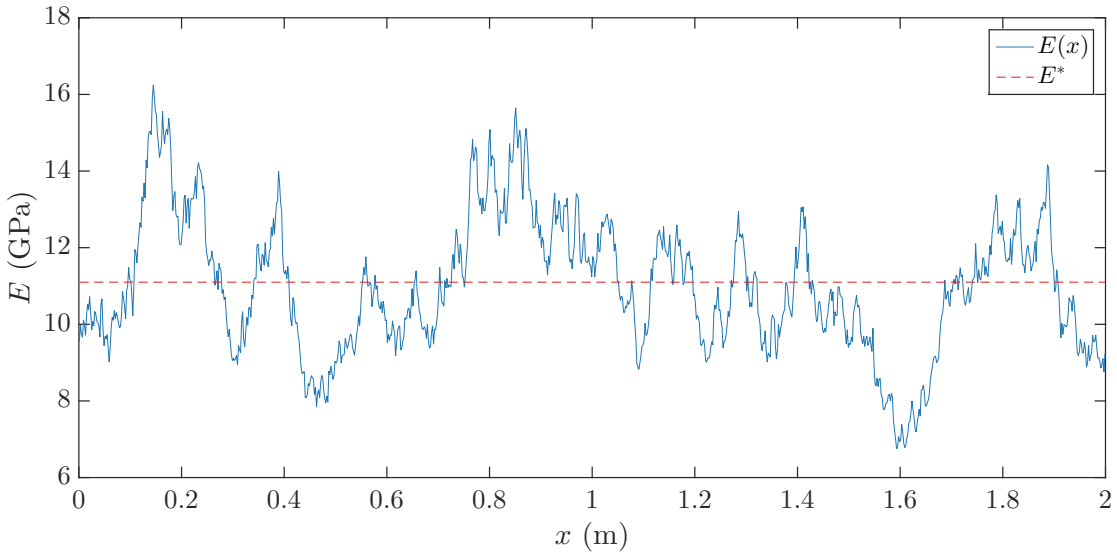


Figure 4.7: A single realisation of the lognormal stiffness profile $E(x)$ and its effective property $E^* = 11.1$ GPa as calculated by the 1D finite element model.

The remainder of this section considers the optimisation of the meta-models to the results of the 1D finite element model with examination of both the rate of convergence and accuracy of the predicted effective properties. The training dataset consisted of $R_T = 20$

realisations of the stiffness profile $E(x)$ and their associated effective properties E^* whilst the remainder of the dataset $R_S = 980$ has been used to evaluate the performance of the meta-models. In the case of 3-point bending, there are two specific details to consider regarding the application of the functional optimisation algorithm to optimise the weighting functions of the meta-models. The first detail to consider is that since the beam is symmetric about the midspan $x = L/2$ then the weighting function must also be similarly symmetric $\omega(x) = \omega(L - x)$ for $0 \leq x \leq L/2$ and, therefore, only half the number of weights N need to be optimised. The second detail to consider is that the functional optimisation algorithm has the possibility to propose a perturbation that results in a negative value for the weighting function $\omega(x)$ at some point in the domain. This is undesirable since negative weights are not physically meaningful and, furthermore, the geometric and harmonic meta-models are ill-behaved for negative inputs. However, rejecting perturbations that result in a negative weighting interferes with the convergence of the optimisation algorithm since it may be necessary to converge to a zero-weighting from below. Consequently, the adopted approach is to allow the weighting function $\omega(x)$ to attain negative values; however, when evaluating the meta-model, any negative weights should be treated as being equal to zero. The parameters of the functional optimisation algorithm, as well as the parameters of the one-dimensional stochastic finite element model, are shown in Table 4.2.

The selected error function between the effective elastic modulus predicted by the meta-models $\{E_A^*, E_G^*, E_H^*\}$ and the finite element model E_{1D}^* is the mean square error since this error function penalises outliers more strongly than alternatives such as the maximum absolute percentage error (Hyndman and Koehler, 2006). Figure 4.8 shows how the error decreases for each meta-model as the number of perturbations N_ξ increases up to 10^5. It is observed, for the initial uniform weighting function ω_0, that the harmonic model E_H^* has the smallest error, the geometric model E_G^* has a larger error whilst the arithmetic model E_A^* has the largest error. The functional optimisation algorithm optimises the geometric model E_G^* slower than the other meta-models and this is attributed to the fact that, for consistency, a constant perturbation standard deviation σ_ξ has been used to optimise all of the meta-models despite the fact that the geometric model E_G^* requires smaller perturbations due to the exponential and logarithmic functions in Equation 4.6. It is observed that after R_ξ perturbations, the mean square error has been reduced by 96.4%, 98.2% and 91.3% for the arithmetic E_A^*, geometric E_G^* and harmonic E_H^* meta-models respectively. The relative decrease in error is the smallest for the harmonic model

Table 4.2: Parameter values for the optimisation of the meta-models to the 1D finite element model.

Parameter name	Symbol	Value	Units
Structural parameters			
Beam length	L	2	m
Second moment of area	I	5×10^{-6}	m^4
Load	P	10	kN
Beam discretisation	N	1000	–
Stiffness parameters			
Mean of stiffness profile	μ	12.0	GPa
Standard deviation of stiffness profile	σ	3.6	GPa
Correlation length of stiffness profile	θ_X	0.6	m
Optimisation parameters			
Number of finite element solves	R	10^6	–
Size of training dataset	R_T	20	–
Size of testing data	R_S	980	–
Number of perturbations	R_ξ	10^5	–
Uniform initial function	ω_0	0.5	–
Perturbation parameters			
Perturbation discretisation	N_ξ	500	–
Mean of perturbations	μ_ξ	0	m^{-1}
Standard deviation of perturbations	σ_ξ	0.1	m^{-1}
Correlation length of perturbations	θ_ξ	2	m

since it does not undergo the coarse adjustment phase due to the fact that its expected value already closely matches that of the effective elastic modulus E^*_{1D}.

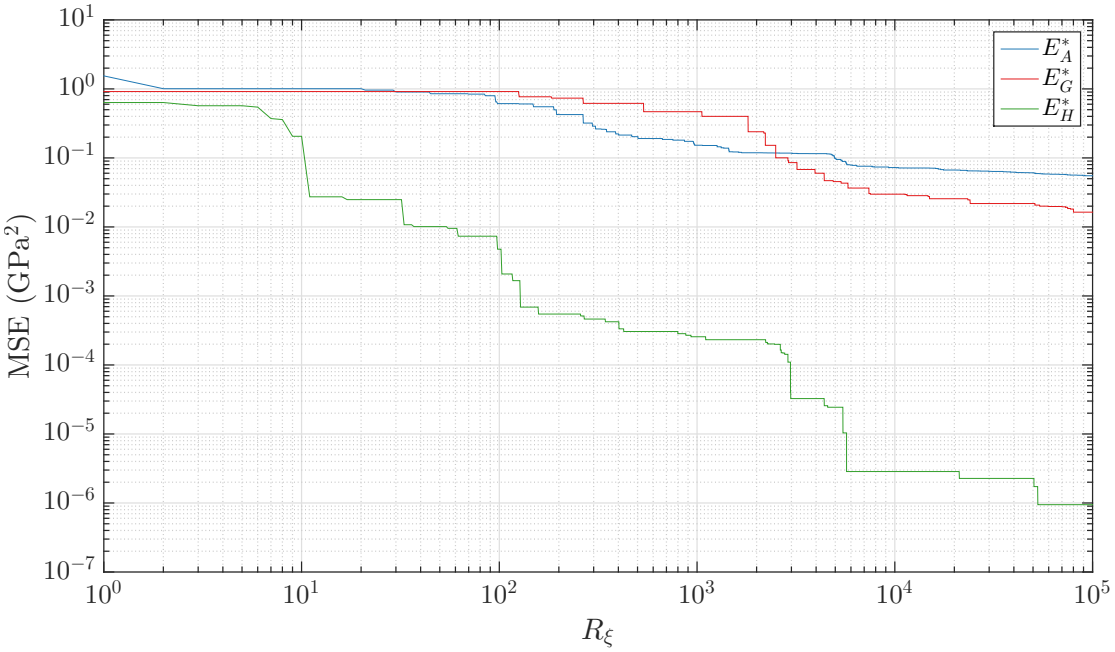


Figure 4.8: Mean square error MSE between the arithmetic E^*_A, geometric E^*_G, harmonic E^*_H meta-models and the one-dimensional effective elastic modulus E^*_{1D} against the number of perturbations R_ξ.

Figure 4.9 shows the optimised arithmetic $\omega_A(x)$, geometric $\omega_G(x)$ and harmonic $\omega_H(x)$ weighting functions compared to the exact weighting function $\omega_X(x)$ derived by Bechtel (1985). It is observed that all the weighting functions assign maximum weighting to the midspan stiffness and a low weighting to the stiffness near the supports of the beam. In particular, close agreement is observed between the exact weighting function $\omega_X(x)$ and weighting function of the harmonic meta-model $\omega_H(x)$ confirming that the functional optimisation algorithm has converged to the exact solution. Additionally, it is noted that the elastic modulus near the supports has no contribution to the effective stiffness of the beam since as $x \to 0$ then the bending moment $M \to 0$ and, consequently, it is asserted that the correct weighting at the supports should be zero. The failure of the arithmetic $\omega_A(x)$ and geometric $\omega_G(x)$ weighting functions to assign zero weighting to the stiffness near the supports is attributed to, as previously identified in Section 4.3, the poor performance of the functional optimisation algorithm at the edges of the domain.

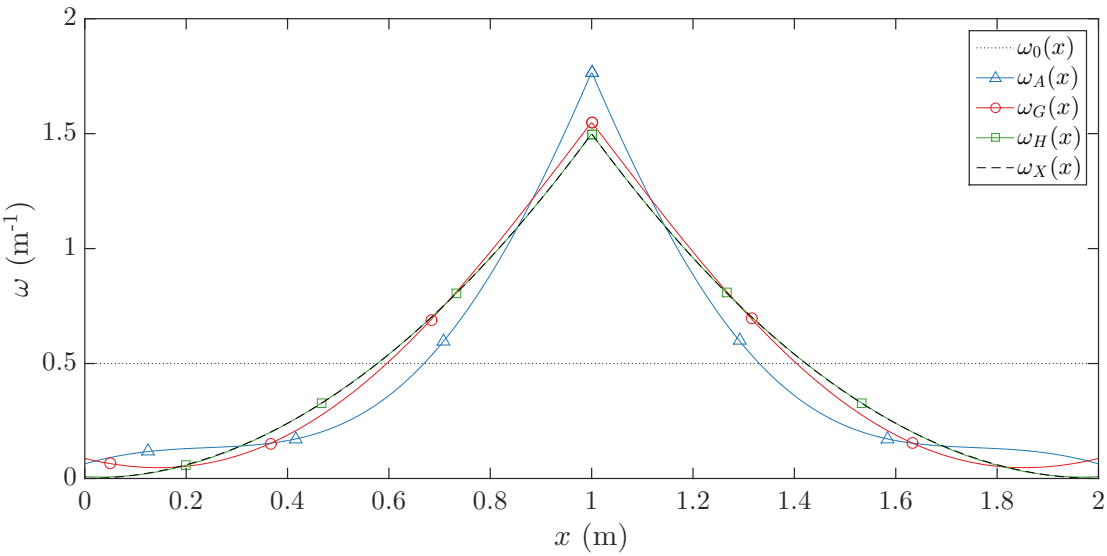


Figure 4.9: Initial $\omega_0(x)$, arithmetic $\omega_A(x)$, geometric $\omega_G(x)$ and harmonic $\omega_H(x)$ weighting functions of the meta-models for $R_\xi = 10^5$ perturbations compared to the exact weighting function $\omega_X(x)$ derived by Bechtel (1985).

The performance of the three meta-models $\{E_A^*,\ E_G^*,\ E_H^*\}$ is evaluated by comparing their prediction of the effective properties to the testing dataset of effective properties $E_{1\mathrm{D}}^*$ obtained by the 1D finite element model. Two different performance metrics are considered, namely the coefficient of determination r^2 and the normalised root mean square error (NRMSE), in order to quantify the residual error of the meta-models remaining after optimisation. The normalised root mean square error, given as a percentage, is considered instead of the mean square error (MSE) since it is more easily interpreted. In addition, two other quantities are reported namely the integral of the optimised weighting function over the domain D (denoted $\int \omega(x)\,\mathrm{d}x$) and the resulting percentage change in the expected value of the meta-model compared to if the weighting function integrated to one (denoted $\Delta\mathbb{E}$). It should be noted that the coefficient of determination r^2 is given by the square of Pearson's correlation coefficient and is a useful performance metric since it quantifies the predictive power of a meta-model independent of its expected value which is dependent on the integral of its weighting function.

Table 4.3 shows the performance metrics of the 1D arithmetic E_A^*, geometric E_G^* and harmonic E_H^* meta-models optimised on the training dataset of $N_T = 20$ finite element solves and evaluated on the testing dataset of $N_S = 980$ finite element solves. It is observed that the arithmetic meta-model E_A^* is the worst performing meta-model with

respect to the two performance metrics, r^2 and NRMSE, and this poor performance is attributed to the inability of E_A^* to suitably model the sensitivity of the effective property E_{1D}^* to minima. In order that the expected value of the arithmetic meta-model E_A^* suitably matches the expected value of the effective property E_{1D}^*, the integral of the weighting function $\omega_A(x)$ has decreased by 4.7% which causes an equivalent reduction in the expected value of E_A^*. In comparison, the geometric meta-model E_G^* offers superior predictive power as quantified by both r^2 and NMRSE and this is due to its increased tendency towards minima which more accurately models the 1D effective property E_{1D}^*. Furthermore, similar to the optimised arithmetic weight function $\omega_A(x)$, the integral of the optimised geometric weighting function $\omega_G(x)$ has also decreased. However, it should be noted that a small decrease in the integral of the geometric weighting function $\omega_G(x)$ causes a large decrease in expected value due to the exponential and logarithmic function in the expression for the geometric mean E_G^* (see Equation 4.6). Finally, the error associated with the optimised harmonic meta-model E_H^* is negligible with respect to the two performance metrics, r^2 and NRMSE, confirming that the functional optimisation algorithm has converged to the true solution. In conclusion, it is evident that the choice of power m and the resulting tendency towards minima has a significant effect on the accuracy of the generalised mean meta-model. However, it has also been shown that the error induced by the choice of a non-exact power m can be mitigated through the relaxation of the integration requirement of the weighting function $\omega(x)$ and this facilitates the use of the arithmetic meta-model Z_A^* to model non-arithmetic effective properties thereby taking advantage of its useful analytical properties as outlined in Section 4.1.

Table 4.3: Performance metrics of the 1D meta-models.

Meta-model	r^2	NRMSE (%)	$\int \omega(x)\,\mathrm{d}V$	$\Delta\mathbb{E}$ (%)
E_A^*	0.968	3.40	0.953	−4.66
E_G^*	0.992	1.66	0.999	−2.28
E_H^*	1.000	0.01	1.000	−0.09

4.6 Two-dimensional meta-modelling

The determination of the effective elastic modulus of a two-dimensional heterogeneous beam requires the use of numerical techniques such as the finite element method. However, it should be noted that there is no software available to perform higher-dimensional stochastic finite element analysis of heterogeneous beams. Consequently, the adopted approach was to develop a deterministic model in the finite element software ABAQUS 6.14 developed by Dassault Systèmes and then to repeatedly sample this model through the Monte Carlo method. The beam was meshed using $N_X = 150$ elements in the x-direction and $N_Y = 30$ elements in y-direction for a total of 4500 plane stress quadrilateral elements with quadratic interpolation and reduced integration. It should be recognised that the development of a finite element model is more complex in the higher-dimensional case due to a number of issues that arise when considering higher-dimensional beam behaviour such as the occurrence of stress concentrations under the point load. The issue of stress concentrations was resolved through the introduction of steel plates of width 30 mm and height 10 mm under the point load and above the supports (see Figure 4.10). Additionally, it was decided that the beam section beyond the supports (as shown by the shaded sections in Figure 4.10) should not be modelled since this region has a negligible contribution to displacement U which was measured at the centroid of the bottom surface of the beam.

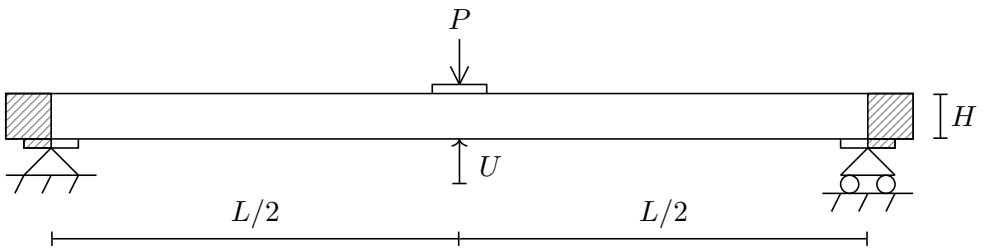


Figure 4.10: Two-dimensional model of 3-point bending with steel plates under the load and above the supports in order to reduce local indentation (shaded beam sections not modelled due to negligible contribution to beam stiffness).

In order to investigate the relationship between one and two-dimensional heterogeneous beam behaviour, it is desired that the displacement associated with the 2D finite element model closely match the displacement of its 1D counterpart. The introduction of the steel plates had the desired effect of reducing local stress concentrations and preventing local indentation in accordance with BS EN 408:2010. However, the steel plates have

the secondary effect of both converting the point load into a distributed load and also extending the support conditions which causes a decrease in displacement thereby causing an increase in the value of the effective property $E^*_{2\mathrm{D}}$. However, this phenomena is to some extent counteracted by the fact that the 2D model includes the effects of shear which is neglected by the 1D model and acts to increase displacement.

The selected standard BS EN 408:2010 requires that the steel plates are of a length no greater than half the depth of the beam which in this specific case corresponds to a length less than 50 mm. A sensitivity analysis was performed to find the length of the plates that minimises the difference between the midspan displacement U of the 1D and 2D finite element models. In the deterministic case of constant modulus of elasticity $E_0 = 12$ GPa, the 1D model with parameters in Table 4.4 predicted a midspan displacement of $U_{1\mathrm{D}} = 27.7776$ mm. The 2D model with plates of length 30 mm and parameters in Table 4.2 predicted a midspan displacement of $U_{2\mathrm{D}} = 27.7775$ mm. The percentage difference of 0.001% between the 1D and 2D finite element models in the deterministic homogeneous case suggests that the effect of introducing the plates, which act to decrease displacement, and the inclusion of the effects of shear, which act to increase displacement, have cancelled out resulting in a negligible difference between the finite element models of different dimension.

It has been shown in the deterministic case that good agreement is achieved between the 1D and 2D finite element models and the next step is to examine the agreement in the stochastic case. In particular, it is noted that in the case of random heterogeneity it is more difficult to achieve equivalence between models of different dimension. The parameters of the 2D random field are equal to those of the 1D random field with mean $\mu = 12$ GPa, standard deviation $\sigma = 3.6$ GPa and higher dimensional correlation function given by the anisotropic Markov correlation function:

$$\rho(s_X, s_Y) = \exp\left(-2\sqrt{\left(\frac{s_X}{\theta_X}\right)^2 + \left(\frac{s_X}{\theta_Y}\right)^2}\right) \tag{4.23}$$

where $\theta_X = 0.6$ m and $\theta_Y = 0.1$ m are the correlation lengths in the x and y-direction respectively. The anisotropic correlation structure has stronger correlations in the longitudinal direction and this is shown in Figure 4.11 which illustrates a single realisation of the lognormal random field.

Table 4.4: Parameter values of the deterministic 2D finite element model.

Parameter name	Symbol	Value	Units
Beam parameters			
Beam length	L	2.00	m
Beam height	H	0.10	m
Beam width	W	0.06	m
Load	P	10	kN
Elastic modulus of beam	E_0	12	GPa
Poisson's ratio of beam	v_p	0.3	–
Discretisation in x-direction	N_X	200	–
Discretisation in y-direction	N_Y	50	–
Element type		CPS8R	
Plate parameters			
Plate length	L_p	0.03	m
Plate height	H_p	0.01	m
Elastic modulus of plates	E_p	210	GPa
Poisson's ratio of plates	v_p	0.2	–

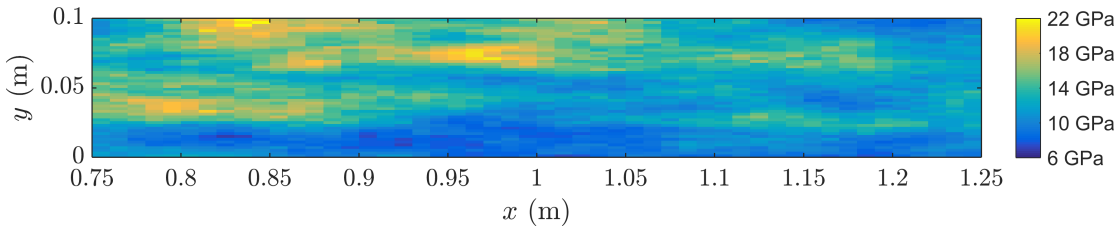


Figure 4.11: Central quarter of a single realisation of the random field $E(x, y)$ and its effective property $E^* = 11.90$ GPa as computed by the 2D finite element model.

A total of 1000 realisations of the 2D random field, with parameters given by Table 4.5, were generated using the MATLAB toolbox `RFbox` through the fast Fourier transform method. For each realisation, a corresponding ABAQUS input file (extension: `.inp`) was written using a script in Python wherein each element in the mesh was assigned a different value of elastic modulus corresponding to the spatial variation of the realisation of the random field. Each input file was submitted to the ABAQUS explicit solver which returns the corresponding output file (extension: `.odb`) containing the output quantities such as displacements, stresses and strains corresponding to that particular realisation of the random field. Each of the output files were read and the midspan displacement extracted using the Python module `odbAccess` which is included in the Python 2.7 interpreter in the ABAQUS 6.14 directory. A total of $R = 1000$ runs were performed with an average solve time of 24.8s for each realisation of the random field on a desktop PC with an i3-4150 CPU and 16 GB of ram. The midspan displacement data was then post-processed in MATLAB and the 2D effective elastic modulus $E^*_{2\mathrm{D}}$ for each realisation was calculated for comparison with the 1D counterparts $E^*_{1\mathrm{D}}$ as computed by the 1D finite element model.

Table 4.5: Parameter values of the 2D random field of elastic modulus.

Parameter name	Symbol	Value	Units
Mean	μ	12.0	GPa
Standard deviation	σ	3.6	GPa
Correlation length in x-direction	θ_X	0.6	m
Correlation length in y-direction	θ_Y	0.1	m
Discretisation in x-direction	N_X	200	–
Discretisation in y-direction	N_Y	50	–
Number of realisations	R	10^3	–

Figure 4.12 shows a comparison between the distribution of the one-dimensional $E^*_{1\mathrm{D}}$ and two-dimensional $E^*_{2\mathrm{D}}$ effective elastic moduli obtained by the stochastic finite element models (SFEM) whilst Table 4.6 shows the sample mean and variance of the effective elastic moduli, $E^*_{1\mathrm{D}}$ and $E^*_{2\mathrm{D}}$, in comparison to the mean and variance of the random field $E(x, y)$. It is observed by inspection that both the 1D and 2D SFEM predict similar distributions for the effective elastic modulus, however, it is worthwhile to comment on

some systematic differences between these distributions of the effective property. The mean of the effective properties, E^*_{1D} and E^*_{2D}, are both lower than the mean of the random field $E(x, y)$ and this is attributed to the non-arithmetic nature of effective elastic modulus E^*, as well as, its sensitivity to local minima of the random field $E(x, y)$. The reduction in expected value is less pronounced in the 2D case since the stress pathways can avoid regions of low stiffness analogous to the way in which flow avoids regions of low permeability (Matheron, 1968). Additionally, it is noted that the reduction in expected value of the effective property increases as the heterogeneity of the beam increases i.e. as the ratio of the correlation length to the length of the domain θ/L decreases. The phenomena of the expected value of the effective property decreasing with the size of the sample has long been recognised for the case of strength and is known as the *size effect* (Weibull, 1939). However, it is important to recognise that the phenomena of size effect also applies to effective modulus of elasticity; albeit to a lesser degree that it applies to effective strength. The reason that the effect is more pronounced in the case of strength is because strength is a minima-type effective property corresponding to a large negative power m in the generalised mean meta-model whilst effective elastic modulus is an average-type effective property corresponding to a power in the range of $-1 \leq m \leq 1$.

The variance of the effective properties, E^*_{1D} and E^*_{2D}, are lower than the variance of the random field $E(x, y)$. This is due to the fact that the effective modulus of elasticity is an average-type effective property which smooths, and hence reduces the variability of, the random field $E(x, y)$. It is important to note that in the case that the field is homogeneous in the y-direction ($\theta_Y \to \infty$) that the 1D and 2D random fields are equivalent and, consequently, the effect of taking the field as heterogeneous in the y-direction ($\theta_Y \neq \infty$) results in the divergence between E^*_{1D} and E^*_{2D}. It is observed in the 2D case that this extra dimension of variability ($\theta_Y \neq \infty$) further reduces the variability of the effective property E^*_{2D}. This is because the 2D effective elastic modulus E^*_{2D} constitutes an average over a larger statistical region and, as the number of random variables being averaged increases, variability in that average decreases. However, it is noted that, in contrast to the reduction in expected value, the reduced variability of the effective elastic modulus E^* has long been recognised by researchers (Bulleit and Chapman, 2004). In conclusion, the difference between the distribution of the 1D and 2D effective properties demonstrates that achieving equivalence between stochastic finite element models of different dimensions is challenging and warrants further investigation.

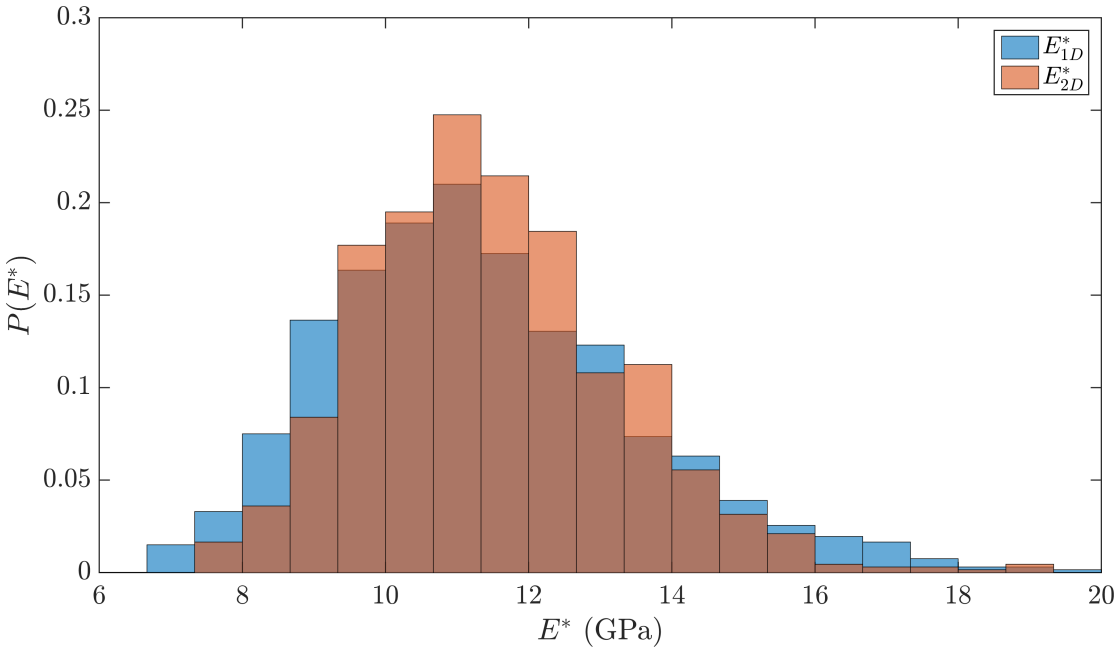


Figure 4.12: Distribution of the effective elastic moduli $E^*_{1\mathrm{D}}$ and $E^*_{2\mathrm{D}}$ obtained by the 1D and 2D stochastic finite element models respectively.

Table 4.6: Statistics of the effective elastic moduli.

Statistic	$E(x,y)$	$E^*_{1\mathrm{D}}$	$E^*_{2\mathrm{D}}$
$\hat{\mu}$	12.00	11.35	11.50
$\hat{\sigma}$	3.60	2.16	1.77

The remainder of this section considers the optimisation of the arithmetic E^*_A, geometric E^*_G and harmonic E^*_H meta-models to the training dataset of 2D finite element solves and the assessment of the performance of these meta-models on a separate testing dataset. Optimisation of the weighting functions $\omega(x,y)$ of the two-dimensional meta-models requires adaptation of the functional optimisation algorithm, as presented in Section 4.3, to the multidimensional case by taking the perturbations to be realisations of a 2D random field $\xi(x,y)$. Furthermore, it is noted that optimisation over the additional spatial dimension is significantly more challenging due to the extra degree of freedom and, consequently, two strategies are adopted to mitigate against this: firstly, the size of the training dataset is increased to $R_T = 100$ solves of the 2D finite element model and, secondly, an informative initial weighting function is adopted instead of the uniform initial weighting function used in Section 4.5. This informative initial weighting function

is given by the point-wise multiplication of the quasi-analytical weighting functions, $\omega_X(x)$ and $\omega_Y(y)$, as detailed in Section 4.4. Consequently, the 2D initial weighting function $\omega_0(x, y)$ is given by:

$$\omega_0(x,y) = \omega_X(x) \cdot \omega_Y(y) = \begin{cases} \dfrac{144x^2\left(y - \frac{H}{2}\right)^2}{L^3H^3} & \text{if } 0 \leq x \leq \dfrac{L}{2} \\ \dfrac{144\left(L-x\right)^2\left(y - \frac{H}{2}\right)^2}{L^3H^3} & \text{if } \dfrac{L}{2} \leq x \leq L \end{cases} \tag{4.24}$$

It is useful to note that since $\int_0^L \omega_X(x)\,\mathrm{d}x = 1$ and $\int_0^H \omega_Y(y)\,\mathrm{d}y = 1$ then similarly $\int_0^L \int_0^H \omega_0(x,y)\,\mathrm{d}x\,\mathrm{d}y = 1$.

The full details of the parameters of the functional optimisation algorithm used to optimise the meta-models to the output of the 2D finite element models are shown in Table 4.7. These parameters are similar to the 1D optimisation parameters shown in Table 4.2, however, a smaller scale parameter σ_ξ of the perturbations has been selected since optimisation begins from an informative initial function which does not require large perturbations. As a rule of thumb, the correlation lengths of the random field perturbations, $\theta_{X,\xi}$ and $\theta_{Y,\xi}$, have been respectively taken equal to the length L and H of the beam.

Figure 4.13 shows the decrease in the mean square error MSE between the arithmetic E_A^*, geometric E_G^*, harmonic E_H^* meta-models and the training dataset of the effective property E_{2D}^* as the number of proposed perturbations R_ξ increases. The coarse and fine tuning stages associated with the acceptance-rejection functional optimisation algorithm are distinctly visible for both the harmonic E_H^* and arithmetic E_A^* meta-models. It is observed that the optimisation algorithm achieves large reductions in mean square error of 85% and 37% for both the arithmetic E_A^* and harmonic E_H^* meta-models respectively whilst, in comparison, the geometric model achieves an error reduction of only 6%. This is due to the geometric model E_G^* already closely matching the expected value of the effective property E_{2D}^* and, as a consequence of this, it does not undergo the coarse adjustment stage. However, an alternative explanation for the lack of optimisation of the geometric weighting function $\omega_G(x, y)$ during the fine adjustment stage is that $\omega_G(x, y)$ is already close to optimal or that, similar to the one-dimensional case, the geometric model E_G^* requires perturbations with a smaller scale parameter σ_ξ than utilised. It is also useful to note that, prior to optimisation, the best performing meta-model was the geometric

Table 4.7: Parameters for the 2D finite element model and optimisation of the meta-models.

Parameter name	Symbol	Value	Units
Optimisation parameters			
Number of finite element solves	R	1000	–
Size of training dataset	R_T	100	–
Size of testing dataset	R_S	900	–
Number of perturbations	R_ξ	10^5	–
Perturbations parameters			
Discretisation in x-direction	N_X	100	–
Discretisation in y-direction	N_Y	50	–
Location parameter	μ_ξ	0	m^{-1}
Scale parameter	σ_ξ	0.01	m^{-1}
Correlation length in x-direction	$\theta_{X,\xi}$	2.0	m
Correlation length in y-direction	$\theta_{Y,\xi}$	0.1	m

mean E_G^* and this is in agreement with existing theory that suggests the geometric mean is the best model for heterogeneous two-dimensional behaviour (Matheron, 1968). However, the results indicate that the optimised harmonic mean meta-model E_H^*, not subject to the requirement that its weighting function integrate to one, achieves superior performance in modelling the effective elastic modulus of randomly heterogeneous two-dimensional beams.

Table 4.8 details the coefficient of determination r^2, normalised root mean square error NRMSE, integral of the weighting function $\int \omega(x, y)\,\mathrm{d}x\,\mathrm{d}y$ and change in the expected value $\Delta\mathbb{E}$ of the four meta-models $\{E_A^*,\ E_G^*,\ E_H^*,\ E_{AH}^*\}$ where E_{AH}^* is the unoptimised hybrid model discussed in Section 4.4. The coefficient of determination r^2, which is a metric of performance independent of the expected value of the meta-model, shows that the harmonic mean E_H^* slightly outperforms both the geometric E_G^* and hybrid E_{AH}^* meta-models whilst the arithmetic meta-model E_A^* performs weakly due to its lack of sensitivity to minima values. In addition, the NRMSE shows that the harmonic mean E_H^* is the best performing meta-model, follow by the geometric mean E_G^*, with both the arithmetic E_A^* and hybrid mean E_{AH}^* performing poorly. The large error associated

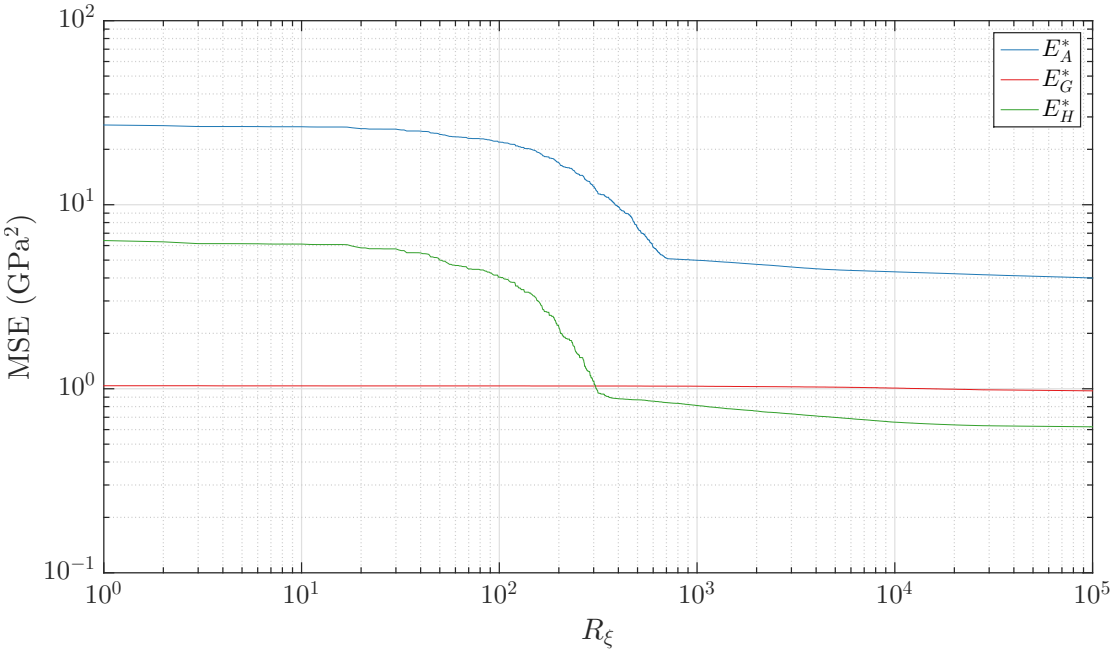


Figure 4.13: Mean square error MSE between the arithmetic E_A^*, geometric E_G^*, harmonic E_H^* meta-models and the two-dimensional effective elastic modulus $E_{2\mathrm{D}}^*$ against the number of perturbations R_ξ.

with the arithmetic mean E_A^* is due to its insensitivity to minima, however, in contrast the performance metric r^2 demonstrates that the hybrid model E_{AH}^* has appropriate sensitivity to minima. The large NRMSE associated with the hybrid model E_{AH}^* proposed by Bechtel (1985) is due to the fact that the weighting function ω_{AH} has not been optimised so that its accuracy can be evaluated and, consequently, E_{AH}^* systematically over-predicts the effective property $E_{2\mathrm{D}}^*$. Additionally, it is noted that the meta-model with the greatest change in its expected value, resulting from the change in the integral of its weighting function, is the arithmetic model E_A^*. Finally, it is observed that the harmonic meta-model increased its expected value whilst the geometric meta-model decreased its expected value and this suggests that the effective elastic modulus of a slender two-dimensional beam is bound by the harmonic and geometric mean.

Figure 4.14 shows the weighting function $\omega_H(x, y)$ of the optimised harmonic mean E_H^* which is the best performing meta-model. It is observed that the effective elastic modulus $E_{2\mathrm{D}}^*$ is most dependent on the stiffness at the top and bottom of the midspan cross-section. This is in agreement with both the conventional theory on the stress distribution of slender beams, as well as, the initial weighting function $\omega_0(x, y)$ obtained by Bechtel (1985) under quasi-analytical theory. Unlike the initial weighting function

Table 4.8: Performance metrics of the 2D meta-models.

Meta-model	r^2	NRMSE (%)	$\int \omega(x,y)\,\mathrm{d}V$	$\Delta\mathbb{E}$ (%)
E_A^*	0.982	2.04	0.961	−4.07
E_G^*	0.996	0.97	0.999	−0.91
E_H^*	0.997	0.84	0.979	+2.10
E_{AH}^*	0.995	2.17	1.000	0

$\omega_0(x,y)$, the harmonic weighting function $\omega_H(x,y)$ includes the effect of shear since it has been optimised to the results of the two-dimensional finite element model. However, in spite of accounting for the effects of shear, the stiffness at both the neutral axis and the supports has negligible contribution to the effective property and this is attributed to the fact that a slender beam has been modelled with length twenty times depth. It is noted that the maximum value of elastic modulus occurs under the point load, with a weighting of 42.4 m^{-2}, whilst another local maxima occurs at the point at which midspan deflection is observed with a weighting of 40.4 m^{-2}. In conclusion, the contribution of this chapter has been to numerically investigate the quasi-analytical theory of Bechtel (1985) with insights into the sensitivity of the effective elastic modulus of a two-dimensional beam to minima including an assessment of the influence of spatial weighting.

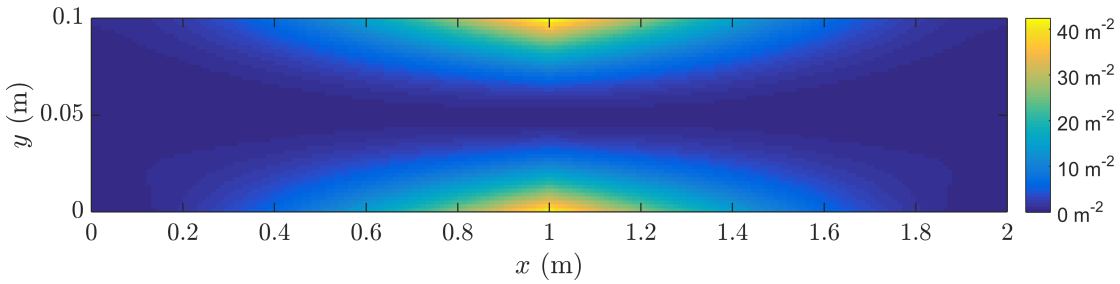


Figure 4.14: Optimised 2D spatial weighting function $\omega_H(x,y)$ of the harmonic mean meta-model E_H^* which models the effective elastic modulus $E_{2\mathrm{D}}$ of a simply supported beam under 3-point loading.

A final remark should be made to acknowledge that the analysis performed in this chapter to investigate the meta-modelling of the effective properties of heterogeneous beams has been subject to a number of methodological limitations. One of these limitations is that

only the discrete cases of the arithmetic ($m = 1$), geometric ($m \to 0$) and harmonic ($m = -1$) means have been considered. It is recommended that this limitation can be alleviated by further developing the theory of meta-modelling so that the power m in the generalised mean meta-model is taken to be a continuous variable that is also optimised to the results of the finite element model. Another limitation of this research has been the sensitivity of the optimisation algorithm to local minima and this implies that it is not known whether the 2D weighting function $\omega_H(x, y)$ shown in Figure 4.14 is a global minima of the error function or merely a local minima. Furthermore, it should be recognised that although the functional optimisation algorithm significantly reduced the mean square error of the 2D meta-models, the residual error of less than 1% in the case of the harmonic mean E_H^* cannot be said to be negligible. In fact, this error is considered to be fundamental since it is not expected to be significantly reduced by either increasing the size of the training dataset or by proposing more perturbations. This is because the generalised weighted mean meta-model, as proposed in Section 4.2, does not account for the so-called *interconnectedness* of the random field (Torquato, 2002). The property of interconnectedness describes the degree to which minima join together to form weak-zones which have a greater effect on the effective property than if the minima were spatially dispersed. It is noted that the interconnectedness of permeability fields of porous media has been analysed extensively within the research discipline of reservoir engineering using Percolation theory (Masihi et al., 2016) and it is suggested that the generalised weighted mean meta-models developed within this chapter should be extended to account for interconnectedness in order to more accurately predict the effective properties of randomly heterogeneous materials.

4.7 Conclusion

This chapter has contributed to the development of the theory of meta-models for the effective properties of heterogeneous materials with particular consideration of the effective modulus of elasticity of heterogeneous beams under 3-point loading. The key achievements of this chapter are summarised as:

- The introduction of a generalised weighted mean meta-model for the effective properties of heterogeneous materials with the capability to model the varying sensitiv-

ity of the effective property to minima of the random field, as well as, accounting for the effect of spatial weighting. In particular, commentary has been provided on the application of mean meta-models for the case of the three Pythagorean means with reference to relevant literature within the research field of reservoir engineering.

- An extension of the acceptance-rejection perturbation algorithm proposed by Bocchini and Deodatis (2008) has been presented where the form of the perturbations is longer deterministic but rather stochastic given by realisations of a random field. This algorithm has been evaluated on a benchmark problem and recommendations have been made for the parameters of the random field perturbations based on an investigation into the convergence characteristics of the algorithm.

- The analytical meta-models have been optimised to a training dataset from both 1D and 2D stochastic finite element models of a heterogeneous beam under 3-point loading. In the 1D case, it has been confirmed that the functional optimisation function converges to the analytical weighting function and, in the 2D case, insights have been obtained into the relationship between the effective property of a heterogeneous two-dimensional beam and the underlying random field of elastic modulus.

The following suggestions are made for future research into the meta-modelling of the effective properties of heterogeneous materials with a view to alleviating some of the methodological limitations identified within this chapter:

- Only three powers of the generalised weighted mean meta-model have been considered corresponding to the arithmetic ($m = 1$), geometric ($m \to 0$) and harmonic ($m = -1$) means under the relaxation of the requirement that the weighting functions integrate to one. It is recommended that future research should consider the development of a methodology that permits the simultaneous optimisation of both the power m and the weighting function ω in order to develop meta-models with increased predictive power.

- The functional optimisation algorithm developed in this chapter treats the parameters (μ_ξ, σ_ξ, θ_ξ) of the random field perturbations as constants to be selected a priori. Future research should consider the development of an adaptive functional

optimisation algorithm based on the recommendations at the end of Section 4.3 wherein the parameters of the perturbations are continually tuned to improve the numerical efficiency and accuracy of the optimisation algorithm.

- In the one-dimensional case, the error associated with the harmonic meta-model became negligible with sufficient optimisation, however, in the two-dimensional case, the error associated with the harmonic meta-model could not be reduced below 0.8%. In order to further decrease the error associated with the multidimensional meta-models, it is recommended that future research extends the generalised weighting mean meta-model to account for the interconnectedness of the random field using percolation theory as discussed in Journel et al. (1986).

Chapter 5

Inference from effective properties

5.1 Introduction

This chapter considers the statistical inference of the parameters of a random field model from experimentally determined material properties which are in fact effective properties of the material since they are determined over a non-zero sample volume. The motivation for the use of probabilistic models is that they facilitate the quantification of risk associated with the uncertain mechanical properties of heterogeneous materials. In particular, the advantage of random field models is that they provide a more accurate representation of the spatial variation of the mechanical properties of heterogeneous structures in comparison to current engineering design methods which are based on an elementary structural theory that intrinsically assumes material homogeneity (Isaksson, 2003). However, a major difficulty encountered in the probabilistic modelling of heterogeneous materials is that structural behaviour is scale dependent and, consequently, material properties that are experimentally determined at one scale are not necessarily representative of the distribution of material behaviour at another scale. Within this context, it should be recognised that the importance of random field models is that they function as a scale-invariant intermediary that mediates between effective material behaviour at different scales. This is because the distribution of the effective property can be determined at any scale from the random field model through the use of Monte Carlo methods in conjunction with a physics-based forward simulator such as the stochastic finite element method. However, it is important to recognise that the accuracy of the

reliability analysis depends on the uncertainty associated with the inferential methodology used to estimate the parameters of the random field in conjunction with the degree to which the effective properties are representative of the underlying distribution of the material property.

The problem of obtaining samples that are representative of the underlying spatial distribution of a material property is complicated by two key factors: the first factor is that only a limited number of effective properties can be determined since the determination of mechanical properties is both time consuming as well as financially expensive and this results in aleatoric uncertainty due to limited sample size; the second factor is that experimentally determined material properties are not point samples of the random field but rather effective properties that are determined over a non-zero sample volume of the material and, consequently, these experimentally determined material properties are not directly statistically representative of the random field which is a source of significant epistemic uncertainty. Furthermore, it should be noted that whilst aleatoric uncertainty can be reduced by increasing the sample size, reduction in epistemic uncertainty requires the development of more sophisticated inferential methodologies. The extent to which effective average-type properties of materials are statistically representative of the underlying random field depends on a number of factors including: the sensitivity of the average to minima of the random field; the extent to which the average exhibits spatial weighting; the size of the sample volume over which the effective property is determined relative to the scale of heterogeneity of the material. Consequently, it is noted that there is potential for large uncertainty associated with the inference of random fields from effective properties and that this motivates an investigation to quantify the uncertainty associated with the parameter estimates of the random field. Finally, it is noted that the analysis in this chapter is inspired by the following quote:

> "So how do we relate local (possibly geometric) average measurements to the point-scale characteristics of our theoretical random field? The simple answer is that in practice so far we do not." (Fenton and Griffiths, 2008, p. 183)

The effective property that is primarily considered within this chapter is the effective modulus of elasticity of timber beams, however, there is also some minor consideration of the effective strength of timber. The decision to consider the material properties of timber is based on a desire to quantify the reliability of both new and heritage timber

structures in addition to the availability of the experimental dataset obtained by Sousa et al. (2014). The benefit of considering the specific case of effective elastic modulus corresponding to an experimental dataset, rather than an abstract effective property, is that this facilitates the investigation of a number of practical issues that arise when fitting a random field model such as the selection of marginal distribution, assessment of stationarity and the treatment of anomalous data. Furthermore, the contribution of this chapter is to provide insights into two different methods to determine the effective elastic modulus of timber in accordance with BS EN 408:2010 which are the so-called local and global procedures. Finally, it is observed that the local and global moduli of elasticity can be formulated under Euler-Bernoulli beam theory as weighted harmonic means and that analysis of these formulations provides a theoretical explanation for the experimentally observed differences between these effective elastic moduli.

The most common approaches within the literature to infer the parameters of a random field model make use of frequentist approaches such as either method of moments or maximum likelihood estimation (Fenton, 1999). It is useful to note that frequentist inference is usually performed under the midpoint approximation which treats the effective property, an average over the sample volume, as a point sample of the random field located at the centroid of the sample volume. It is argued within this chapter that the midpoint approximation introduces significant epistemic bias into the parameter estimates of the random field and that these biases should be quantified since they may lead to an unconservative calculation of risk. Unfortunately, accurate determination of the epistemic bias is complicated by the fact that the uncertainty associated with the parameter estimates depends on the true parameters of the random field which are unknown and need to be inferred. The approach adopted within this chapter is to perform a computer experiment involving the simulation of random field realisations, whose parameters are given by the method of moment estimators under the midpoint approximation, and to analyse the discrepancy between the simulated and experimentally determined effective properties in order to gain insights into inferential uncertainty. It should be recognised that this computer experiment to quantify uncertainty is an important development on previous research that has not taken into account that the effective modulus of elasticity is a non-arithmetic mean (Bulleit and Chapman, 2004). Consequently, this approach is the first step towards an improved inferential methodology for the estimation of the parameters of a random field from experimentally determined material properties.

In order to clearly define the scope of this chapter, it is useful to consider the meta-problem framework detailed in Chapter 1 and, additionally, particular consideration should be given to the meta-problems that are addressed by this chapter in relation to the meta-problems addressed by previous chapters. The first half of this thesis has principally been concerned with the predictive meta-problems, for instance Chapter 3 considered *meta-problem 1 – deterministic prediction* and *meta-problem 2 – stochastic prediction* in the one-dimensional case, whilst Chapter 4 considered *meta-problem 1 – deterministic prediction* for the case of multidimensional heterogeneity. It is important that the prediction meta-problems have been considered first since an understanding of the forward prediction process, which tends to be well-defined, is critical to developing an approach to the reverse process of inference which, similar to many inversion problems, tends to be ill-defined. In particular, this chapter is concerned with problems of inference with a specific focus on *meta-problem 3 – stochastic inference* which is the problem of inferring the parameters of a random field from experimentally determined effective properties. However, this chapter also has important implications on *meta-problem 4 – deterministic inference* due to the fact that the accurate inference of a realisation depends on the parameters of the random field since these parameters dictate the expected value, variability and smoothness of the realisations.

This chapter consists of six sections in total: the first section is *introduction* which contains this overview of the chapter; the second section is *probabilistic modelling of timber* which considers the literature on the probabilistic modelling of the mechanical properties of timber; the third section is *determination of the effective elastic modulus of timber* which provides an overview of the experimental procedure to determine the local and global elastic moduli including analytical expressions for the weighting functions of these effective elastic moduli; the fourth section is *analysis of experimental data* which investigates estimation of the parameters of a random field model from experimental data under the midpoint approximation; the fifth section is *uncertainty quantification* which details the results of the computer experiment to quantify the aleatoric and epistemic uncertainty associated with the parameter estimates and comments on whether the local or global moduli of elasticity are superior for the estimation of random field parameters; the sixth and final section is *conclusion* which summarises the main contributions of this chapter and provides recommendations for future work.

5.2 Probabilistic modelling of timber

Timber is a sawn wood product that is used as a structural construction material and offers a natural alternative to more commonly used materials such as concrete or steel. This biological material has an excellent strength to weight ratio and good flexural resistance which means that it is well suited for usage as a flexural beam. Furthermore, the key advantages of timber over man-made materials are its environmentally sustainable characteristics as well as its aesthetic appeal. However, in the consideration of timber as a structural material it is important to recognise that wood is grown to meet the needs of the tree and is not optimised for use within construction. In particular, the natural formation of timber results in a number of disadvantages that are associated with its sensitivities to both environmental factors and defects such as knots. This motivates the adoption of a reliability based approach to the structural design of timber with a view to managing the risk associated with its uncertain mechanical properties.

In order to evaluate the risk associated with using timber as a structural material, it is important to identify the hazards that are associated with this material and this begins with consideration of the microstructure of wood. At the cellular level, wood consists of an irregular random honeycomb of long thin tubular fibres that are primarily orientated parallel to the trunk of the tree which is known as the along-grain direction (Astley et al., 1997). Additionally, the material that forms the cell wall is a natural fibre composite consisting of cellulose, the fibre, and lignin which is the matrix (Desch and Dinwoodie, 1996, p. 17). It should be recognised that the tubular microstructure of wood results in highly anisotropic material properties with against-grain material properties being significantly inferior to along-grain properties. For instance, the tension strength of timber has been found to be 30–50 times smaller perpendicular to the grain than in the along-fibre direction and the elastic modulus perpendicular to the grain has been found to be 50–80 times smaller than the elastic modulus parallel to the grain (Thelandersson, 2003, p. 19-20). These anisotropic qualities cause timber to perform well in flexure; however, the performance of timber in shear is poor and this explains the reason why the majority of failures of timber observed in practice have resulted from tension perpendicular to the grain which has caused the timber to split along planes parallel to the fibre orientation. Furthermore, it is noted that the tensile failure of timber is associated with rupture of the cell walls resulting in extremely brittle material behaviour (Hoffmeyer, 2003, p. 141).

In comparison, the compressive failure of timber is associated with a gradual folding of the cell walls resulting in more ductile material behaviour. Consequently, the effective tensile strength of timber is considered to be extremely sensitive to minima of the strength field and this can be modelled using the generalised mean meta-model (see Chapter 4) by taking the power $m \to -\infty$. Furthermore, the reduced sensitivity of the effective compressive strength of timber to minima can be similarly modelled using the generalised mean meta-model by taking the power such that $-\infty < m < -1$.

Other hazards associated with timber that result from the biological nature of the microstructure of wood are its sensitivities to a number of environmental factors such as moisture, fire and decay. The cell wall of wood is porous to allow the tree to transport water and nutrients which, despite being a beneficial property for the tree, is a distinct disadvantage for the structural material of timber since this porosity causes high sensitivity to atmospheric moisture. In particular, the mechanical properties of timber are adversely affected as the moisture content increases up to the fibre saturation point and, consequently, timber is typically dried before use in order to mitigate against this (Porteous and Kermani, 2007, p. 9). It is also important to recognise that wood based products are primarily composed of cellulose and lignin which are combustible and, consequently, wood based products often require treatment with flame-retardant chemicals (Porteous and Kermani, 2007, p. 47). Finally, timber is vulnerable to decay resulting from attack by fungi, insects or molluscs which can be mitigated against through the use of treatments such as tar oil, organic solvents or water borne preservatives (McKenzie and Zhang, 2007, p. 10).

In addition to the sensitivities associated with the biological microstructure of wood, timber also has a number of defects relating to the macroscale formation of the structure of the tree. The most severe type of defect associated with timber are knots (Johansson, 2003, p. 26) which are formed when wood fibres are redirected to form an efficient structural connection between the trunk and a branch of the tree (Thelandersson, 2003, p. 15). However, when the trunk is sawn to produce the structural material of timber, these knots transform from an asset into a severe liability. This is because the presence of knots alters the orientation of the tubular microstructure, a phenomena known as *grain deviation*, which results in large decreases in strength and stiffness due to the severely anisotropic properties of timber. The magnitude of the decrease in mechanical properties depends on a number of factors including the size of the knot, or cluster of knots, and

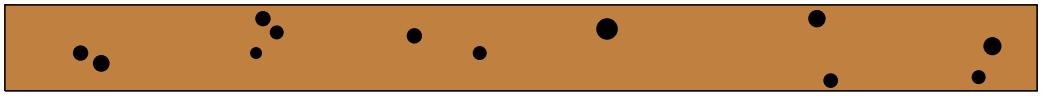
whether the knot is alive or enclosed (McKenzie and Zhang, 2007, p. 4). Furthermore, the sensitivity of timber to knots has been identified as the most dominant factor in the structural performance of timber and it has been observed through experimental investigation that the failure of timber occurs at knots in 95% (Schniewind and Lyon, 1971) and 91% of cases (Johansson et al., 1998). Consequently, it is evident that in the majority of cases the effective strength of timber is determined by the presence of knots, however, in a minority of cases it should be recognised that the determining factor is the variability of sections of wood without knots which are known as *clear wood*.

In order to manage the risk associated with the hazards of timber identified within this section it is desirable to make use of probabilistic methods. One approach is to probabilistically model the intervariability of timber which is the variability of the effective strength f^* or stiffness E^* between members. A significant cause of the intervariability of timber is the sensitivity of wood to random defects; for instance, the presence of knots implies that the expected effective strength f^* of an element decreases with its size since a large element has an increased chance of having a critical defect and this phenomena has traditionally been modelled using weakest link theory (Weibull, 1939). ===note that the occurrence and magnitude of these defects is random which results in considerable uncertainty as to the strength of any particular timber member. In practice, the approach to mitigate against this uncertainty is to sort each member into a strength class prior to structural usage on the basis of the prediction of the effective strength f^* of that particular member. Unfortunately, the direct determination of effective strength f^* involves destruction of the sample itself and, consequently, effective strength is predicted through highly correlated properties, known as *indicating properties*, which can instead be obtained non-destructively. One example of an indicating property is the number, position and size of knots which can be determined on the basis of a visual assessment in accordance with BS EN 14081:2005. However, this chapter primarily considers the indicating property of effective elastic modulus which typically has a coefficient of determination with effective strength in the range of 0.51–0.73 (Johansson, 2003, p. 25). Furthermore, whilst there are many methods to determine the effective elastic modulus E^*, such as machine grading and vibration testing, this chapter considers the static determination of E^* through a 4-point bending testing in accordance with BS EN 408:2010. It should be noted that many distributions have been used to model the intervariability of timber including normal, lognormal and Weibull distributions (Isaksson, 2003). However, the disadvantage of directly modelling intervariability is that the distribution of

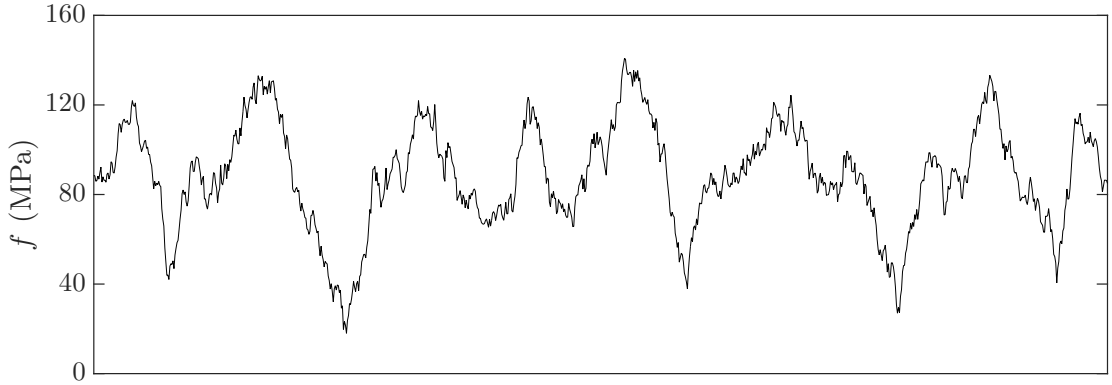
the material property is scale-dependent and this motivates the probabilistic modelling of the scale-invariant material profile itself.

The probabilistic modelling of the intravariability of timber is concerned with modelling the variability of strength $f(x)$ or stiffness $E(x)$ within the member itself. A model for intravariability that has drawn significant attention is the weak-zone model (Riberholt and Madsen, 1979) that has been utilised and further developed by many authors to model the sensitivity of timber to defects (Isaksson, 2003, Köhler et al., 2007, Fink and Kohler, 2014). Figure 5.1 shows a timber beam with knots and illustrates the hypothetical variation and weak-zone model of the strength profile. The weak-zone model treats the strength of clear wood as constant and models strength decreases as solely resulting from the presence of defects such as knots. The occurrence of these knots is modelled as a Poisson point process with constant intensity and the strength of the weak-zone is typically modelled as lognormally or Weibull distributed. Additionally, the assumption that clear wood has constant material properties can also be found in a recently developed automatic grading procedure that utilises the fact that irregularities in wood result in different light scatterings, known as the tracheid effect (Nyström, 2003), in order to automatically detect grain direction thereby inferring the decrease in material properties associated with grain deviation (Olsson et al., 2013). One line of conceptual investigation that is pursued within this chapter is consideration of the extent to which the weak-zone model is not only an appropriate model for the strength profile $f(x)$ but also the stiffness profile $E(x)$. This is because these material properties are highly correlated and it is conjectured here that the correlation at the mesoscale between the material profiles, $f(x)$ and $E(x)$, is even greater than that observed at the macro-scale between the effective properties, f^* and E^*.

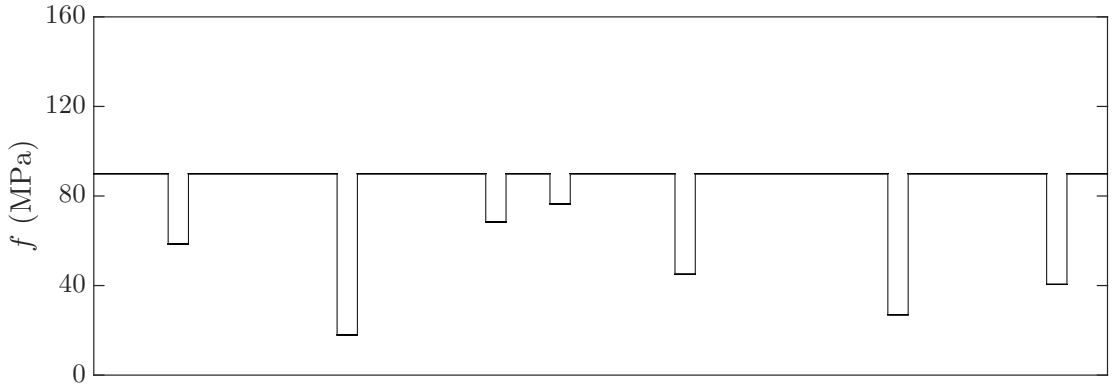
A major limitation of the weak-zone model is the assumption that all variability in the mechanical properties of timber can be attributed to the presence of defects since clear wood is assumed to have constant material properties. It is important to recognise that this assumption is not supported by experimental research which has found the properties of clear wood to be variable with significant coefficients of variation (Zhu et al., 2001, Xavier et al., 2007, 2009, Dill-Langer et al., 2003). The negligence of the variability of clear wood means that the marginal distribution of the material property has an imposed upper bound associated with truncation of the right-tail of the distribution and this is arguably not representative of the true variation of material properties. On the basis



(a) Timber beam with knots



(b) Hypothetical spatial variation of the strength profile $f(x)$



(c) Weak-zone model of the spatial variation of the strength profile $f(x)$

Figure 5.1: Two alternative representations of the spatial variation of the one-dimensional strength profile $f(x)$ of a timber beam with knots.

of the formulation of the effective property in terms of a generalised power mean (see Chapter 4), it is argued that the weak-zone model is most appropriate for the tensile strength of timber since this is brittle material behaviour without stress redistribution and, consequently, the left-tail of the distribution associated with minima is the dominant factor. However, it is asserted that the weak-zone model is less appropriate for the compressive strength of timber since this is a ductile failure mechanism that facilitates the redistribution of stress to strong zones associated with the right-tail of the distribution and this phenomena is not accounted for by the weak-zone model. Finally, it is contended that the weak-zone model is an inappropriate model for elastic modulus since, despite

having a tendency towards minima, it is not affected by minima to nearly the same extent as effective strength and, consequently, the variability of clear wood must be considered as a non-negligible cause of variation in the effective elastic modulus.

An alternative model for the intravariability of timber is the random field which, in contrast to the weak-zone model, treats the variation in material properties as continuous. Random field models have been used by many authors to model the intravariability of both the elastic modulus (Vanmarcke and Grigoriu, 1983, García and Rosales, 2017, Shen et al., 2014, Füssl et al., 2016, Kukla and Owczarek, 2005) and strength of randomly heterogeneous beams (Köhler et al., 2007, Sasikumar et al., 2014, Moshtaghin et al., 2016). The advantages of random field models over the weak-zone model are, firstly, that the continuous realisations of the random field are a more accurate representation of the real variation in the material properties of timber and, secondly, that it is possible to arbitrarily specify the marginal distribution so that the right-tail variation of the material properties of clear wood is not neglected. However, the utilisation of random field models is not without its difficulties since careful consideration is required of two key issues relating to both the heterogeneity of timber and the methodologies to infer the parameters of the random field.

The first issue is whether a continuous model is appropriate to model the heterogeneity of timber which can be considered to be a discrete phenomena that occurs at two distinct scales. At the microscale, the structure of timber consists of long thin tubes primarily orientated in the along-grain direction where any point in the material corresponds to either a solid or a void. The discrepancy between the discrete nature of this microscale heterogeneity and the continuity of the random field model is resolved through the mesoscale continuum approximation proposed by Ostoja-Starzewski and Wang (1999) which considers the random field model to be the result of passing of an averaging window over the underlying binary structure. At the macroscale, the heterogeneity of timber can to a large extent be attributed to knots which are a discrete phenomena associated with the formation of the branches of the tree and, consequently, it is important to consider whether it is appropriate to represent this phenomena with a continuous model. The approach adopted by some authors has been to restrict their random field model to only apply to the case of clear wood (Moshtaghin et al., 2016). However, it is suggested here that the mesoscale continuum approximation can be utilised to not only average over binary microscale heterogeneity, but also to average over discrete macroscale heterogeneity

resulting from the presence of knots. This is because, provided that the magnitude of the minima associated with the knot is appropriately modelled, the effect of averaging over macroscale variation using the mesoscale continuum approximation is to reduce the gradient around the knots and, consequently, the use of the mesoscale continuum approximation is conservative since the capacity for stress redistribution is underestimated.

The second issue associated with the application of random field models is the accurate determination of the random field parameters. In particular, it is noted that this problem is more complex in the two-dimensional case since the anisotropic nature of wood requires the estimation of two distinct correlation parameters, along and against-grain correlation lengths, in order to appropriately model the anisotropic heterogeneity of timber. In an ideal scenario, it would be desirable to utilise an inferential methodology that estimates the value of these parameters so that the likelihood of the observed data is maximised. However, since the likelihood function associated with effective elastic moduli is intractable, the approach used herein is to instead rely on method of moments estimators. A further issue is the incompatibility between the inferential requirement for point observations of the underlying random field and the reality that material properties can only be measured over a non-zero volume. This issue is often resolved through the use of the midpoint approximation (Kiureghian and Ke, 1988) which has been utilised by researchers for the cases of tensile loading (Brandner and Schickhofer, 2014), 3-point (Arwade et al., 2009) and 4-point bending (Sousa et al., 2016) as well as machine grading (Lam et al., 1994, Kline et al., 1986). The midpoint approximation treats the effective property E^*, obtained over the sample volume, as a point observation of the random field $E(x)$ at the centroid x_c of the sample volume. Figure 5.2 illustrates the error $\epsilon = E(x_c) - E^*$ that results from usage of the midpoint approximation. It is one of the contributions of this chapter to conduct an uncertainty analysis that quantifies the epistemic and aleatoric uncertainty associated with the midpoint approximation and to propose an improved inferential methodology that utilises approximate Bayesian computation in order to obtain the joint posterior distribution on the parameter estimates.

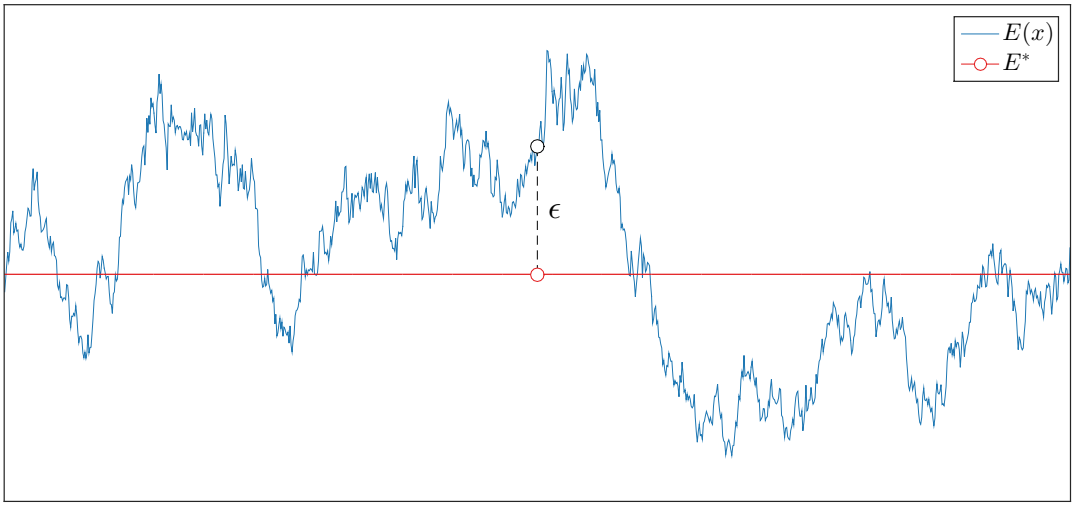


Figure 5.2: Midpoint approximation error ϵ between a realisation of the stiffness profile $E(x)$ and its effective property E^*.

5.3 Determination of the effective elastic modulus of timber

The determination of the effective elastic modulus E^* of timber is not only important for assessment of the serviceability limit state but also the ultimate limit state due to its correlation with the effective strength f^* of timber. The standard considered within this thesis to determine the effective elastic modulus E^* is BS EN 408:2010 which details the test procedure for the static four-point bending of a simply supported beam, as illustrated in Figure 5.3, and specifies two different methods for calculating the effective elastic modulus E^*. The first method determines an effective property, known as the local modulus of elasticity E_l^*, which is based on the local displacement U_l given by the relative midspan displacement of the beam with respect to the displacements at either side of a centrally placed displacement gauge of length $5H$ where H is the height of the beam. The benefit of local displacement U_l is that it does not include displacement due to shear, however, the disadvantages are that the magnitude of displacement is smaller, leading to greater relative measurement error, and that the associated effective property E_l^* is not representative of the bending stiffness of the whole span but rather a small region located between the loading pins. The second method determines an effective property, known as the global modulus of elasticity E_g^*, based on the global displacement U_g given by the absolute midspan displacement. The benefit of the global

elastic modulus E_g^* is that it is an average over, and hence representative of, the stiffness of the whole span; however, the disadvantage is that the global elastic modulus E_g^* is based on the global displacement U_g which includes the effects of both shear and local indentation.

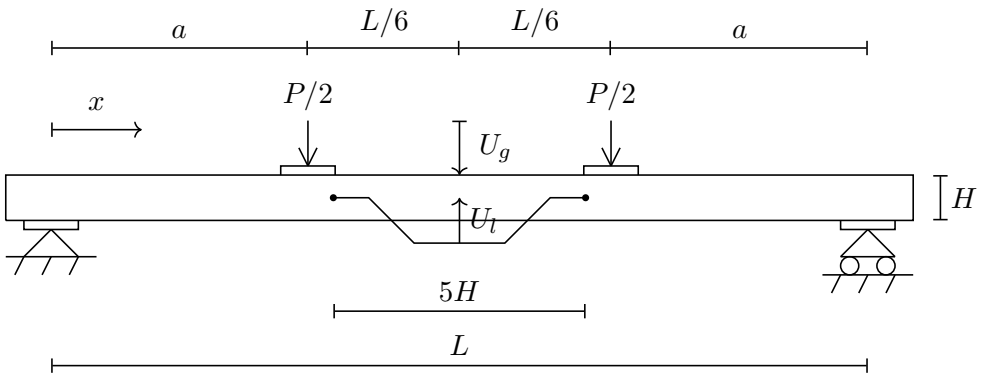


Figure 5.3: Set-up of the 4-point bending test according to BS EN 408:2010 with local U_l and global U_g displacement for the calculation of the local E_l^* and global E_g^* effective moduli of elasticity respectively.

According to BS EN 408:2010, the expression for the local modulus of elasticity E_l^* is given by:

$$E_l^* = \frac{25aH^2P}{16IU_l} \tag{5.1}$$

where I is the second moment of area of the beam. Similarly, the expression for the global modulus of elasticity E_g^* is given by:

$$E_g^* = \frac{Pa(3L^2 - 4a^2)}{48IU_g} \tag{5.2}$$

where the shear modulus G has been taken to be infinite so that the contribution of shear to the global displacement U_g is neglected. It should be noted that BS EN 408:2010 requires that the distance a from the support to the load satisfy the following inequality:

$$\frac{3L}{10} \leq a \leq \frac{5L}{14} \tag{5.3}$$

It is of importance to obtain an effective modulus of elasticity E^* that is most representative of in situ structural behaviour. This is because over-estimation of the effective property leads to under-design of the structure, which is unsafe due to the risk of structural failure; however, on the other hand, under-estimation leads to over-design which is both unsustainable and uneconomic. As a consequence, there has been extensive discussion and experimental investigation into the difference between the local E_l^* and global E_g^* elastic moduli (Boström, 1999, Solli, 2000). In particular, the experimental investigation conducted by Nocetti et al. (2013) has shown that the local elastic modulus E_l^* has a higher mean and standard deviation than the global elastic modulus E_g^*. It is the objective of the remainder of this section to develop a theoretical explanation for these experimental observations through consideration of the weighting functions, $\omega_l(x)$ and $\omega_g(x)$, of the local E_l^* and global E_g^* effective elastic moduli respectively.

As shown in Chapter 3, the effective elastic modulus of an Euler-Bernoulli beam is given by a weighted harmonic mean:

$$E^* = \left(\int_0^L \omega(x) \cdot E(x)^{-1} \, \mathrm{d}x \right)^{-1} \tag{5.4}$$

In the case of the global modulus of elasticity E_g^*, the weighting function $\omega_g(x)$ is given by (see Appendix C.1):

$$\omega_g(x) = \begin{cases} \dfrac{12x^2}{a(3L^2 - 4a^2)} & \text{if } 0 \leq x \leq a \\ \dfrac{12x}{3L^2 - 4a^2} & \text{if } a \leq x \leq \dfrac{L}{2} \\ \dfrac{12(L-x)}{3L^2 - 4a^2} & \text{if } \dfrac{L}{2} \leq x \leq L - a \\ \dfrac{12(L-x)^2}{a(3L^2 - 4a^2)} & \text{if } L - a \leq x \leq L \end{cases} \tag{5.5}$$

Similarly, noting that the distance from the left support to the left-side of the displacement gauge is given by $(10a + L)/12$, that the length of the displacement gauge is given by $5(L - 2a)/6$ and that the distance from the left support to the right-side of the displacement gauge is given by $(11L - 10a)/12$, then the weighting function $\omega_l(x)$ for the local effective elastic modulus E_l^* is given by (see Appendix C.2):

$$\omega_l(x) = \begin{cases} 0 & \text{if } 0 \leq x \leq \dfrac{10a + L}{12} \\ \dfrac{12(12x - 10a - L)}{25(L - 2a)^2} & \text{if } \dfrac{10a + L}{12} \leq x \leq \dfrac{L}{2} \\ \dfrac{12(11L - 10a - 12x)}{25(L - 2a)^2} & \text{if } \dfrac{L}{2} \leq x \leq \dfrac{11L - 10a}{12} \\ 0 & \text{if } \dfrac{11L - 10a}{12} \leq x \leq L \end{cases} \tag{5.6}$$

Figure 5.4 shows a plot of the local $\omega_l(x)$ and global $\omega_g(x)$ weighting functions for three different values of the distance a from the supports to the point load. It can be seen that both weighting functions monotonically increase towards, and attain a maximum at, the midspan $x = L/2$. However, the global weighting function $\omega_g(x)$ is zero only at the supports whilst the local weighting function $\omega_l(x)$ assigns a weighting of zero to all values of the stiffness profile $E(x)$ outside of the displacement gauge. It is observed that between the loading points, both the local $\omega_l(x)$ and global $\omega_g(x)$ weighting functions are linear whilst, beyond the loading points, the global weighting function $\omega_g(x)$ is quadratic. Ridley-Ellis et al. (2009) produced a plot similar to Figure 5.4 through a numerical experiment which investigates the influence of a single weak-zone on the effective local E_l^* and global E_g^* moduli of elasticity. It is noted that the close resemblance between these figures is due to the fact that the numerical experiment conducted by Ridley-Ellis et al. (2009) utilised a one-dimensional finite element model which, in effect, approximates the analytical weighting functions given by Equations 5.5 – 5.6.

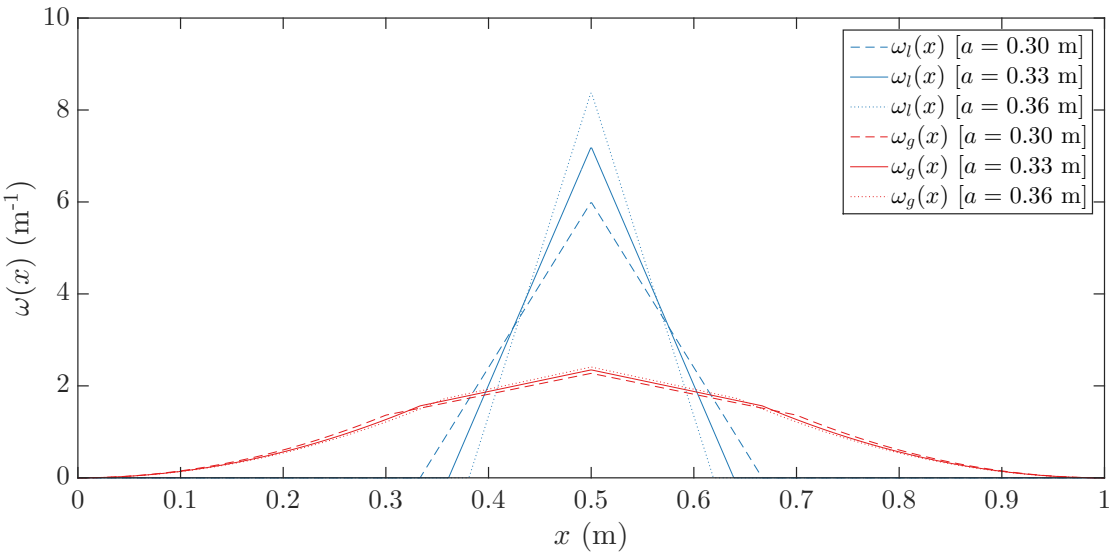


Figure 5.4: Local $\omega_l(x)$ and global $\omega_g(x)$ weighting functions for three different values of the distance a from the supports to the point load ($L = 1$ m).

The experimentally observed differences between the local E_l^* and global E_g^* elastic moduli can be explained through consideration of their respective weighting functions. Firstly, it is important to observe that the local elastic modulus E_l^* constitutes an average over a smaller statistical region and hence is less representative of whole span stiffness than the global elastic modulus E_g^*. The observation of Nocetti et al. (2013) that the expected value of E_l^* is higher than the expected value of E_g^* is explained by considering that, whilst both effective properties E_l^* and E_g^* are harmonic means that tend towards minima, only the global effective property E_g^* will be affected by minima of the stiffness profile $E(x)$ outside of the displacement gauge. Similarly, the observation that the variance of E_l^* is higher than the variance of E_g^* is explained by considering that since E_g^* is an average over a greater statistical region it will have lower variance since the average of a greater number of variables is less variable. In addition to explaining experimental observations, it is also possible to understand the effect of varying the distance a from the support to the load on the effective property E^* through analysis of the weighting functions. It is observed, as a increases, that both elastic moduli, E_l^* and E_g^*, become less representative of whole span stiffness which causes an increase in both the expected value and variance of the effective elastic moduli. However, it is important to recognise that the relative increase in the expected value and variance is greatest for the local effective property E_l^* which is significantly more sensitive to variation in the distance a than the global effective property E_g^*.

5.4 Analysis of experimental data

This section details the utilisation of method of moment estimators to infer the parameters of a random field model from a 4-point bending dataset detailed in Sousa et al. (2014). The experimental investigation involved sawing 16 old chestnut beams ($300 \times 15 \times 3$ cm) into 48 boards ($300 \times 4 \times 3$ cm) and then sequentially determining local E_l^* and global E_g^* elastic moduli over seven segments of each board. It should be noted that the sawing process resulted in a loss of 3 cm of section height from each beam leading to 1.5 cm of vertical separation between the boards as shown in Figure 5.5 (b). For each board, 4-point bending tests were performed over 60 cm spans centred over the $N_S = 7$ segments (as shown in Figure 5.5 (c)) and it is noted that the overlap between each bending test and its neighbour was at least 20 cm. For the first and final bending

test, the domain was offset by 2 cm to allow sufficient space for the insertion of steel plates under the supports in order to reduce local indentation. The length of the displacement gauge for the local elastic modulus E_l^* was 20 cm, the inter-pin distance was 24 cm and the distance from the support to the point load was $a = 18$ cm. Additionally, it is noted that during testing one of the boards broke meaning that effective elastic moduli could not be determined for that particular segment and, consequently, a total of 335 samples of both the local E_l^* and global E_g^* were determined.

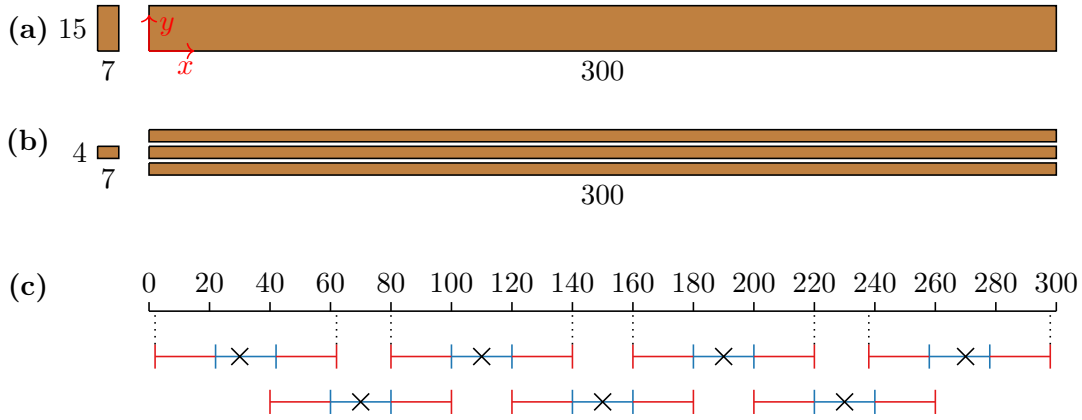


Figure 5.5: Illustration of the experimental procedure (all units in cm) where (a) illustrates the whole beam, (b) beam subdivided into boards and (c) domains of the local elastic moduli (⊢—⊣), domains of the global elastic moduli (⊢—⊣) and the locations of the midpoint approximation (×).

Figure 5.6 shows the marginal distribution of the local E_l^* and global E_g^* elastic moduli of the boards and Table 5.1 shows their sample statistics including mean $\hat{\mu}$, standard deviation $\hat{\sigma}$ and skewness $\hat{\gamma}$. It is observed that the distribution of the local effective elastic modulus E_l^* has both increased expected value and variance compared to the global effective elastic modulus E_g^* which agrees with both the experimental observations of Nocetti et al. (2013) and the analysis of the weighting functions presented in the previous section. Additionally, it can be seen that the distribution of the local elastic modulus E_l^* is approximately symmetric whilst the distribution of the global elastic modulus E_g^* is moderately negatively skewed. A maximum value of 32.3 GPa is observed on the right tail of the distribution of the local modulus of elasticity E_l^* and it has been investigated whether this value was an experimental anomaly that has potentially resulted from an incorrect test procedure. Based on an investigation of the adjacent

segments and global modulus of elasticity over the same section, this maximum has been found to be reflective of the true variability of the old chestnut beams and is not considered to be an anomaly. It is noted that caution should be exercised in the dismissal of anomalous values since this leads to a decrease in the estimate of the variability of the distribution which could lead to the under-design of timber structures.

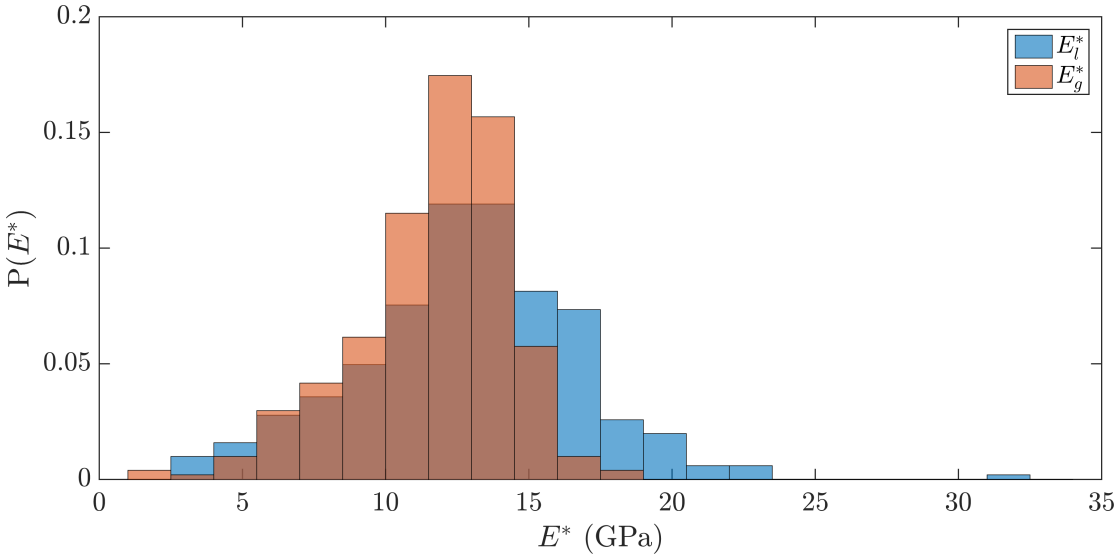


Figure 5.6: Histogram of the experimentally determined local E_l^* and global E_g^* moduli of elasticity.

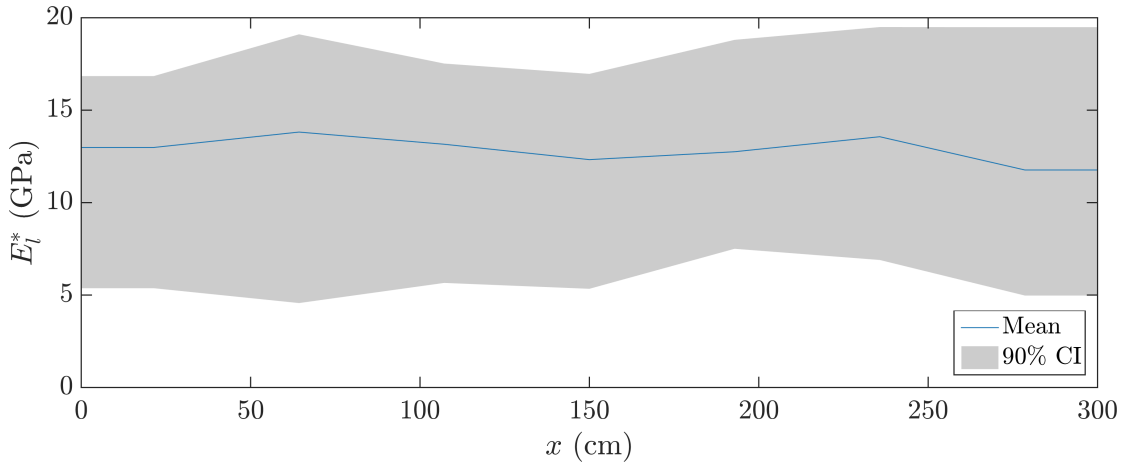
Table 5.1: Sample statistics of the local E_l^* and global E_g^* elastic moduli.

Test	$\hat{\mu}$ (GPa)	$\hat{\sigma}$ (GPa)	$\hat{\gamma}$
E_l^*	12.91	3.92	0.15
E_g^*	11.66	2.65	−0.79

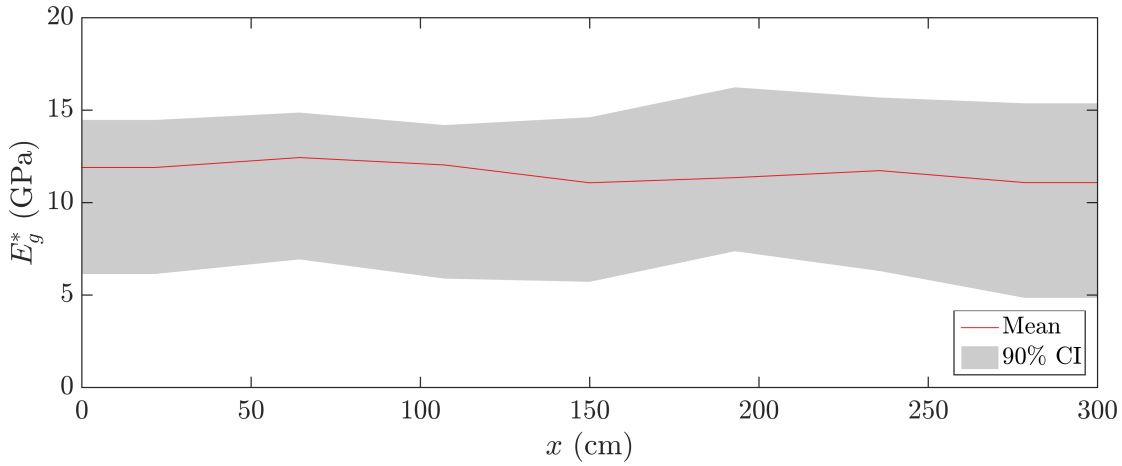
5.4.1 Marginal distribution

One of the first considerations when fitting a random field model is whether the distribution is stationary with respect to the specified spatial dimensions. The stationarity of the marginal distribution of the effective elastic moduli is assessed by inspection of the spatial plots of the mean trend and confidence intervals computed from the empirical cumulative distribution function using linear interpolation. Figure 5.8 shows the variation with the along-grain x-direction of the mean and 90% confidence intervals of both

the local E_l^* and global E_g^* elastic moduli. It can be seen that there is moderate spatial variation in the mean and confidence intervals for both moduli of elasticity. The problem of whether any apparent trends are systematic in nature or merely random fluctuations is one of the fundamental challenges associated with the inference of random fields. It is noted by Fenton (1999) that, in the face of uncertainty, the conservative approach is to attribute any apparent trends to random fluctuations since this leads to a higher estimate of variability. Consequently, the variations in the mean and 90% confidence intervals are attributed to random fluctuations resulting from limited statistical certainty rather than the result of a deterministic trend and, therefore, both the local E_l^* and global E_g^* elastic moduli are modelled as stationary in the x-direction.



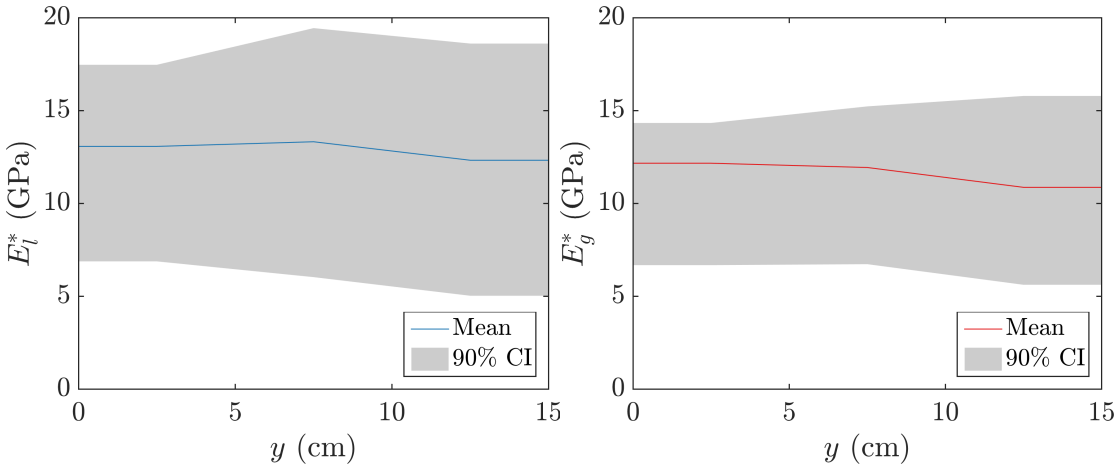
(a) local modulus of elasticity E_l^*



(a) global modulus of elasticity E_g^*

Figure 5.8: Plot of the spatial variation in the mean and 90% confidence intervals of both effective elastic moduli with the along-grain x-direction.

In addition to consideration of the stationarity of the marginal distribution for seven lags in the x-direction, the stationarity of both effective elastic moduli is also considered for three lags in the y-direction. Figure 5.9 shows plots of the spatial variation in the mean and 90% confidence intervals of both the local E_l^* and global E_g^* elastic moduli in the against-grain y-direction. A visual assessment suggests that in the y-direction there is a slight negative trend in the mean and a slight positive trend in the variance for both E_l^* and E_g^*. However, as a result of the limited number of lags associated with the y-direction, in addition to the weakness of the trend, it is not possible to determine whether this is a random fluctuation resulting from statistical uncertainty or a systematic trend. Consequently, since the inclusion of a trend could lead to an unconservative estimate of variance, the marginal distribution of both E_l^* and E_g^* are modelled as fully stationary in both in the x and y-directions.

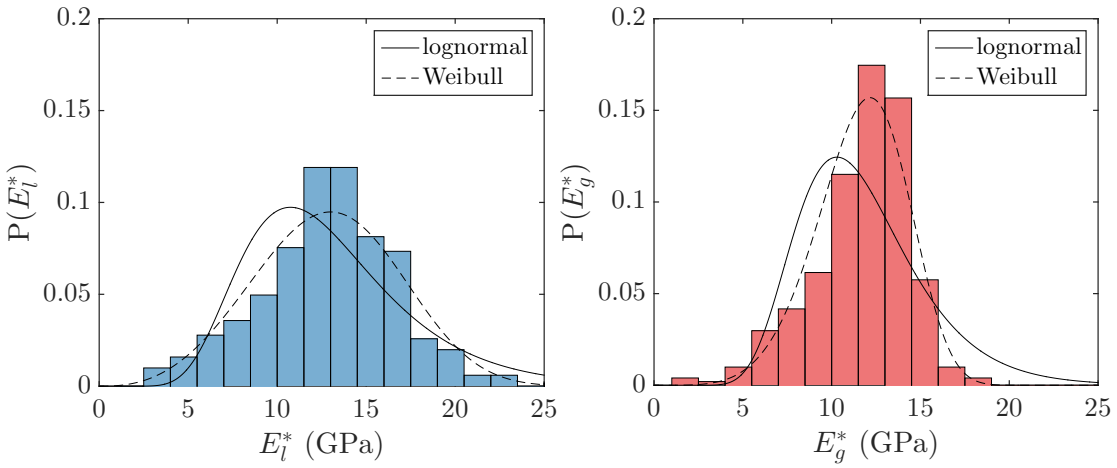


(a) local modulus of elasticity E_l^* (b) global modulus of elasticity E_g^*

Figure 5.9: Spatial variation in the mean and 90% confidence intervals of both effective elastic moduli with the against-grain y-direction.

Following the determination that a stationary random field appropriately models both the local E_l^* and global E_g^* moduli of elasticity, the next consideration is the choice of marginal distribution. Two distributions are considered, namely the lognormal and Weibull distribution, whose parameters are found through maximum likelihood estimation under the assumption of statistical independence. Figure 5.10 shows histograms of the marginal distribution of the effective elastic moduli with fitted lognormal and Weibull distributions whilst Table 5.2 details the null hypothesis test and the Anderson-Darling test statistic for both fitted distributions. The null hypothesis H_0 was rejected at the

5% significance level for both distributions fitted to both effective properties and it is noted that the Anderson-Darling test statistic A^2 is significantly lower for the Weibull distribution in comparison to the lognormal distribution. This is because the lognormal distribution has a strictly positive skewness whilst the Weibull distribution can have either a positive or negative skewness (Jiang and Murthy, 2011). As a consequence of this, the Weibull distribution more accurately models the moderate negative skewness of the global elastic modulus E_g^* and the approximate symmetry of the local elastic modulus E_l^*. In contrast, the fitted lognormal distribution poorly models both the mode and the right tail of both effective elastic moduli. Unfortunately, simulation of a random process with a specified correlation structure and an arbitrary marginal distribution, such as the Weibull distribution, requires the use of the Fast Fourier transform simulation method (Grigoriu, 1995) including numerical determination of the underlying Gaussian spectral density function (Shields et al., 2011). Therefore, in order to avoid these technical complications, the lognormal marginal distribution is selected due to the availability of analytic relationships between the statistics of the underlying normal and the transformed distribution (Vanmarcke, 1988). It is noted that the error induced by the use of the lognormal distribution instead of the Weibull distribution is discussed in Subsection 5.5.4. Finally, it is noted that the realisations of the lognormal random field have been simulated using the covariance matrix decomposition method (see Chapter 2).



(a) local modulus of elasticity E_l^* (b) global modulus of elasticity E_g^*

Figure 5.10: Histograms of the marginal distribution of the effective moduli of elasticity with fitted lognormal and Weibull distributions.

Table 5.2: Null hypothesis test H_0 at 5% significance level and Anderson-Darling test statistic A^2 for distributions fit to both the local E_l^* and global E_g^* moduli of elasticity.

Test	Lognormal		Weibull	
	Reject H_0	A^2	Reject H_0	A^2
E_l^*	1	8.34	1	1.84
E_g^*	1	13.5	1	1.54

5.4.2 Correlation structure

Following the specification of the marginal distribution, the next step is to specify the correlation structure thus defining the full joint distribution of the random field. The selected two-dimensional correlation function has separate correlation lengths in the along-grain x and against-grain y-directions in order to model the anisotropic nature of the timber microstructure as discussed in Section 5.2. The selected correlation function is the two-dimensional anisotropic Markov correlation function given by:

$$\rho(s_X, s_Y) = \exp\left(-2\sqrt{\left(\frac{s_X}{\theta_X}\right)^2 + \left(\frac{s_Y}{\theta_Y}\right)^2}\right) \tag{5.7}$$

where s_X and s_Y are the separation of points, θ_X and θ_Y are the correlation lengths, in the x and y-directions respectively. By considering spatial separation only in the x-direction ($s_Y = 0$), the two-dimensional correlation function simplifies to the one-dimensional Markov correlation function:

$$\rho_X(s_X) = \exp\left(-\frac{2|s_X|}{\theta_X}\right) \tag{5.8}$$

An estimate $\hat{\theta}_X$ of the correlation length in the x-direction is found by first computing the sample correlation function $\hat{\rho}(s_X)$, known as the *correlogram* (Cressie, 1993), and then a non-linear least squares algorithm is used to find the value of the correlation length θ_X that minimises the misfit ϵ between the theoretical correlation function $\rho(s_X)$ and the sample correlation $\hat{\rho}(s_X)$. The misfit ϵ is given by the weighted square error:

$$\epsilon = \sum_{k=0}^{N_S-1} w_k \Big(\rho_X(s_k) - \hat{\rho}_X(s_k)\Big)^2 \tag{5.9}$$

where w_k is the weight associated with the k^{th} lag s_k of the correlation function. These weights are often taken to be uniform (Lloret-Cabot et al., 2014); however, it is the suggestion of this thesis that it should be taken into account that the sample correlation at higher lags is associated with fewer observations which results in greater uncertainty. Consequently, the approach pursued here is to weight the correlation estimate at the k^{th} lag according to the number of samples associated with that lag. In addition, a simpler estimate of the correlation structure is also considered that is only based on the lag-1 correlation $\hat{\rho}_1$ since it is less computationally expensive to numerically quantify the uncertainty associated with this estimate in comparison to the estimate based on the full correlation structure associated with N_S lags. This is because a non-linear optimisation algorithm is not required to obtain the correlation length, instead, the lag-1 estimate $\hat{\theta}$ of the correlation length is given by:

$$\hat{\theta} = -\frac{2L^*}{\ln(\hat{\rho}_1)} \tag{5.10}$$

where L^* is the separation between the midpoints of the board segments given by $L^* = 40$ cm.

Figure 5.11 shows the sample correlation function $\hat{\rho}_l(s_X)$ for the local modulus of elasticity E_l^* as well as fitted full and lag-1 theoretical correlation functions $\rho_l(s_X)$ in the along-grain x-direction. It is observed that the correlation in the x-direction initially exhibits rapid decay, however, the correlation associated with higher lags does not appear to settle to zero. The correlation not decaying to zero is a property of long-memory processes (Beran et al., 2013), also known as *fractal processes* (Mandelbrot and Van Ness, 1968), and it is noted that these processes are associated with infinite variance and correlation length. However, the determination of whether this is evidence of a fractal process is beyond the scope of this research and, consequently, the value of correlation associated with the higher lags is treated as a random fluctuation resulting from the limited sample size. It is observed that since the lag-1 theoretical correlation function $\hat{\rho}_l(s_X)$ [lag-1] does not take into account the correlation observed at higher lags its value is lower than the full theoretical correlation function $\hat{\rho}_l(s_X)$ [full]. As detailed in Table

5.3, the estimate of the correlation length $\hat{\theta}_X$ of the local elastic modulus E_l^* in the x-direction obtained from the lag-1 estimate of the correlation structure is 10.6% lower than the estimate obtained from the full autocorrelation structure.

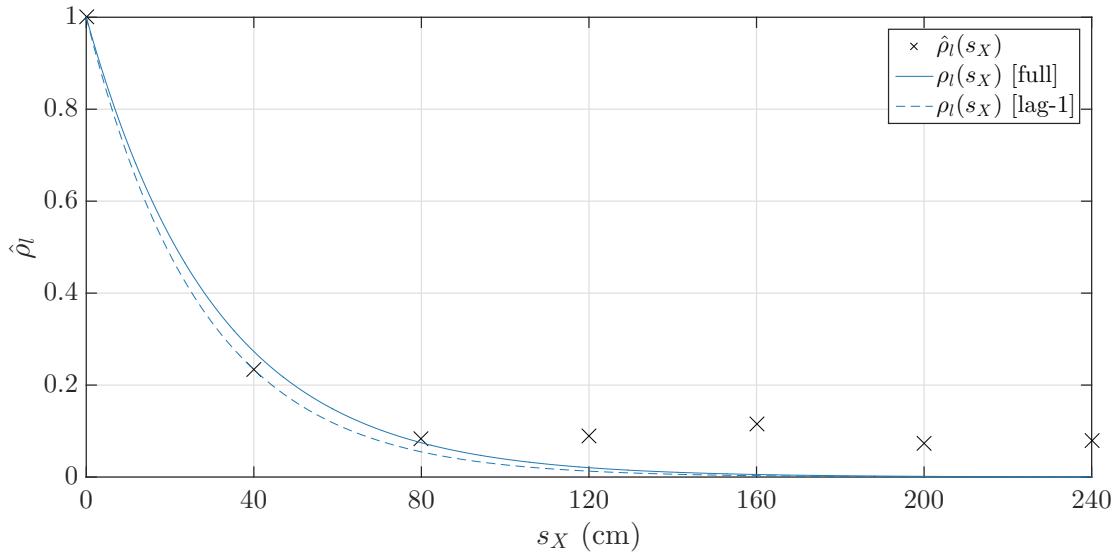


Figure 5.11: Sample correlation function $\hat{\rho}_l(s_X)$ for the local modulus of elasticity E_l^* against separation s_X in the along-grain x-direction with fitted full and lag-1 theoretical correlation functions $\rho_l(s_X)$.

Figure 5.12 shows that the sample correlation function $\hat{\rho}_g(s_X)$ for the global modulus of elasticity E_g^* with fitted full and lag-1 correlation functions $\rho_g(s_X)$ in the along-grain x-direction. It is observed that, in the x-direction, the correlations associated with the global elastic modulus E_g^* are higher than those associated with the local elastic modulus E_l^*. This is attributed to the global weighting function $\omega_g(x)$ being more uniform over the domain, thereby averaging over a larger statistical region, which results in increased smoothing of the stiffness profile $E(x)$ thus inflating the measured correlation. Similar to the local elastic modulus E_l^*, the estimate of the correlation length $\hat{\theta}_X$ of the global elastic modulus E_g^* in the x-direction obtained from the lag-1 estimate of the correlation structure is 20.4% lower than the estimate obtained from the full autocorrelation structure.

The procedure to obtain estimates of the along-grain correlation length θ_X can be repeated to obtain estimates of the against-grain correlation length θ_Y by considering separation only in the y-direction ($s_X = 0$). Figure 5.13 shows that the sample correlation functions $\hat{\rho}(s_Y)$ for the local E_l^* and global E_g^* moduli of elasticity with fitted full and lag-1 correlation functions $\rho(s_Y)$ in the against-grain y-direction. It is observed that

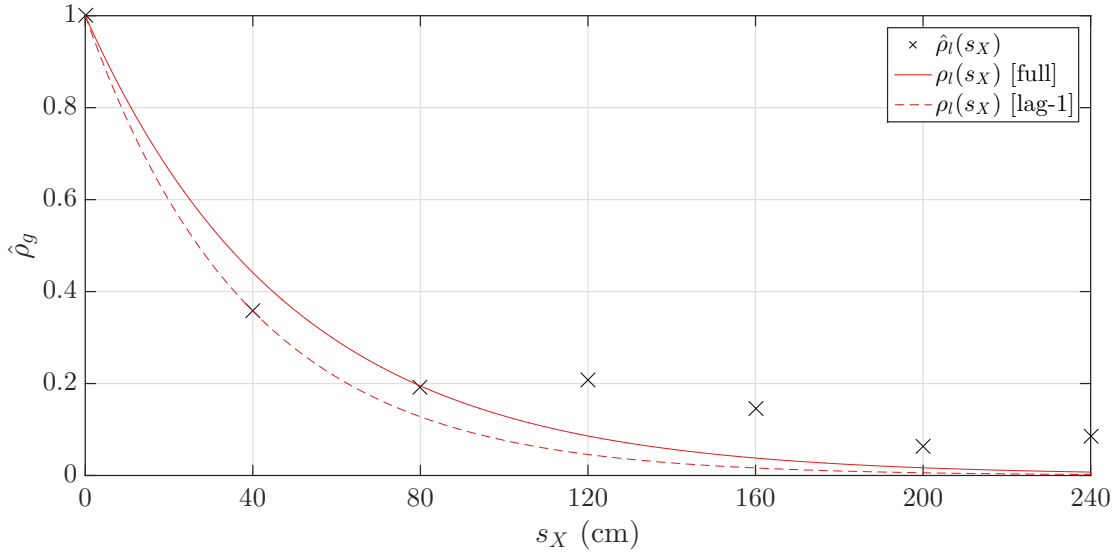
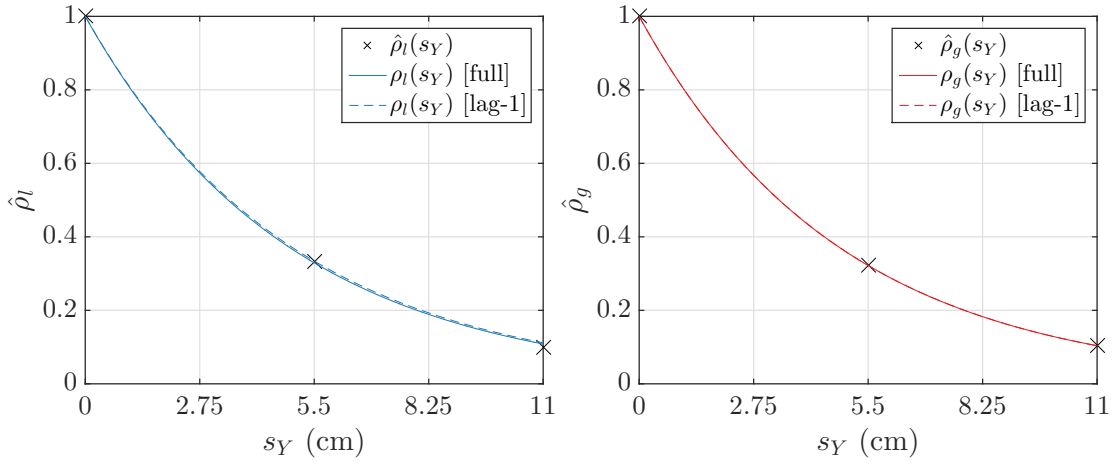


Figure 5.12: Sample correlation function $\hat{\rho}_g(s_X)$ for the global modulus of elasticity E_g^* against separation s_X in the along-grain x-direction with fitted full and lag-1 theoretical correlation functions $\rho_g(s_X)$.

there is much greater agreement between the estimates of the correlation structure of the local E_l^* and global E_g^* elastic moduli in the y-direction in comparison to the correlation estimates in the x-direction. Furthermore, there is also greater agreement between lag-1 and full autocorrelation estimates which is partly attributed to the greater statistical certainty associated with the larger number of observations of each lag in the y-direction.



(a) local modulus of elasticity E_l^*

(b) global modulus of elasticity E_g^*

Figure 5.13: Sample correlation functions $\hat{\rho}(s_Y)$ for both moduli of elasticity in the against-grain y-direction with fitted full and lag-1 theoretical correlation functions $\rho(s_Y)$.

Table 5.3: Correlation length estimates inferred from the local E_l^* and global E_g^* elastic moduli.

Test	$\hat{\theta}_X$ (cm)		$\hat{\theta}_Y$ (cm)	
	full	lag-1	full	lag-1
E_l^*	61.6	55.1	9.9	10.0
E_g^*	97.8	77.8	9.7	9.7

5.5 Uncertainty quantification

This section considers the quantification of the uncertainty associated with the parameters of the random field model inferred from the experimental dataset of Sousa et al. (2014) as detailed in the previous section. The motivation for this uncertainty quantification is that it is suggested, based on a qualitative analysis of the formulation of the effective property as a weighted harmonic mean in Section 5.3, that the parameter estimates are subject to large systematic biases due to the use of the midpoint approximation. In particular, it is noted that computer experiments utilising mathematical models can be used to simulate physical experiments for a fraction of both the financial cost and time investment (Sacks et al., 2004). As a result of this, computer experimentation offers a viable method to quantify the uncertainty associated with an experimental procedure for which physical reproduction would be uneconomic. The traditional problem considered within uncertainty quantification is to calculate the variability in the output for a given variability in the input and this is known as forward uncertainty quantification. However, an alternative problem is inverse uncertainty quantification which is the process of deducing the variability in the input of a model from known variability in the output (Wua et al., 2018). The approach to inverse uncertainty quantification adopted within this section is to perform a computer experiment to gain insights into the variability of the input, the vector random field parameters $\boldsymbol{\Phi} = \{\mu, \sigma, \theta_X, \theta_Y\}$, from the output, the vector of effective properties $\boldsymbol{E}^*$.

The computer experiment has been designed to closely replicate the experimental procedure of Sousa et al. (2014) with the boards modelled as one-dimensional Euler-Bernoulli beams. It should be recognised that the computer experiment contained within this chapter is subject to a number of limitations; for instance, quantification of the un-

certainty in the against-grain correlation length $\hat{\theta}_Y$ is neglected in order to reduce the computational burden associated with the two-dimensional case. Realisations of the lognormal random field are generated using the covariance matrix decomposition simulation method (see Chapter 2) with $N_X = 360$ elements in the along-grain x-direction and $N_Y = 3$ elements in the against-grain y-direction which represents the three boards that the beam is sawn into and, consequently, the elastic modulus of each board is modelled by a one-dimensional random process. It is important that the stiffness profiles of the boards belonging to the same beam are cross-correlated since treating the boards as statistically independent would artificially decrease the aleatoric uncertainty. Once the stiffness profiles have been simulated for each board, the next step is to sequentially calculate the local and global elastic moduli over the $N_S = 7$ segments using the harmonic mean formulation and weighting functions detailed in Section 5.3 thereby replicating the experimental procedure conducted by Sousa et al. (2014). For illustrative purposes, a single realisation of the stiffness profile $E(x)$ of one of the boards is shown in Figure 5.14 along with the calculated local E_l^* and global E_g^* elastic moduli.

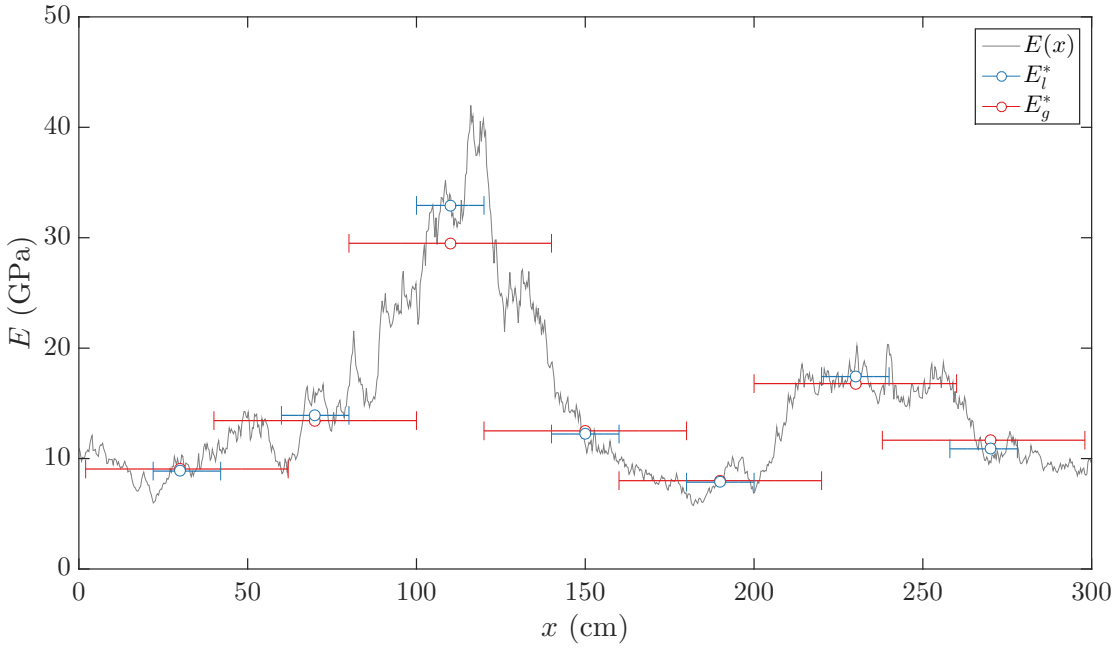


Figure 5.14: A realisation of the lognormal stiffness profile $E(x)$ with local E_l^* and global E_g^* elastic moduli with the associated averaging region and location of the midpoint approximation indicated by a circle.

The Monte Carlo method is used to estimate the distributions of the parameter estimates inferred from the effective elastic moduli and then, additionally, to quantify the

associated aleatoric and epistemic uncertainty. The statistics of these distributions are referred to as *meta-statistics* in order to distinguish them from the statistics of the random field. In total, four meta-statistics are reported for each parameter estimate: two of which are raw and two of which are normalised. The first raw meta-statistic is the sample mean Mean[.] and it is useful to note that the deviation of this meta-statistic from the true value of the parameters ($\mu = 12.91$ GPa, $\sigma = 3.92$ GPa, $\theta_X = 55.1$ cm) is a measure of the epistemic uncertainty. The second raw meta-statistic is the sample standard deviation Std[.] which quantifies the aleatoric uncertainty in each of the parameter estimates of the random field. The aleatoric uncertainty is due to a number of factors including the non-ergodicity of the realisations of the lognormal stiffness profile $E(x)$ as well as the limited number of boards N_B that have been sampled. The first normalised meta-statistic is the percentage bias Bias[.] which is given by:

$$\text{Bias}\left[\hat{\mu}\right] = \frac{100\%}{R}\sum_{r=1}^{R}\left(\frac{\hat{\mu}_r - \mu}{\mu}\right) \tag{5.11}$$

where R is the number of runs of the simulated experiment, $\hat{\mu}_r$ is the parameter estimate associated with the r^{th} simulation and μ is the true value of the parameter. The meta-statistic Bias[.] is reported in order to facilitate comparison of the epistemic uncertainty between different parameter estimates. However, it should be recognised that the estimate given by the meta-statistic Bias[.] consists of bias due to both the midpoint approximation, as well as, the bias associated with the method of moment estimators presented in Section 5.2. The second normalised meta-statistic is the maximum absolute percentage error MAPE[.] which is given by:

$$\text{MAPE}\left[\hat{\mu}\right] = \frac{100\%}{R}\sum_{r=1}^{R}\left|\frac{\hat{\mu}_r - \mu}{\mu}\right| \tag{5.12}$$

The utility of this meta-statistic is that it evaluates the total uncertainty resulting from the combination of both aleatoric and epistemic uncertainty. The following section presents the results of the computer experiment, with parameters in Table 5.4, that quantifies the uncertainty in the estimates of the location $\hat{\mu}$, scale $\hat{\sigma}$ and correlation parameter $\hat{\theta}_X$. The meta-statistics are reported for each parameter of the random field inferred from both the local and global elastic moduli. In addition, the meta-statistics of the parameter estimates inferred directly from the stiffness profile $E(x)$ are also reported

since the bias in these estimates is only due to the method of moment estimators and, consequently, this enables assessment of the proportion of bias that is due to the method of moment estimators in comparison to the bias resulting from use of the midpoint approximation.

Table 5.4: Parameter values of the computer experiment to quantify uncertainty.

Parameter	Symbol	Value	Units
Experimental parameters			
Number of runs	R	10^6	–
Number of beams	N_M	16	–
Number of boards	N_B	48	–
Number of segments	N_S	7	–
Span length	L_0	60	cm
Separation between segment midpoints	L^*	40	cm
Distance from support to load	a	18	cm
Gauge length	L_1	20	cm
Load	P	10	kN
Board parameters			
Board length	L	300	cm
Board height	H	4	cm
Board width	W	7	cm
Area moment of inertia	I	37	cm^4
Random field parameters			
Mean of elastic modulus	μ	12.91	GPa
Standard deviation of elastic modulus	σ	3.92	GPa
Correlation length in x-direction	θ_X	55.1	cm
Correlation length in y-direction	θ_Y	10.0	cm
Discretisation in x-direction	N_X	360	–
Discretisation in y-direction	N_Y	3	–

5.5.1 Distribution of the location parameter

Figure 5.15 shows the distribution of the location parameter estimate $\hat{\mu}$ obtained from each of the tests whilst Table 5.5 details the four associated meta-statistics. It is noted that the bias in the location parameter estimate $\hat{\mu}$ estimated directly from the stiffness profile $E(x)$ has been found to be negligible despite the sample mean not being an unbiased estimator for correlated samples. Additionally, it is observed that both the local E_l^* and global E_g^* effective properties have decreased expected value compared to the stiffness profile $E(x)$ which has an expected value of $\mu = 12.91$ GPa. This is explained by considering that both effective elastic moduli, E_l^* and E_g^*, are given by harmonic means which tend towards the least element of a set and, consequently, these effective properties are disproportionately affected by regions of low stiffness which act to decrease their expected value. Furthermore, it has been found that the decrease in expected value of the location parameter estimate $\hat{\mu}$ is smaller in the case of the local elastic modulus E_l^*. This is because weak-zones near the supports do not affect the local elastic modulus E_l^* however, in comparison, these weak zones do affect the global elastic modulus E_g^*.

It is observed that the estimates of the location parameter estimate $\hat{\mu}$ inferred from the local E_l^* and global E_g^* elastic moduli both have a similar variance. In particular, it is noted that the aleatoric uncertainty associated with the location parameter estimate $\hat{\mu}$ is similar to the base aleatoric uncertainty associated with direct inferences from the stiffness profile $E(x)$. This is due to the fact that the variability of the arithmetic mean of a set of random variables is not significantly different than the variability of the harmonic mean of the same set. Additionally, it is observed that the standard deviation, as quantified by the meta-statistic Std[.], is slightly greater for the local elastic modulus E_l^* since it is an average over a smaller region of the stiffness profile $E(x)$ of the beam in comparison to the global elastic modulus E_g^* and, as the number of random variables decreases, the variability of that average increases. The meta-statistic MAPE[.] for each of the tests $\{E(x), E_l^*, E_g^*\}$ shows that the epistemic uncertainty due to the midpoint approximation is of a similar magnitude relative to the magnitude of the aleatoric uncertainty associated the experimental set-up as detailed in Table 5.4.

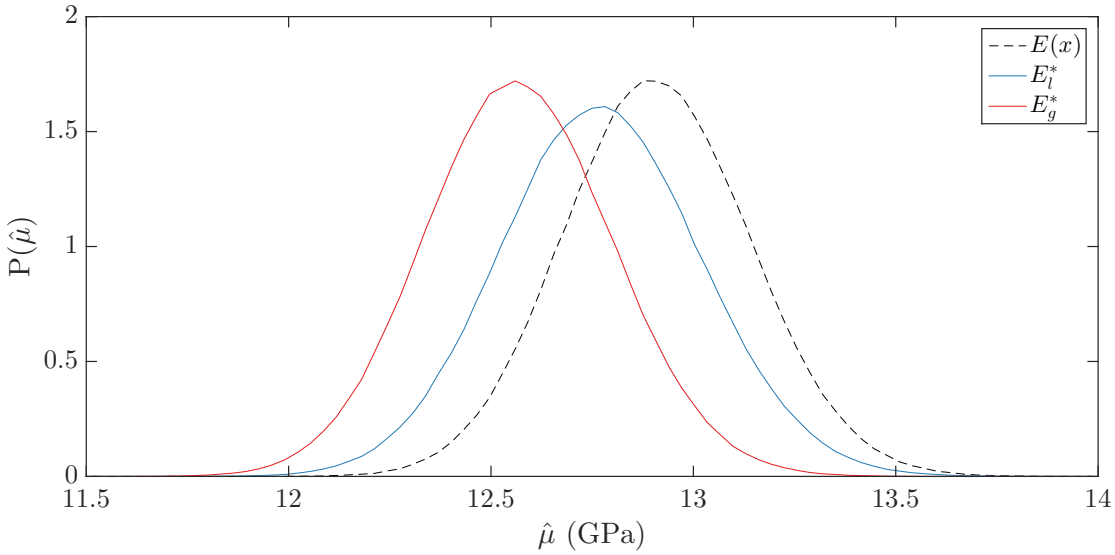


Figure 5.15: Distribution of the location parameter estimate $\hat{\mu}$ inferred from the local elastic moduli E_l^*, global elastic moduli E_g^* and the base stiffness profile $E(x)$.

Table 5.5: Meta-statistics of the location parameter estimate $\hat{\mu}$.

Test	Mean[$\hat{\mu}$] (GPa)	Std[$\hat{\mu}$] (GPa)	Bias[$\hat{\mu}$] (%)	MAPE[$\hat{\mu}$] (%)
$E(x)$	12.91	0.231	0.00	1.43
E_l^*	12.77	0.248	−1.07	1.77
E_g^*	12.57	0.233	−2.64	2.76

5.5.2 Distribution of the scale parameter

Figure 5.16 shows the distribution of the scale parameter estimate $\hat{\sigma}$ obtained from each of the tests whilst Table 5.6 details the four associated meta-statistics. It is observed that the estimates of the scale parameter $\hat{\sigma}$ obtained from the local E_l^* and global E_g^* effective properties underestimate the true variability of the stiffness profile $E(x)$. This is potentially unconservative since underestimation of the scale parameter of the stiffness profile $E(x)$ results in the beam being modelled as inappropriately homogeneous which leads to under-design. Similar to the location parameter estimate $\hat{\mu}$, the bias in the scale parameter estimate $\hat{\sigma}$ is negative and the magnitude of the reduction in the expected value is once again greatest for inferences from the global elastic modulus E_g^*. However, it should be noted that the relative reduction in expected value is significantly greater for the scale parameter estimate $\hat{\sigma}$ than it is for the location parameter estimate $\hat{\mu}$. In addition, the meta-statistic Bias[.] shows that the estimator of standard deviation is negatively biased for the stiffness profile $E(v)$ and, consequently, it is concluded that the estimator of the standard deviation has a negative bias of approximately 0.26%. Therefore, approximately 0.26 percentage points of the bias associated with the elastic moduli, E_l^* and E_g^*, results from estimator bias and cannot be attributed to usage of the midpoint approximation.

It is observed that there is not a significant variation between the meta-statistic Std[.] associated with each test $\{E(x), E_l^*, E_g^*\}$ and, consequently, it is concluded that estimating the location μ and scale σ parameters of the stiffness profile $E(x)$ from its effective properties does not result in significant increases in aleatoric uncertainty. Additionally, in contrast to the location parameter estimate, the meta-statistic MAPE[.] shows that the epistemic uncertainty associated with the scale parameter estimate $\hat{\sigma}$ is significantly greater than the aleatoric uncertainty. In conclusion, the parameter estimates of the location $\hat{\mu}$ and scale $\hat{\sigma}$ parameters both experience a reduction in expected value when estimated from the effective properties. However, it should be noted that whilst underestimation of the location parameter μ leads to over-design, in contrast, underestimation of the scale parameter σ leads to under-design since the material is modelled as being unsuitably homogeneous. In particular, identification of these epistemic biases motivates the development of improved inferential methodologies to estimate the random field parameters so that the stochastic finite element model accurately quantifies the risk associated with heterogeneous structures.

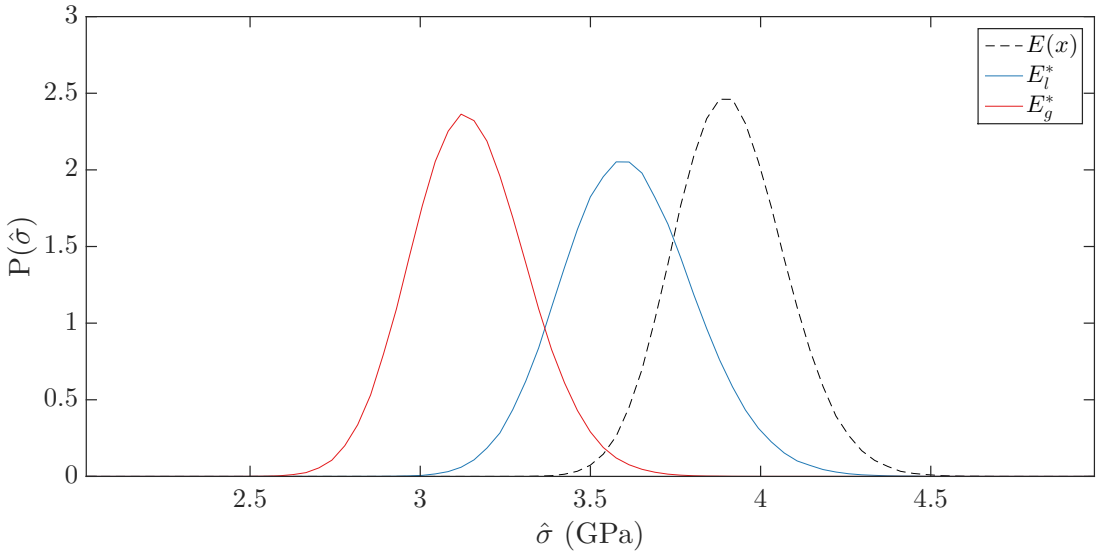


Figure 5.16: Distribution of the scale parameter estimate $\hat{\sigma}$ inferred from the local elastic moduli E_l^*, global elastic moduli E_g^* and the base stiffness profile $E(x)$.

Table 5.6: Meta-statistics of the scale parameter estimate $\hat{\sigma}$.

Test	Mean[$\hat{\sigma}$] (GPa)	Std[$\hat{\sigma}$] (GPa)	Bias[$\hat{\sigma}$] (%)	MAPE[$\hat{\sigma}$] (%)
$E(x)$	3.91	0.162	−0.25	3.3
E_l^*	3.61	0.195	−7.82	8.1
E_g^*	3.15	0.170	−19.73	19.7

5.5.3 Distribution of the correlation parameter

Figure 5.17 shows the distribution of the correlation parameter estimate $\hat{\theta}_X$ obtained from each of the tests whilst Table 5.7 details the associated meta-statistics. It is observed that the correlation parameter estimates $\hat{\theta}_X$ obtained from effective properties, E_l^* and E_g^*, exhibit large positive epistemic biases in contrast to the negative biases observed for both the location $\hat{\mu}$ and scale $\hat{\sigma}$ parameter estimates. In particular, it is noted that the increase in the expected value is greatest for the correlation parameter estimate $\hat{\theta}_X$ inferred from the global elastic modulus E_g^*. This is because the global elastic modulus E_g^* is an average over a larger statistical region which results in a greater smoothing of the stiffness profile $E(x)$ thus inflating the measured correlation. Additionally, the meta-statistic Bias[.] associated with the correlation parameter estimate $\hat{\theta}$ directly inferred from the base stiffness profile $E(x)$ indicates that the lag-1 estimator of the correlation length, given by Equation 5.10, has a negative bias of approximately 1%. The small magnitude of this underestimation suggests that the lag-1 estimator is a good estimator of the correlation length θ_X provided the number of samples is sufficiently large. However, the negative bias of this estimator implies that the inflation of correlation associated with inferences from the effective properties is greater, by approximately a single percentage point, than that suggested by the Bias[.] meta-statistic in Table 5.7.

It is observed that the aleatoric uncertainty associated with the correlation length estimate $\hat{\theta}_X$ inferred under the midpoint approximation from the effective elastic moduli, E_l^* and E_g^*, is significantly higher than the base aleatoric uncertainty associated with direct inference of the correlation length θ_X from the stiffness profile $E(x)$. This is to be expected since the estimator of the sample correlation function, given by Equation 2.69, depends on estimates of both the location $\hat{\mu}$ and scale parameter $\hat{\sigma}$ and, consequently, the uncertainty associated with these parameter estimates is propagated into the estimate of the correlation length θ_X. In addition, the MAPE meta-statistic shows that both the aleatoric and epistemic uncertainties have a similar contribution to the total uncertainty associated with the correlation length estimate $\hat{\theta}_X$. It is concluded that the correlation structure of the effective elastic moduli, E_l^* and E_g^*, is not necessarily representative of the correlation structure of the stiffness profile $E(x)$. Furthermore, it has been identified that the correlation parameter θ_X inferred from the effective elastic moduli is systematically over-estimated; however, it should be noted that it is not possible to make a general conclusion on whether this overestimation leads to under or over-design.

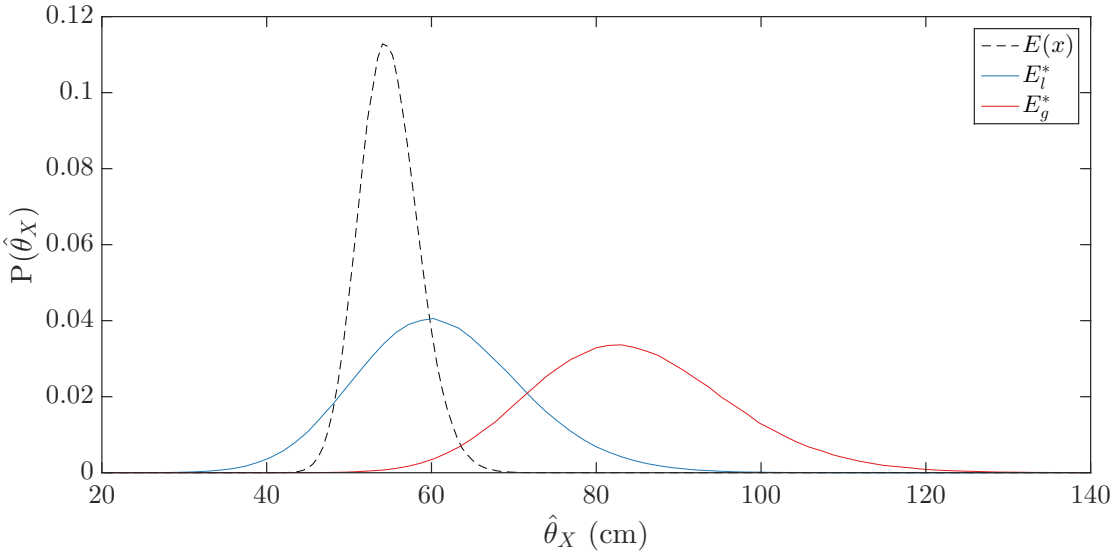


Figure 5.17: Distribution of the correlation parameter estimate $\hat{\theta}_X$ inferred from the local elastic moduli E_l^*, global elastic moduli E_g^* and the base stiffness profile $E(x)$.

Table 5.7: Meta-statistics of the correlation parameter estimate $\hat{\theta}_X$.

Test	Mean$[\hat{\theta}_X]$ (m)	Std$[\hat{\theta}_X]$ (m)	Bias$[\hat{\theta}_X]$ (%)	MAPE$[\hat{\theta}_X]$ (%)
$E(x)$	54.9	3.57	−0.4	5.2
E_l^*	61.2	10.10	11.0	16.8
E_g^*	84.5	12.15	53.4	53.4

5.5.4 Discussion of results

The conclusions of the computer experiment conducted to quantify uncertainty are that the estimation of random field parameters from the experimentally determined local E_l^* and global E_g^* elastic moduli under the midpoint approximation results in minor negative epistemic bias in the location parameter estimate $\hat{\mu}$, moderate negative epistemic bias in the scale parameter estimate $\hat{\sigma}$ and large positive epistemic bias in the correlation parameter estimate $\hat{\theta}_X$. Furthermore, the aleatoric uncertainty associated with the location $\hat{\mu}$ and scale $\hat{\sigma}$ parameter estimates inferred from the effective properties has been found to be only slightly increased in comparison to the base aleatoric uncertainty. In contrast, the aleatoric uncertainty associated with the correlation length estimate $\hat{\theta}_X$ inferred from the effective properties has been found to be significantly greater than the base aleatoric uncertainty. Additionally, the sign of the epistemic bias in the parameter estimates has been found to be consistent for both the local E_l^* and global E_g^* moduli of elasticity and it is noted that the magnitude of all the meta-statistics is always greater for the global elastic modulus E_g^* in comparison to the local elastic modulus E_l^*. As a result of this, it is concluded that the utilisation of the midpoint approximation is less appropriate for the global elastic modulus E_g^* and more appropriate for the local elastic modulus E_l^* due to the central concentration of the local weighting function $\omega_l(x)$.

It is important to recognise that the computer experiment detailed in this section, as well as the associated uncertainty quantification, has been subject to a large number of limitations including: the introduction aleatoric uncertainty into the quantification of uncertainty through the use of Monte Carlo simulation; the effect of shear and indentation on the global elastic modulus E_g^* have been neglected; in order to reduce the computational burden, the parameters of the underlying distribution have been assumed based on estimates obtained under the midpoint approximation; only the lag-1 correlation has been considered instead of the full autocorrelation structure; the random field has been approximated with a discretised representation suitable for simulation; experimental error has been neglected and has instead been attributed to the variability of the random field. The result of these limitations is that the quantification of uncertainty cannot be treated as exact, however, this does not discredit the general insights yielded by the computer experiment into the uncertainty associated with the inference of the random field parameters from experimentally determined effective properties. In particular, it is noted that this approach is a significant advance on previous research

that has been under the assumption that the effective elastic modulus of a beam is an unweighed arithmetic mean (Bulleit and Chapman, 2004) which neither accounts for the disproportionate contribution of zones of low stiffness to effective modulus of elasticity nor the influence of spatial weighting associated with bending tests.

Additionally, it should be recognised that the poor fit of the lognormal distribution is expected to have decreased the accuracy of the distributions of the parameter estimates presented in this section, however, it should be noted that the use of the lognormal distribution has no implications on the on the accuracy of the parameter estimates reported in Section 5.4. Finally, it should be noted that the computer experiment has only been run for one set of random field parameters ($\mu = 12.91$ GPa, $\sigma = 3.92$ GPa, $\theta_X = 55.1$ cm); however, it is expected that the trends are expected to hold for different parameter values with the magnitude of the trend increasing with the heterogeneity of the beam i.e. as either the scale parameter σ increases or as the correlation ratio θ_X/L decreases. Furthermore, the observation that the midpoint approximation is most appropriate for the local effective property E_l^* should be treated with caution since the smaller epistemic error associated with the local effective property E_l^* is still of a significant magnitude. In conclusion, it has been identified that random field parameters inferred under the midpoint approximation are subject to large epistemic biases and likely underestimate the true variability of material properties.

5.6 Conclusion

This chapter has investigated the inference of the parameters of a random field from experimentally determined effective properties with specific consideration of the effective elastic moduli of timber. The key achievements of this chapter are summarised as:

- A literature review on the probabilistic modelling of timber has been conducted with consideration of the risk associated with the mechanical properties of timber resulting from its sensitivities to environmental conditions and defects such as knots. Furthermore, the experimentally determined differences between the local and global effective elastic moduli have been discussed and an analytical explanation for these differences has been developed based on an analysis of the local and global weighting functions derived under Euler-Bernoulli beam theory.

- A lognormal random field model has been fitted to the experimental four-point dataset of Sousa et al. (2016) using method of moment estimators under the midpoint approximation and the estimates for the location, scale and correlation parameters have been reported. In particular, there has been extensive consideration of stationarity, regression of the sample correlation function and the selection of the marginal distribution with insights into the choice between the lognormal and Weibull distributions.

- A computer experiment has been performed to quantify the uncertainty associated with the parameter estimates of the random field model obtained under the midpoint approximation. It is concluded that the location and scale parameters are systematically underestimated whilst the correlation parameter is systematically overestimated. Moreover, it has been found that the location parameter is associated with small aleatoric certainty, the scale parameter estimate is associated with moderate aleatoric uncertainty and the correlation parameter estimate is associated with large aleatoric uncertainty.

In conclusion, random fields are an attractive probabilistic model for the spatial variation of material properties, however, additional research is required to further develop and verify methodologies to accurately infer their parameters from experimentally determined material properties.

Chapter 6

Conclusion

This thesis has considered the application of random fields to model the effective property of materials with spatially stochastic mechanical properties. This is important since the suitability of random field models to model material heterogeneity has implications on the accuracy of the quantification of structural reliability obtained through the stochastic finite element method. There has been extensive investigation of the relationship between the effective elastic modulus of a simply supported timber beam and the log-normal stiffness profile. The main research topic that has been investigated within this thesis is the extent to which the effective property is sensitive to minima of the random field of elastic modulus and determination of the influence of spatial weighting. It is noted that the investigation of this research topic has led to the development of an analytical approach to determine the moments of displacement of an Euler-Bernoulli beam and a quasi-analytical approach to determine the moments of the effective elastic modulus. In the one-dimensional case, the accuracy of these quasi-analytical moments has been evaluated against a stochastic finite element model and, in the two-dimensional case, an acceptance-rejection perturbation algorithm has been developed to optimise a weighted mean meta-model to the results of a stochastic finite element model in order to approximate the higher-dimensional effective modulus of elasticity. Furthermore, a computer experiment has been conducted to quantify the uncertainty associated with the random field parameter estimates inferred from experimentally determined effective properties. Finally, it is suggested that the identification of large epistemic uncertainty in the parameter estimates motivates the development of improved inferential methodologies.

6.1 General conclusions

The objective of this section is to present the general conclusions of this thesis with respect to three key criteria namely the *analytical*, *numerical* and *inferential insights* into the effective properties of randomly heterogeneous beams. These insights lay the foundation for the development of an increasingly sophisticated theory of heterogeneous beams and, in order to alleviate some of the methodological limitations associated with these insights, recommendations are made in Section 6.2 for further research.

Analytical insights

This thesis has considered the development of a theory to describe the relationship between the effective properties of a material and the underlying random field that models the continuous variation of material properties. The approach adopted in the one-dimensional case was to analytically derive this relationship and it has been shown, in the first half of Chapter 3, that the effective elastic modulus of an Euler-Bernoulli beam can be formulated as a weighted harmonic mean. The weighting function of this harmonic mean has been derived for a number of important loading conditions of a simply supported beam including 3-point, 4-point and uniformly distributed loading. Furthermore, expressions are also presented in Chapter 5 for the weighting functions of the local and global moduli of elasticity determined in compliance with BS EN 408:2010. Additionally, it has been shown in the second half of Chapter 3 that the weighted mean formulation of the effective elastic modulus facilitates the derivation of analytical expressions for the first two moments of deflection and quasi-analytical expressions for the first two moments of the effective elastic modulus of an Euler-Bernoulli beam with a lognormally distributed stiffness profile. Finally, analytical contributions have been achieved in Chapter 2 to the general theory of random fields including the derivation of the constant of the power correlation function as well as the periodic definition of the discretised spectral density function.

Numerical insights

It has been observed in Chapter 4 that, in the multidimensional case, the relationship between the effective property and the random field of the material property is not analytical and, consequently, this necessitates the use of numerical methods. One of the

numerical techniques considered within this thesis is the stochastic finite element method, however, the disadvantage of this approach is that it may be prohibitively computationally expensive for large models especially when implemented using Monte Carlo methods. In Chapter 4, a generalised mean meta-model has been introduced for the effective properties of randomly heterogeneous materials that, when optimised on a small number of finite element solves, offers a computationally efficient surrogate to accurately predict the effective elastic modulus of heterogeneous materials. An additional benefit of this meta-model is that it provides insights into research questions concerning the sensitivity of the effective elastic modulus to both spatial weighting and minima of the stiffness field and it noted that these insights could not have been obtained through the stochastic finite element method due to its opaque black-box nature. Furthermore, in the second half of Chapter 3, a one-dimensional stochastic finite element model has been used to show, for low coefficients of variation of the stiffness profile, that the quasi-analytical theory of heterogeneous beams closely approximates the numerically determined moments of the effective elastic modulus. Finally, Chapter 2 contained an evaluation of the numerical efficiency of three different simulation methods with conclusions on which method is most efficient, as well as containing useful observations on the efficient numerical computation of the likelihood of samples from a multivariate Gaussian distribution.

Inferential insights

Inferential insights have been provided throughout this thesis on the suitability of random fields to model material heterogeneity including a discussion on a range of topics such as the mesoscale continuum approximation and the choice of marginal distribution with specific attention given to the material properties of timber. In Chapter 2, frequentist estimation using either method of moments or maximum likelihood estimation has been considered including adaptation of these estimators to the case of multiple realisations. In particular, this thesis has extensively considered the discrepancy between the fact that traditional inferential methodologies assume point samples of the random field and the reality that effective material properties are experimentally determined over a non-zero sample volume. It has been identified that this discrepancy is typically resolved through the use of the midpoint approximation and, based on the computer experiment detailed in Chapter 5, it has been demonstrated that this approximation is a source of significant epistemic bias. Specifically, it has been shown that typically the location parameter of the random field model is slightly underestimated, that the scale parameter is moderately

underestimated and that the correlation parameter is greatly overestimated. This implies that caution should be exercised with regards to parameter values inferred under these methodologies since it will lead to the material being modelled as more homogeneous than it truly is. It is recommended that a future research topic of considerable importance is the development of inferential methodologies that avoid the epistemic error associated with the midpoint approximation as well as quantifying aleatoric uncertainty.

6.2 Recommendations for further research

This section contains recommendations for research to the further develop the theory of the effective properties of heterogeneous beams and overcome the methodological limitations identified within this thesis. In particular, two key areas of research are prioritised for further development and recommended as subjects of future research. The first key area is the development of *improved analytical expressions* for the relationship between the effective properties of a material and the underlying random field model and the second key area is the development of *improved inferential methodologies* for the estimation of random field parameters from experimentally determined effective properties.

Improved analytical expressions

The motivation for the development of improved analytical expressions is that an analytical theory of heterogeneous beams is less computationally expensive, more accurate and offers greater insight in comparison to numerical methods. In Chapter 3, a procedure has been outlined for the derivation of weighting functions through the manipulation of the Euler-Bernoulli beam equation. However, it should be noted that the limitation of this approach is that the derivation must be repeated for each boundary and loading condition of interest. In order to further develop the theory of heterogeneous beams, it is desirable that a general expression is derived for the weighting function of an Euler-Bernoulli beam under arbitrary loading and boundary conditions in terms of an integral of the bending moment. In addition, it is noted that Chapter 3 contains useful expressions for the first two moments of displacement of an Euler-Bernoulli beam in terms of the weighting functions and a scale factor. It is suggested that this result could be further strengthened by deriving an expression, in terms of the weighting functions, for the n^{th} moment of displacement of an Euler-Bernoulli beam with arbitrary boundary

conditions. Finally, in Chapter 4, a generalised weighted mean meta-model has been developed for the effective properties of randomly heterogeneous materials. However, it has been identified that a key limitation of this meta-model is that it fails to account for the interconnectedness of the underlying random field and it is recommend that the generalised weighted mean meta-model can be improved through the introduction of a factor that accounts for interconnectedness in accordance with Percolation theory as discussed at the end of Chapter 4.

Improved inferential methodologies

It has been shown in Chapter 5 that the traditional approach to estimate the parameters of a random field from experimentally determined effective properties through the use of method of moment estimators under the midpoint approximation results in significant epistemic bias. It is recommended that future research focus on the development of improved inferential methodologies that avoid the use of the midpoint approximation and account for inferential uncertainty under a Bayesian framework. In particular, it is suggested that the inferential methodology employ the technique of approximate Bayesian computation in order to avoid issues relating to the intractability of the likelihood function associated with experimentally determined material properties such as the effective modulus of elasticity. In particular, it is suggested that the proposed inferential methodology sample parameter values from the joint prior distribution, simulate realisations of the random field, determine the associated effective properties through a forward simulator and, finally, obtain samples from the posterior distribution based on an acceptance criteria which compares summary statistics of the simulated effective properties to summary statistics of the experimentally determined effective properties. The major advantage of this proposed Bayesian inferential methodology is that it would facilitate the scale-dependent reliability analysis of heterogeneous structures through the posterior predictive so that the quantification of risk accounts for inferential uncertainty.

Bibliography

R. J. Adler and J. E. Taylor. *The geometry of random fields*. Springer, New York, 2007.

G. B. Arfken, H. J. Weber, and F. E. Harris. *Mathematical methods for physicists*. Elsevier, Oxford, 7th edition, 2013.

S. R. Arwade and G. Deodatis. Variability response functions for effective material properties. *Probabilistic Engineering Mechanics*, 26(2):174–181, 2011.

S. R. Arwade, P. L. Clouston, and R. Winans. Measurement and stochastic computational modeling of the elastic properties of parallel strand lumber. *Journal of Engineering Mechanics*, 135(9):897–905, 2009.

R. J. Astley, J. J. Harrington, and K. A. Stol. Mechanical modelling of wood microstructure, an engineering approach. *IPENZ Transactions*, 24(1):21–29, 1997.

S. Axler. *Linear algebra done right*. Springer, New York, 2nd edition, 1997.

N. Bakhvalov and G. Panasenko. *Homogenisation: Averaging processes in periodic media*. Kluwer Academic Publishers, Dordrecht, The Netherlands, 1989.

K.-J. Bathe. *Finite element procedures*. Prentice Hall, London, 1996.

N. C. Beaulieu and Q. Xie. An optimal lognormal approximation to lognormal sum distributions. *IEEE Transactions on Vehicular Technology*, 53(2), 2004.

F. K. Bechtel. Beam stiffness as a function of pointwise E with application to machine stress rating. In *Symposium on forest products research international - achievements and the future*, Pretoria, 22nd - 26th April 1985. National Timber Research Institute of the South African Council for Scientific and Industrial Research.

F. K. Bechtel. Estimating local compliance in a beam from bending measurements part I: computing "span function". *Wood and Fiber Science*, 39(2):250–259, 2007.

J. Beran, Y. Feng, S. Ghosh, and R. Kulik. *Long-memory processes: probabilistic properties and statistical methods*. Springer, London, 2013.

P. Bocchini and G. Deodatis. Critical review and latest developments of a class of simulation algorithms for strongly non-Gaussian random fields. *Probabilistic Engineering Mechanics*, 23(4), 2008.

L. Boström. Determination of the modulus of elasticity in bending of structural timber – comparison of two methods. *Holz als Roh- und Werkstoff*, 57(2):145–149, 1999.

G. E. P. Box, G. M. Jenkins, G. C. Reinsel, and G. M. Ljung. *Time series analysis: forecasting and control*. Wiley, Hoboken, New Jersey, 5th edition, 2016.

R. N. Bracewell. *The Fourier transform and its applications*. McGraw Hill, Boston, 3rd edition, 2000.

R. Brandner and G. Schickhofer. Spatial correlation of tensile perpendicular to grain properties in Norway spruce timber. *Wood Science and Technology*, 48(2):337–352, 2014.

D. L. Brown and M. Vasilyeva. A generalized multiscale finite element method for poroelasticity problems I: Linear problems. *Journal of Computational and Applied Mathematics*, 294:372–388, 2016.

A. E. Bryson. Optimal control-1950 to 1985. *IEEE Control Systems Magazine*, 16(3): 26–33, 1996.

BS EN 14081:2005. Timber structures - Strength graded structural timber with rectangular cross section - Part 1: General requirements. Standard, British Standard Institution, London, 2005.

BS EN 178:2010. Plastics - Determination of flexural properties. Standard, British Standard Institution, London, 2010.

BS EN 408:2010. Timber structures - structural timber and glued laminated timber - determination of some physical and mechanical properties. Standard, British Standard Institution, London, 2000.

N. Buannic and P. Cartraud. Higher-order effective modelling of periodic heterogeneous beams - part I: asymptotic expansion method. *International Journal of Solids and Structures*, 38(40-41):7139–7161, 2001.

W. M. Bulleit and R. A. Chapman. Characterization of the correlation structure of lumber strength properties. *Wood Science and Technology*, 38(4):285–296, 2004.

O. S. Bursi and J. P. Jaspart. Benchmarks for finite element modelling of bolted steel connections. *Journal of Constructional Steel Research*, 43(1-3):17–42, 1997.

W. T. Cardwell and R. L. Parsons. Average permeabilities of heterogeneous oil sands. *Transactions of the AIME*, 160(1):34–42, 1945.

S. Casciati and M. Domaneschi. Random imperfection fields to model the size effect in laboratory wood specimens. *Structural Safety*, 29(4):308–321, 2007.

G. Casella and R. L. Berger. *Statistical inference*. Thomson Learning, Pacific Grove, California, 2nd edition, 2002.

T.-P. Chang and H.-C. Chang. Stochastic dynamic finite element analysis of a nonuniform beam. *International Journal of Solids and Structures*, 31(5):587–597, 1994.

J.-P. Chilès and P. Delfiner. *Geostatistics: modeling spatial uncertainty*. Wiley, Hoboken, New Jersey, 2nd edition, 2012.

S.-K. Choi, R. V. Grandhi, and R. A. Canfield. Structural reliability under non-Gaussian stochastic behaviour. *Computers and Structures*, 82(13-14):1113–1121, 2004.

Y. H. Chok, M. B. Jaksa, W. S. Kaggwa, D. V. Griffiths, and G. A. Fenton. Neural network prediction of the reliability of heterogeneous cohesive slopes. *International Journal for Numerical and Analytical Methods in Geomechanics*, 40(11):1556–1569, 2016.

J. W. Cooley and J. W. Tukey. An algorithm for the machine calculation of complex Fourier series. *Mathematics of Computation*, 19(90):297–301, 1965.

D. Coronelli and P. Gambarova. Structural assessment of corroded reinforced concrete beams: Modeling guidelines. *Journal of Structural Engineering*, 130(8):1214–1224, 2004.

N. A. C. Cressie. *Statistics for spatial data*. Wiley, New York, revised edition, 1993.

A. J. Desbarats. Spatial averaging of transmissivity in heterogeneous fields with flow toward a well. *Water Resources Research*, 28(3):757–767, 1992.

H. E. Desch and J. M. Dinwoodie. *Timber - Structure, properties, conversion and use.* Macmillan, Basingstoke, Hampshire, 7th edition, 1996.

C. A. Desoer and E. S. Kuh. *Basic circuit theory.* McGraw Hill, New York, 1969.

J. Devore. *Probability and statistics for engineering and the sciences.* Brooks Cole, Boston, 8th edition, 2012.

G. Dill-Langer, R. C. Hidalgo, F. Kun, Y. Moreno, S. Aicher, and H. Herrmann. Size dependency of tension strength in natural fiber composites. *Physica A: Statistical Mechanics and its Applications*, 325(3-4):547–560, 2003.

J. L. Doob. *Stochastic processes.* Wiley, New York, classics library edition, 1997.

S. Dreyfus. The numerical solution of variational problems. *Journal of Mathematical Analysis and Applications*, 5(1):30–45, 1962.

I. Elishakoff, Y. Ren, and M. Shinozuka. Some exact solutions for the bending of beams with spatially stochastic stiffness. *International Journal of Solids and Structures*, 32 (16):2315–2327, 1995.

C. A. Felippa. Solution of linear equations with skyline-stored symmetric matrix. *Computer & Structures*, 5(1):13–29, 1975.

G. A. Fenton. *Simulation and analysis of random fields.* PhD thesis, Princeton University, 1990.

G. A. Fenton. Error evaluation of three random field generators. *Journal of Engineering Mechanics*, 120(12):2478–2497, 1994.

G. A. Fenton. Estimation for stochastic soil models. *Journal of Geotechnical and Geoenvironmental engineering*, 125(6):470–485, 1999.

G. A. Fenton and D. V. Griffiths. *Risk assessment in geotechnical engineering.* Wiley, Hoboken, New Jersey, 2008.

G. Fink and J. Kohler. Model for the prediction of the tensile strength and tensile stiffness of knot clusters within structural timber. *European Journal of Wood and Wood Products*, 72(3):331–341, 2014.

R. O. Foschi. A procedure for the determination of localized modulus of elasticity. *Holz als Roh- und Werkstoff*, 45:257–260, 1987.

S. Fuchs, F. Schütz, H.-J. Förster, and A. Förster. Evaluation of common mixing models for calculating bulk thermal conductivity of sedimentary rocks: Correction charts and new conversion equations. *Geothermics*, 47(1):40 – 52, 2013.

J. Füssl, G. Kandler, and J. Eberhardsteiner. Application of stochastic finite element approaches to wood-based products. *Archive of Applied Mechanics*, 86(1-2):89–110, 2016.

D. A. García and M. B. Rosales. Deflections in sawn timber beams with stochastic properties. *European Journal of Wood and Wood Products*, 75(5):683–699, 2017.

B. Gaspar, A. P. Teixeira, and C. G. Soares. Assessment of the efficiency of Kriging surrogate models for structural reliability analysis. *Probabilistic Engineering Mechanics*, 37:24–34, 2014.

I. M. Gelfand and S. V. Fomin. *Calculus of variations*. Prentice Hall, Englewood Cliffs, New Jersey, revised English edition, 1963.

M. Grigoriu. On the spectral representation method in simulation. *Probabilistic Engineering Mechanics*, 8(2):75–90, 1993.

M. Grigoriu. *Applied non-Gaussian processes: Examples, theory, simulation, linear random vibration, and MATLAB solutions*. Prentice Hall, London, 1995.

M. Grigoriu. Material responses at micro- and macro-scales. *Computational Materials Science*, 107:190–203, 2015.

B. Hajek. *Random processes for engineers*. Cambridge University Press, Cambridge, England, 2015.

A. M. Hasofer and N. C. Lind. Exact and invariant second-moment code format. *Journal of the Engineering Mechanics Division*, 100(1):111–121, 1974.

W. K. Hastings. Monte Carlo sampling methods using Markov chains and their applications. *Biometrika*, 57(1):97–109, 1970.

N. J. Higham. Computing the nearest correlation matrix - a problem from finance. *IMA Journal of Numerical Analysis*, 22(3):329–343, 2002.

P. Hoffmeyer. Strength under long-term loading. In S. Thelandersson and H. J. Larsen, editors, *Timber engineering*, chapter 8, pages 131–152. Wiley, Chichester, 2003.

R. V. Hogg, J. M. McKean, and A. T. Craig. *Introduction to mathematical statistics*. Pearson, Boston, Massachusetts, 7th edition, 2013.

R. A. Horn and C. R. Johnson. *Matrix analysis*. Cambridge University Press, Cambridge, second edition, 2013.

J. R. M. Hosking and J. R. Wallis. Parameter and quantile estimation for the generalized pareto distribution. *Technometrics*, 3(29):339–349, 1987.

K. H. Huebner, D. L. Dewhirst, D. E. Smith, and T. G. Byrom. *The finite element method for engineers*. Wiley, New York, 4th edition, 2001.

R. J. Hyndman and A. B. Koehler. Another look at measures of forecast accuracy. *International Journal of Forecasting*, 22(4):679–688, 2006.

T. Isaksson. Structural timber - variability and statistical modelling. In S. Thelandersson and H. J. Larsen, editors, *Timber engineering*, chapter 4, pages 45–66. Wiley, Chichester, 2003.

R. Ishida. Stochastic finite element analysis of beam with statistical uncertainties. *AIAA Journal*, 39(11):2192–2197, 2001.

G. M. Jenkins and D. G. Watts. *Spectral analysis and its applications*. Holden-Day, San Francisco, California, 1968.

R. Jiang and D. N. P. Murthy. A study of weibull shape parameter: Properties and significance. *Reliability Engineering & System Safety*, 96(12):1619–1626, 2011.

C.-J. Johansson. Grading of timber with respect to mechanical properties. In S. Thelandersson and H. J. Larsen, editors, *Timber engineering*, chapter 3, pages 23–43. Wiley, Chichester, 2003.

C.-J. Johansson, L. Böstrom, L. Bräuner, P. Hoffmeyer, C. Holmquist, and K. H. Solli. Laminations for glued laminated timber: establishment of strength classes for visual strength grades and machine settings for glulam laminations of nordic origin: a nordic wood project. *Swedish National Testing and Research Institute*, 1998.

A. G. Journel and C. J. Huijbregts. *Mining geostatistics*. Academic Press, London, 1978.

A. G. Journel, C. Deutsch, and A. J. Desbarats. Power averaging for block effective permeability. In *Proceedings of SPE California Regional Meeting*, Oakland, California, 2nd - 4th April 1986. Society of Petroleum Engineers.

G. Kallianpur. *Stochastic filtering theory.* Springer, New York, 1980.

G. Kandler and J. Füssl. A probabilistic approach for the linear behaviour of glued laminated timber. *Engineering Structures*, 148(1):673–685, 2017.

A. Kefal, A. Tessler, and E. Oterkus. An enhanced inverse finite element method for displacement and stress monitoring of multilayered composite and sandwich structures. *Composite Structures*, 179:514–540, 2017.

P. R. King. The use of field theoretic methods for the study of flow in a heterogeneous porous medium. *Journal of Physics A: Mathematical and General*, 20:3935–3947, 1987.

A. D. Kiureghian and J.-B. Ke. The stochastic finite element method in structural reliability. *Probabilistic Engineering Mechanics*, 3(2), 1988.

D. E. Kline, F. E. Woeste, and B. A. Bendtsen. Stochastic model for modulus of elasticity of lumber. *Wood and Fiber Science*, 18(2):228–238, 1986.

V. K. R. Kodur and M. M. S. Dwaikat. Response of steel beam–columns exposed to fire. *Engineering Structures*, 31(2):369–379, 2009.

J. Köhler and S. Svensson. Probabilistic representation of duration of load effects in timber structures. *Engineering Structures*, 33(2):462–467, 2011.

J. Köhler, J. D. Sørensen, and M. H. Faber. Probabilistic modeling of timber structures. *Structural Safety*, 29(4):255–267, 2007.

A. N. Kolmogrov. Interpolation and extrapolation of stationary random sequences. *Izvestiia Akademii Nauk SSSR Seriia Matematicheskaia*, 5:3–14, 1941.

D. G. Krige. A statistical approach to some basic mine valuation problems on the Witwatersrand. *Journal of the Southern African Institute of Mining and Metallurgy*, 52(9):201–203, 1951.

S. Kukla and A. Owczarek. Stochastic vibration of a Bernoulli-Euler beam under random excitation. *Scientific Research Institute of the Institute of Mathematics and Computer Science*, 4(1):71–78, 2005.

F. Lam, R. O. Foschi, J. D. Barrett, and Q. Y. He. Modified algorithm to determine localized modulus of elasticity of lumber. *Wood Science and Technology*, 27(2):81–94, 1991.

F. Lam, Y.-T. Wang, and J. D. Barrett. Simulation of correlated nonstationary lumber properties. *Journal of Materials in Civil Engineering*, 6(1):34–53, 1994.

G. E. Latta and J. A. Bailie. On the autocorrelation functions of wind generated ocean waves. *Zeitschrift für angewandte Mathematik und Physik ZAMP*, 19(4):575–586, 1968.

T. M. H. Le, D. Gallipoli, M. Sánchez, and S. Wheeler. Stability and failure mass of unsaturated heterogeneous slopes. *Canadian Geotechnical Journal*, 52(11):1747–1761, 2015.

J.-F. Le Gall. *Brownian motion, martingales, and stochastic calculus*. Springer, Berlin, 2013.

M. Lloret-Cabot, G. Fenton, and M. Hicks. On the estimation of scale of fluctuation in geostatistics. *Georisk: Assessment and Management of Risk for Engineered Systems and Geohazards*, 8(2):129–140, 2014.

M. Loève. *Probability theory*, volume II. Springer, New York, 4th edition, 1978.

B. B. Mandelbrot and J. W. Van Ness. Fractional Brownian motions, fractional noises and applications. *SIAM Review*, 10(4):422–437, 1968.

A. Maniatty, N. Zabaras, and K. Stelson. Finite element analysis of some inverse elasticity problems. *Journal of Engineering Mechanics*, 115(6):1303–1317, 1989.

M. Masihi, P. A. Gago, and P. R. King. Estimation of the effective permeability of heterogeneous porous media by using percolation concepts. *Transport in Porous Media*, 114(1):169–199, 2016.

G. Matheron. Composition des perméabilitiés en milieu poreux hétérogène. *Revue de l'institut Francais du pérole et annales des combustibles liquides*, 23(2):201–218, 1968.

G. Matheron. The intrinsic random functions and their applications. *Advances in Applied Probability*, 5(3):439–468, 1973.

W. M. C. McKenzie and B. Zhang. *Design of Structural Timber to Eurocode 5*. Palgrave Macmillan, Basingstoke, England, 2007.

G. Montavon, W. Samek, and K.-R. Müller. Methods for interpreting and understanding deep neural networks. *Digital Signal Processing*, 73(1):1–15, 2018.

D. C. Montegomery, C. L. Jennings, and M. Kulahci. *Introduction to time series analysis and forecasting*. Wiley, Hoboken, New Jersey, 2008.

A. F. Moshtaghin, S. Franke, T. Keller, and A. P. Vassilopoulos. Random field-based modeling of size effect on the longitudinal tensile strength of clear timber. *Structural Safety*, 58:60–68, 2016.

B. Mosley, J. Bungey, and R. Hulse. *Reinforced concrete design to Eurocode 2*. Palgrave Macmillan, Basingstoke, England, 6th edition, 2007.

T. Most and C. Bucher. Probabilistic analysis of concrete cracking using neural networks and random fields. *Probabilistic engineering mechanics*, 22(2):219–229, 2007.

M. Nocetti, L. Brancheriau, M. Bacher, M. Brunetti, and A. Crivellaro. Relationship between local and global modulus of elasticity in bending and its consequence on structural timber grading. *European Journal of Wood and Wood Products*, 71(3):297–308, 2013.

J. Nyström. Automatic measurement of fiber orientation in softwoods by using the tracheid effect. *Computers and Electronics in Agriculture*, 41(1-3):91–99, 2003.

D. S. Oliver. The averaging process in permeability estimation for well-test data. *SPE Formation Evaluation*, 5(3):319–324, 1990.

A. Olsson, J. Oscarsson, E. Serrano, B. Källsner, M. Johansson, and B. Enquist. Prediction of timber bending strength and in-member cross-sectional stiffness variation on the basis of local wood fibre orientation. *European Journal of Wood and Wood Products*, 71(3):319–333, 2013.

M. Opper and D. Saad. *Advanced mean field theories: Theory and practice*. MIT Press, Cambridge, Massachusetts, 2007.

M. Ostoja-Starzewski. Material spatial randomness: From statistical to representative volume element. *Probabilistic Engineering Mechanics*, 21(2):112–132, 2006.

M. Ostoja-Starzewski. *Microstructural randomness and scaling in mechanics of materials*. Taylor & Francis, Boca Raton, Florida, 2008.

M. Ostoja-Starzewski and X. Wang. Stochastic finite elements as a bridge between random material microstructure and global response. *Computer Methods in Applied Mechanics and Engineering*, 168(1-4):35–49, 1999.

C. J. Paciorek. *Nonstationary Gaussian processes for regression and spatial modelling.* Carnegie Mellon University, Pennsylvania, 2003.

A. Papoulis. *The Fourier integral and its applications.* McGraw Hill, New York, 1962.

G. A. Pavliotis and A. M. Stuart. *Multiscale methods: Averaging and homogenization.* Springer, Berlin, 2007.

V. Picheny and D. Ginsbourger. Noisy kriging-based optimization methods: A unified implementation within the diceoptim package. *Computational Statistics and Data Analysis*, 71:1035–1053, 2014.

J. Pierce-Brown, L. C. Neves, and D. L. Brown. Uncertainty quantification for random fields estimated from effective moduli of elasticity. In *8th international workshop on reliable engineering computing: Computing with confidence*, pages 51–62, Liverpool, UK, July 2018.

E. Polizzi and A. H. Sameh. A parallel hybrid banded system solver: the SPIKE algorithm. *Parallel Computing*, 32(2):177–194, 2006.

D. J. Pope and F. W. Matthews. A comparison of deconvolution techniques to improve mor estimation from stress grading machine output. *Wood Science and Technology*, 29(6):431–439, 1995.

J. Porteous and A. Kermani. *Structural timber design to eurocode 5.* Blackwell, Oxford, 2007.

W. H. Press, S. A. Teukolsky, W. T. Vetterling, and B. P. Flannery. *Numerical recipes in Fortran 77.* Cambridge University Press, Cambridge, England, 2nd edition, 1997.

C. E. Rasmussen and C. K. I. Williams. *Gaussian processes for machine learning.* MIT Press, Cambridge, Massachusetts, 2006.

R. Redwood and S. H. Cho. Design of steel and composite beams with web openings. *Journal of Construction Steel Research*, 25(1-2):23–41, 1993.

H. Riberholt and P. H. Madsen. Strength distribution of timber structures - Measured variation of the cross sectional strength of structural lumber. Technical Report 114, Structural Research Laboratory - Technical University of Denmark, 1979.

S. O. Rice. Mathematical analysis of random noise. *Bell System Technical Journal*, 23 (3):282–332, 1944.

D. Ridley-Ellis, J. Moore, and A. Khokhar. Random acts of elasticity: MoE, G and EN408. *Wood EDG Conference 23rd April 2009 in Bled, Slovenia*, 2009.

C. Robert. Generalized inverse normal distributions. *Statistics & Probability Letters*, 11 (1):37–41, 1991.

C. P. Robert and G. Casella. *Monte Carlo statistical methods*. Springer, New York, 2nd edition, 2004.

G. O. Roberts and J. S. Rosenthal. Optimal scaling for various Metropolis-Hastings algorithms. *Statistical Science*, 16(4):351–367, 2001.

J. Sacks, W. J. Welch, T. J. Mitchell, and H. P. Wynn. Design and analysis of computer experiments. *Statistical Science*, 82(13-14):1113–1121, 2004.

P. Sasikumar, R. Suresh, and S. Gupta. Stochastic finite element analysis of layered composite beams with spatially varying non-Gaussian inhomogeneities. *Acta Mechanica*, 225(6):1503–1522, 2014.

E. M. Scheuer and D. S. Stoller. On the generation of normal random vectors. *Technometrics*, 4(2):278–281, 1962.

A. P. Schniewind and D. E. Lyon. Tensile strength of redwood dimension lumber. II. Prediction of strength values. *Forest Products Journal*, 21(8):45–55, 1971.

L. F. Shampine. Vectorized adaptive quadrature in MATLAB. *Journal of Computational and Applied Mathematics*, 211(2):131–140, 2008.

L. Shen, M. Ostoja-Starzewski, and E. Porcu. Bernoulli–Euler beams with random field properties under random field loads: fractal and Hurst effects. *Archive of Applied Mechanics*, 84(9-11):1595–1626, 2014.

M. D. Shields, C. Deodatis, and P. Bocchini. A simple and efficient methodology to approximate a general non-Gaussian stationary stochastic process by a translation process. *Probabilistic Engineering Mechanics*, 26(4):511–519, 2011.

M. Shinozuka and G. Deodatis. Simulation of multidimensional Gaussian stochastic fields by spectral representation. *Applied Mechanics Review*, 49(1):29–53, 1996.

M. Shinozuka and C.-M. Jan. Digital simulation of random processes and its applications. *Journal of Sound and Vibration*, 25(1):111–128, 1972.

K. H. Solli. Modulus of elasticity - local or global values. In *Proceedings of the 6th world conference on timber engineering*, Whistler, Canada, 31st July - 3rd August 2000.

H. S. Sousa, J. M. Branco, and P. B. Lourenço. Prediction of global bending stiffness of timber beams by local sampling data and visual inspection. *European Journal of Wood and Wood Products*, 72(4):453–461, 2014.

H. S. Sousa, J. M. Branco, and P. B. Lourenço. Use of bending tests and visual inspection for multi-scale experimental evaluation of chestnut timber beams stiffness. *Journal of Civil Engineering and Management*, 22(6):728–738, 2016.

P. D. Spanos and R. Ghanem. Stochastic finite element expansion for random media. *Journal of Engineering Mechanics*, 115(5):1035–1053, 1989.

G. Stefanou. The stochastic finite element method: Past, present and future. *Computer Methods in Applied Mechanics and Engineering*, 198(9-12):1031–1051, 2009.

M. L. Stein. *Interpolation of spatial data - some theory for Kriging*. Springer, New York, 1999.

M. G. Stewart. Mechanical behaviour of pitting corrosion of flexural and shear reinforcement and its effect on structural reliability of corroding RC beams. *Structural Safety*, 31(1):19–30, 2009.

O. Straka, J. Duník, M. Šimandl, and J. Havlík. Aspects and comparison of matrix decompositions in unscented Kalman filter. In *2013 American Control Conference*, pages 3075–3080, Washing, DC, USA, June 2013. IEEE.

B. Sudret. Meta-models for structural reliability and uncertainty quantification. In *Asian-Pacific symposium on structural reliability and its applications*, pages 1–24, Singapore, 23rd - 25th May 2012.

B. Sudret and A. D. Kiureghian. Stochastic finite element methods and reliability: A state-of-the-art report. 2000.

J. L. Synge and B. A. Griffith. *Principles of mechanics*. McGraw-Hill, New York, 2nd edition, 1949.

K. Y. Sze, X. H. Liu, and S. H. Lo. Popular benchmark problems for geometric nonlinear analysis of shells. *Finite elements in analysis and design*, 40(11):1551–1569, 2004.

S. E. Taylor and D. A. Bender. Stochastic model for localized tensile strength and modulus of elasticity in lumber. *Wood and Fiber Science*, 1991.

J. S. Temenoff and A. G. Mikos. *Biomaterials: The intersection of biology and material science*. Pearson Prentice Hall, 2008.

S. Thelandersson. Introduction: Wood as a construction material. In S. Thelandersson and H. J. Larsen, editors, *Timber engineering*, chapter 2, pages 15–22. Wiley, Chichester, 2003.

S. Torquato. *Random heterogeneous materials - microstructure and macroscopic properties*. Springer, New York, 2002.

G. E. Uhlenbeck and L. S. Ornstein. On the theory of the Brownian motion. *Physical review*, 36(5):823–841, 1930.

E. Vanmarcke. *Random fields: Analysis and synthesis*. MIT Press, Cambridge, Massachusetts, 3rd edition, 1988.

E. Vanmarcke. *Random Fields: Analysis and Synthesis*. The MIT Press, 2015.

E. Vanmarcke and M. Grigoriu. Stochastic finite element analysis of simple beams. *Journal of Engineering Mechanics*, 109(5):1203–1214, 1983.

G. G. Wang and S. Shan. Review of metamodeling techniques in support of engineering design optimization. *Journal of Mechanical Design*, 129(4):370–380, 2007.

Y. T. Wang and R. O. Foschi. Random field stiffness properties and reliability of laminated wood beams. *Structural Safety*, 11(3-4):191–202, 1992.

W. Weibull. The phenomenon of rupture in solids. In *Proceedings of the Royal Swedish Institute*, number 151, Stockholm, 1939.

R. Wicklin. Compute the log-determinant of a matrix. `https://blogs.sas.com/content/iml/2012/10/31/compute-the-log-determinant-of-a-matrix.html`, 2012. Accessed: 09-08-2018.

N. Wiener. Differential-space. *Journal of Mathematics and Physics*, 2(1-4):131–174, 1923.

N. Wiener. *Extrapolation, interpolation, and smoothing of stationary time series with engineering applications*. MIT Press, Cambridge, Massachusetts, 1st paperback edition, 1964.

X. Wua, T. Kozlowskia, H. Meidanib, and K. Shirvan. Inverse uncertainty quantification using the modular Bayesian approach based on Gaussian process, Part 1: Theory. *Nuclear Engineering and Design*, 335:417–431, 2018.

J. Xavier, S. Avril, F. Pierron, and J. Morais. Novel experimental approach for longitudinal-radial stiffness characterisation of clear wood by a single test. *Holzforschung*, 61(5):573–581, 2007.

J. Xavier, M. Oliveira, J. Morais, and T. Pinto. Measurement of the shear properties of clear wood by the arcan test. *Holzforschung*, 63(2):217–225, 2009.

D.-F. Xia, S.-L. Xu, and F. Qi. A proof of the arithmetic mean-geometric mean-harmonic mean inequalities. *RGMIA Research Report Collection*, 2(1):85–87, 1999.

A. M. Yaglom. *An introduction to the theory of stationary random functions*. Dover, Mineola, New York, revised English edition, 1962.

J. Zhang and B. Ellingwood. Orthogonal series expansions of random fields in reliability analysis. *Journal of Engineering Mechanics*, 120(12):2660–2677, 1994.

J. Zhu, A. Kudo, T. Takeda, and M. Tokumoto. Methods to estimate the length effect on tensile strength parallel to the grain in Japanese larch. *Journal of Wood Science*, 47(4):269–274, 2001.

O. C. Zienkiewicz and R. L. Taylor. *The finite element method for soil and structural mechanics*. Elsevier, Oxford, 6th edition, 2005.

Appendices

Appendix A

Calculations for Chapter 2

A.1 Constant of the power correlation function

The power correlation function is given by:

$$\rho_P(s) = \exp\left(-C\left(\frac{|s|}{\theta}\right)^{\lambda}\right) \quad \text{if } C, \lambda, \theta > 0 \tag{A.1}$$

It is of interest to derive an expression for the constant C. If the correlation length θ is to satisfy the definition provided by Vanmarcke (1988) then the following requirement must be met:

$$2\int_0^{\infty} \rho_P(s)\,\mathrm{d}s = \theta \tag{A.2}$$

$$2\int_0^{\infty} \exp\left(-C\left(\frac{|s|}{\theta}\right)^{\lambda}\right)\,\mathrm{d}s = \theta \tag{A.3}$$

The following identity relating the integral of the exponential function to the Gamma function $\Gamma(.)$ is used to evaluate this integral:

$$\int_0^{\infty} t^u e^{-t}\,\mathrm{d}t = \Gamma(1+u) \tag{A.4}$$

Making use of the following substitutions:

$$t = C\left(\frac{s}{\theta}\right)^{\lambda} \tag{A.5}$$

$$u = \theta\left(\frac{x}{C}\right)^{\lambda^{-1}} \tag{A.6}$$

$$\mathrm{d}s = \frac{\theta}{\lambda C^{\lambda^{-1}}} t^{\lambda^{-1}-1} \tag{A.7}$$

The integral of the exponential function is then given by:

$$\int_0^{\infty} \exp\left(-C\left(\frac{|s|}{\theta}\right)^{\lambda}\right) \mathrm{d}s = C^{-\lambda^{-1}}\theta\Gamma(1+\lambda^{-1}) \tag{A.8}$$

Substituting this result into Equation A.3 and manipulating yields the desired expression for the constant C:

$$2C^{-\lambda^{-1}}\theta\Gamma(1+\lambda^{-1}) = \theta \tag{A.9}$$

$$C^{-\lambda^{-1}} = \frac{1}{2\Gamma(1+\lambda^{-1})} \tag{A.10}$$

$$C = \left(\frac{1}{2\Gamma\left(1+\lambda^{-1}\right)}\right)^{-\lambda} \tag{A.11}$$

A.2 Spectral representations for FFT

This section contains the derivation of the computational forms, suitable for the fast Fourier transform (FFT) algorithm, of the 1D and 2D spectral representations of a random field. It is noted that these manipulations are based on Euler's formula:

$$e^{ix} = \cos x + i \sin x \tag{A.12}$$

$$\mathrm{Re}\left\{e^{ix}\right\} = \cos x \tag{A.13}$$

where Re{.} is the real part operator.

The manipulation of a random process $Z(x)$ with the random phase angle representation into a form suitable for the FFT algorithm is given by:

$$Z(x_j) = \sum_{m=0}^{M-1} C_m \cos(f_m x_j + \phi_m) \tag{A.14}$$

$$= \mathrm{Re}\left\{ \sum_{m=0}^{M-1} C_m e^{i f_m x_j} \right\} \tag{A.15}$$

The manipulation of a random process $Z(x)$ with the random amplitude representation into a form suitable for the FFT algorithm is given by:

$$Z(x_j) = \sum_{m=0}^{M-1} \left(A_m \cos(f_m x_j) + B_m \sin(f_m x_j) \right) \tag{A.16}$$

$$= \mathrm{Re}\left\{ \sum_{m=0}^{M-1} (A_m - iB_m)(\cos(f_m x_j) + i \sin(f_m x_j) \right\} \tag{A.17}$$

$$= \mathrm{Re}\left\{ \sum_{m=0}^{M-1} (A_m - iB_m) e^{i f_m x_j} \right\} \tag{A.18}$$

The manipulation of a random field $Z(x, y)$ with the random amplitude representation into a form suitable for the FFT algorithm is given by:

$$Z(x_j, y_k) = \sum_{n=0}^{N-1} \sum_{m=0}^{M-1} \left(A_{m,n} \cos(f_m x_j + f_n y_k) + B_{m,n} \cos(f_m x_j + f_n y_k) \right) \tag{A.19}$$

$$= \mathrm{Re}\left\{ \sum_{n=0}^{N-1} \sum_{m=0}^{M-1} (A_{m,n} - iB_{m,n}) e^{i(f_m x_j + f_n y_k)} \right\} \tag{A.20}$$

$$= \mathrm{Re}\left\{ \sum_{n=0}^{N-1} \sum_{m=0}^{M-1} (A_{m,n} - iB_{m,n}) e^{i f_m x_j} e^{i f_n y_k} \right\} \tag{A.21}$$

$$= \mathrm{Re}\left\{ \sum_{n=0}^{N-1} e^{i f_n y_k} \sum_{m=0}^{M-1} (A_{m,n} - iB_{m,n}) e^{i f_m x_j} \right\} \tag{A.22}$$

A.3 Statistical properties of CMD

The covariance matrix decomposition (CMD) method decomposes the random vector $\boldsymbol{Z}$ according to $\boldsymbol{Z} = \mu + \sigma \boldsymbol{\psi} \boldsymbol{\xi}$. The expected value of $\boldsymbol{Z}$ can be shown to be given by μ as follows:

$$\mathbb{E}\left[\boldsymbol{Z}\right] = \mathbb{E}\left[\mu + \sigma\boldsymbol{\psi}\boldsymbol{\xi}\right] \tag{A.23}$$

$$= \mathbb{E}\left[\mu\right] + \mathbb{E}\left[\sigma\boldsymbol{\psi}\boldsymbol{\xi}\right] \tag{A.24}$$

$$= \mathbb{E}\left[\mu\right] + \sigma\boldsymbol{\psi}\mathbb{E}\left[\boldsymbol{\xi}\right] \tag{A.25}$$

$$= \mu \tag{A.26}$$

The covariance of $\boldsymbol{Z}$ can be shown to be given by $\boldsymbol{\Sigma}$ as follows:

$$\mathbb{E}[(\boldsymbol{Z} - \mu)(\boldsymbol{Z}^T - \mu)]] = \mathbb{E}[(\sigma\boldsymbol{\psi}\boldsymbol{\xi})(\sigma\boldsymbol{\psi}\boldsymbol{\xi})^T] \tag{A.27}$$

$$= \mathbb{E}[\sigma^2\boldsymbol{\psi}\boldsymbol{\xi}\boldsymbol{\xi}^\intercal\boldsymbol{\psi}^\intercal] \tag{A.28}$$

$$= \sigma^2\boldsymbol{\psi}\mathbb{E}[\boldsymbol{\xi}\boldsymbol{\xi}^\intercal]\boldsymbol{\psi} \tag{A.29}$$

Noting that since $\boldsymbol{\psi}$ is a column vector of independent mean-zero unit variance normal random variables then $\mathbb{E}[\boldsymbol{\xi}\boldsymbol{\xi}^\intercal] = \boldsymbol{I}$ where $\boldsymbol{I}$ is the identity matrix and thus:

$$\mathbb{E}[(\boldsymbol{Z} - \mu)(\boldsymbol{Z}^T - \mu)]] = \sigma^2\boldsymbol{\psi}\boldsymbol{I}\boldsymbol{\psi}^\intercal \tag{A.30}$$

$$= \sigma^2\boldsymbol{\rho} \tag{A.31}$$

$$= \boldsymbol{\Sigma} \tag{A.32}$$

Appendix B

Calculations for Chapter 3

B.1 Interchange of the order of integration

An interchange in the order of integration is useful to reduce multiple integrals into a simpler integral. The displacement of a simply supported beam is given by the following double integral:

$$U(x) = \frac{1}{I}\int_{0=u}^{x=u}\int_{0=v}^{u=v}\frac{M(v)}{E(v)}\,\mathrm{d}v\,\mathrm{d}u - \frac{x}{LI}\int_{0=u}^{L=u}\int_{0=v}^{u=v}\frac{M(v)}{E(v)}\,\mathrm{d}v\,\mathrm{d}u \tag{B.1}$$

Figure B.1 illustrates the domains of integration for the first term of Equation B.1. The domains of integration of the second term are identical except that the upper limits are given by $u = L$ and $v = L$ instead of $u = x$ and $v = x$ respectively.

Through the use of Fubini's theorem, the order of integration can be changed in the iterated integral such that:

$$U(x) = \frac{1}{I}\int_{0=v}^{x=v}\int_{v=u}^{x=u}\frac{M(v)}{E(v)}\,\mathrm{d}u\,\mathrm{d}v - \frac{x}{LI}\int_{0=v}^{L=v}\int_{v=u}^{L=u}\frac{M(v)}{E(v)}\,\mathrm{d}u\,\mathrm{d}v \tag{B.2}$$

Figure B.2 illustrates the exchanged domains of integration for the first-term of Equation B.2. Similarly, the domains of integration of the second term are identical except that the upper limits are given by $u = L$ and $v = L$ instead of $u = x$ and $v = x$ respectively.

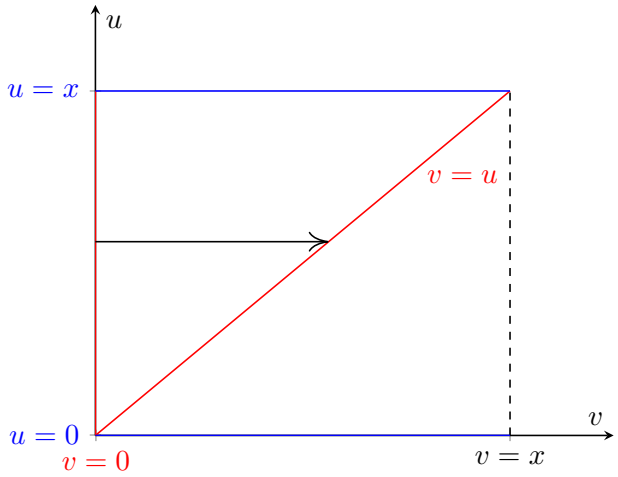


Figure B.1: Domain of integration for the first-term of Equation B.1.

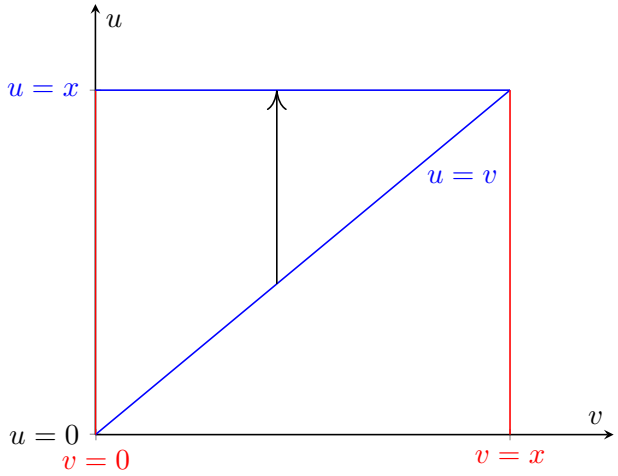


Figure B.2: Domain of integration for the first-term of Equation B.2.

The double integral is then reduced to a single integral through the following evaluation of the inner integral of both the first and second term:

$$U(x) = \frac{1}{I}\int_0^x \frac{M(v)}{E(v)} \int_v^x \mathrm{d}u\,\mathrm{d}v - \frac{x}{LI}\int_0^L \frac{M(v)}{E(v)} \int_v^L \mathrm{d}u\,\mathrm{d}v \tag{B.3}$$

$$= \frac{1}{I}\int_0^x \frac{M(v)(x-v)}{E(v)}\,\mathrm{d}v - \frac{x}{LI}\int_0^L \frac{M(v)(L-v)}{E(v)}\,\mathrm{d}v \tag{B.4}$$

B.2 Equation of deflection for three-point loading

Substituting the 3-point bending moment $M_3(v)$ given by Equation 3.11 into the equation for the displacement of a simply supported beam given by Equation 3.10 and assuming

the location of displacement x is in the second half of the beam $L/2 \leq x \leq L$ gives:

$$U(x) = \frac{P}{2I}\Bigg(\int_0^{L/2} -\frac{v(x-v)}{E(v)}\,\mathrm{d}v + \int_{L/2}^{x} -\frac{(L-v)(x-v)}{E(v)}\,\mathrm{d}v \\ - \frac{x}{L}\left[\int_0^{L/2} -\frac{v(L-v)}{E(v)}\,\mathrm{d}v + \int_{L/2}^{L} -\frac{(L-v)^2}{E(v)}\,\mathrm{d}v\right]\Bigg) \tag{B.5}$$

Expanding the brackets gives:

$$U(x) = \frac{P}{2I}\Bigg(\int_0^{L/2} -\frac{v(x-v)}{E(v)}\,\mathrm{d}v + \int_{L/2}^{x} -\frac{(L-v)(x-v)}{E(v)}\,\mathrm{d}v \\ + \int_0^{L/2} \frac{xv(L-v)}{LE(v)}\,\mathrm{d}v + \int_{L/2}^{L} \frac{x(L-v)^2}{LE(v)}\,\mathrm{d}v\Bigg) \tag{B.6}$$

Splitting the domain of integration of the fourth term in agreement with the domains of integration of the second term and ensuring all terms have a common denominator of $LE(v)$ gives:

$$U(x) = \frac{P}{2LI}\Bigg(\int_0^{L/2} -\frac{Lv(x-v)}{LE(v)}\,\mathrm{d}v - \int_{L/2}^{x} \frac{L(L-v)(x-v)}{LE(v)}\,\mathrm{d}v + \int_0^{L/2} \frac{xv(L-v)}{LE(v)}\,\mathrm{d}v \\ + \int_{L/2}^{x} \frac{x(L-v)^2}{LE(v)}\,\mathrm{d}v + \int_{x}^{L} \frac{x(L-v)^2}{LE(v)}\,\mathrm{d}v\Bigg) \tag{B.7}$$

Noting that $xv(L-v) - Lv(x-v) = v^2(L-x)$ and $x(L-v)^2 - L(L-v)(x-v) = v(L-v)(L-x)$ and combining terms with the same domains of integration in the second half of the beam $L/2 \leq x \leq L$ gives the desired expression for displacement $U(x)$:

$$U(x) = \frac{P}{2LI}\left(\int_0^{L/2} \frac{v^2(L-x)}{E(v)}\,\mathrm{d}v + \int_{L/2}^{x} \frac{v(L-v)(L-x)}{E(v)}\,\mathrm{d}v + \int_{x}^{L} \frac{x(L-v)^2}{E(v)}\,\mathrm{d}v\right) \tag{B.8}$$

B.3 Weighting function for uniformly distributed loading

Substitution the equation for the bending moment resulting from uniformly distributed loading of magnitude ψ, given by Equation 3.22, into the equation for the deflection of a simply supported beam, given by Equation 3.10, gives:

$$U(x) = \frac{1}{I}\int_0^x \frac{\psi v(L-v)(x-v)}{2E(v)}\,\mathrm{d}v - \frac{x}{LI}\int_0^L \frac{\psi v(L-v)^2}{2E(v)}\,\mathrm{d}v \tag{B.9}$$

Spitting the domain of integration of the second term in agreement with the domain of integration of the first term and factoring out ψ/I gives:

$$U(x) = \frac{\psi}{I}\left[\int_0^x \frac{v(L-v)(x-v)}{2E(v)}\,\mathrm{d}v - \frac{x}{L}\int_0^x \frac{v(L-v)^2}{2E(v)}\,\mathrm{d}v - \frac{x}{L}\int_x^L \frac{v(L-v)^2}{2E(v)}\,\mathrm{d}v\right] \tag{B.10}$$

$$= \frac{\psi}{I}\left[\int_0^x \frac{vL(L-v)(x-v)}{2LE(v)}\,\mathrm{d}v - \int_0^x \frac{xv(L-v)^2}{2LE(v)}\,\mathrm{d}v - \int_x^L \frac{xv(L-v)^2}{2LE(v)}\,\mathrm{d}v\right] \tag{B.11}$$

Noting that $vL(L-v)(x-v) - xv(L-v)^2 = -v^2(L-v)(L-x)$ and combining terms with the same domains of integration gives:

$$U(x) = \frac{\psi}{I}\left[-\int_0^x \frac{v^2(L-v)(L-x)}{2LE(v)}\,\mathrm{d}v - \frac{x}{L}\int_x^L \frac{v(L-v)^2}{2E(v)}\,\mathrm{d}v\right] \tag{B.12}$$

Under the assumption that the beam is homogeneous with constant modulus of elasticity $E_0^*(x)$, the displacement $U(x)$ is given by:

$$U(x) = \frac{\psi x(L^3 - 2Lx^2 + x^3)}{24E_0^*(x)I} \tag{B.13}$$

An equation for the effective property $E_0^*(x)$ is obtained in terms of displacement $U(x)$ by changing the subject of the equation:

$$E_0^*(x) = \frac{\psi x(L^3 - 2Lx^2 + x^3)}{24U(x)I} \tag{B.14}$$

Substituting the equation for deflection $U(x)$ into this equation gives:

$$E_0^*(x) = \frac{x\left(L^3 - 2Lx^2 + x^3\right)}{24\left[\int_0^x \frac{v^2(L-v)(L-x)}{2LE(v)}\,\mathrm{d}v - \int_x^L \frac{xv(L-v)^2}{2LE(v)}\,\mathrm{d}v\right]} \tag{B.15}$$

The effective property $E_0^*(x)$ for a simply supported beam under uniformly distributed loading is then expressed as a weighted harmonic mean:

$$E_0^*(x) = \left(\int_0^L \omega_0(v|x) \cdot E(v)^{-1}\,\mathrm{d}v\right)^{-1} \tag{B.16}$$

where the weighting function $\omega_0(v|x)$ is given by:

$$\omega_0(v|x) = \begin{cases} \dfrac{12(L-v)v^2}{Lx(L^2 + Lx - x^2)} & \text{if } 0 \le x \le v \\ \dfrac{12(L-v)^2 v}{L(L-x)(L^2 + Lx - x^2)} & \text{if } v \le x \le L \end{cases} \tag{B.17}$$

B.4 Weighting function for four-point loading

An expression for midspan deflection U of a simply supported beam is obtained by substituting $x = L/2$ into Equation 3.10:

$$U(L/2) = \frac{1}{I}\int_0^{L/2} \frac{M(v)(L/2 - v)}{E(v)}\,\mathrm{d}v - \frac{1}{2I}\int_0^L \frac{M(v)(L-v)}{E(v)}\,\mathrm{d}v \tag{B.18}$$

Substituting the expression for the bending moment $M_4(v)$, given by Equation 3.26, into the expression for the midspan displacement, given by Equation B.18, gives:

$$\begin{aligned} U_4 = \frac{P}{I}\Bigg[&- \int_0^{L/3} \frac{2v(L/2 - v)}{4E(v)}\,\mathrm{d}v - \int_{L/3}^{L/2} \frac{2L(L/2 - v)}{12E(v)}\,\mathrm{d}v \\ &+ \int_0^{L/3} \frac{v(L-v)}{4E(v)}\,\mathrm{d}v + \int_{L/3}^{2L/3} \frac{L(L-v)}{12E(v)}\,\mathrm{d}v + \int_{2L/3}^{L} \frac{(L-v)^2}{4E(v)}\,\mathrm{d}v\Bigg] \end{aligned} \tag{B.19}$$

Combining terms with similar domains of integration and simplifying gives:

$$U_4 = \frac{P}{I}\Bigg[\int_0^{L/3} \frac{v^2}{4E(v)}\,\mathrm{d}v + \int_{L/3}^{L/2} \frac{Lv}{12E(v)}\,\mathrm{d}v + \int_{L/2}^{2L/3} \frac{L(L-v)}{12E(v)}\,\mathrm{d}v + \int_{2L/3}^{L} \frac{(L-v)^2}{4E(v)}\,\mathrm{d}v\Bigg] \tag{B.20}$$

Under the assumption that the beam is homogeneous with constant modulus of elasticity E_4^*, the midspan displacement is given by:

$$U_4 = \frac{23L^3P}{648IE_4^*} \tag{B.21}$$

An equation for the effective property E_4^* is obtained in terms of midspan displacement U_4 by changing the subject of Equation B.21:

$$E_4^* = \frac{23L^3P}{648IU_4} \tag{B.22}$$

Substituting the equation for displacement given by Equation B.20 into the expression for the effective property given by Equation B.22 yields:

$$E_4^* = \frac{23L^3}{648\left(\displaystyle\int_0^{L/3} \frac{v^2}{4E(v)}\,\mathrm{d}v + \int_{L/3}^{L/2} \frac{Lv}{12E(v)}\,\mathrm{d}v + \int_{L/2}^{2L/3} \frac{L(L-v)}{12E(v)}\,\mathrm{d}v + \int_{2L/3}^{L} \frac{(L-v)^2}{4E(v)}\,\mathrm{d}v\right)} \tag{B.23}$$

The effective elastic modulus E_4^* for four-point bending is then expressed as a weighted harmonic mean:

$$E_4^* = \left(\int_0^L \omega_4(v) \cdot E(v)^{-1}\,\mathrm{d}v\right)^{-1} \tag{B.24}$$

where the weighting function $\omega_4(v)$ is given by:

$$\omega_4(v) = \begin{cases} \dfrac{324v^2}{23L^3} & \text{if } 0 \leq v \leq \dfrac{L}{3} \\ \dfrac{108v}{23L^2} & \text{if } \dfrac{L}{3} \leq v \leq \dfrac{L}{2} \\ \dfrac{108(L-v)}{23L^2} & \text{if } \dfrac{L}{2} \leq v \leq \dfrac{2L}{3} \\ \dfrac{324(L-v)^2}{23L^3} & \text{if } \dfrac{2L}{3} \leq v \leq L \end{cases} \tag{B.25}$$

B.5 Moments of the reciprocal of a lognormal random variable

Let X be lognormally distributed random variable $X \sim \ln\mathcal{N}(\mu_N, \sigma_N^2)$ with expected value given by $\mu = \mathbb{E}[X]$ and variance given by $\sigma^2 = \mathrm{Var}[X]$. The mean μ_N and variance σ_N^2 of the underlying normal distribution are given by:

$$\mu_N = \ln\left(\frac{\mu}{\sqrt{1+\frac{\sigma^2}{\mu^2}}}\right) \tag{B.26}$$

$$\sigma_N^2 = \ln\left(1+\frac{\sigma^2}{\mu^2}\right) \tag{B.27}$$

Let Y be lognormally distributed given by the reciprocal of X:

$$Y = \frac{1}{X} \sim \ln\mathcal{N}(-\mu_N, \sigma_N^2) \tag{B.28}$$

with expected value given by:

$$\mu_Y = \mathbb{E}[Y] = \exp\left(-\mu_N + \frac{\sigma_N^2}{2}\right) \tag{B.29}$$

and variance given by:

$$\sigma_Y^2 = \mathrm{Var}[Y] = \left(\exp(\sigma_N^2) - 1\right)\exp(-2\mu_N + \sigma_N^2) \tag{B.30}$$

An expression for the expected value of the reciprocal random variable Y can be obtained in terms of μ and σ by substituting Equations B.26 and B.27 into Equation B.29:

$$\mu_Y = \exp\left(-\ln\left(\frac{\mu}{\sqrt{1+\frac{\sigma^2}{\mu^2}}}\right) + \frac{\ln\left(1+\frac{\sigma^2}{\mu^2}\right)}{2}\right) \tag{B.31}$$

$$= \exp\left(\ln\left(\frac{\sqrt{1+\frac{\sigma^2}{\mu^2}}}{\mu}\right) + \ln\left(\sqrt{1+\frac{\sigma^2}{\mu^2}}\right)\right) \tag{B.32}$$

$$= \exp\left(\ln\left(\frac{1+\frac{\sigma^2}{\mu^2}}{\mu}\right)\right) \tag{B.33}$$

$$= \frac{\mu^2+\sigma^2}{\mu^3} \tag{B.34}$$

Similarly, an equation for the variance of the reciprocal random variable Y can be obtained by substituting Equations B.26 and B.27 into Equation B.30:

$$\sigma_Y^2 = \left[\exp\left(\ln\left(1+\frac{\sigma^2}{\mu^2}\right)\right) - 1\right]\exp\left(-2\ln\left(\frac{\mu}{\sqrt{1+\frac{\sigma^2}{\mu^2}}}\right) + \ln\left(1+\frac{\sigma^2}{\mu^2}\right)\right) \tag{B.35}$$

$$= \frac{\sigma^2}{\mu^2}\exp\left(\ln\left(\frac{1+\frac{\sigma^2}{\mu^2}}{\mu^2}\right) + \ln\left(1+\frac{\sigma^2}{\mu^2}\right)\right) \tag{B.36}$$

$$= \frac{\sigma^2}{\mu^2}\exp\left(\ln\left(\frac{1+2\frac{\sigma^2}{\mu^2}+\frac{\sigma^4}{\mu^4}}{\mu^2}\right)\right) \tag{B.37}$$

$$= \frac{\sigma^2}{\mu^2}\left(\frac{\mu^4+2\sigma^2\mu^2+\sigma^4}{\mu^6}\right) \tag{B.38}$$

$$= \frac{\sigma^2\left(\mu^2+\sigma^2\right)^2}{\mu^8} \tag{B.39}$$

Appendix C

Calculations for Chapter 5

C.1 Weighting function for the global modulus of elasticity

Figure C.1 illustrates the experimental setup for the determination of local and global effective properties according to BS EN 408:2010. The calculation of the global effective property E_g^* is based solely on midspan displacement $U(x_c)$ whilst the local effective property E_l^* is calculated based on the local midspan displacement U_l which is given by the magnitude of midspan displacement $U(x_c)$ relative to the displacements either side of the displacement gauge namely $U(x_l)$ and $U(x_r)$.

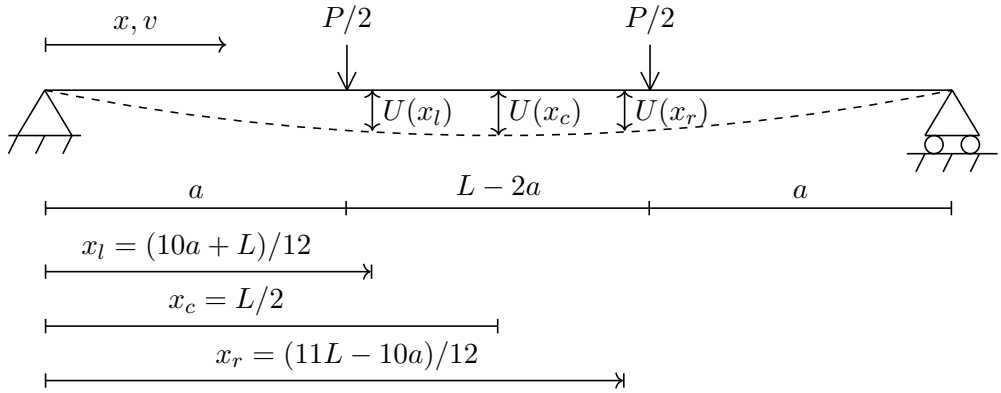


Figure C.1: Locations of displacement for the calculation of the local E_l^* and global E_g^* effective elastic moduli.

The internal bending moment for four-point loading as shown in Figure C.1 is given by:

$$M_4(v) = \begin{cases} -\dfrac{Pv}{2} & \text{if } 0 \le v \le a \\ -\dfrac{Pa}{2} & \text{if } a \le v \le L-a \\ -\dfrac{P(L-v)}{2} & \text{if } L-a \le v \le L \end{cases} \tag{C.1}$$

Substituting the 4-point bending moment $M_4(v)$ given by Equation C.1 into the equation for the displacement of a simply supported beam given by Equation 3.10 and taking the location of displacement to be in the middle sector of the beam $a \le x \le L-a$ gives:

$$\begin{aligned} U_4(x) = \frac{1}{I}\Bigg[&- \int_0^a \frac{Pv(x-v)}{2E(v)}\,\mathrm{d}v - \int_a^x \frac{Pa(x-v)}{2E(v)}\,\mathrm{d}v \\ &+ \frac{x}{L}\left(\int_0^a \frac{Pv(L-v)}{2E(v)}\,\mathrm{d}v + \int_a^{L-a} \frac{Pa(L-v)}{2E(v)}\,\mathrm{d}v + \int_{L-a}^{L} \frac{P(L-v)^2}{2E(v)}\,\mathrm{d}v \right) \Bigg] \end{aligned} \tag{C.2}$$

Expanding the bracket, factoring out P and making the denominators of all the terms equal to $2LE(v)$ gives:

$$\begin{aligned} U_4(x) = \frac{P}{I}\Bigg[&- \int_0^a \frac{vL(x-v)}{2LE(v)}\,\mathrm{d}v - \int_a^x \frac{aL(x-v)}{2LE(v)}\,\mathrm{d}v + \int_0^a \frac{xv(L-v)}{2LE(v)}\,\mathrm{d}v \\ &+ \int_a^{L-a} \frac{ax(L-v)}{2LE(v)}\,\mathrm{d}v + \int_{L-a}^{L} \frac{x(L-v)^2}{2LE(v)}\,\mathrm{d}v \Bigg] \end{aligned} \tag{C.3}$$

Noting that $xv(L-v) - vL(x-v) = v^2(L-x)$ and combing the first and third term which have the same domains of integration yields:

$$\begin{aligned} U_4(x) = \frac{P}{I}\Bigg[&\int_0^a \frac{v^2(L-x)}{2LE(v)}\,\mathrm{d}v + \int_a^x \frac{av(L-x)}{2LE(v)}\,\mathrm{d}v \\ &+ \int_x^{L-a} \frac{ax(L-v)}{2LE(v)}\,\mathrm{d}v + \int_{L-a}^{L} \frac{x(L-v)^2}{2LE(v)}\,\mathrm{d}v \Bigg] \end{aligned} \tag{C.4}$$

An expression for midspan displacement $U_4(x_c)$ is obtained by substituting $x = x_c = L/2$ into Equation C.4 as follows:

$$U_4(x_c) = \frac{P}{I}\Bigg[\int_0^a \frac{v^2}{4E(v)}\,\mathrm{d}v + \int_a^{L/2} \frac{av}{4E(v)}\,\mathrm{d}v + \int_{L/2}^{L-a} \frac{a(L-v)}{4E(v)}\,\mathrm{d}v + \int_{L-a}^{L} \frac{(L-v)^2}{4E(v)}\,\mathrm{d}v\Bigg] \tag{C.5}$$

In the case of a homogeneous beam with constant modulus of elasticity E_g^* then midspan displacement is given by:

$$U_4(x_c) = \frac{Pa(3L^2 - 4a^2)}{48E_{\mathrm{g}}^* I} \tag{C.6}$$

An expression for the global effective property E_g^* is obtained by rearranging the subject of the equation:

$$E_{\mathrm{g}}^* = \frac{Pa(3L^2 - 4a^2)}{48U_4(x_c)I} \tag{C.7}$$

Substituting the expression for midspan displacement $U_4(x_c)$ given by Equation C.5 into the expression for the effective property E_g^* given by C.7 gives:

$$E_{\mathrm{g}}^* = \frac{a(3L^2 - 4a^2)}{48\left(\int_0^a \frac{v^2}{4E(v)}\,\mathrm{d}v + \int_a^{L/2} \frac{av}{4E(v)}\,\mathrm{d}v + \int_{L/2}^{L-a} \frac{a(L-v)}{4E(v)}\,\mathrm{d}v + \int_{L-a}^{L} \frac{(L-v)^2}{4E(v)}\,\mathrm{d}v\right)} \tag{C.8}$$

The global effective property E_g^* is then expressed as a weighted harmonic mean:

$$E_g^* = \left(\int_0^L \omega_g(v) \cdot E(v)^{-1}\,\mathrm{d}v\right)^{-1} \tag{C.9}$$

where the global weighting function $\omega_g(v)$ is given by:

$$\omega_g(v) = \begin{cases} \dfrac{12v^2}{a(3L^2-4a^2)} & \text{if } 0 \le v \le a \\ \dfrac{12v)}{3L^2-4a^2} & \text{if } a \le v \le L/2 \\ \dfrac{12(L-v)}{3L^2-4a^2} & \text{if } L/2 \le v \le L-a \\ \dfrac{12(L-v)^2}{a(3L^2-4a^2)} & \text{if } L-a \le v \le L \end{cases} \tag{C.10}$$

C.2 Weighting function for the local modulus of elasticity

This appendix contains a derivation of an expression for the weighting function $\omega_l(v)$ of the local modulus of elasticity continuing the analysis from Appendix C.1. The first step is to consider expressions for the displacement at the left $U(x_l)$ and right $U(x_r)$ of the strain gauge. An expression for the displacement $U(x_l)$ at the left-side of the displacement gauge is obtained by evaluating Equation C.4 at $x = x_l = (10a + L)/12$ giving:

$$\begin{aligned} U(x_l) = \frac{P}{I}\Bigg[& \int_0^a \frac{23v^2}{72E(v)}\,\mathrm{d}v + \int_a^{x_l} \frac{23vL}{216E(v)}\,\mathrm{d}v \\ & + \int_{x_l}^{2L/3} \frac{13L(L-v)}{216E(v)}\,\mathrm{d}v + \int_{2L/3}^{L} \frac{13(L-v)^2}{72E(v)}\,\mathrm{d}v \Bigg] \end{aligned} \tag{C.11}$$

An expression for the displacement $U(x_r)$ at the right-side of the displacement gauge is obtained by evaluating Equation C.4 at $x = x_r = (11L - 10a)/12$ giving:

$$\begin{aligned} U(x_r) = \frac{P}{I}\Bigg[& \int_0^a \frac{13v^2}{72E(v)}\,\mathrm{d}v + \int_a^{x_r} \frac{13vL}{216E(v)}\,\mathrm{d}v \\ & + \int_{x_r}^{L-a} \frac{23L(L-v)}{216E(v)}\,\mathrm{d}v + \int_{L-a}^{L} \frac{23(L-v)^2}{72E(v)}\,\mathrm{d}v \Bigg] \end{aligned} \tag{C.12}$$

The local displacement U_l is given by BS EN 408:2010 as follows:

$$U_l = U(x_c) - \left(\frac{U(x_l) + U(x_r)}{2}\right) \tag{C.13}$$

Substituting the expressions for midspan displacement $U(x_c)$ given by Equation C.5, displacement at the left-side of the strain gauge $U(x_l)$ given by Equation C.11 and displacement at the right-side of the strain gauge $U(x_r)$ given by Equation C.12 into the expression for local displacement U_l gives:

$$\begin{aligned} U_l = \frac{P}{I}\Bigg[& \int_0^a \frac{v^2}{4E(v)}\,\mathrm{d}v + \int_a^{L/2} \frac{av}{4E(v)}\,\mathrm{d}v + \int_{L/2}^{L-a} \frac{a(L-v)}{4E(v)}\,\mathrm{d}v + \int_{L-a}^{L} \frac{(L-v)^2}{4E(v)}\,\mathrm{d}v \\ & - \int_0^a \frac{23v^2}{144E(v)}\,\mathrm{d}v - \int_a^{x_l} \frac{23vL}{432E(v)}\,\mathrm{d}v - \int_{x_l}^{2L/3} \frac{13L(L-v)}{432E(v)}\,\mathrm{d}v - \int_{2L/3}^{L} \frac{13(L-v)^2}{144E(v)}\,\mathrm{d}v \\ & - \int_0^a \frac{13v^2}{144E(v)}\,\mathrm{d}v - \int_a^{x_r} \frac{13vL}{432E(v)}\,\mathrm{d}v - \int_{x_r}^{L-a} \frac{23L(L-v)}{432E(v)}\,\mathrm{d}v - \int_{L-a}^{L} \frac{23(L-v)^2}{144E(v)}\,\mathrm{d}v \Bigg] \end{aligned} \tag{C.14}$$

In order that there is no overlap between the domains of integration of different terms, the integrals are split in compliance with the six domains of integration shown in Figure C.2.

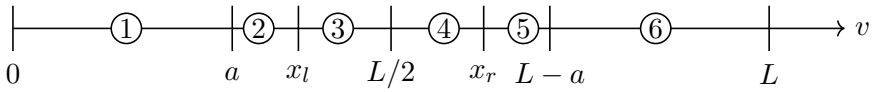


Figure C.2: Six domains of integration associated with Equation C.14.

It is noted that the terms associated with integrals over domains 1, 2, 5 and 6 cancel with the remaining terms corresponding to integrals over domains 3 and 4. Consequently, the equation of local displacement U_l given by Equation C.14 simplifies to give:

$$U_l = \frac{P}{I}\left[\int_{x_l}^{L/2} \frac{a(12v - 10a - L)}{48E(v)}\,\mathrm{d}v + \int_{L/2}^{x_r} \frac{a(11L - 10a - 12v)}{48E(v)}\,\mathrm{d}v \right] \tag{C.15}$$

Under the assumption that the beam is homogeneous with constant modulus of elasticity E_l^* then local displacement U_l is given by:

$$U_l = \frac{25Pa(L-2a)^2}{576E_l^* I} \tag{C.16}$$

An expression for the effective property E_l^* is given by the following change of subject:

$$E_l^* = \frac{25Pa(L-2a)^2}{576\,U_l\,I} \tag{C.17}$$

Substituting the expression for displacement U_l given by Equation C.15 into the expression for the effective property E_l^* gives (noting that a, P and I cancel):

$$E_l^* = \frac{25(L-2a)^2}{12\left[\displaystyle\int_{x_l}^{L/2} \frac{12v-10a-L}{E(v)}\,\mathrm{d}v + \int_{L/2}^{x_r} \frac{11L-10a-12v}{E(v)}\,\mathrm{d}v\right]} \tag{C.18}$$

The effective property E_l^* is then expressed as a weighted harmonic mean:

$$E_l^* = \left(\int_0^L \omega_l(v)\cdot E(v)^{-1}\,\mathrm{d}v\right)^{-1} \tag{C.19}$$

where the weighting function $\omega_l(v)$ is given by:

$$\omega_l(v) = \begin{cases} 0 & \text{if } 0 \le v \le x_l \\ \dfrac{12(12v-10a-L)}{25(L-2a)^2} & \text{if } x_l \le v \le L/2 \\ \dfrac{12(11L-10a-12v)}{25(L-2a)^2} & \text{if } L/2 \le v \le x_r \\ 0 & \text{if } x_r \le v \le L \end{cases} \tag{C.20}$$